PNNL-11304
UC-721

Potential for Criticality in Hanford Tanks Resulting from Retrieval of Tank Waste

G. A. Whyatt
R. J. Serne
S. V. Mattigod
Y. Onishi
M. R. Powell
J. H. Westsik, Jr.
L. M. Liljegren
G. R. Golcar
K. P. Recknagle
P. M. Doctor
V. G. Zhirnov
J. Dixon

September 1996

Prepared for the U.S. Department of Energy
under Contract DE-AC06-76RLO 1830

Pacific Northwest National Laboratory
Operated for the U.S. Department of Energy
by Battelle

Battelle

PNL-11304

PACIFIC NORTHWEST NATIONAL LABORATORY
operated by
BATTELLE
for the
UNITED STATES DEPARTMENT OF ENERGY
under Contract DE-AC06-76RLO 1830

Printed in the United States of America

Available to DOE and DOE contractors from the Office of Scientific and Technical Information, P.O. Box 62, Oak Ridge, TN 37831; prices available from (615) 576-8401.

Available to the public from the National Technical Information Service, U.S. Department of Commerce, 5285 Port Royal Rd., Springfield, VA 22161

PNNL-11304
UC-721

Potential for Criticality in Hanford Tanks Resulting from Retrieval of Tank Waste

G. A. Whyatt
R. J. Serne
S. V. Mattigod
Y. Onishi
M. R. Powell
J. H. Westsik, Jr.
L. M. Liljegren
G. R. Golcar
K. P. Recknagle
P. M. Doctor
V. G. Zhirnov
J. Dixon

September 1996

Prepared for
the U.S. Department of Energy
under Contract DE-AC06-76RLO 1830

Pacific Northwest National Laboratory
Richland, Washington 99352

Foreword

Much of this document was prepared in coordination with the preparation of the draft of WHC-SD-WM-TI-757, Rev 0 (Serne et al., 1996), with substantial information in common. The scope of Serne et al. focused on safe storage and this document focuses on the segregation that may occur during retrieval of sludge from waste tanks. Some information in Serne et al. (1996) does not relate to retrieval and is not included in this document, while other subject areas have been expanded from the Serne et al. (1996) document.

Summary

This draft report contains evaluations intended to assess the potential for criticality occurring as the result of retrieval of waste tank sludge from single-shell tanks (SST) and double-shell tanks (DST). The evaluations are focused on the potential for segregation of fissile material creating locally concentrated regions within a tank that could cause a criticality. The current analysis focuses specifically on mixer pump operation in SY-102, and sluicing retrieval of C-106 solids to tank AY-102. These two tanks were singled out for scrutiny, based on their high plutonium inventories and due to near term plans for retrieval operations. Qualitative conclusions can be made for mixer pump operation and sluicing within other tanks, based on the analysis of C-106 and SY-102. This evaluation found no credible mechanism through which a criticality could be achieved during retrieval of these tanks. Although numerical probabilities have not been calculated, the probability of a criticality occurring during retrieval is clearly remote.

Waste in tanks may be categorized as supernatant, salt cake, or sludge. The low solubility of plutonium in the high pH supernatants results in very low plutonium inventories in supernatant and salt cake. Further, a review of plutonium chemistry supports the assertion that criticality resulting from soluble plutonium will not occur. Thus, of the three waste types, only the sludge poses a potential concern.

The average fissile concentration within any given DST is sufficiently low that, if the material is uniform, criticality is not possible. For example, the minimum areal concentration of Pu-239 (Pu) in water to achieve criticality is 2583 g/m^2 (240 g/ft^2). This criterion is conservative when applied to waste sludge (Rogers 1993). When applied to the floor area of a 22.9 m (75-ft) diameter storage tank, this implies a minimum inventory of 1060 kg Pu. This total is roughly equal to the conservative estimate of 1000 kg for the total plutonium inventory of all Hanford tanks. Alternatively, using the conservative waste model developed by Rogers (1993), the minimum Pu concentration to allow criticality in sludge of infinite geometry is 2.6 g/l. By contrast, conservatively high estimates of the Pu content of sludge in C-106 is 0.13 g/l and in SY-102 is 0.15 g/l which indicates a factor of safety of 20 and 17, respectively. Both C-106 and SY-102 contain sufficient iron to satisfy the minimum safe iron to plutonium (Fe:Pu) mass ratio of 160. Therefore, any process that concentrates both the Pu and iron fractions of the sludge without affecting the Fe:Pu ratio cannot result in a criticality.

However, the waste within each tank is not uniform initially, and the retrieval process could potentially sort particles of different composition based on differences in density, size, surface properties, or chemistry. If such sorting occurs to a sufficient extent and some mechanism were to arrange the fissile material into a suitable geometry, then a criticality becomes possible. This issue is the one this report addresses.

Figure S.1 provides a conceptualization of the logic used for resolution of the retrieval criticality issue. The criticality issue could potentially be resolved, if the plutonium exists initially in a state where

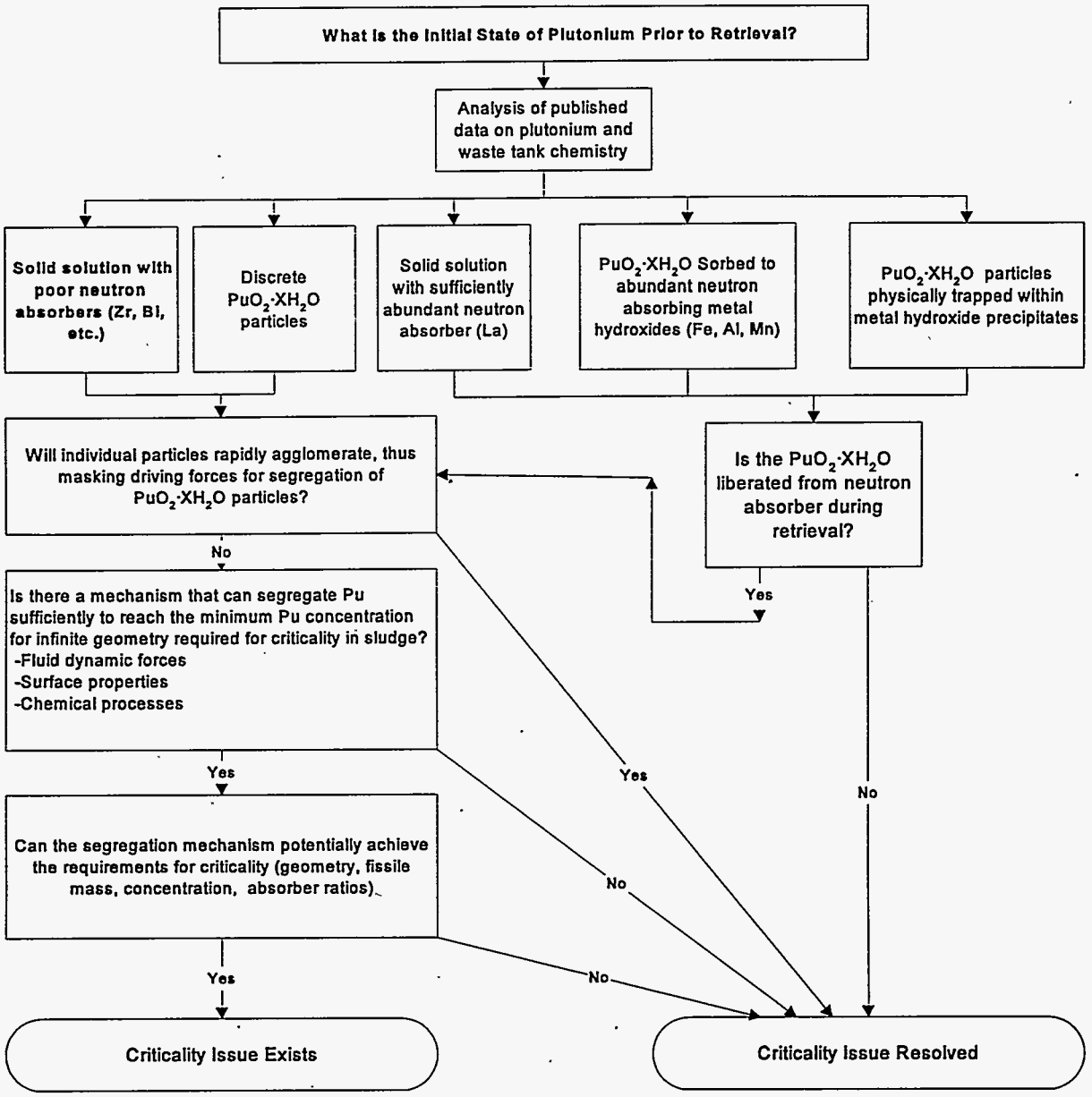

Figure S.1. Flowchart for Resolution of Criticality Issue Related to Segregation During Retrieval

it is intimately associated with effective neutron absorbers. For this reason, the initial state of the plutonium within the sludge is of great interest. A thorough review of literature was conducted in an attempt to resolve the initial state of plutonium in sludge. The literature review determined that while sorption to iron or formation of a solid solution with a good neutron absorber is possible, discrete PuO_2 xH_2O particles (either existing free or physically trapped by other precipitates) or Pu in solid solution with a poor neutron absorber are also possibilities. If the Pu is strongly sorbed to iron, or if it exists in solid solution with adequate quantities of a good neutron absorber such as lanthanum, no issue arises

because the neutron absorber will prevent criticality. Further, fluid forces during retrieval and possible dilution with inhibited water would not be expected to liberate the Pu in these cases. Other possible states include the possibility that either the plutonium exists as separate particles initially or that fluid forces liberate the plutonium particles during retrieval. Because this first possible route to issue resolution cannot be established to high confidence, the dynamics of particle segregation must be evaluated.

The second mechanism that can prevent segregation of a fissile particulate is agglomeration. If fissile particulates are agglomerated with other particles, the physical properties of the agglomerate will determine segregation. While agglomeration may lead to more rapid settling and cause solids to settle out of a fluid, the settling will be determined by the properties of the agglomerate rather than any unique properties of the fissile material and a criticality will not be possible. There is very strong evidence that the waste particles will agglomerate. The most direct evidence of agglomeration is a comparison of TEM data with measured sedimentation velocities and particle size data, generated using light scattering techniques. TEM measurements show the primary particles of the sludge are submicron while sedimentation and particle sizing information indicate much larger particles. The reason is that sedimentation and light scattering techniques measure the properties of agglomerates of the waste particles, not the individual particles. In addition, conservative calculations lead to the conclusion that rapid formation of flocs will occur, provided the salt concentration is at least 0.1 molar in the supernatant, the pH is at least 10, and the mixing intensity is sufficiently low to permit flocculation. Rapid flocculation will prevent segregation of the fissile material.

While agglomerates within the waste are likely to be broken up by the pumps, and possibly fluid jets, associated with retrieval operations, they are expected to reform under conditions suitable for settling of solids. The kinetics of the agglomerate breakup/reformation process have not been extensively studied, but hot-cell settling tests imply that agglomerates will reform quickly once mechanical disruption (such as mixing) stops.

Selective agglomeration (where a single type of particle preferentially agglomerates with itself) should not occur under the pH and saline conditions existing within the tanks. Conceptually, it is possible for particles that are agglomerated to selectively agglomerate if a chemical reaction were to cement chemically-similar particles together. Through repeated cycles of breakup and reagglomeration, these particles could stick together in larger clumps. It is not expected that Pu should show this type of behavior, although some submicron SiO_2 agglomerates have been observed by TEM. The available evidence suggests the plutonium will be agglomerated with other materials and will not segregate from the waste.

Although PuO_2 is not believed to exist as super micron, discrete, non-agglomerated particles, the potential for segregation of this type of particle was evaluated in order to provide a defense in depth. Modeling was performed to evaluate the potential for segregation using simplified 1-dimensional models, as well as full 3-dimensional TEMPEST models, to simulate the fluid dynamic processes occurring during retrieval. Particle size distributions, based on light scattering measurements, were used with the assumption that these represent individual particle sizes with each particle having a unique

composition (PuO_2 xH_2O for plutonium). In separate 1-dimensional cases, the plutonium was assumed to exist uniformly across the size distribution, or as monodisperse particles with sizes between 5 and 20 microns. Simplified models indicated the minimum concentrations to allow criticality for C-106 solids could not be obtained under these conditions by simple settling. In the case of SY-102, the segregation was only sufficient to reach the minimum concentration when plutonium was assumed to be the smaller, monodisperse particles. In this case, concentrations in excess of 2.6 g/l are predicted to occur in very thin layers near the top of the sludge layer that contain less than 10% of the plutonium inventory. Based on the concentration and mass of the plutonium in this layer, the material in the concentrated layer would not attain criticality even if skimmed from the remainder of the waste and collected into a sphere. Thus, simple settling does not provide sufficient segregation to create a criticality concern. This statement is true under the conservative assumptions (made only to allow analysis) that light scattering particle size distributions represent primary particles of unique composition and that agglomeration does not interfere with segregation.

Full 3-dimensional modeling was preformed specifically for mixer pumps in SY-102, for withdrawal of slurried solids from C-106, and for introduction of C-106 solids to AY-102. This modeling was performed to determine if the flowing fluid might deposit particles of a given type in a specific area and, in this way, achieve higher degrees of concentration than in the simple settling case. This modeling indicated the largest degree of enrichment in fissile content was less than a factor of 2.5, well below the minimum required enrichment factors of 17 (SY-102) or 20 (C-106) to reach a concentration of 2.6 g/l. The results indicate much less segregation than in the simple settling model due to:

1. TEMPEST averages concentration across each node and therefore cannot resolve very thin layers less than 1 node thick. Due to geometric concerns, very thin layers of concentrated material are not a criticality concern.)

2. The greatest degree of concentration in the simple settling scenarios without flocculation occurs for the last particles to settle, while the TEMPEST models only provide information on the first layers of sludge to form, due to computational times required for the problems.

3. Flow patterns may reduce segregation compared to simple settling. For example, as sludge is introduced to AY-102, a density current forms that carries the slurry to the bottom of the tank and minimizes the potential for segregation.

In any case, the degree of segregation observed for the full 3-dimensional model does not raise any concern related to criticality.

In TEMPEST, particles follow the fluid streamlines and settle relative to these streamlines at a terminal settling velocity. This approach does not account for particle momentum and does not model effects related to particle acceleration or deceleration relative to the fluid. For this reason the mining literature was reviewed for analogous separations processes to determine which ones may be applicable. The Pu particles are expected to be micron sized with an upper limit in the 10 to 20 micron range. This size is below the normal particle range for either gravity separations or flotation processes.

To achieve gravity segregation would require the addition of centrifugal forces, rhythmic shaking of a surface with a thin flowing film with collection and refinement of the product or other processes that would not be expected to occur within a waste tank. While it is possible that very localized concentrated regions could occur, the possibility of a large scale segregation by gravity means does not appear credible. Segregation of plutonium by selective flotation of the plutonium appears highly unlikely. If the proper organic molecules were present to allow flotation they would be expected to float other metal hydroxides along with the plutonium at the pH conditions typical of waste storage tanks. However, even if selective flotation were assumed to occur, the material would spread out in a form layer across the tank and the 2583 g/m^2 (240 g/ft^2) areal limit for criticality would apply to the uniform layer. Thus, the entire plutonium content of a waste tank could be concentrated into a foam layer without resulting in a criticality. Also, attachment to or extraction into a separate organic layer are possible scenarios for segregation. Neither SY-102, C-106 nor AY-102 are known to have separate organic layers which eliminates this mechanism from consideration.

Neutronics calculations provide the final line of defense in the case that criticality will not occur during retrieval. No additional criticality calculations were performed as part of this study, although a few useful benchmarks developed elsewhere are included. The geometric, critical mass, absorber content and moderation considerations adds an additional margin of safety on top of the convincing evidence that segregation sufficient to result in criticality will not occur.

This page intentionally left blank.

Contents

Figures

Tables

Acronyms and Abbreviations

ALC	Air-lift circulator
CRW	Cladding removal waste
DBP	Dibutyl phosphate
DBBP	Dibutyl butylphosphonate
DF	Decontamination factor
DLVO	Derjaguin, Landau, Verwey, and Overbeek, developers of the theory
DST	Double shell tank
EDDA	ethylenediaminediacetic acid
ED3A	Ethylenediaminetriacetic acid
E_2DTA	diethylenediaminetetraacetic acid*
EDTA	Ethylenediaminetetraacetic acid
E'S	Energy dispersive spectroscopy
Eh	Oxidation-reduction potential
ESP	Environmental Simulation Program
EXAFS	X-ray absorption fine structure spectroscopy
GC/FID	Gas chromatography/Flame ionization detection
GC/FTIR	Gas chromatography/Fourier transform infrared spectrometry
GC/MS	Gas chromatography/Mass spectrometry
GMIN	Geochemistry code that uses Gibbs Free Energy Minimization techniques*
HEDDA	N-hydroxyethylene-diaminediacetic acid
HEDTA	Hydroxyethylenediaminetetraacetic acid
HEIDA	N-(2-Hydroxyethyl) iminodiacetic acid*
HLW	High level waste
HPLC	High Pressure Liquid Chromatography
IC	Ion chromatography
IDA	Iminodiacetic acid
LC	Liquid chromatography
LC/UV	Liquid chromatography/Ultraviolet spectrometry
LMWA	Low molecular weight organic acids
MeEDD'A	N-Methylethylenediamine-N, N'-diacetic acid*
NCAW	Neutralized Current Acid Waste
ND	Not detected
NIDA	Nitrosoiminodiacetic acid
NMR	Nuclear magnetic resonance spectroscopy
NPH	Normal paraffin hydrocarbons
NTA	Nitrilotriacetic a
PNNL	Pacific Northwest National Laboratory
Pu	Pu-239
PUREX	Name of the PUREX facility, Hanford Site
REDOX	Name of the REDOX facility, Hanford Site
SEM	Scanning electron microscopy
SORWT	Sort on Radioactive Waste Type
SRS	Savannah River Site
SST	Single shell tank

TBP	Tributyl phosphate
TEM	Transmission Electron Microscopy
TEMPEST	Transient Energy Momentum and Pressure Equations Solutions in Three Dimensions
TOC	Total organic carbon
TRU	Transuranic waste
TWRS	Tank Waste Remediation System
XANES	X-ray absorption near edge spectroscopy
XAS	X-ray absorption spectroscopy
XRD	X-ray diffraction
*	Degradation fragment of EDTA

1.0 Introduction

This report assesses the potential during retrieval operations for segregation and concentration of fissile material to result in a criticality. The sluicing retrieval of C-106 sludge to AY-102 and the operation of mixer pumps in SY-102 are examined in some detail. These two tanks (C-106, SY-102) were selected because of the near term plans for retrieval of these tanks and their high plutonium inventories relative to other tanks. Although all underground storage tanks are subcritical by a wide margin if assumed to be uniform in composition, the possibility retrieval operations could preferentially segregate the plutonium and locally concentrate it sufficiently to result in criticality was a concern. This report examines the potential for this segregation to occur.

The report follows the logic provided in Figure 1.1. The approach has been to assemble a defense-in-depth by examining a number of mechanisms that may prevent criticality from occurring. Because various points of reference for criticality have been developed previously by others, this study did not perform any additional neutronic calculations.

Chapter 2 provides an in-depth review of plutonium chemistry including speciation in solution, redox, hydrolysis, complexation, solubility and sorption processes, as well as an estimation of the upper bound on a discrete plutonium particle size. It was initially hoped this line of investigation would demonstrate the plutonium would be chemically bonded to abundant neutron aborbers, such as aluminum and iron, and that physical processes would not be able to separate the plutonium from neutron absorbers. However, the study concludes that chemical bonding between the Pu and neutron absorbers cannot be proven with existing data. Thus, the fissile material may or may not be separable by physical means.

Chapter 3 examines the potential for flocculation of waste particles as a mechanism for preventing segregation of plutonium particles. Strong evidence is provided that waste particles are agglomerated and that plutonium exists within flocs of other waste particles. Data obtained using scanning electron microscopy (SEM) are provided that indicate the actual sludge particles are primarily submicron in size. In contrast, hot cell sedimentation data using actual waste sludge and light-scattering particle size measurements indicate much larger particle sizes. This difference can be explained if the sedimentation and light scattering measurements are actually measuring particle flocs rather than primary particles. In addition, conservative calculations are presented to demonstrate that particles less than about 10 μm should be agglomerated under conditions typically encountered in waste tanks.

Following the defense-in-depth approach, considerable effort was expended to examine the potential for particle segregations if the conclusions in Chapter 3 were not correct. For this examination, the optical light scattering particle size measurements were assumed to represent the actual sizes of primary particles of discrete composition. Modeling was performed including simple 1-dimensional models (4.1), as well as full 3-dimensional TEMPEST models (4.2). In addition, observations of segregation made during operation of an experimental 1/12-scale mixer pump are presented (4.3), as well as a

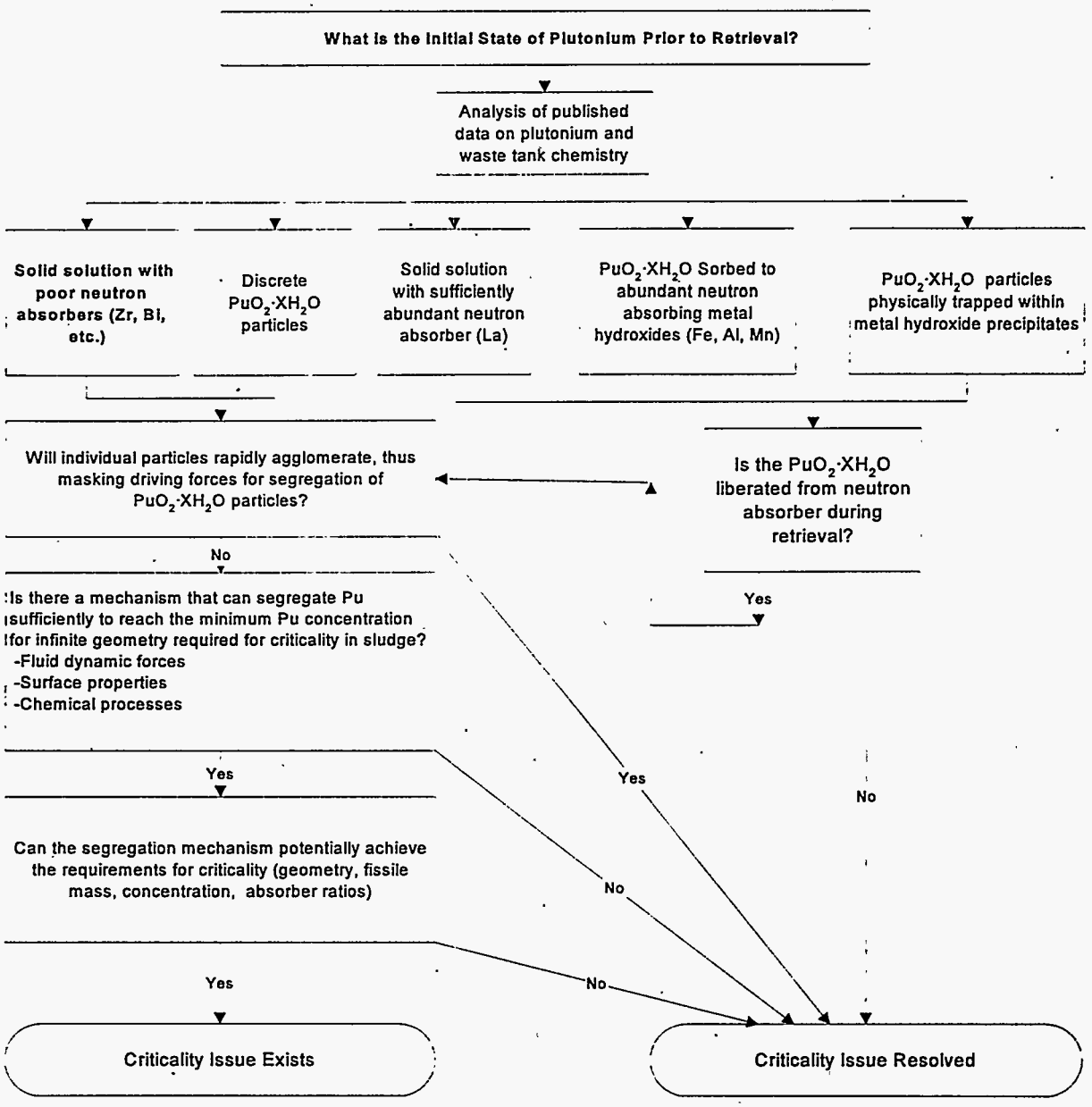

Figure 1.1. Flowchart for Resolution of Criticality Issue Related to Segregation During Retrieval

review of particle segregations that are performed in the mineral processing industry (4.4). While some minor segregation may occur during retrieval operations, the analysis of segregation processes fails to find any credible process through which the fissile material could segregate sufficiently to achieve criticality.

Criticality benchmarks provide the last line of defense that a criticality will not occur. Several factors which interact in a nonlinear fashion determine whether a particular arrangement of material will or will not achieve criticality. While these relationships are complex, a number of simple conservative benchmarks or safe limits can be used to understand the degree of concentration required to actually achieve criticality. Some of these limits are provided in Chapter 5. The information in Chapter 5 was developed elsewhere and is repeated here only for convenience. Criticality calculations were not performed as part of this study. Conclusions are summarized in Chapter 6.

Additional information on selected topics is provided in the appendixes. Appendix A contains information on waste streams transferred to tank farms; Appendix B provides a literature review of liquid flow and solid transport mechanisms; Appendix C provides a calculation of the pumping rate for an air-lift circulator; Appendix D evaluates the significance of organic complexes of Pu(IV); Appendix E describes some experiments that could provide additional support to the criticality issue; and Appendix F provides a discussion of the data available on the identify of solid phases within tank sludges at Hanford.

This page intentionally left blank.

2.0 Chemical Processes That Control Fate of Plutonium and Neutron Absorbers

This chapter focuses on the chemistry of plutonium and selected neutron absorbers. At present, expert opinion differs about which process precipitation or adsorption, dominates partitioning of the plutonium between solid and solution phases in the tanks. Although both views, are discussed because existing literature on general actinides and Hanford Site tanks waste is not comprehensive, no conclusion was reached as to which hypothesis is correct. An abbreviated test plan is included as Appendix F which outlines testing to determine which hypothesis is correct. The authors agree the plutonium in the Hanford Site tanks, based on proposed retrieval activities or continued safe storage, will not be found in supernate solution or salt cake at high enough concentrations to cause a criticality. Also, the tank supernate will always have enough neutron absorber to promote subcriticality.

2.1 Solution Species

In aqueous solutions, plutonium exhibits multiple oxidation states (3+, 4+, 5+, 6+, and 7+) depending on factors such as pH, presence of complexants and reductants, and radiolysis. In some systems, several oxidation states of this element may coexist at equilibrium (Choppin 1983). Typically, the lower oxidation states of plutonium are stable in highly acidic conditions. As alkalinity increases, the higher oxidation states tend to be stable. One factor that influences the solution speciation properties of plutonium, such as hydrolysis, and complexation, is its dominant redox status. Therefore, to accurately assess the overall behavior of plutonium in solution, knowing the redox status of the system is important.

2.1.1 Redox Status

Pu(III) is the stable redox species under highly acidic conditions and in the presence of a reducing agent. Pu(IV) species are stable under moderately reducing conditions. Pu(V) is stable under a narrow range of redox and pH conditions and has a strong tendency to disproportionate into IV and VI redox states (Choppin 1983). However, it has been noted that Pu(V) may be stable and the dominant species only when present in ultra-trace (picomolar) concentration (Hanson 1980). Under oxidizing conditions Pu(VI) is the dominant form in solution. Typical oxidation potentials for plutonium are shown in Table 2.1.

The oxidation potentials indicate that increasing alkalinity results in a decreasing tendency for plutonium to form oxidized species. Disproportionation reactions are also involved in overall redox reactions of plutonium; however, typically the disproportionation mechanism is more important at high concentrations of plutonium and low concentrations of oxidizing agents (Cleveland 1979). Kinetics of plutonium redox reactions are significantly affected by the presence of complexing ligands. Data also shows that, because Pu(IV) forms stronger complexes than other redox species, its oxidation or reduction to other forms is significantly retarded, and the redox conversion from other valence states to Pu(IV)is enhanced (Cleveland 1979).

Table 2.1. Oxidation-Reduction Potentials for Plutonium

Reaction	Oxidation Potentials (volts)		
	pH = 0	pH = 8	pH = 14
$Pu(III) \rightarrow Pu(IV) + e^-$	+0.982	-0.39	-1.04
$Pu(IV) \rightarrow Pu(V) + e^-$	+1.17	+0.70	+0.52
$Pu(V) \rightarrow Pu(VI) + e^-$	+0.916	+0.60	+0.16

Significant quantities of data have been collected for redox reactions of plutonium. However, this data was derived from experiments conducted mainly in acid media to separate plutonium for defense purposes. Similar redox data is limited for plutonium in highly alkaline, high ionic strength, mixed electrolyte medium, and at higher than ambient temperatures (similar to conditions that exist in tanks containing HLW).

Recent experiments, conducted by Yamaguchi et al. (1994) and Delegard (1995) on plutonium solubility in highly alkaline solutions in the presence of a reductant, $NaNO_2$, indicate that plutonium in solution exists mainly in the tetravalent state. Specifically, plutonium solubility experiments conducted by Delegard (1995) in a reductant-containing $NaOH/Na_2CO_3$ solution indicated that all detectable plutonium in solution existed in the tetravalent redox state. These results suggest that, under ambient temperature conditions, and in HLW solutions containing mainly [$\geq$ 0.5 M concentrations of NaOH, $NaNO_3$, $NaAl(OH)_4$, and $NaNO_2$], all the dissolved plutonium may exist in the tetravalent state.

2.1.2 Hydrolysis

Hydrolysis reactions of plutonium involve the formation of soluble complexes or solid phases with hydroxyl ions. Therefore, plutonium hydrolysis species depend strongly on the concentration of hydroxyl ions in solution among other factors. Because the available data presented in Section 2.1.1 indicates that soluble plutonium in HLW tanks may exist mainly in the tetravalent state, all discussion of hydrolysis reactions will be restricted to Pu(IV) species. Pu(IV) hydrolyzes more readily than all other redox species of plutonium (Baes and Mesmer 1976). The order of hydrolysis of plutonium redox species follows the sequence Pu(IV) > Pu(III) > Pu(VI) > Pu(V). Depending on the total concentration of plutonium in solution, hydrolysis may also cause polymer formation. Typically, polymerization occurs when total plutonium concentration in solution exceeds 10^{-6} M (Choppin 1983). Also, the presence of other complexing ligands inhibits polymer formation (Cleveland 1979). When total Pu(IV) concentration is $<10^{-6}$ M, hydrolysis reactions result in the formation of monomeric species. The speciation scheme can be expressed as:

$$Pu^{4+} + x\ OH^- = Pu(OH)_x^{x-4} \qquad (2.1)$$

Depending on the pH of the solution, the number of hydroxyls (x) coordinating plutonium may range from 1 to 4 or perhaps larger. Solubility data for tetravalent actinides (Rai and Ryan 1983, Rai et al. 1995) indicate lack of amphoteric behavior, thus the formation of Pu $(OH)_5^-$ species in solution appears to be unproven. However, solubility data obtained by Delegard (1987) in sodium hydroxide solutions ranging in concentration from 1 to 15 M, indicate amphoteric behavior suggesting that negatively charged hydrolytic species of Pu(IV) may exist.

The stability constants for Pu(IV) hydrolytic species are listed in Table 2.2. The constants indicate that plutonium in the tetravalent state forms more stable complexes than plutonium in tri-, penta-, and hexavalent states. Increasing hydroxyl concentration (increasing pH) results in the dominance of hydrolytic species with increasing numbers of OH^- coordinating with plutonium.

Table 2.2. Stability Constants for Hydrolytic Species of Pu(IV)

Hydrolysis Reaction	log K
$Pu^{4+} + OH^- = Pu(OH)^{3+}$	13
$Pu^{4+} + 2\ OH^- = Pu(OH)_2^{2+}$	26
$Pu^{4+} + 3\ OH^- = Pu(OH)_3^{+}$	37
$Pu^{4+} + 4\ OH^- = Pu(OH)_4^{0}$	47

2.1.3 Complexation

Plutonium forms complexes with a number of inorganic and organic ligands. The tendency to form complexes depends on the ionic potential defined as a ratio of formal charge and the ionic radius of an ion. Among plutonium redox species, Pu(IV) exhibits the highest ionic potential, therefore Pu(IV) forms the strongest plutonium complexes with various ligands.

Typical Hanford Site HLW contains ligands, such as NO_3, NO_2, CO_3, PO_4, SO_4 F, Cl, oxalate, citrate, EDTA, and HEDTA. Reviews of existing literature indicate that Pu(IV) complexes have been studied extensively because they occur during the plutonium separation process. The tabulated data shows the Pu(IV) complexes containing NO_3, SO_4, F, and Cl form rather weak complexes, so these complexes may not be significant in Hanford Site HLW. Although phosphate, citrate, oxalate, and EDTA ligands form very strong complexes with the Pu(IV) ion, the concentrations of these complexes will not be significant in Hanford Site HLW because the ligand concentrations in the waste solution are typically two orders of magnitude or more less than the strongly complexing hydroxyl ions. A sample calculation showed (Appendix D) that in a typical waste tank supernatant, the concentrations of

Pu-hydroxyEDTA complexes would be insignificant as compared to the concentrations of Pu-hydroxycarbonate complexes. Typical stability constants for Pu(IV) complexes are tabulated in Table 2.3.

Table 2.3. Stability Constants for Pu(IV) Complexes

Species	Log K	Species	log K
$PuCl^{3+}$	0.9	$Pu(OH)_2(CO_3)_2^{2-}$	34
PuF^{3+}	8	$Pu(OH)_4(CO_3)_2^{4-}$	50
$PuNO_3^{3+}$	1.8	$Pu(citrate)^{3+}$	~16
$PuSO_4^{2+}$	6	$Pu(Citrate)_2^{2+}$	~30
$Pu(SO_4)_2^0$	3.5	$PuOH(EDTA)^{2+}$	~17
$PuHPO_4^{2+}$	13	$Pu(C_2O_4)^{2+}$	~9
$Pu(HPO_4)_2^0$	24	$Pu(C_2O_4)_2^0$	~8
$Pu(HPO_4)_3^{2-}$	33	$Pu(C_2O_4)_3^{2-}$	~7
$Pu(HPO_4)_4^{4-}$	43	$Pu(C_2O_4)_4^{4-}$	~4

Based on solubility data, Lierse (1985) has suggested the existence of a series of Pu-carbonate complexes namely, $PuCO_3^{2+}$, $Pu(CO_3)_2^0$, $Pu(CO_3)_3^{2-}$, $Pu(CO_3)_4^{4-}$, and $Pu(CO_3)_5^{6-}$. However, no spectroscopic data support the existence of these species. Because solubility data can be interpreted on the basis of any number of hypothetical species, the existence of such species are uncertain without additional confirmatory spectroscopic data.

Recently, based on solubility and spectroscopic data, Yamaguchi et al. (1994) showed that under alkaline conditions, Pu(IV)-OH-CO_3 mixed ligand complexes may form the dominant dissolved species in alkaline-carbonate solutions. Solubility experiments in high ionic strength solutions containing NaOH and Na_2CO_3 also have shown that plutonium mixed ligand species are the principal aqueous species (Delegard 1995). Photoacoustic spectroscopic data generated by Tait et al. (1995) has also confirmed the existence of three different Pu(IV)-OH-CO_3 mixed ligand species, although these investigators could not determine the ligand stoichiometry. These investigators interpreted the data in terms of the existence of $Pu(OH)_x(CO_3)_y^{(3-x-2y)}$, $Pu(OH)_x(CO_3)_{y+1}^{(3-x-2y-2)}$, and $Pu(OH)_{x+1}(CO_3)_y^{(3-x-2y-1)}$ species. The distribution of these species, as a function of pH and total aqueous carbonate concentrations, is shown in Figures 2.1 and 2.2. The data indicates the $Pu(OH)_{x+1}(CO_3)_y^{(3-x-2y-1)}$ species is dominant under all conditions examined in these experiments. The stoichiometries of these mixed ligand species for various values of x and a unit value of y were computed and compared with the stoichiometries of mixed ligand species predicted by Yamaguchi et al. (1994) in Table 2.4.

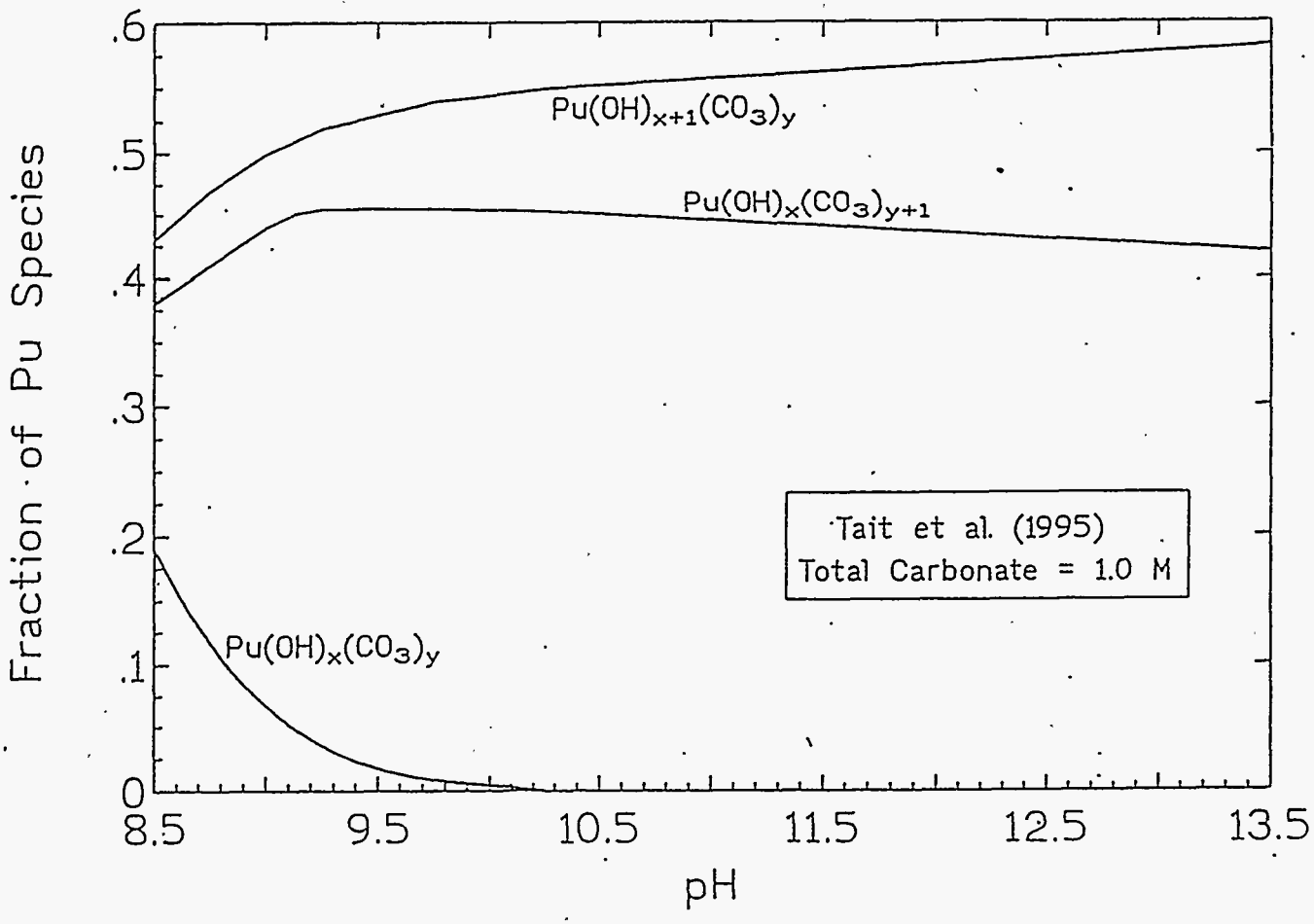

Figure 2.1. Distribution of Pu(IV)-Hydroxycarbonate Species as a Function of pH at Fixed Total Carbonate Concentration of 1.0 M

The data in Table 2.4 show that in all cases, except two, the predicted stoichiometry based on data presented by Tait et al. (1995) does not conform with stoichiometries of species predicted by Yamaguchi et al. (1994). Only in two cases, when x is 2 and y is 1, and when x is 1 and y is 2, does one of the predicted species [$Pu(OH)_2(CO_3)^{2-}$] based on the data presented by Tait et al. (1995) agree with a species predicted by Yamaguchi et al. (1994). The stochiometries based on the suggested condition for charge $4-(x+2(y+1)) \leq -1$ from Tait et al. (1995) results in the set of species listed in the first column of Table 2-4[a]. Only one species from the speciation scheme of Tait et al. ($Pu(OH)_2(CO_3)_2^{2-}$) with either of the two species suggested by Yamaguchi et al. (1994). According to Yamaguchi et al. (1994) data, the dominant species at pH values above about 11 would be $Pu(OH)_4(CO_3)_2^{4-}$. The speciation scheme

(a) In a recent unpublished manuscript, Tait et al. (personal communication) indicate that x and y may be 1 and 2, respectively.

proposed by Tait et al. (1995) does not provide a comparable species. Therefore, the data generated by Yamaguchi et al. (1994) and Tait et al. (1995) disagree about the number of complexes, their stochiometries, and the range of species dominance.

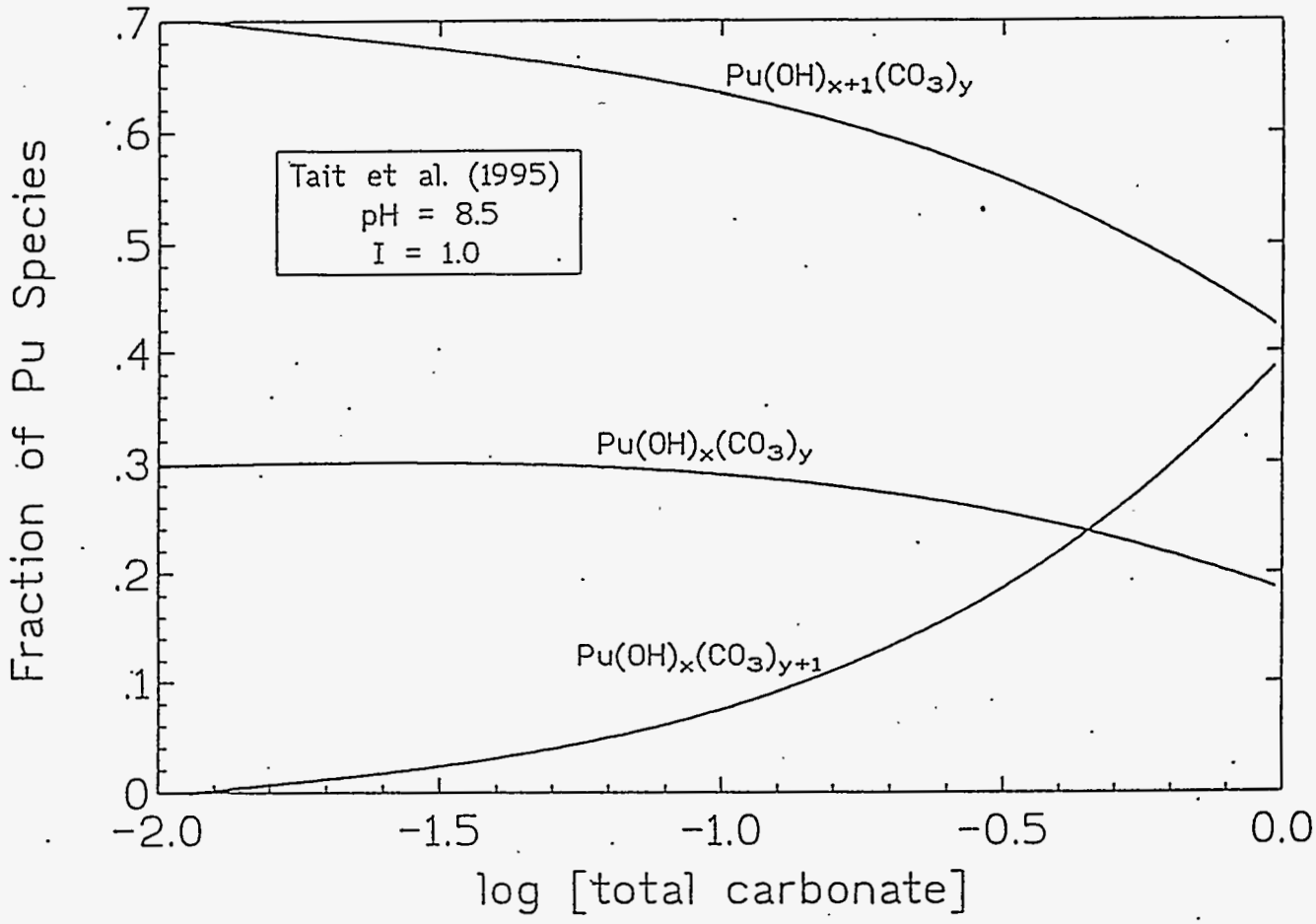

Figure 2.2. Distribution of Pu(IV)-Hydroxycarbonate Species as a Function of Total Carbonate Concentration at a Fixed pH Value of 8.5

Although experimental data is available that confirms the existence of Pu(IV)-OH-CO_3 mixed ligand species, the existing data from spectroscopy and solubility are contradictory. Until the stiochiometry question is resolved, the data set of Yamaguchi et al. (1994) was used in all speciation calculations. Predicted speciation of Pu(IV) species as a function of pH and carbonate concentrations are shown in Figures 2.3 and 2.4. The computations show that, at low carbonate concentrations (0.001 M), various hydrolytic species predominate up to a pH value of about 6.5. At a pH between 6.5 and 10, $Pu(OH)_2(CO_3)^{2-}$ is the dominant aqueous species. At higher pH values, the neutral hydrolytic species, $Pu(OH)_4^0$ makes up about 90 % of the dissolved Pu(IV) species. With increasing carbonate

concentration, the speciation picture shows significant changes. Under these conditions, the range of dominance of $Pu(OH)_2(CO_3)^{2-}$ species extends over about 7 orders of magnitude (from a pH of about 3.5 to 10.5). At pH values above ~11, $Pu(OH)_4(CO_3)^{4-}$ will be the dominant aqueous species in solution.

Table 2.4. Probable Stochiometries of Pu(IV)-OH-CO_3 Mixed Ligand Aqueous Species

Tait et al. (1995)			Yamaguchi et al. (1994)
x = 1, y =1	x = 2, y =1	x = 3, y =1	
$PuOHCO_3^+$	$Pu(OH)_2CO_3^0$	$Pu(OH)_3CO_3^-$	$Pu(OH)_2(CO_3)^{2-}$
$PuOH(CO_3)^-$	$Pu(OH)_2(CO_3)_2^{2-}$	$Pu(OH)_3(CO_3)^{3-}$	$Pu(OH)_4(CO_3)_2^{4-}$
$Pu(OH)_2CO_3^0$	$Pu(OH)_3CO_3^-$	$Pu(OH)_4CO_3^{2-}$	--

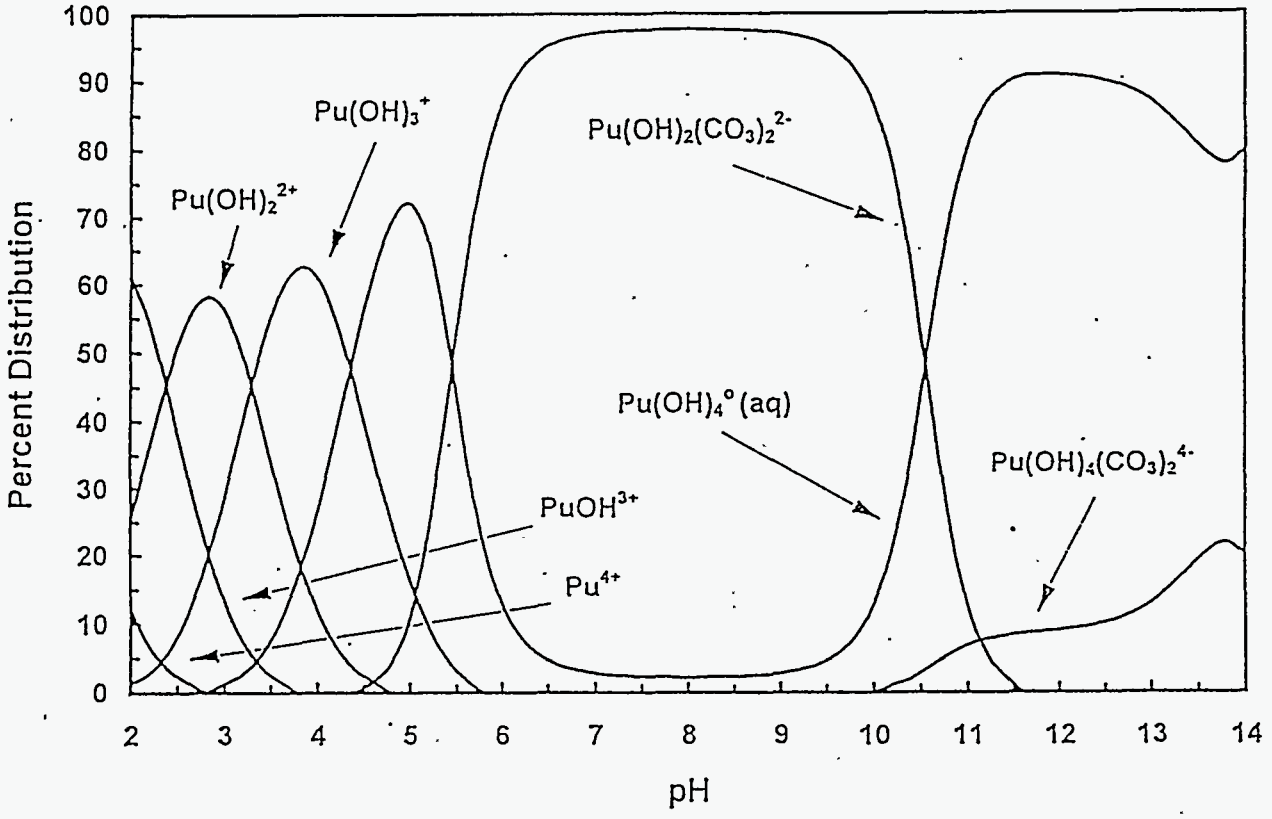

Figure 2.3. Computed Distribution of Pu(IV) Aqueous Species as a Function of pH at a Fixed Total Carbonate Concentration of 0.001 M

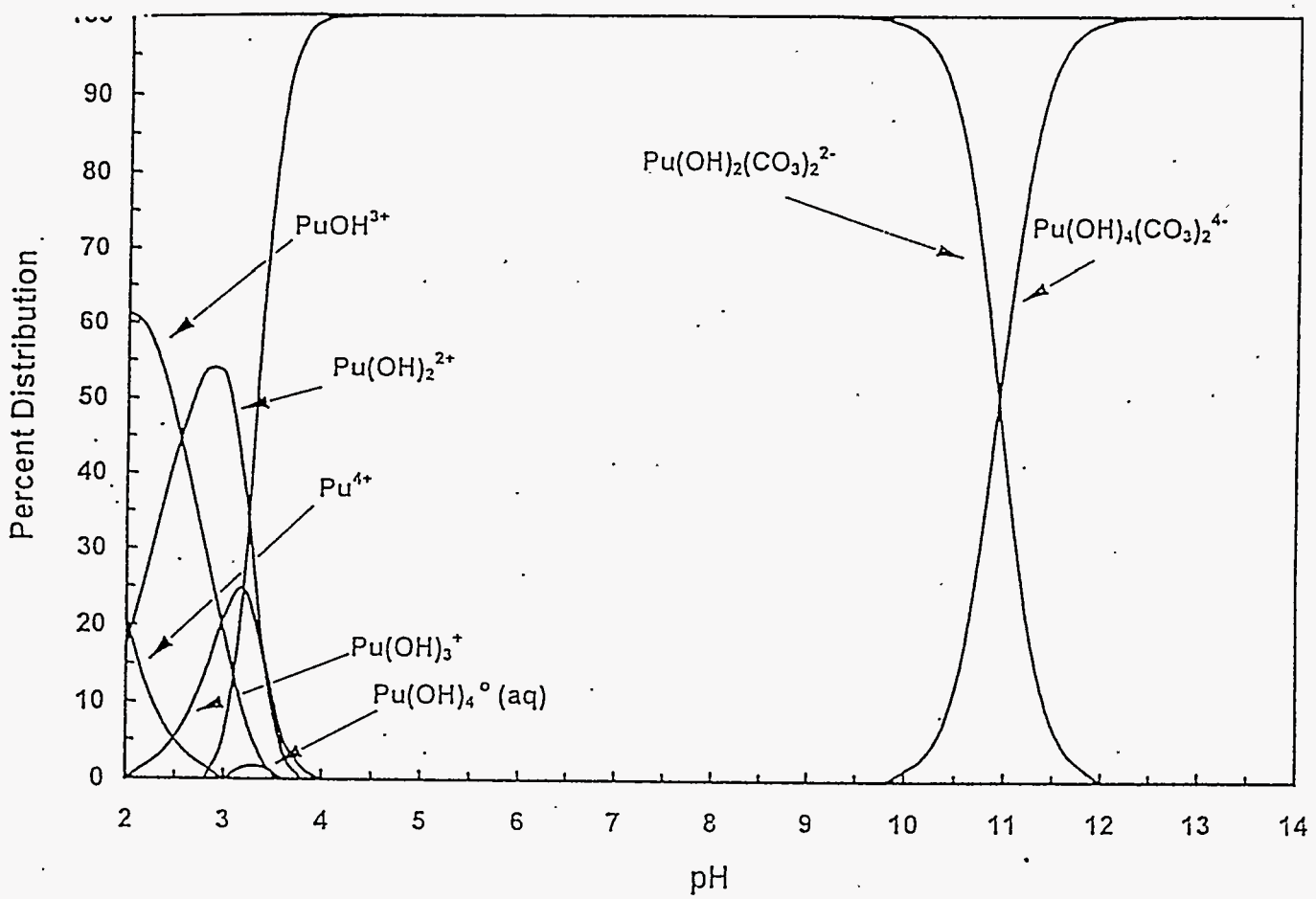

Figure 2.4. Computed Distribution of Pu(IV) Aqueous Species as a Function of pH at a Fixed Total Carbonate Concentration of 0.5 M

The data suggests the typical solution composition of HLW in Hanford Site tanks probably includes Pu(IV)-OH-CO_3 mixed ligand complexes as the dominant aqueous species. However, equilibrium calculations or spectroscopic measurements are needed to confirm the presence of these dominant species in HLW supernatants.

2.1.4 Ionic Strength Effects

Ionic strength is a measure of the total electrolyte concentration. This concentration is defined as one-half the sum of the products of total concentrations and the charge on the electrolyte components in a waste solution. Ionic strength of a solution affects a number of reaction parameters related to complex formation, complex stability, solubility, and adsorption.

Available stability data (up to 4 M ionic strength) indicates that plutonium-complex species tend to become less stable with increasing ionic strength. For instance, the stability of $Pu(OH)^{3+}$ species decreases by about an order of magnitude when the ionic strength increases from 0 to 2 M. The stability of a weaker complex, such as $PuNO_3^{3+}$, also decreases by an order of magnitude when the ionic strength increases from 0 to 4 M. However, the magnitude of plutonium-complex stability constants in HLW solutions (typically ~9 M) is difficult to assess because no experimental data exists on solutions at these very high ionic strengths. Consequently, if the magnitude of change in stability is assumed to be similar for all complex species, the type of dominant species can be expected to be the same, even at higher ionic strengths. Thus, the assumption is the mixed hydroxide-carbonate solution species will predominate in the tank supernate liquids.

2.1.5 Temperature Effects

Higher than ambient temperatures will affect the reaction kinetics and chemical equilibrium of the HLW system. The bulk of published data on stability for hydrolytic and complex species for Pu(IV) was typically obtained at ambient temperatures. Therefore, to assess the effects of higher temperatures (up to boiling) on the supernatant chemistry of HLW stored in tanks, it is necessary to know how the ambient temperature stability constants change, as a function of increasing temperature.

Literature review identified only one source of higher temperature complex stability data for plutonium species (Lemire and Tremaine 1980). The data used in this report was derived from their work using theoretical calculations instead of actual measurements. Typically, these calculations indicate the stability constants of soluble Pu(IV) complexes (with inorganic ligands besides OH^-) increase by one or two orders of magnitude when the solution temperature increases from 25° to 100°C.

2.1.6 Radiolysis Effects

Alpha emissions from Pu-239 produce free radicals which are powerful redox agents. These free radicals may induce Pu redox reactions resulting in the formation of various valence species. Such self-catalyzed Pu reactions are categorized as radiolytic effects. Most of the studies of radiolysis effects have been conducted in highly acidic solutions. Only a limited number of experiments have been conducted where the radiolytic effects have been studied using near neutral or slightly alkaline solution. Available data show that radiolysis in such solutions in the presence of ligands, such as Cl, SO_4, NO_3, and CO_3, causes oxidation of reduced Pu species (Sullivan 1983). Pikaev (1996) presented data on gamma ray induced radiolysis of alkaline aqueous solutions of Np and Pu that showed the net reaction formed more reducing conditions and Pu(V) and Np(V) aqueous species were reduced to (IV) species. Camaioni et al. (1994) performed gamma irradiation tests on a simulated organic-rich Hanford site tank waste supernatant and found the net radiolysis species were reductants.

Two recent reports from the Savannah River Site (SRS), using simulated HLW solutions similar to the supernatant solutions in Hanford tanks, suggest the following. For solutions that contain NaOH, $NaNO_3$, $NaNO_2$, $NaAlO_2$, Na_2CO_3, and Na_2SO_4 in concentrations similar to those found in Hanford tanks, the effects of gamma Co-60 radiation of up to ~10^7 rads at a dose rate of 4 x 10^4 R/hr on Pu solubility

was insignificant. However, at higher NaOH concentrations an increase occurred in Pu solution concentrations in small vials that were irradiated versus control vials that contained Pu hydrous oxide precipitates and the highly caustic solution. Details are summarized as follows based on the references, Karraker (1994, 1995).

Various simulated tank solutions with the components noted in the previous paragraph were prepared and inoculated with enough Pu stock solution in 0.25 M nitric acid to cause Pu precipitation. Small vials of the Pu slurry were then gamma irradiated with a Co-60 source. Following 3 to 10 days of irradiation, the samples and the non-irradiated controls were analyzed for soluble Pu, based on filtration through 0.2 μm membranes. Based on wet chemical procedures, some Pu speciation data were also obtained. The Pu speciation discussions are based on the assumption that only Pu(IV) would be retained on anion exchange resins; while Pu(VI), Pu(V), and Pu(IV) polymer would not be strongly retained on the resin and could be easily rinsed out prior to rinsing the Pu(IV) with stronger reagents. It should be noted that all the data collected at SRS show solution Pu concentrations below 0.02 g/l when Pu(IV) was used and 0.13 g/l when Pu(VI) was used. In other words, although some increase is indicated in Pu solution concentration in some solutions that are outside the range generally found in tanks, none of the results show solution concentrations above about one-tenth the minimum criticality value of 2.6 g/l discussed in Bratzel et al.(1996).

Karraker found that Pu solution concentrations in the presence of excess hydrous Pu-oxide, increased up to 5 to 10 times, versus nonirradiated controls, in slurries that were irradiated and contained at least 2.75 M NaOH and contained $NaNO_3$ and $NaNO_2$. The effects were especially found in solutions with NaOH concentrations above 6 M. When no sodium nitrite was present, Pu solution concentrations did not increase until the hydroxide content reached >6 M. Karraker hypothesizes the increased Pu solubility may be caused by radiolysis species that are capable of oxidizing the Pu(IV) to a higher valence state. One possible reactive specie that is formed by radiolysis is hydrogen peroxide (H_2O_2). Karraker performed some experiments where hydrogen peroxide was added to NaOH solutions that contained Pu precipitate/slurry and found that hydrogen peroxide did increase Pu solubility when present in concentrations $>10^{-4}$ M. Further, the hydrogen peroxide degraded to water and oxygen with a half-life of 100 to 300 minutes. If hydrogen peroxide is formed during radiolysis, it could be constantly supplied at a rate faster than it degrades naturally and thus could be ever present in the waste tanks.

Karraker also tested Pu(VI) stock solutions using a slight excess of permanganate in solution. The Pu(VI) acidic solution was mixed with simulated alkaline tank solution. A precipitate formed and the slurries were used in experiments like those just described. Control and irradiated slurries were filtered after several days and solution Pu concentrations were measured. Aliquots of the filtrate were measured as created and after treatment with ferrous iron solution and $NaNO_2$ to reduce all the Pu to the +4 valence state. Running both analyses allows an estimate of Pu speciation. Karraker found that Pu(VI) is stable for at least 25 days. After irradiation, the observed Pu concentration in solution drops, as long as the hydroxide is below 8 M in pure NaOH solutions and in mixed NaOH, $NaNO_3$, and $NaNO_2$ solutions, as long as the hydroxide is at least 4 M. However, the speciation of the solution Pu remains (VI) which might conflict with the concept that the irradiation is reducing the Pu valence state. For similar tests where the Pu stock solution was initially Pu(IV), the end speciation showed some transformation to

Pu(VI) when NaOH solutions were used solely. The higher the free hydroxide, the more soluble Pu converted to Pu(VI) in both the control and irradiated samples. No speciation work was performed in the presence of other salts, such as nitrite, nitrate, sulfate, carbonate and the myriad other components in actual tank waste.

The Karraker results might appear to conflict somewhat with the Russian results (Pikaev 1996), dependent upon interpretation of the reason why the Pu valence state remaining in solution remains (VI) but the overall concentration drops. None of the work available considers the impacts of beta and alpha radiolysis, which exhibit different abilities to create radiolysis reactants, and the enormous number of reactions that may form other reactive species or, conversely, rapidly consume radiolysis species. It is impossible to quantify the impacts of radiolysis on Pu chemistry in the tanks. However, none of the observed Pu solution concentrations in the tests discussed exceed 0.13 g/l, which is 20 times below the Pu concentration of concern to criticality.

No other radiolysis experimental data was found that is relevant for the highly alkaline and ionic strength solutions that are typical of Hanford Site HLW supernatants which also typically contain reductive NO_2^- anion. One other general review of radiation effects on solution chemistry was found (Serne 1989) that also suggests the issue is far from being understood. Although specific radiolysis data for actual tank solutions do not exist, several cited references and Delegard's solubility data (1995) indicate that the radiolysis effects on Pu in Hanford site HLW solutions maintain reducing conditions relative to Pu aqueous chemistry.

2.2 Solubility

The concept of solubility/precipitation is well-established from first principles. The concept often is used in bounding fate and transport analyses to estimate the distribution of actinides between the solution phase and the solid phase. For discussions and examples of why/how solubility is a valuable construct for addressing fate of plutonium and other radionuclides, see Nitsche (1991), Pennders et al. (1985), Pryke (1985), Pryke and Rees (1986), Rai and Ryan (1984), and Rees (1985). Solubility constructs for pure or solid solution phases give an upper bound on the concentrations that are expected in a mobile solution phase in equilibrium with solids; any coincident adsorption-desorption reactions should only cause lower amounts of the contaminant to be found in solution.

2.2.1 Precipitation of Plutonium Hydroxide Phase

In its simplest form, solubility calculations require identification of the solubility-controlling solid and the predominant aqueous species that forms when the controlling solid dissolves. If several aqueous species contribute significantly to the overall solution concentration, their forms and stabilities also must be identified. The thermodynamic solubility product or constant, K_{sp}, and the stability constant(s), K_i, that describe(s) the formation of the predominant aqueous species can then be used to calculate the total solution concentration that should be present in the system of interest. This method is true for the example inside a particular Hanford Site tank. Literature is available that supports the choice of a partially crystalline Pu(IV) oxide described as $PuO_2 \cdot xH_2O$ as the solubility-controlling solid in the

chemical environments inside a Hanford Site tank. Key references where efforts were made to directly determine the nature of the plutonium solid are Rai et al. (1980), Delegard (1987), Yamaguchi et al. (1994), and Carteret (1996)[a]. Other references that provide empirical data on observed plutonium solution concentrations in chemical environments similar to those inside a Hanford Site tank, but do not attempt to directly determine which solid phase is present, include Hobbs et al.(1993), Hobbs and Edwards (1993), Hobbs (1995), Delegard et al.(1984), Delegard and Gallagher (1983), and Delegard (1995). However, in a recent study involving waste supernatants, Hobbs and Karraker[b] identified $PuO_2 \cdot xH_2O$ in the precipitated phase. The solubility data from Yamaguchi et al. (1994), Delegard (1995), Hobbs et al. (1993), and Hobbs (1995), plotted as a function of total carbonate concentration in Figure 2.5, show that in all these experiments, $PuO_2 \cdot xH_2O$ was most likely the solubility-controlling solid phase.

Some of the experiments conducted by Hobbs and his coworkers involved aluminum and iron. Plutonium and uranium were found to coprecipitate with the aluminum and iron. Hobbs and Karraker[a] believe that such phenomena are probably $PuO_2 \cdot xH_2O$ colloids coagulated by aluminum and iron hydroxides, rather than the formation of true solid solution phases. It is important to remember that coagulation is a proven chemical process used in water treatment plants to remove colloidal suspended impurities (Clark 1990). Solids resulting from coagulation differ from solid solution phases in two distinct ways. First, in a coagulated mass, pure phase colloids are enclosed in the major phases (consisting of distinct gel phases), whereas, solid solutions are constituted of ions of comparable ionic radii substituting in a single solid phase. Second, in a coagulated solid mass, the solubility of ions is controlled by each distinct relatively pure solid phase. Solid solutions control the solubility of all constituent ions in the discrete phase by the dissolution of the single solid solution phase. The plutonium solubility data, which agrees with the solubility of relatively pure phase $PuO_2 \cdot xH_2O$ (Figure 2.5), suggests the precipitation of plutonium observed in Hobbs' experiments was more likely the result of coagulation, rather than true solid solution formation with Al and Fe hydroxides.

Identification of the predominant aqueous solution species expected in Hanford Site tanks is less certain, but likely candidates are $Pu(OH)_2(C0_3)_2^{2-}$ when the free hydroxide content is low (<0.01 M or ~pH≤10) and total carbonate is ≥0.1 M (see Section 2.1). At pH values of 12 to 13 and total inorganic carbon of ≥0.1 M, where carbonate is the predominant inorganic carbon species, the proposed soluble complex is $Pu(OH)_4(C0_3)_2^{4-}$ (see Section 2.1).

This selection of $Pu(OH)_4(CO_3)_2^{4-}$ is supported by data presented in Yamaguchi et al. (1994); Delegard (1995), where data in Delegard (1987) are reinterpreted; and Tait et al. (1995). The literature contains numerous articles for less alkaline, lower pH, and lower salinity waters common in lakes, rivers, and oceans that suggest the predominant aqueous species should be Pu(V) species. However, these reports are unconvincing, given the highly sensitive nature of speciation to key variables (such as pH, Eh) and the concentration of dissolved ligands, such as carbonate.

(a) *Trip Report: Russian Retrieval Technical Exchange* (unpublished). Westinghouse Handord Company, Richland, Washington.
(b) Personal communication, July 1996.

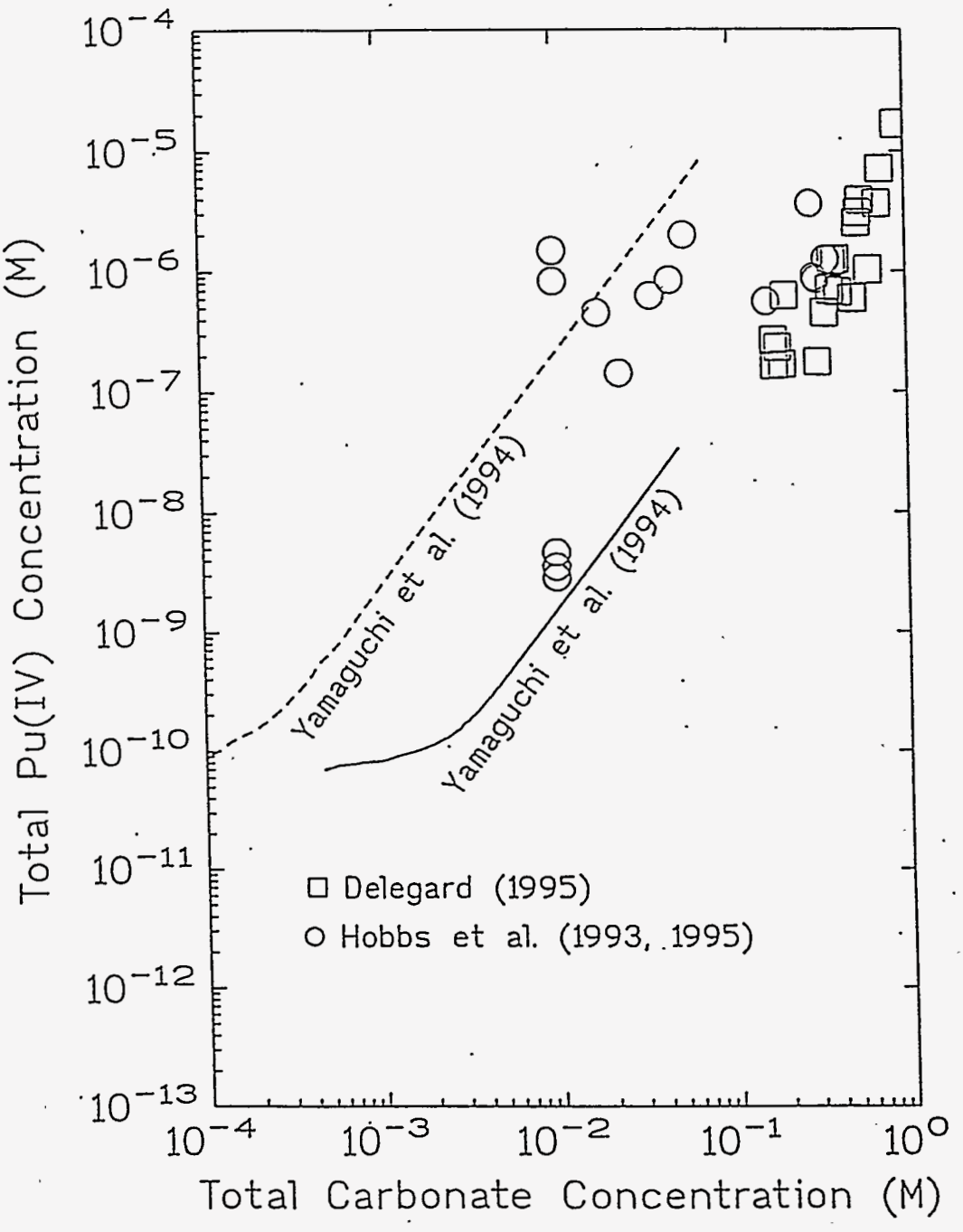

Figure 2.5. Experimental Data for Solubility of $PuO_2 \cdot xH_2O$ as a Function of pH and Total Carbonate Concentration

Waste stream data from the Hanford Site (Agnew 1995, 1996) indicate the wastes were probably oversaturated with respect to $PuO_2 \cdot xH_2O$ (Figure 2.6). The degree of oversaturation of each waste stream can be more accurately evaluated using a chemical equilibrium code, such as GMIN (see Felmy 1995)or Environmental Simulation Program (ESP v5.0) developed by OLI Systems Inc. Given the $PuO_2 \cdot xH_2O$ as the solubility-controlling solid and the choice of either $Pu(OH)_2(C0_3)_2^{2-}$ or $Pu(OH)_4(C0_3)_2^{4-}$ as the dominant aqueous species, depending on pH in the presence of at least 0.1 M total carbonate, the total plutonium solution concentration in Hanford Site tanks can be predicted. Expected plutonium solution concentrations for high pH tanks should be $\sim 10^{-7}$ M (0.025 ppm) at carbonate concentrations of ≥ 0.1, but ≤ 1.0 M as long as pH >12 and $\sim 10^{-5}$ M (2.5 ppm) at carbonate concentrations of ≥ 1.0 M (as long as pH >12). However, if pH is 10 or less, these plutonium solution values would increase by ~300 for tanks with high carbonate, but little free hydroxide.

Based on studies by Rai and Ryan (1984), Delegard (1987), and Kim and Kanellakopulos (1989). The assumption is the $PuO_2 \cdot xH_2O$ in waste tanks is aging toward a more stable and partly crystalline phase. If this assumption is so, the expected solution concentrations will be at least an order of magnitude less than the concentrations supported by freshly precipitated $PuO_2 \cdot xH_2O$, as shown in Figure 2.5. The cited laboratory studies by Hobbs and coworkers (the open circles in Figure 2.5) and Delegard (the open squares) corroborate the simple solubility estimates (the dashed and solid lines). Characterization data for supernatants and drainable solutions from Hanford Site waste tanks (Van Vleet 1993a,b; Sederburg 1994, listed in Table 2.5) plot near or slightly below the lines, depending on specific tank carbonate and free hydroxide concentration (Figure 2.7). This relationship suggests the plutonium-controlling solid is most likely $PuO_2 \cdot xH_2O$ or a less soluble, more crystalline (aged) $PuO_2 \cdot xH_2O$. Plutonium solution concentrations in the range of 0.1 to 100 ppm, represented by the solubility considerations, are thousands to about 30 times lower than the values needed to allow nuclear criticality to occur in solution. Bratzel et al. (1996) and Waltar et al. (1996) present additional discussion on the plutonium concentrations necessary to reach criticality. Therefore, criticality is implausible in tank supernate solutions.

Because of changes in ionic strength, the presence of other common inorganic ligands, such as nitrate, nitrite, aluminate, sulfate, and phosphate are not expected to have any significant influence. The general impact of total dissolved salts (that is, ionic strength) on thermodynamic activity and solubility also is not expected to change these estimates significantly. The key variables that control the solubility of plutonium in Hanford Site tanks are free hydroxide and carbonate content.

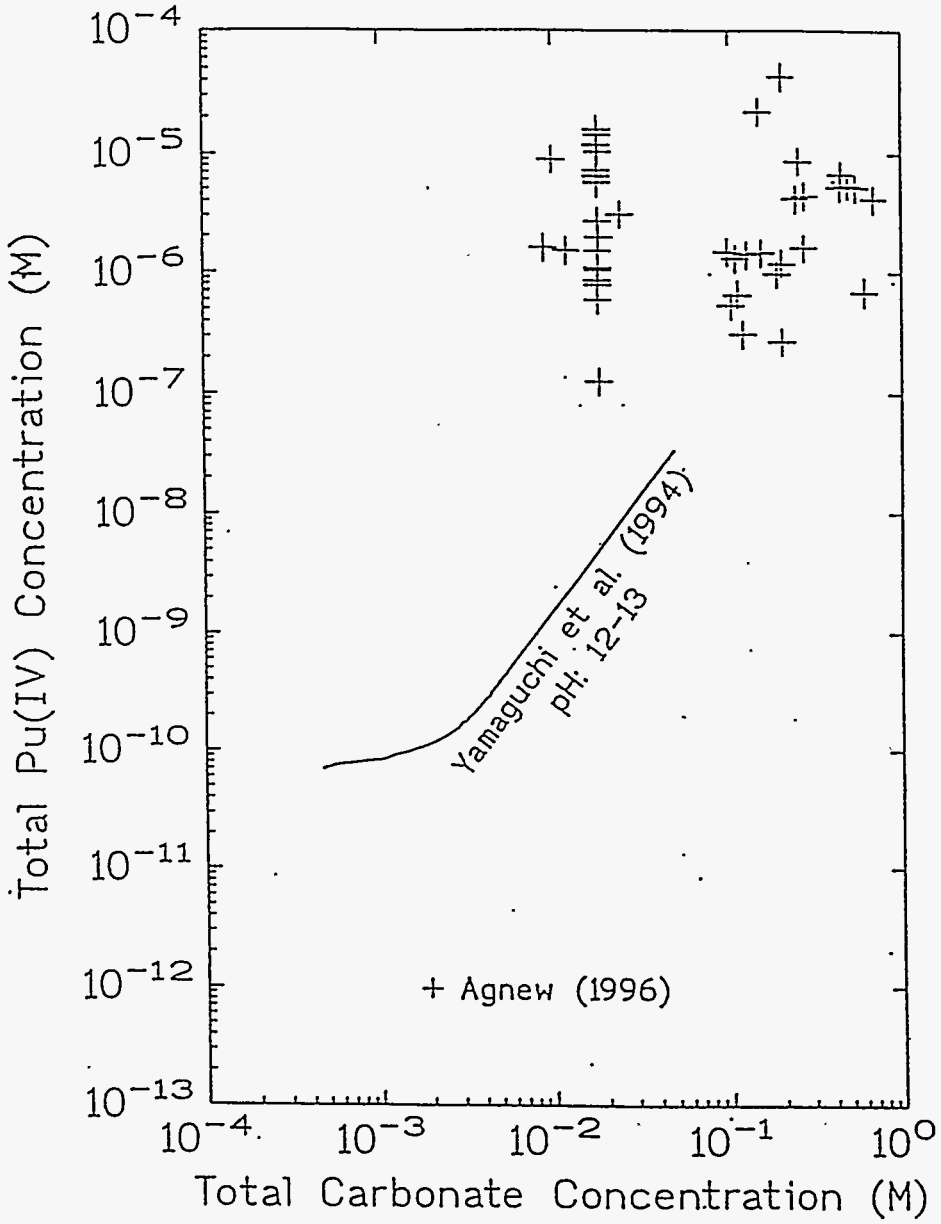

Figure 2.6. Hanford Waste Stream Data Compared with the Experimental Equilibrium Solubility of $PuO_2 \cdot xH_2O$

Table 2.5. Total Dissolved Plutonium, Carbonate, and Hydroxyl

Tank No.	Pu	CO_3	OH	Tank No.	Pu	CO_3	OH
	Total Concentration				Total Concentration		
AX-101	5.18	0.66	-0.45	SX-104	7.32	0.66	-0.30
AX-103	11.6	-0.04	-0.39	T-102	7.78	0.75	0.32
B-102	6.84	1.08	1.29	T-103	7.35	0.61	0.34
B-103	7.11	0.75	0.88	T-107	6.09	0.43	1.60
B-106	6.23	0.88	1.51	T-108	6.35	0.10	0.03
B-109	7.91	3.50	-0.11	T-109	6.71	0.27	0.42
BX-106	8.05	0.03	-0.32	T-112	6.90	1.08	0.31
BX-107	5.54	0.56	0.96	T-204	5.29	0.10	0.70
BX-109	7.17	0.45	0.96	TX-103	6.08	0.64	-0.14
BX-110	8.26	0.54	-0.14	TX-104	5.87	0.33	-0.48
BX-111	8.23	0.22	-0.54	TX-107	5.02	0.50	0.64
BX-112	6.11	0.46	1.14	TY-104	6.89	0.18	1.89
C-102	6.40	0.46	0.06	U-106	8.41	1.16	-0.07
C-106	4.83	0.13	0.89	U-202	8.37	0.75	-0.09
C-107	4.50	0.50	0.77	AN-104	6.15	0.55	-0.60
C-110	5.52	0.60	0.31	AN-107	5.22	-0.05	1.30
C-112	7.88	0.28	0.31	AW-105	10.10	1.55	0.49
C-201	3.83	0.41	0.47	AW-106	7.73	0.57	-0.41
C-204	8.31	0.94	1.72	AY-101	6.25	0.51	0.32
S-103	4.20	1.17	-0.07	AY-102	7.80	1.21	0.53

*All data from Van Vleet (1993a, b), except data for waste tanks C-106, and AY-102 are from Sederburg (1994).

2.2.2 Organics Present in Hanford Site Tanks and Their Influence on Solubility and Plutonium Speciation

Measurements have been taken of the total organic carbon content in supernate solution, sludge slurry, and perhaps salt cake for Hanford Site tanks. However, only a few tanks have been studied in enough detail to evaluate the types and amounts of organic components present in supernate and sludge. Data specific to Hanford Site tanks has been found in Campbell et al. (1994a, b, c), Campbell et al. (1995a, b), Lokken et al. (1986), Pool and Bean (1994), Wahl et al. (1995), and WHC (1995a).

Much of the material in these documents describes the development of analytical procedures to measure selected organic compounds in the complex tank waste matrix, a difficult task. To date, the organic analyses attempted have emphasized measuring chelating agents, chelating agent fragments, butyl phosphates, low-molecular-weight water-soluble organic acids, and normal paraffin hydrocarbons (NPH).

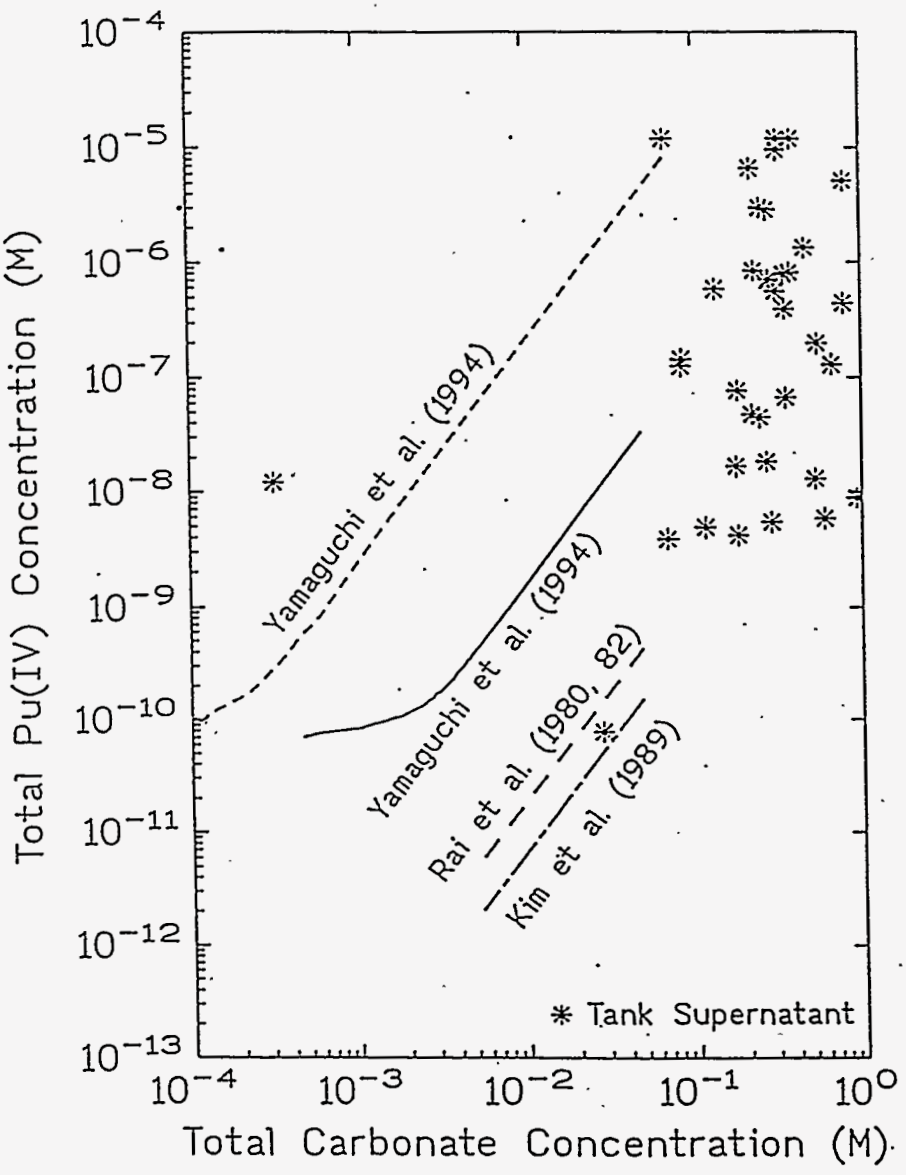

Figure 2.7. Hanford Waste Tank Supernatant Data Compared with the Experimental Solubility and Aged $PuO_2 \cdot xH_2O$ Solids

To evaluate how well the analyses have identified the major organic compounds present in the tank materials, chemists have tried to calculate mass balances by comparing the organic carbon mass in the species identified with the total organic carbon measured in bulk material removed from the tanks. The bulk material consists of supernate solutions and solids, mainly sludge slurries.

Not all organic carbon is identified by all the techniques used to measure total organic carbon. Two commonly used methods to measure total organic carbon in tank materials are as follows:

- Hot persulfate oxidation, which acidifies a tank sample to drive off inorganic carbon. The remaining sample is then oxidized using a silver catalyst, heat, and persulfate to form carbon dioxide gas, which is collected and analyzed. This method assumes the acidification and sparging do not liberate volatile organic material. Long chain organics such as NPH, surfactants, acetone, butanol, benzene, and organic polymers do not react quantitatively using this technique.

- Combustion, where the sample is heated to 600°C in the presence of oxygen gas. The resultant carbon dioxide is measured to quantify the organic carbon content.

Analysts believe that combustion may more accurately measure total organic carbon, but it is not generally used on actual tank samples. The hot persulfate method is favored, so the actual amount of organic carbon in the tanks may be ~0.5 to 2 % by weight higher in tank solids and 0.5 to 1.5 % higher in tank supernate than generally reported. The types of organic carbon that have been found to predominate in aqueous phases in tank samples (chelators, chelator fragments, and low molecular weight organic acids) react quantitatively using the persulfate technique. Therefore, the mass of carbon species identified can be compared with the total organic carbon value to estimate how much organic carbon has not yet been identified.

The results of the mass balance check for the amount of organic carbon identified using detailed speciation techniques versus total organic carbon are improving. The current range is between ~50 and 90 %, with an average of 80 to 90 %. This improvement is mostly because cation exchange techniques are now used to remove radioactive constituents, especially cesium and strontium, from tank samples. After the radioactive constituents are removed, the samples can be transferred from the hot cell to fume hoods for analysis, using techniques specific for extracting organic materials. Performing detailed work in a fume hood, instead of being limited to the crude operations that can be performed in a hot cell, lead to significant improvement in mass balance on organic carbon.

The following sample treatment and detailed organic analysis techniques are currently in use. To create hydrophilic samples, about 2 to 5 g of tank solids are stirred overnight with 10 to 20 mL of distilled water. The solution is filtered through 0.45-μm membranes in a hot cell. Newer procedures are then used to run the solution through a cation-exchange column (10 g of AG50W-X8 resin). This procedure removes cationic radionuclides, so the ion-exchange treated solution can be removed from the hot cell. Using the old methods, work on the radioactive sample continued in the hot cell. The water extract or a subsample is next dried, using nitrogen blowdown techniques. The evaporites are next mixed with BF_3/methanol and heated to 100°C for 1 hour to derivatize the hydrophilic organic species present. After cooling, chloroform is added and the resultant organic solution is added to an aqueous buffer solution of 0.1 M KH_2PO_4. The aqueous and chloroform phases are well-mixed and allowed to separate. The chloroform phase, which contains derivatized organics, is saved for analysis by GC/MS (gas chromatogrphy/mass spectrometry)to identify the organic species that are present and then by

GC/FID (gas chromatography/flame ionization detection) to determine how much of each is present. Using this process to form methyl esters of the organic compounds makes them easier to analyze using GC/MS.

This procedure was used to measure the water-soluble chelating agents, chelating agent fragments, and a few organic acids in the tank solids. Similar procedures were used on tank supernate solution with a one-to-one mix of supernate solution and distilled water. Another subsample of the water leachate (after cation exchange treatment) is run directly by liquid chromatography (LC) or ion chromatography (IC) to quantify the low-molecular-weight organic acids (LMWA). LC/UV techniques were used to measure water-soluble low-molecular-weight organic acids, such as the oxalic, glycolic, formic, succinic, and acetic acids present in the tanks as salts.

A second tank sample (tank solids or discrete organic solution phases) was equilibrated three times with an organic solvent (chloroform or methylene chloride) to leach hydrophobic organics from the tank material. The organic solvent extract was then concentrated by partial evaporation and analyzed by GC/MS to identify the hydrophobic organics, such as NPH, which are long-chained hydrocarbons (C_{12} to C_{15}), and tributyl phosphate (TBP) and its degradation products.

The results of organic speciation measurements on tank samples from DST SY-101 and SY-103 are shown in Tables 2.6 through 2.9. Results for SST C-103 are shown in Tables 2.10 through 2.12. Tables 2.6 through 2.9 suggest the following conclusions for the DST.

- Oxalate, the predominant LMWA, is present at much higher levels in the sludge solids than in the supernate solution. These levels may be caused by the insolubility of many metal oxalates.

- Proportionately more chelators and chelator fragments were found in the supernate solution than in the solids. However, because the solids in the tanks can have higher total organic carbon (TOC), the absolute concentration of chelators in the solids can be as high as or higher than in the supernate solution. EDTA is the predominant chelator present. The NPH content in tank samples analyzed to date is small (less than 7 % of the TOC).

Table 2.6. Organic Content (by Class) in Tank SY-101

Core #	Chelators (mg C/g)	LMWA (mg C/g)	NPH (mg C/g)	Identified (%)
R4258 (solid)	4.7	3.3	1.44	87
R4259 (solid)	3.3	4.5	--	77
R4260 (solid)	4.8	4.4	0.41	91
R4261 (solid)	6.4	2.5	0.67	81
R4262 (solid)	2.2	5.8	0.02	73
R4263 (solid)	3.6	6.8	--	93

Table 2.7. Average Organic Content of SY-101 Core Samples

Constituent (mg C/g)	Drainable Liquid composite segs 2-7	Solids composite segs 10-14
TOC	10.9	11.1
NIDA	1.04	0.82
NTA	0.33	0.22
Citric acid	0.32	0.31
ED3A	0.30	0.28
EDTA	2.23	0.80
HEDTA	-	-
Other fragments	0.61	0.42
Succinic acid	0.07	0.05
Oxalic acid	1.8	5.7
Acetic acid	-	-
Formic acid	1.4	0.62
Glycolic acid	0.54	-
NPH	0.80	0.02
Mass balance on C	79%	83%

Table 2.8. Organic Carbon Analyses for Tank SY-103 Samples

Constituent (mg C/g)	Drainable liquid composite segs 2-7	Solids composite segs 10-14
TOC	6.4	10.5
NIDA	0.2	0.16
NTA	0.14	0.16
Citric acid	0.42	0.56
ED3A	0.25	0.16
EDTA	0.55	0.65
HEDTA	0.03	<0.01
Other fragments	<0.01	0.14
Succinic acid	0.02	0.02
Oxalic acid	-	6.0
Acetic acid	0.6	0.7
Formic acid	1.2	0.9
Glycolic acid	-	tbd
NPH	tbd	tbd
Mass balance on C	53%	90%

Table 2.9. Summary of Organic Types in Tank Samples

Type	Tank SY-101		Tank SY-103	
	Supernate	Solids	Supernate	Solids
chelators	44	26	23.4	18.3
LMWA	35	57	28.1	72.4
NPH	7	4	NA*	NA*
Org. C Mass Bal.	86	87	51.5	90.7
NA* = Not available				

Table 2.10. Organic Compounds and Other Inorganic Species Found in Organic Layer of Tank C-103

Species	Weight %
TBP	47.2
Tridecane (C_{13})	11.4
Tetradecane (C_{14})	6.0
Dodecane (C_{12})	2.8
DBBP	1.9
Pentadecane (C_{15})	0.9
Various branch alkanes	3.5
Water	1.3
Ammonia	<0.003
Water-soluble anions	<0.005
Water-soluble cations	<0.010
Gross Alpha Emmitters	550 (pCi/g)
Plutonium	$2.43 \cdot 10^{-3}$ ppm
Gross Beta Emitters	$1.05 \cdot 10^{+5}$ (pCi/g)
^{90}Sr	$5.5 \cdot 10^{+5}$ (pCi/g)
^{137}Cs	$4.1 \cdot 10^{+4}$ (pCi/g)
Others	$\sim 1.0 \cdot 10^{+3}$ (pCi/g)
Total	75.0

Table 2.11. Analysis of Supernate Solution in Tank C-103

Constituent	Concentration (units are ppm unless specified)
Gross Alpha Emitters	$4.35 \cdot 10^{+4}$ pCi/mL
Gross Beta Emitters	$7.06 \cdot 10^{+7}$ pCi/mL
Cs-137	$5.79 \cdot 10^{+7}$ pCi/mL
Co-60	$5.11 \cdot 10^{+4}$ pCi/mL
Cations	
Ammonia	0.23
Sodium	32,800
U	2100
K	320
Zr	300
Ni	72
Cr	57
Ca	5
Fe	3
Anions	
Nitrite	24,800
Sulfate	3,230
Nitrate	2,590
Phosphate	2,200
Floride	1,200
Chloride	430
Inorganic Carbon	5,175
Organic Carbon	7,200
pH	10
Density	1.078 g/mL @ 25°C
Viscosity	0.015-0.045 poise @ 25°C dependent on shear rate

Table 2.12. Organic Carbon Analyses on Tank C-103 Samples

Sample #	Solids	
	TOC (mg C/g)	Oxalate (mg C/g)
Core 63-Seg. 2(upper)	8.5	2.66
Core 63-Seg. 2(lower)	10.2	--
Core 63-Seg. 3(upper)	7.6	1.94
Core 63-Seg. 3(lower)	8.9	--
Core 63-Seg. 4	4.5	2.32
Core 66-Seg. 3 (upper)	8.9	3.92
Core 66-Seg. 3 (lower)	--	2.96
Core 66-Seg. 4	9.2	2.96
Sample #	Liquids	
Solids	TOC (mg/mL)	Oxalate (mg/mL)
Core 63-Seg. 1	7.71	3.36
Core 63-Seg. 2	7.61	--
Core 63-Seg. 4	--	3.36
Core 66-Seg. 1	--	3.14
Core 66-Seg. 2	--	3.1
Core 66-Seg. 3	--	2.96
Core 66-Seg. 4	--	2.73

In the mid 1980s, Lokken et al. (1985) performed organic analyses on supernate solutions from double-shell tanks AN-107 and AZ-102, which have been categorized as complex concentrate, using a deriving technique similar to the one currently used. The analytes were then measured using GC/MS and GC/FTIR. NTA, HEDTA, EDTA, and citric acid were identified at millimolar concentrations. The mass balance of total organic carbon was only 40 %. Using HPLC techniques, some other classes of organic compounds, such as mono- and di-carboxylic acids, long-chained alkanes ranging from C-23 to C-35, and phthalate esters, were identified. By the end of 1986, the mass balance had been improved to 75 %. The final results for the AN-107 supernate waste solution are shown in Table 2.13. The report also describes organic aging studies performed on simulated complex concentrate for 85 days at room temperature and in the absence of radiation. Even under these mild conditions, chelators (such as EDTA and HEDTA) showed significant degradation (~70 %), NTA showed no degradation, and citric acid showed 18 % degradation. The chelator fragments identified were similar to those found in the actual waste, suggesting that EDTA and HEDTA would exhibit significant degradation in Hanford Site tanks. The degradation products identified accounted for only 41 % of the loss of EDTA and HEDTA, which suggests that other fragments not amenable to GC/MS analysis, such as amines, were likely formed also.

Table 2.13. Organic Species Identified in Tank AN-107 Supernate Solution

Compound	mM	mg C/mL
Chelates/Complexants		
Citric Acid	64.39	4.61
HEDTA	37.53	4.53
EDTA	31.41	3.77
Methane Tricarboxylic Acid*	17.32	1.45
NTA	7.33	0.53
Chelator Fragments	--	--
ED3A	17.91	1.72
HEDDA	2.39	0.26
E_2DTA	2.28	0.23
HEIDA	2.14	0.18
MeEDD'A	1.02	0.08
Others	--	0.14
Carboxylic Acids		
Docos-13en-oic	2.50	0.67
Hexanedioic	2.04	0.15
Hexadecanoic	2.04	0.39
Phthalic	1.10	0.10
Nonanedioic	0.83	0.07
Tetradecanoic	0.68	0.12
Pentanedioic	0.60	0.04
Octadecanoic	0.54	0.11
Hydroxybutanedioic	0.33	0.01
Butanedioic	0.10	0.01
Alkanes		
C-23 to C-35	7.77	2.50
Phthalate Esters		
Dibutylphthalate	1.24	0.23
Dioctylphthalate	0.05	0.01
Total Organic Carbon		44.0
* Identification of this species is now considered erroneous (J. A. Campbell, personal communication 1996).		

The total organic carbon content of the complex concentrate waste liquor in Tank AN-107 is over four times higher than in tanks from the SY tank farm. The citric acid content in AN-107 supernate is about 10 times more concentrated and the HEDTA is at least an order of magnitude more concentrated.

The other chelators are present in about the same concentrations as found in the SY tanks' supernate solution and sludges. Fragments, such as ED3A and IDA are also present in AN-107 at several times higher concentrations than are found in SY tank supernates. The AN-107 supernate contains numerous long-chained carboxylic acids not identified in the SY tanks. Conversely, the SY tank supernate solutions appear to contain shorter chained carboxylic acids. The hydrocarbon content in the AN-107 solution is larger than in the SY samples and appears to contain compounds with longer chains than the NPH identified in SY tanks.

SST C-103 has a distinct organic solution layer floating on top. Some of this material was diluted 10,000 times with methylene chloride and analyzed by GC/MS using the chemical ionization mode to determine molecular weight. High-resolution mass spectrometry also was used to identify the compounds. Table 2.10 lists the organic carbon species results for this organic layer. The relative weight of TBP plus DBBP to NPH is about 2:1. The so-called missing mass in the organic layer was mostly inorganic (perhaps colloidal suspension) matter that was identified by SEM as metal-sulfate salts; alumino-silicate particles; calcium phosphate particles; and iron, chromium, and aluminum hydrous oxide particles.

A sample of Tank C-103 aqueous supernate layer was mixed with equal portions of distilled water and extracted three times with methylene chloride. The organic extracts were then conditioned and evaporated to 1 ml volume and analyzed by GC/MS. The only organics (water-insoluble) found in the liquid phase were TBP at 80 ppm, DBBP at 7ppm, and NPH at ~1 to 3 ppm.

Data on the chemical composition of the aqueous phase (supernate solution) underlying the discrete organic phase in Tank C-103 are shown in Table 2.11. The aqueous phase was measured for inorganic cations, anions, carbon, and radionuclides and for some physical properties, such as viscosity and density. This phase was measured also for the water-insoluble organics just noted and the water-soluble organics mentioned in the next paragraph. Other data currently available on the water-soluble portion of supernate tank solids from Tank C-103 are shown in Table 2.12. The TOC values were determined using the persulfate oxidation method. The oxalate values were determined by ion chromotography. The TOC content of the tank liquids and solids from this SST is slightly lower than for the DST (see Table 2.6), but more oxalate is present in SST liquids than in DST liquids and less oxalate is present in SST solids than in DST solids.

From the small amount of data available, the tank supernate aqueous solutions is estimated to contain up to 3.8 mg of C/g of solution of EDTA, which is the strongest complexing agent for plutonium, iron, and aluminum, as well as most other metals present in the tanks. (See the discussion of complex stability constants in Section 2.1 and Table 2.3 for details.) One mole of EDTA contains 10 carbon moles, so the highest concentration of EDTA measured to date in supernate solution is ~0.04 M. All other identified chelating agents are present at lower concentrations. The highest concentration of LMWA (about 2.0 mg C/ml) found in tank supernate solutions occurs in SST. One mole of oxalic acid contains two carbon atoms, thus the molarity of the supernate solution would be 0.15 M. The SST studied also had an immiscible liquid organic layer, consisting primarily of TBP and degradation products. TBP is a known complexing agent for plutonium. But the analyses for plutonium and other radionuclides in this discrete

organic layer (see Table 2.11) are quite low compared to the aqueous phase. Further, the concentration of plutonium in either the organic liquid or the supernate is much lower than values needed to reach a criticality threshold.

Campbell et al. (1995b) state that Tank C-102 formerly contained a floating organic-solvent layer, but that much of this material was pumped to Tank C-103. Further salt-well pumping reduced the Tank C-102 liquid levels so that no free-standing liquids were present. Based on the data in Table 2.14, NPH are still present in the tank solids, likely as coatings on the solids. An analysis of the headspace in Tank BY-108 suggests it may have contained a discrete organic layer floating on top of aqueous layers before interim stabilization by salt-well pumping. Tank C-103 currently does contain a discrete organic layer that has been verified by sampling (Postma et al. 1994). The solids in Tanks C-102 and C-103 are described as being sludge; the solids in Tank BY-108 are described as salt cake. The solids (see Table 2.15) in the lower part of Tank BY-108 riser 17 and all solids from riser 16 appear to have less TOC and hydrophobic organics than tanks that originally had organic layers, but have sludge instead of salt cake as the solids.

Table 2.14. Organic Species Measured in Tanks C-102 and C-204

Sample Description	Species	Concentration (mg C/g)
C-102 Sludge Sample (drainable liquid minimal)		
Upper part of core	TOC	7.00
	NPH	7.97
	TBP	2.06
Lower part of core	TOC	6.00
	NPH	17.17
	TBP	2.74
C-204 Solids Sample (drainable liquid minimal)		
Auger core sample	TOC	60*
	NPH	trace
	TBP	330*
	DBP	2.5*
	EDTA	ND
	NTA	ND
	HEDTA	ND
	acetic acid	<0.1*
	formic acid	<0.1*
	oxalic acid	<0.1*
* per gram wet weight. Moisture content is ~55%; multiply values by 2.2 to get dry weight ND. Not detected		

Table 2.15. Organic Species Measured in Tank BY-108

Solid Sample (drainable liquid limited)		
Sample Description	Species	Concentration (mg C/g)
Riser 17, upper part of core	TOC	16.6
	NPH	ND
	TBP	ND
Riser 17, lower part of core	TOC	0.5
	NPH	ND
	TBP	ND
Riser 16	TOC	1.2
	NPH	ND
	TBP	ND
ND = Not detected		

Campbell et al. (1995a, b) describe several aging mechanisms that should change the nature and quantity of organics in the discrete organic layers present in some tanks, and likely in aqueous layers (although this is not stated in the reports). The high caustic content of the Hanford Site tanks should result in saponification of TBP to DBP (dibutyl phosphate). Because DBP is much more water-soluble than TBP, it should be extracted from the discrete organic phase into the aqueous fluids. Further, TBP undergoes radiolytic decomposition.

The NPH in the discrete floating organic layers in a few tanks is somewhat volatile under tank heat conditions. NPH decomposes radiolytically to carboxylic acids that are much more water-soluble than NPH. Therefore, the carboxylic acids will migrate toward the aqueous layers and some of the for long-chained acids perhaps precipitate and coat the inorganic sludges. Also, the passive ventilation systems present in some tanks have allowed some NPH to escape from the tank headspace.

The organic ligands present in Hanford Site tanks that could influence plutonium solubility are found at relatively low concentrations, compared to free hydroxide and carbonate. Most ligands are also chemically unstable and are continually being transformed into molecules with even weaker complex-forming capabilities.

Delegard and Gallagher (1983) show in an empirical fashion that relatively high concentrations of chelating agents [HEDTA to 0.1 M, EDTA to 0.05 M, hydroxyacetate to 0.1 M, and citrate to 0.03 M] did not increase the solubility of plutonium in tank environments. Toste et al. (1984, 1987) discuss procedures to analyze for specific chelating/complexing agents in complex waste streams. They also present data on an actual Hanford Site tank waste complex concentrate in which much of the soluble organic materials are identified as degradation products of parent ligands commonly used to extract fission products.

Camaioni et al. (1995) also discuss ongoing work that shows radiation can degrade the complexing agents. Babad[a] says the half-life data for EDTA measured by Camaioni et al. (1995) as a function of gamma dose rate equals about half the EDTA that degrades every 15 years. Presently, the issue of organic constituents is considered insignificant to increasing plutonium solubility. To more quantitatively evaluate this factor, a few speciation calculations could be performed for supernate solutions with the highest concentration of EDTA presently found in tank supernates (~0.04 M).

2.2.3 Effects of Other Parameters on Plutonium Solubility

At present, the possibility of large oxidation-reduction potential (Eh) and pH gradients in the tanks that could significantly affect plutonium are not considered credible. Some tanks (Tanks AN-107 and C-106) may not contain as much free hydroxide as most other tanks, but evidence does not indicate that pH varies dramatically in individual tanks. The Eh in Hanford tanks was purposefully adjusted by adding sodium nitrite to lower the oxidation-reduction potential into a range that should minimize corrosion of the tank walls. The presence of excess nitrite can keep plutonium in the Pu(IV) valence state (Yamaguchi et al. 1994). This statement is consistent with the conclusions and choice of solubility-controlling solids and predominant aqueous plutonium species presented in this report. Eh is difficult to measure and many articles in the literature suggest that complex solutions and slurries with solids often show that some constituents are not in equilibrium with the measured Eh. No evidence suggests that plutonium or iron, a key neutron absorber that is also redox-sensitive, is behaving in unanticipated ways that could suggest that non-equilibrium reactions related to redox are dominant.

The effect of temperature on solubility for the chosen plutonium-controlling solid and predominant aqueous species is difficult to quantify. Sparse empirical data is found on the tank environment and only theoretical estimates are found of the thermodynamic data needed to calculate the effects of temperature, using known chemical constructs that rely on enthalpy and heat-capacity measurements. Using the estimation technique presented by Lemire and Tremaine (1980), the solubility for amorphous Pu(IV) oxide/hydroxide would not be significantly affected by temperatures up to 100°C. Required thermodynamic data for even the simple system, Pu-OH-H_2O, is not precisely known and is essentially nonexistent for complex systems, such as Pu-OH-CO_2-H_2O. Direct experimental observations of temperature effects on plutonium solubility in tank-related solutions are available in Hobbs et al.(1993), where tests at 60°C showed no difference in observed plutonium solution concentrations from tests at room temperature.

The small amount of available literature and calculations that extrapolate from tests involving few chemical components suggest that radiolysis will not have an important effect on plutonium solubility. Alpha decay is much more influential than beta or gamma decay in directly changing the solubility of solids and the tanks do not contain high levels of alpha emitters. Also the large inventory of solids in the tanks can readily buffer the hydrolysis species that form when ionizing radiation reacts with water. Some of the reaction products can change pH and Eh in the absence of large sources of buffering material

---

(a) Personal communication from H. Babad (WHC) to R. J. Serne (PNNL) 1996.

(generally solids). Thus, the first impression is that radiolysis will not be a key parameter in changing the probability of nuclear criticality in Hanford Site tanks during continued inactive storage or active retrieval.

2.2.4 Solid Solution Phases

Plutonium recovery chemistry using the bismuth phosphate process depends on the tendency of plutonium to form solid solutions with bismuth and lanthanum ions. Studies conducted by Grebenshchikova et al. (1967a, b) indicated that Pu(IV) formed solid solutions with lanthanum oxalates. Also, tests by Hodgson et al. (1985) have shown that when Zircalloy cladding removal wastes were treated with sodium hydroxide, transuranic constituents coprecipitated with zirconium hydroxide. As part of the plutonium separation process, data has been accumulated about the formation of plutonium solid solutions. This data (Coleman 1965, Penneman et al. 1988) about known Pu(IV) solid solutions is listed in Table 2.16.

Table 2.16. Solid Solution Compounds Pu(IV)

Compound	Major Component Ions forming Solid Solutions with Pu(IV)					
	Bi (III)	Ce(III)	La(III)	Th(IV)	U(IV)	Zr(IV)
Hydroxide	•	•	•	•	•	•
Phosphate	•				•	•
Oxalate	•		•	•	•	
Iodate		•	•	•		•
Fluoride			•			
Peroxide				•		
Molybdate						•
Tungstate		•		•	•	
Arsenate	•					•
Pyrophosphate				•		
Hypophosphate				•		

Solid solution formation is a subset of coprecipitation phenomena in which two or more ions form a single solid phase. The solubility of a solid solution phase regulates the solution concentrations of each constituent ion at levels that may be significantly different from the solution concentrations of pure solid phases of each of the ions (Walton 1967). Typically, one of the conditions for solid solution formation is the ionic radii of constituent ions should not differ significantly from each other (within 15 to 20 % as cited in Walton 1967). Based on ionic radii data (Shannon 1976), the ionic radii of Pu(IV) were compared with those of other ions in the Hanford Site waste stream to determine which may potentially form solid solution phases with Pu(IV). The data show (Table 2.17) that only bismuth, cerium, lanthanum, thorium, uranium(IV), and zirconium are likely to form true solid solutions with Pu(IV). The Pu(IV) ion is too large to form solid solutions with either aluminum or iron in sixfold coordination.

Therefore, the observed removal of Pu(IV) from suspended colloidal form by aluminum and Fe(III) hydroxide gels is probably a coagulation phenomenon, rather than the formation of thermodynamically definable solid solution phases, which involves removing Pu(IV) from the dissolved aqueous phase and substituting it into structural sites in gel phases.

Table 2.17. Differences in Ionic Radii Between Pu(IV) and Potential Solid Solution Forming Ions in Hanford Site Waste Streams (%)

Ions	Coordination Number*	
	VI	VIII
Bi(III)	-17	-8
Ce (III)	-15	-16
La(III)	-17	-17
Th(IV)	-9	-9
U(IV)	-3	-4
Zr(IV)	+19	+14
Al(III)	+61	--
Fe(III)	+33	--
* Ionic radii data from Shannon (1976).		

Some experimental data confirm the potential formation of Pu(IV) solid solutions in certain Hanford Site waste streams. For instance, bench-scale tests on cladding removal wastes (CRW) conducted by Hodgson et al. (1985) showed that Pu(IV) can coprecipitate with lanthanum as a solid solution. Their data (Figure 2.8) showed the decontamination factor (the ratio of initial plutonium concentration in solution to the plutonium solution concentration in equilibrium with the solid solution phase) ranged from 3 to 61 and was a function of lanthanum concentration. The decontamination factor (DF) of plutonium showed an exponential relationship with lanthanum concentration represented by Equation 2.2.

$$DF = 47.4e^{(219.0X)} - 46.6e^{(98.9X)} + 4108.6X \qquad (2.2)$$

Where X represents the molar concentration of lanthanum.

These data showed the mole fraction of plutonium in the lanthanum solid phase ranged from 2.9×10^{-3} to 3.18×10^{-2}, depending on the amount of lanthanum added to induce the precipitation of solid solution phases. Calculations indicate that, within the range of lanthanum concentrations used in these experiments, the resulting solid solutions would contain lanthanum/plutonium mole ratios from 30 to 349. Hodgson et al. (1985) also indicated that when CRW was neutralized with sodium hydroxide,

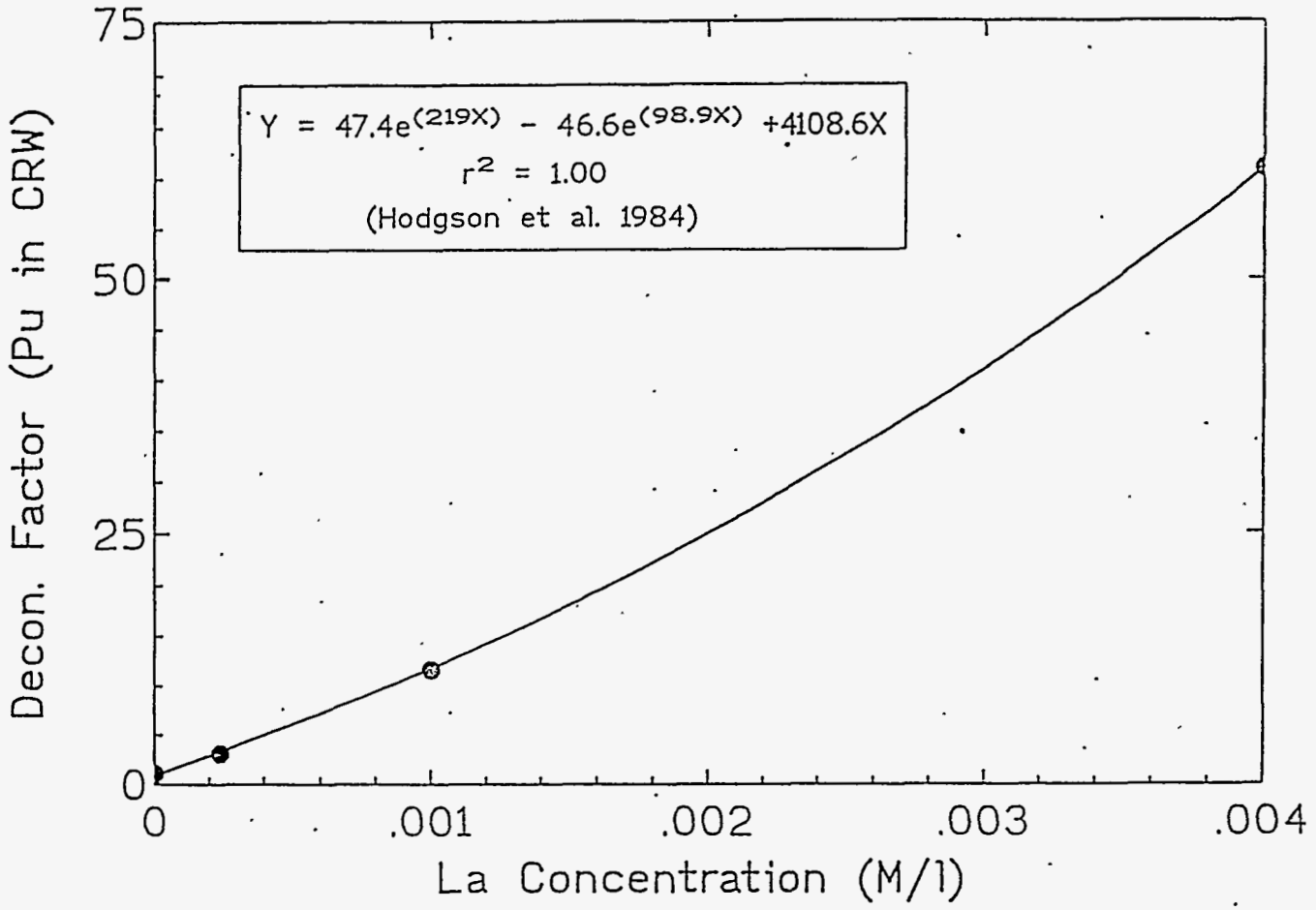

Figure 2.8. Experimental Data for Decontamination Factor of Pu in Cladding Removal Waste as a Function of Added La Concentration

soluble TRU elements were found to precipitate with zirconium hydroxide. The decontamination factors for Pu(IV) coprecipitating as solid solution with zirconium hydroxide were estimated to range from 10 to 100[(a)].

Available data indicate that some of the Hanford site waste streams resulting from the bismuth phosphate process contained Bi, La (used for coprecipitating Pu in $BiPO_4$ and LaF_3 solid phases), and Ce (used as an oxidizer and a carrier precipitant for Ce-144, a fission product). Waste streams containing Th(IV) were generated during the thoria campaigns of 1966 and 1970 (Agnew 1995). Therefore, Hanford waste streams containing constituents such as Bi, Ce, La, and Zr upon neutralization

(a) Personal communication between J. L. Swanson and C. V. Mattigod, Pacific Northwest National Laboratory, June 1996.

may have precipitated as solid solution phases with Pu(IV). Although Hanford site waste streams also contained U, it is unlikely that Pu(IV) would have coprecipitated with U solid phases because uranium in these wastes exist mainly in U(VI) oxidation state (Agnew 1995).

2.2.5 Crystallization and Particle Size of Precipitated Phases

It is possible to estimate the upper size limit that crystalline particles may have and still remain x-ray diffraction amorphous to analysis using standard mineralogy techniques. That is, even crystalline particles will appear to be amorphous (showing no consistent lattice structure) if the average size of the particles is extremely small. Based on discussions in Klug and Alexander (1974), Bish and Post (1989), and Amonette and Zelazny (1994), the estimate of the minimum size for crystallites to be measured by traditional powder X-ray diffraction, as a very broad peak, is 0.003 to 0.004 μm. According to Bartram (1967), crystallites smaller than 0.003 μm do not scatter the primary X-ray beam coherently; they contribute only to the background. Therefore, crystallites smaller than 0.003 μm have only short-range structural ordering and are x-ray amorphous. Peaks are still broad when the crystal size is close to 0.1 μm (Hsu 1977), so care should be taken when reviewing literature to attempt to discern whether the author is calling a mineral completely amorphous based on absolutely no diffraction patterns above a background noise, such as particles below 0.003 to 0.004 μm would give, or the author is calling very broad peaks amorphous. An author with this bent might call such very broad spectra, resulting from particles as large as 0.1 μm, amorphous.

A quantitative equation to estimate the crystallite size is known as the Scherrer equation and is defined as follows (Smith 1989):

$$D = (K \bullet \lambda)/[b \bullet \cos(\Theta)] \qquad (2.3)$$

where D = crystallite size in (Å)
K = a shape constant (usually ~0.9)
λ = the wavelength of the incident X-ray in (Å)
b = the half-width of the diffraction profile due to the sample (measured breadth minus instrumental blank breadth at same wavelength)
Θ = diffraction angle
Å = angstroms (10^{-4} μm).

Equation 2.3 cannot be used to estimate the size of a crystal when the sample gives no peak distinguishable from the instrument background (where b becomes zero), but experts on XRD have used the value of, 0.003 to 0.004 μm, as an estimate.

Thus, if the initial precipitates, formed by the fast neutralization of the Hanford Site acidic waste streams with sodium hydroxide, are actually forming crystalline particles of less than 0.003 to 0.004 μm,the particles would appear as amorphous to the traditional instrumentation (powder X-ray diffraction) used to identify solids with long-range structural ordering.

As described in various articles (Schwertmann and Cornell 1991, Stumm and Morgan 1981, Hsu 1977, and Cornell and Schwertmann 1979), many common oxides (such as aluminum, iron, copper, and zinc) appear to form very small crystallites that are interpreted as being amorphous at first, but grow and become crystalline with time. Schwertmann and Hsu prefer to think that the iron and aluminum crystallites, respectively, were essentially crystalline from the start, but the individual particles were too small to yield measurable x-ray diffraction patterns. These authors are considered by many earth scientists to be the leading experts on the mineralogy and soil chemistry of these two important compounds and several of them endorse their concepts.

Because small particles exhibit very large surface energy (Stumm and Morgan 1981), they are thermodynamically less stable than larger particles of the same mineral. This instability is a driving force for the small particles to agglomerate into more stable larger particles. When the particles reach a size above perhaps 0.003 μm, they start looking crystalline to X-ray diffraction analyzers. In nature and in the laboratory, crystalline ferric oxides and aluminum oxides often are found as discrete particles of 0.1 to 10 μm.

Schwertmann and Cornell (1991) show that pure ferric oxides follow the stated trends and transform into several larger-sized crystalline forms in a few days to a few weeks, depending on the chemical and thermal conditions. Cornell and Schwertmann (1979), Hsu (1977), and others concede that recrystallization to form larger particles can be retarded or inhibited by other dissolved species in the system. Some of the most efficient inhibitors of recrystallization are simple organic acids, such as citrate and, to a much lesser extent, oxalate and fulvic acids from the decay of plant matter. Interestingly, these simple acids become much less effective at pH values of 11 or higher, which is the pH range most common in Hanford Site tanks.

Various mechanisms have been proposed to explain how crystalline growth to larger sizes is inhibited. One process is the adsorption of the organic acids onto either the very small crystals' surfaces or the larger crystals' surfaces that already appear crystalline, blocking further crystal growth. Another process could be the complexation of soluble iron to the extent the system becomes undersaturated in iron and the crystals tend to redissolve to reestablish equilibrium. In some instances the organic acid does not stop crystal growth, but does change the type of ferric oxide that dominates (hematite versus goethite). The explanation for this phenomenon is the organic acid adsorbs onto specific sites on the surface of the iron oxide lattice. The presence of the organic acid blocks further growth (bonding of more ferric and oxide molecules) along that direction of the crystal. Because the difference between ferric oxide minerals often is only the number of molecules that attach to one or another axis in 3-dimensional space, if one axis gets blocked, growth will occur on the other axis, which changes the type of mineral formed.

Hsu (1977) discusses the inhibition/retardation of particle growth for crystalline aluminum hydroxide (gibbsite and bayerite, $Al(OH)_3$) and aluminum oxyhydroxides (boehmite and diaspore, AlOOH). Anions, such as sulfate, phosphate, and silicate, that have a strong affinity for Al^{3+} in solution can tie up the Al^{3+} ions and sterically hinder the growth of the Al-OH polymer units that become these solids after enough of them have aggregated. The organic acids, such as citrate, impede aluminum hydroxide and

oxyhydroxide in the same way as for the iron hydrous oxides (Kwong and Huang 1975). Again, the impact of these other ligands (anions) on the tank solutions is not easily quantified, but some indications are that the high pH, elevated temperatures, and long periods (~30 to 50 years) available for reaction, favor the eventual recrystallization of partly crystalline products. Evidence in the Hanford Site, Savannah River, and Russian literature germane to defense waste tanks indicates that crystalline aluminum and iron hydroxide, oxide, and oxyhydroxide compounds are present (Hobbs 1995, Zakharova and Ermolaev 1995, Carteret[a] 1996). No literature studies have been identified that discuss the particle size or nature of plutonium solids within Hanford Site or other nuclear defense sludges. However, expecting that plutonium would act similarly to metals such as iron and aluminum is logical.

Another interesting phenomenon is the variability of a compound's solubility as a function of particle size. According to Stumm and Morgan (1981), finely divided particles (small crystallites) exhibit higher solubility than large crystals. Consequently, small crystals are thermodynamically less stable and should recrystallize into large ones. For particles smaller than about 1 μm or with a specific surface area greater than a few m^2/g, the surface energy is large enough to influence the surface properties of the particle and the free energy of the solid. Experimenters such as Schindler (1967) and Schindler et al. (1965) investigated the effect of particle size (and surface area of the particle) on the solubilities of ZnO, $Cu(OH)_2$, and CuO. Stumm and Morgan (1981) show the solubility of the various compounds changes, as a function of surface area by a theoretical ratio that relates the change in free energy of the particles to surface tension at the solid-solution interface. For ZnO, the solution concentration of zinc decreases by almost 30 times as the particle size of the ZnO increases from 0.0046 to 0.0560 μm, although these particle sizes are generally smaller than those usually measured for the aluminum and iron oxides. Further, the particle size plays a role in transforming one polymorph to another, such as $Cu(OH)_2$ to CuO or $Zn(OH)_2$ to ZnO. As discussed in Stumm and Morgan (1981), Schindler et al. (1965) describe how copper oxide that is 10 times more stable than copper hydroxide becomes less stable as the particle size decreases until, at a size of 0.004 μm, the CuO is less stable than $Cu(OH)_2$. This situation is because the oxide exhibits a higher surface tension (interfacial energy) than the hydroxide and a cross-over in overall Gibbs free energy (thermodynamic stability) occurs as the particle size decreases for both compounds. The authors and cited experimental investigators suggest this is why copper hydroxide forms first; acid solutions of copper ion are neutralized. This phenomenon may be another mechanism that explains why scientists find or claim that hydroxides form first during the rapid neutralization of acidic solutions, but that, with time, crystalline oxides are found.

As discussed previously, detailed solubility data as a function of particle size (and surface area of the particle) is available for only a few solids, such as ZnO, $Cu(OH)_2$, and CuO. A literature search revealed that similar solubility versus particle size data for $PuO_2 \cdot xH_2O$ is not available. However, it the relationship between solubility and particle size for $PuO_2 \cdot xH_2O$ is assumed similar to that for ZnO and $Zn(OH)_2$, the particle size of fresh and aged $PuO_2 \cdot xH_2O$ can be estimated. The implication of this assumption is the differences in crystal structures of $Zn(OH)_2$ and $PuO_2 \cdot xH_2O$ do not affect the relationship.

(a) *Trip Report: Russian Retrieval Technical Exchange* (unpublished). Westinghouse Handord Company, Richland, Washington.

Because freshly precipitated $PuO_2 \cdot xH_2O$ is x-ray amorphous, the bulk of this material may consist of particles smaller than 0.004 μm. Studies conducted by Andelman and Rozzell (1970) showed the bulk of freshly precipitated $PuO_2 \cdot xH_2O$ exists as colloids that cannot be settled through centrifuging. Studies of long-term aging of $PuO_2 \cdot xH_2O$ by Rai et al. (1980) and Delegard (1987) showed decreases in solubility, which indicates that particle growth occurred, along with a concomitant increase in crystallinity (long-range structural ordering). Furthur, X-ray diffraction data obtained on aged (over 3 years) $PuO_2 \cdot xH_2O$ precipitates showed the precipitate had crystallized, resulting in particle growth and decreased solubility (Rai et al. 1980).

Therefore, assuming the solubility-particle size relationship for zinc hydroxide precipitates observed by Schindler (1967) applies to $PuO_2 \cdot xH_2O$ precipitates, and using the data for equilibrium solubilities of fresh and aged precipitates from Rai et al. (1980) and Delegard (1987), we can calculate the following relationship can be calculated for the average diameter of the smallest particle sizes that control plutonium solubility.

$$d \text{ (Angstroms)} = 2740 \exp (3 \times \Delta \log K_{sp}) + 35 \qquad (2.4)$$

Where d = particle diameter of plutonium oxide in angstroms

$\Delta \log K_{sp}$ = the difference in equilibrium solubility between the crystalline phase and a phase with lower crystallinity.

The solubility data obtained by Rai et al. (1980) indicated the solubilities between freshly precipitated and aged $PuO_2 \cdot xH_2O$ differed by about two orders of magnitude. Using this assumption, the smallest particles in aged $PuO_2 \cdot xH_2O$ material have an average diameter of about 0.3 μm. This calculation provides the smallest particle size that controls the solubility. The largest particle size can be estimated based on the particle-size distribution data obtained by Andelman and Rozell (1970). This data showed the upper bound is approximately an order of magnitude higher than the smallest particle size in the plutonium-hydroxide colloidal mass. From this, aged Pu(IV) oxyhydroxide is estimated as about 60 % of the particles by mass less than 2 μm in size. About 40 % of the mass of aged particles may range from about 2 to 8 μm in size. As shown by Andelman and Rozell (1970), ionic strength, presence of ligands, and other particulates will affect the particle size distribution of $PuO_2 \cdot xH_2O$.

In summary, the particle sizes of precipitates in the Hanford Site tank sludge should be the same as those assessed from literature data. Some of the chemists on the review team believe that all the metals present in the acid waste stream that form insoluble hydroxide-like phases, and probably those that form insoluble phosphate, sulfate, or carbonate compounds, follow a similar path. First, particles that range from less than nanometer (<0.001 μm) to 0.004 μm form, but have fixed chemical structures. Over time, these crystallites grow, driven by the thermodynamic need to shed excess surface energy, eventually reaching a threshold size that is identified as crystalline using traditional techniques, such as powder X-ray diffraction. Their size at this point is somewhere larger than 0.003 μm, depending on the criteria used for defining the X-ray diffraction peaks as sharp enough to qualify as crystalline. Crystalline compounds of these metal oxides/hydroxides formed in the laboratory or isolated from natural soils/sediments often range in size from 0.1 to 10 μm.

This crystal growth process has been recognized for at least a century. In early literature, it is referred to as Ostwald Ripening. A succinct definition of Ostwald Ripening is the process wherein small crystals, which are more soluble than large ones, dissolve and reprecipitate onto larger particles.

The concept of solubility/precipitation is more well-developed from first principles than is adsorption/desorption and is often used in bounding fate and transport analyses to estimate the distribution of contaminants between the solution and solid phases. Solubility constructs give an upper bound on the concentrations expected to be in a mobile solution phase in equilibrium with solids; any coincident adsorption-desorption reactions should only cause lower amounts of the contaminant to be found in solution. Because adsorption processes are less well understood and quantifiable than solubility, a complete review takes longer and can lead to less definitive results. Section 2.3 summarizes the findings on plutonium adsorption in tank-like environments.

2.3 Adsorption

Adsorption reactions are less well quantified than solubility reactions and generally lead to even lower concentrations of such materials as plutonium in solution. Most of the waste streams disposed of in tanks were acid liquids bearing high concentrations of dissolved metals such as aluminum, iron, chromium, manganese, bismuth, zirconium, and uranium, and low concentrations of plutonium that were neutralized with NaOH, and sometimes carbonate-bearing solids. The rapid neutralization of acidic metal-bearing solutions with caustic leads to the precipitation of large amounts of oxyhydroxide solids (sludge).

Such neutralization not only precipitated the bulk of the metals in the waste, but coprecipitated or adsorbed various trace metals, such as plutonium, associated with reprocessing or waste management. Such sludge materials were allowed to settle in cascaded single-shell waste tanks. The essentially radionuclide-free supernate was then released to soil columns in a variety of engineered structures. Most reprocessing and product purification operations either used iron-containing reagents in sufficient quantities to moderate any fissile materials present or added iron-containing reagents during waste neutralization steps. Thus, the adsorption literature review focussed on adsorption/coprecipitation of plutonium onto iron and aluminum and, to a much lesser extent, oxides of manganese and chromium.

The same parameters that affect solubility were investigated:

1. Hydrolysis—pH effects
2. Soluble inorganic and organic complexation
3. Radiolysis
4. Redox
5. Ionic strength
6. Temperature effects on parameters 1 through 5
7. Time (aging, recrystallization).

2.3.1 Introduction

Adsorption is the process of net accumulation of ionic or molecular species at the interface between a solid phase and an aqueous phase. Adsorption differs from precipitation in that adsorption is a 2-dimensional process and precipitation connotes a 3-dimensional process of solid growth (Corey 1981). Although both these phenomena basically involve mass transfer of ionic and molecular species from aqueous phase to solid phase, the fundamental molecular processes differ significantly. Thus, data from any experiment that relies solely on monitoring mass transfer between liquid and solid phases, without measuring other important factors, cannot be used to distinguish between adsorption and precipitation.

The fact that mass transfer data fits any one of several adsorption isotherms does not confirm that adsorption is the controlling phenomenon. Extensive discussions about distinguishing between the 2- and 3-dimensional mass transfer processes (adsorption and precipitation) have been provided by Corey (1981) and Sposito (1986). The difficulty in distinguishing between these two processes based on insufficient or inadequate data led Sposito (1986) to formulate the following two rules:

- The adherence of experimental sorption data to an adsorption isotherm equation provides no evidence the actual mechanism occurring is an adsorption process.

- The experimental observation that an ion-activity product is smaller than a corresponding solubility product constant provides no evidence the principal mass transfer mechanism is adsorption.

The first rule is based on the fact that both adsorption and precipitation data can be fitted with well-known isotherms. Data fit to an isotherm cannot be used as unequivocal proof the principal process is adsorption. The second rule is based on formation of solid solutions, possibly resulting in measured solubility products that are less than solubility products for pure precipitates. Another mechanism that can be misinterpreted as adsorption is the coagulation of pure-phase colloids by solid-phase substrates. This mechanism is especially true for the case of tri- and tetravalent cations such as lanthanides and actinides (Kinniburgh and Jackson 1981). These ions undergo strong hydrolysis resulting in precipitation of colloidal hydroxides (Kepak 1971). These radiocolloids are hard to detect in the presence of a large amount of another solid. Their coagulation and settling with the other solids may lead to misinterpreting the observed reaction as true adsorption.

Following a detailed discussion of adsorption versus precipitation phenomena, Corey (1981) set forth the following six conditions that help in interpreting and judging the validity of existing adsorption data. These conditions also help in guiding investigators in designing appropriate adsorption experiments.

1. Even though bonding mechanisms are similar, specific adsorption is a 2-dimensional phenomenon, whereas precipitation is a 3-dimensional process.

2. Ions specifically adsorbed on substrates form solid solutions that are similar to solid solutions that form from the conventional precipitation process.

3. Relatively small deviations from theoretical concentrations may occur for precipitated solids at solubility equilibrium because particle sizes differ, polymorphic forms are present, or solid solutions form.

4. Concentrations of ions that are minor constituents in natural systems are usually controlled by either solid-solution equilibria or adsorption reactions.

5. Heterogeneous nucleation of a new solid phase, involving adsorbed ions, occurs only when a critical supersaturation is exceeded. Below critical supersaturation, ideal adsorption reactions may prevail.

6. Interpretations of many adsorption reactions are suspect because they are carried out in systems supersaturated with respect to potential new solid phases involving the ion of interest.

A review of adsorption and related processes led Davis and Hayes (1986) to conclude that interfacial reactions at solid surfaces, such as adsorption, ion exchange, and precipitation, are interrelated and detailed studies are needed to identify the dominant mechanism.

During the last two decades, a class of adsorption models, based on electrostatic interactions between adsorbates and sorbent surfaces, has increasingly been used in interpreting experimental data. Detailed descriptions and comparisons of these models have been provided by Westall and Hohl (1980), Benjamin and Leckie (1981), Morel et al. (1981), Barrow and Bowden (1987), and Davis and Kent (1990). These models provide molecular-level interpretation of adsorption phenomena compared to non-electrostatic models (isotherm models). However, the fact these models can be applied to experimental data does not prove that adsorption is the controlling phenomenon in such experiments. Application of Corey's validity criteria and direct determination of species on solid surfaces via various spectroscopic techniques is also necessary to establish that adsorption is the dominant process in the system being investigated (Sposito 1986).

2.3.2 Adsorption Substrates in Waste Tank Environment

The HLW generated during the plutonium separation process was rapidly neutralized (caustic strike) before storage in waste tanks. Experimental data from literature indicate that such rapid neutralization of acidic solutions containing iron and aluminum causes the formation of microcrystalline/x-ray amorphous ferric hydroxide (ferrihydrite) and aluminum hydroxide precipitates. Hanford Site HLW compositions indicate these two solids form major adsorption substrates for plutonium in tank sludges. When no complexing ligands are present (such as dissolved carbonate), freshly precipitated iron and aluminum hydroxide exhibit large surface areas and are capable of adsorbing large amounts of dissolved cationic species. Such high cationic adsorption capacities are caused by the large number of negatively charged adsorption sites these substrates contain as a consequence of deprotonation of surface hydroxyl groups. Increasing the solution hydroxyl concentration (increasing pH) results in increasing deprotonation of surface hydroxyl groups. The cation adsorption capacities of these substrates increase as a function of increasing pH.

Most of the high-level radioactive waste solutions generated from chemical operations at the Hanford Site were acidic solutions containing metals dissolved in nitric acid. Concentrations of dissolved plutonium (typically $<10^{-5}$ M plutonium) that were not recovered in processing were also present in these waste solutions. Before sending the waste to underground tanks, the acid was neutralized with excess sodium hydroxide (containing unknown concentrations of sodium carbonate) to prevent corrosion of the carbon steel tanks. Metals, including plutonium, that were insoluble in basic solutions were precipitated as oxyhydroxides during neutralization. These oxyhydroxides are the major components of sludge in the tanks.

Concentrations of plutonium were very small, compared to the other metals from the processing operations that were dissolved in the waste solutions (Braun et al. 1994). Typical mole ratios of iron/plutonium and aluminum/plutonium in the Hanford Site waste streams were 12,000 and 28,000, respectively, for bismuth phosphate waste; 1,400 and 132,000, respectively, for REDOX waste; 63,000 and 1,400,000, respectively, for PUREX aluminum-clad waste; 3,300 and 13,000, respectively, for PUREX Zirflex waste; and 100 and 7400 respectively for plutonium finishing wastes. These ratios do not include iron added to the waste as a criticality control. In addition to iron and aluminum, other dissolved metals, such as uranium, zirconium, manganese, bismuth, chromium, nickel, and tin, were present in the acid waste and were precipitated as oxyhydroxides.

For example, the waste composition in Tank C-106 (Sederburg 1994) consists mainly of sludge solids (746,000 L) and liquid supernate solution (182,000 L). The tank received tributyl phosphate waste from the uranium recovery process from 1954 to 1963, neutralized PUREX acid waste from 1958 to 1963, aluminum cladding waste from 1958 to 1963, PUREX organic wash waste from 1969 to 1974, and B Plant complexed waste from 1974 to 1978. These wastes resulted in a sludge with high concentrations of iron, aluminum, silicon, and phosphate. The iron/plutonium and aluminum/plutonium mole ratios are about 4500 and 5800 in the sludge. The supernate solution has high concentrations of sodium (4.0 M), nitrate (1.1 M), and carbonate (0.75 M). The plutonium concentration in the supernate is 0.0035 g/L (1.5×10^{-5} M).

In a nitric acid solution containing Pu(IV) as the only dissolved hydrolyzable metal ion, neutralization with sodium hydroxide, as required for waste solutions sent to the tanks, would produce plutonium polymer along with plutonium hydroxide. However, because of the low solubility of iron and aluminum hydroxides and their much higher initial concentrations in the waste solution, these compounds may precipitate first as the waste is neutralized and plutonium may be coprecipitated with them. A comparison of solubilities (with only dissolved hydrolytic species—no other complexants present) of crystalline $PuO_2 \cdot xH_2O$ (Allard 1982 and Rai et al. 1980), amorphous $Fe(OH)_3$ (Lindsay 1979), and crystalline $Al(OH)_3$ (gibbsite) (Lindsay 1979) suggests this possibility. Assuming no significant kinetic differences, iron may precipitate before any plutonium can precipitate as plutonium oxyhydroxide during the waste neutralization process. Thus, the iron hydroxide sludge would be present and capable of adsorbing the plutonium from the solution before it could form its own precipitate. However, no experimental data derived under waste tank conditions exists to corroborate this hypothesis.

Amorphous iron is slightly less soluble than crystalline plutonium hydroxide and much less soluble than amorphous plutonium hydroxide. Because the waste contains thousands of times more iron and aluminum than plutonium, the possibility exists that a pure plutonium phase (plutonium hydroxide or polymer) may not form. Rather, the plutonium may be adsorbed on the iron and aluminum hydroxides that may precipitate first in much larger quantities.

Typical concentrations of plutonium in the acid wastes range from 10^{-5} to 10^{-6} M in the acid wastes. At these low concentrations, incipient polymerization of plutonium hydroxide may require a relatively high pH. Also, polymerization is not instantaneous, but requires an induction period before it is formed (Toth et al. 1981). Although polymer formation is unlikely, any polymer that is formed has a strong affinity to adhere to other particles suspended in solution or on nearby surfaces (Dran et al. 1994).

Several likely coprecipitation mechanisms are important. First, sorption of plutonium hydroxide on the large surface areas of the solid metal oxyhydroxides is the most important mechanism. The sorption capacity (in terms of available sorption sites) for iron oxyhydroxide gel has been estimated to be about 500 μmoles/mmole iron (Kinniburgh and Jackson 1981). This capacity greatly exceeds the molar ratios of plutonium/iron in the waste tank sludges, which range from about 0.016 to 10 μmole plutonium/mmole of iron.

The hydrolysis of metal ions has been studied extensively (Baes and Mesmer 1976). As these hydrolysis reactions occur, a tendency has been shown for the ions to aggregate through hydroxyl bridging, forming dimers, trimers, or extensive polymeric networks that can reach colloid dimensions. These polymers can then condense with the loss of water to form oxygen-bridged polymeric species (Thiyagarajan et al. 1990). The polymers can contain more than one metal hydroxide (those of other metal ions present in the initial solution mixtures) bonded to the polymer. For example, if U(VI) is present during $PuO_2 \cdot xH_2O$ and $Th(OH)_4$ polymerization, the U(VI) is bonded through hydroxyl bridges to the polymer (Toth et al. 1981, 1984). Hydroxyl bridge bonding is similar to that proposed for surface complexation models of sorption of hydrolyzable metal ions on oxide surfaces (Schindler 1981 and Davis et al. 1978). Surface complexation models have been successfully used to predict sorption of uranyl ions onto amorphous iron oxyhydroxide, goethite, and hematite solids (Hsi and Langmuir 1985). Structures of uranyl (VI) complexes at the surface of clay minerals have been identified by Chisholm-Brause et al. (1994). These studies suggest the trace levels of $PuO_2 \cdot xH_2O$ formed during neutralization of acidic wastes may be bonded to other oxyhydroxides present in much greater abundance in the sludge waste.

These observations indicate that sorption may be one of the mechanisms for removing plutonium from solution. However, because none of the experimental observations were conducted under precisely the conditions existing in Hanford Site waste tanks, some extrapolation is needed to determine that adsorption is the dominant mechanism.

Several changes take place as the precipitated substrates begin to age in the supernatant waste solution. One of these changes is the microcrystalline particles growing into larger crystalline particles that produce distinctive x-ray diffraction patterns. Experimental data shows that, with aging under very

high pH conditions, ferric hydroxide precipitate converts to a well-crystallized oxyhydroxy mineral, goethite (FeOOH) and, with continued aging, to a crystalline oxide phase, hematite (Fe_2O_3). Similarly, the aluminum hydroxide precipitate converts first to a more crystalline gibbsite and, with continued aging, to an oxyhydroxy phase known as boehmite (AlOOH).

The second change, that occurs as the precipitated substrates age to more crystalline phases, is the cation adsorption capacity of the substrates with higher crystallinity is reduced. These materials with larger size crystallites contain smaller surface areas, and so have fewer ionizable surface hydroxyl sites. Goethite, hematite, and boehmite types of phases have been identified in some of the HLW sludges from the Hanford Site and Russia (Liu et al. 1995; Zakharova and Ermolaev 1995). However, data does not exist regarding the rate of crystallization of fresh precipitates when aged under very high ionic strengths, higher temperatures, and in the presence of high concentrations of both inorganic and organic ligands—conditions typically encountered in tanks containing HLW. Therefore, estimating the relative proportions of different crystalline phases that currently exist in the waste tank sludges is difficult. Hanford site HLW sludge data (Appendix F) indicate that major waste constituents (Al and Fe)not only exist as pure phase hydroxides and oxyhydroxides but also as solid solution hydroxides, oxyhydroxides, silicates and phosphates. Therefore, it appears the HLW sludge chemistry is much more complex than hypothesized precipitation of mainly hydroxide phases upon neutralization.

2.3.3 Tetravalent Plutonium Adsorption on Iron and Aluminum Oxide/Hydroxide Substrates

Empirical data does not exist regarding adsorption of Pu(IV) species on iron- and aluminum-oxide/hydroxide substrates under typical HLW tank conditions (very high ionic strengths, higher temperatures, and high concentrations of both inorganic and organic ligands). However, a number of investigators have examined potential adsorption of plutonium on minerals, soils, and other geological substrates. Experiments conducted by Ticknor (1993) showed that plutonium sorbed on goethite and hematite from slightly basic solutions [(pH: 7.5) containing high dissolved salts, but extremely low bicarbonate concentrations (8.2×10^{-6} to 2.9×10^{-4} M)] with affinities reflected by distribution coefficients, K_d, ranging from 170 to 1400 mL/g.

According to Pius et al. (1995), significant removal of Pu(IV) from solutions containing 0.1 to 1 M concentrations of sodium carbonate was observed with alumina, silica gel, and hydrous titanium oxide as substrates. These investigators also noted the presence of carbonate lowered the sorption distribution coefficient for these adsorbents. However, even at 0.5 M carbonate, the coefficients were 60 mL/g, 1300 mL/g, and 15,000 mL/g, respectively, for alumina, silica gel, and hydrous titanium oxide. In another study using bicarbonate solutions, the distribution coefficient for Pu(IV) sorption on alumina was lowered to about 30 mL/g at 0.5 M bicarbonate (Charyulu et al. 1991). However, the initial concentrations of Pu(IV) used by these investigators ranged from 8.4×10^{-6} to 4.2×10^{-5} M, which means the solutions were probably supersaturated with respect to $PuO_2 \cdot xH_2O$ solid phase. Because the experimental conditions used by Pius et al. (1995), and Charyulu et al. (1991) do not fit Corey's criteria, the principal mechanism of plutonium removal from solution could have been precipitation as easily as adsorption.

Barney et al. (1992) measured adsorption of plutonium from carbonate-free wastewater solutions onto commercial alumina adsorbents over a pH range of 5.5 to 9.0. Plutonium adsorption K_d values increased from about 10 mL/g at a pH of 5.5 to about 50,000 mL/g at a pH of 9.0. The slopes of the K_d compared to the pH curves were close to one, indicating that one hydrogen ion is released to the solution for each plutonium ion that is adsorbed on the alumina surface. This behavior is typical of adsorption reactions of multivalent hydrolyzable metal ions with oxide surfaces. Changing the initial concentration of plutonium from about 10^{-9} to 10^{-10} M did not affect the Kd values, which showed that plutonium precipitation was not significant in these tests. Also, the initial plutonium concentrations were below the measured solubility limits of plutonium hydroxide. This experiment demonstrated that in carbonate-free systems, plutonium would be adsorbed on alumina substrates.

Delegard et al. (1984), Delegard and Gallagher, (1983), performed tests to identify tank waste components that could significantly affect sorption of plutonium on three shallow sediments typical of the Hanford Site. They found that sorption was decreased by the chelating agents, 0.05 M ethylenediaminetetraacetate (EDTA) and 0.1 M N-2-hydroxyethylethylenediaminetriacetate (HEDTA), but not by low concentrations of carbonate (0.05 M). Delegard's data also showed that roughly a two-fold increase in ionic strength caused an order of magnitude decrease in plutonium adsorption. Sorption of Pu(IV) on a Hanford Site shallow sediment from a synthetic groundwater containing very low (0.003 M) carbonate ranged from about 5000 mL/g to 30,000 mL/g (Barney 1992).

Another study of Pu(IV) adsorption on goethite was conducted by Sanchez et al. (1985). The experimental conditions used by these investigators were evaluated for assessing whether the reaction being studied was indeed adsorption. The initial Pu(IV) concentrations used in their experiments were 10^{-10} and 10^{-11} moles per liter. These concentrations are well below the equilibrium saturation levels for $PuO_2 \cdot xH_2O$. The equilibrating solutions used in these experiments contained salts such as $NaNO_3$, NaCl, Na_2SO_4, and $NaHCO_3$ and did not contain any ionic constituents that may have potentially formed solid solution precipitates. Therefore, it is reasonably certain the dominant reaction being studied was adsorption and not precipitation of pure or solid solution phases.

The Pu(IV) adsorption data obtained in 0.1 M $NaNO_3$ electrolyte medium (Figure 2.9) indicated an isotherm typical of metal or metal-like complex species adsorption on substrate (Benjamin and Leckie 1981). Such a situation indicates that Pu(IV) is adsorbing onto the ionized hydroxyl sites in the form of Pu^{4+} and its hydrolytic species, $PuOH^{3+}$, $Pu(OH)_2^{2+}$, $Pu(OH)_3^{+}$, and $Pu(OH)_4^{0}$, with metal ion and the metal-ion part of the complex adsorbing onto the surface. The adsorption isotherm obtained at the higher initial concentration (10^{-10} M) of total soluble Pu(IV) showed the adsorption edge (pH value at which 50 % adsorption occurs) increased towards a higher pH value, which is typical of the metal-like adsorption behavior of adsorbing species (Benjamin and Leckie 1981). Adsorption data for another tetravalent actinide (thorium) generated by LaFlamme and Murray (1987) (see Figure 2.10) and Righetto et al. (1988) confirms the typical adsorption behavior generally observed for higher valence actinides adsorbing onto iron and aluminum oxides, hydroxides, and oxyhydroxide surfaces.

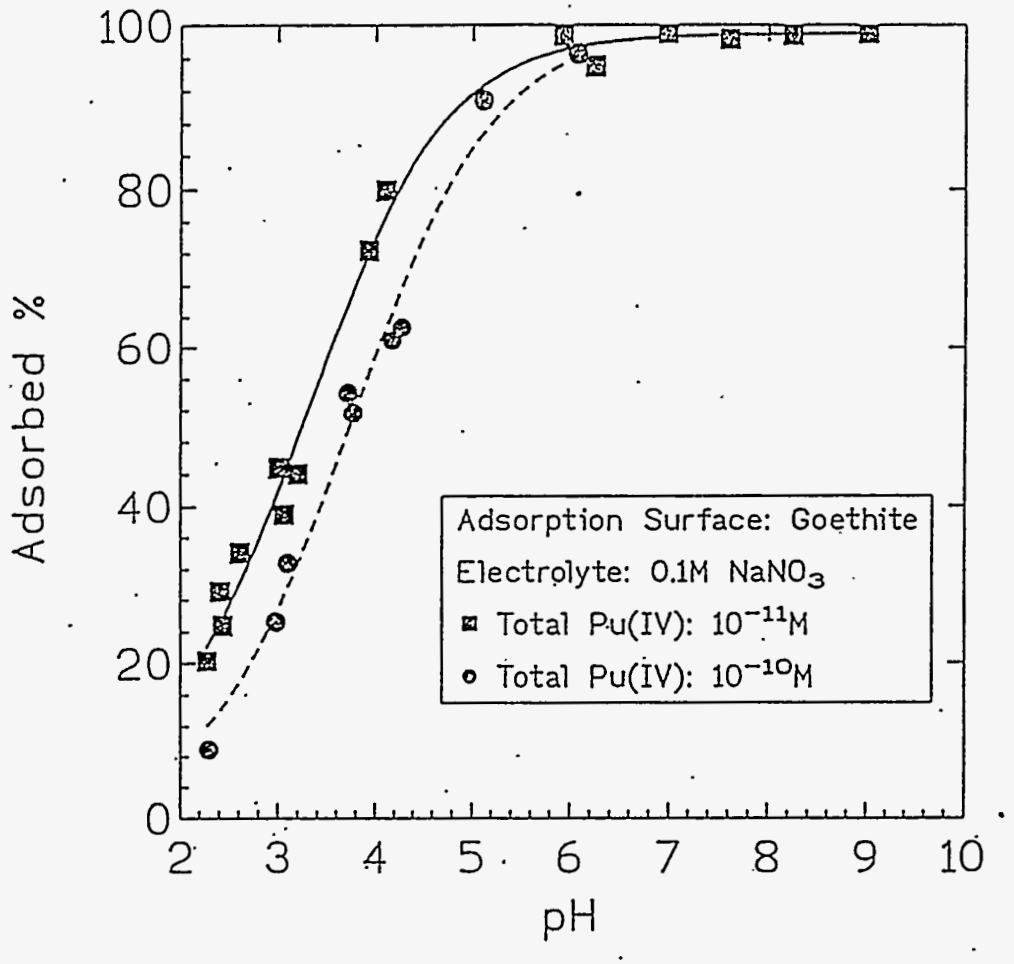

Figure 2.9. Adsorption Isotherms for Pu (IV) Adsorption on Goethite at Fixed Electrolyte Concentration

The Pu(IV) adsorption data obtained in a medium of 0.1 M $NaNO_3$ represents the condition where only free cation and the hydrolytic species are the adsorbing species. Extensive experimental observations have shown that, when present, strong complexing agents have a significant effect on the metal ion adsorption (Benjamin and Leckie 1981). This modified adsorption behavior in the presence of complex-forming ligands is characterized by Benjamin and Leckie as ligand-like adsorption. Sanchez et al. (1985) also conducted experiments to examine the effect of dissolved carbonate (from 10 to 1000 meq/L) on the adsorption of Pu(IV) on goethite. Their adsorption data showed that at a fixed pH value of 8.6, increasing carbonate concentration decreased the adsorption of plutonium (Figure 2.11). This data demonstrated that practically no Pu(IV) adsorption occurred on goethite when the total carbonate concentration approached 1000 meq/l (0.5 M CO_3).

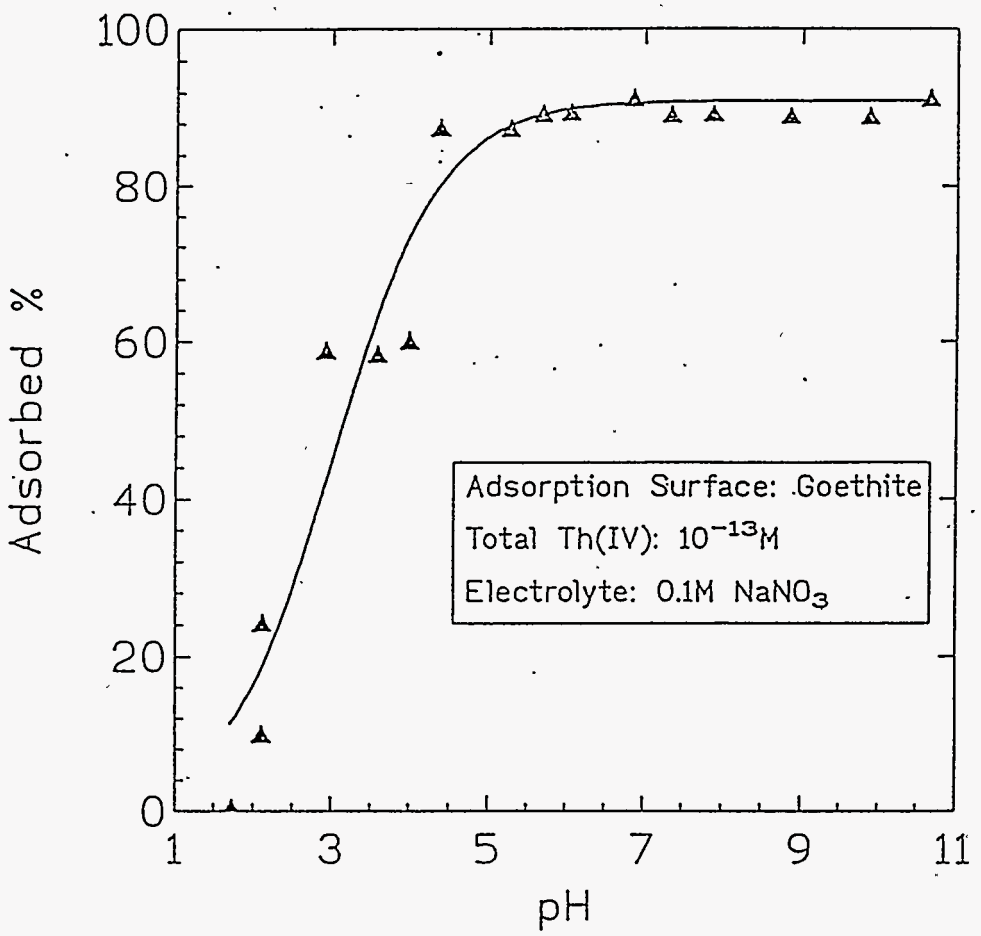

Figure 2.10. Adsorption Isotherms for Th (IV) Adsorption on Goethite at Fixed Electrolyte Concentration

Such complete suppression of Pu(IV) adsorption was attributed to the presence of anionic plutonium-hydroxy carbonate species in solution and to the fact that goethite at this pH contains mainly negatively charged sites that have negligible affinity to adsorb anionic species. This adsorption behavior of Pu(IV) in the presence of carbonate ions that form strong hydroxy carbonate complexes (see Section 2.1) is typical of ligand-like adsorption of metal ions described by Benjamin and Leckie (1981). Ligand-like adsorption is described as adsorption of a metal-ligand complex that is analogous to adsorption of the free ligand species. Also, the metal-ligand complexes may not adsorb at all, if these complexes are highly stable.

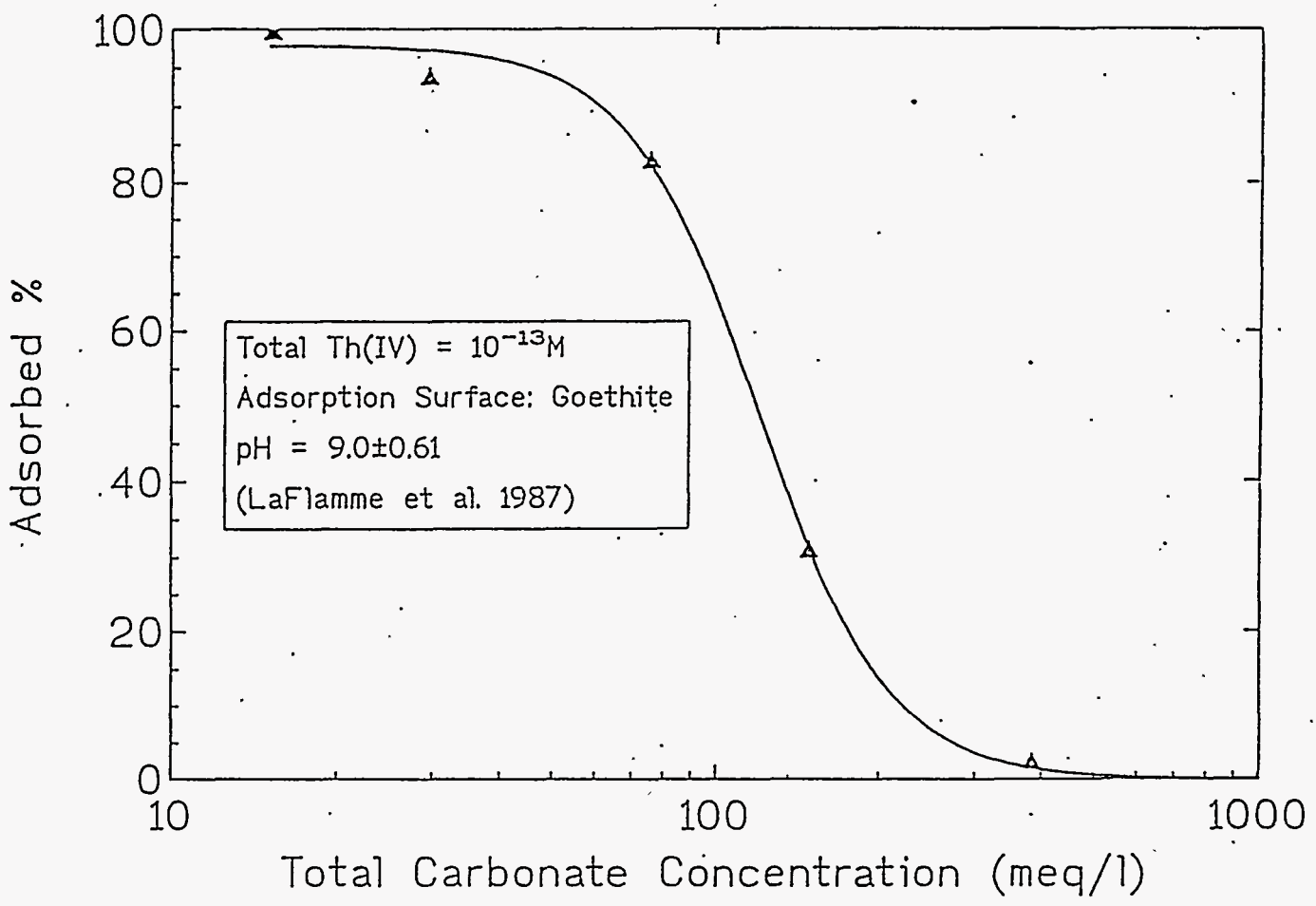

Figure 2.11. Experimental data for Pu(IV) Adsorption on Goethite as a Function of Total Dissolved Carbonate Concentration at a Fixed pH Value of 8.6

Th(IV) showed similar adsorption behavior in the presence of total carbonate concentrations ranging from 10 to 1000 meq/l (LaFlamme and Murray 1987, (see Figure 2.12)). Righetto et al. (1988) conducted a study on adsorption of Th(IV) species, a surrogate for Pu(IV) on aluminum oxide surfaces. These data showed that in solutions containing 100 meq/l of carbonate concentration, significant reduction in Th(IV) adsorption occurred when pH increased from 8.5 to 9.8. This experiment (Righetto et al. 1988) also showed that under these pH conditions, the presence of an organic ligand also significantly retarded Th(IV) adsorption on aluminum oxide.

These data clearly demonstrate that increasing total carbonate and hydroxyl solution concentrations significantly decrease tetravalent actinide adsorption on iron and aluminum oxide, and oxyhydroxide surfaces. Using these data, an adsorption envelope was developed to represent the behavior of Pu(IV) on goethite in the presence of increasing carbonate concentrations and pH. The three-dimensional graph

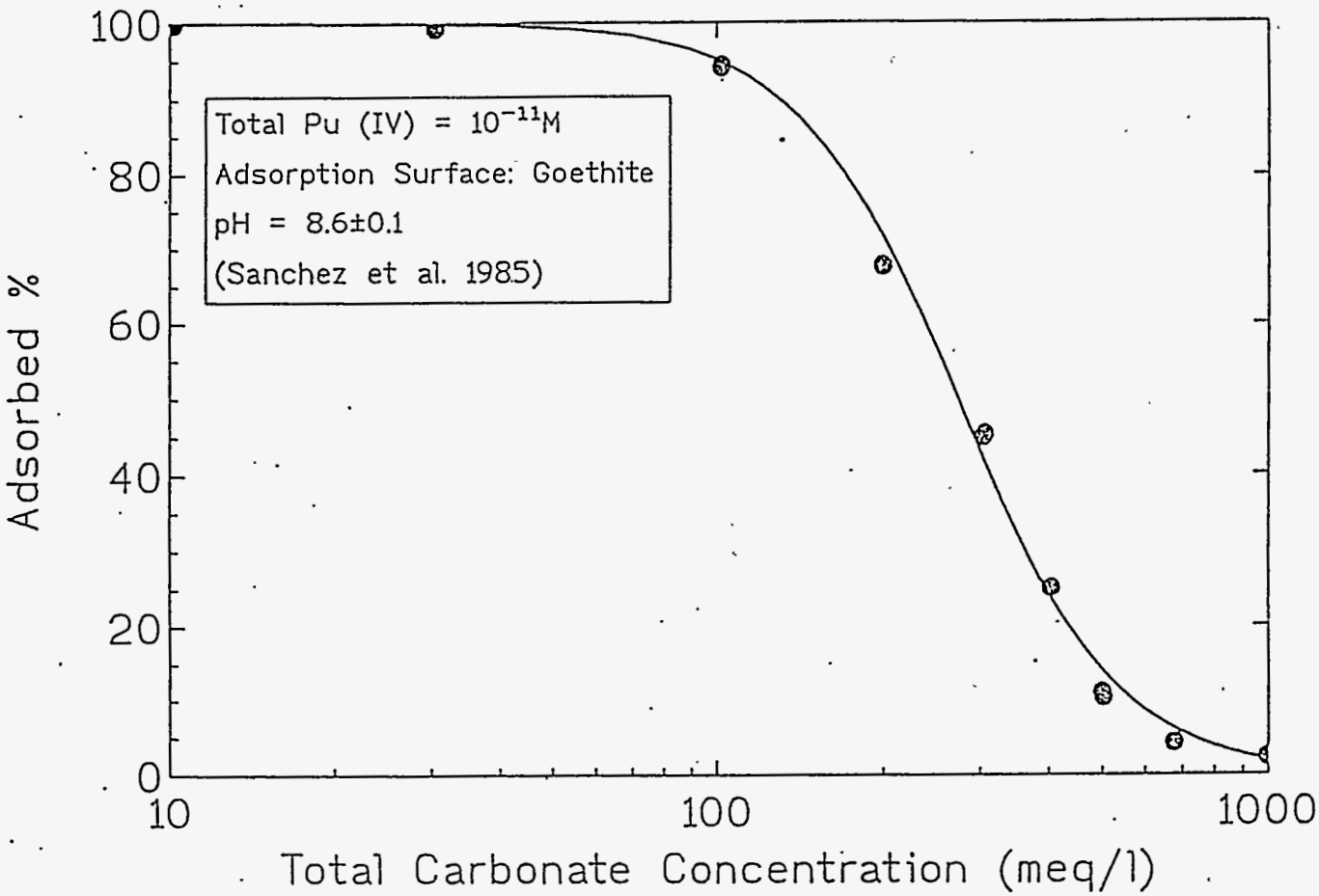

Figure 2.12. Experimental Data for Th(IV) Adsorption on Goethite as a Function of Total Dissolved Carbonate Concentration at a Fixed pH Value of 9.0

(Figure 2.13) represents the different degrees of Pu(IV) adsorption on goethite as a function of two variables (dissolved carbonate and hydroxyl concentrations). Two contour plots (Figures 2.14 and 2.15) are also provided to help visualize adsorption isopleths in carbonate-pH and carbonate- adsorption planes. The adsorption envelope (Figures 2.13 through 2.15) shows that Pu(IV) adsorption onto goethite may be completely suppressed under certain combinations of carbonate and hydroxyl concentrations.

Similar suppression of adsorption of higher valence state actinides in the presence of carbonate and hydroxyl ions has been observed by a number of investigators. Some of these studies include Pu(V) adsorption on goethite (Sanchez et al. 1985); adsorption of U(VI) on goethite (Tripathi 1984, Hsi and Langmuir 1985, Koehler et al. 1992), ferrihydrite (Payne et al. 1992), and clinoptilolite (Pabalan and Turner 1992); and Np(V) adsorption on ferrihydrite, hematite, and kaolinite (Koehler et al. 1992).

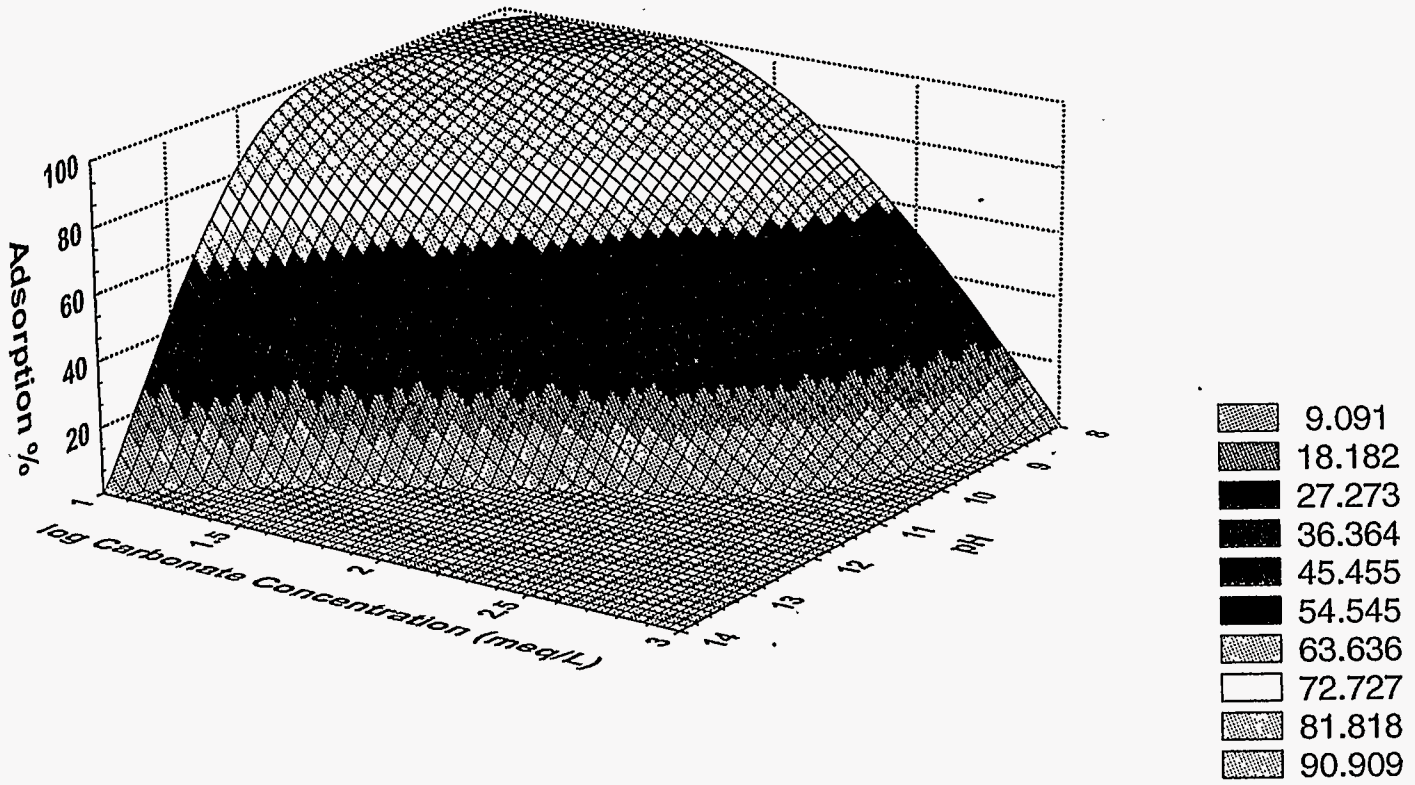

Figure 2.13. Estimated Pu(IV) Adsorption Envelope as a Function of pH and Total Dissolved Carbonate Concentration

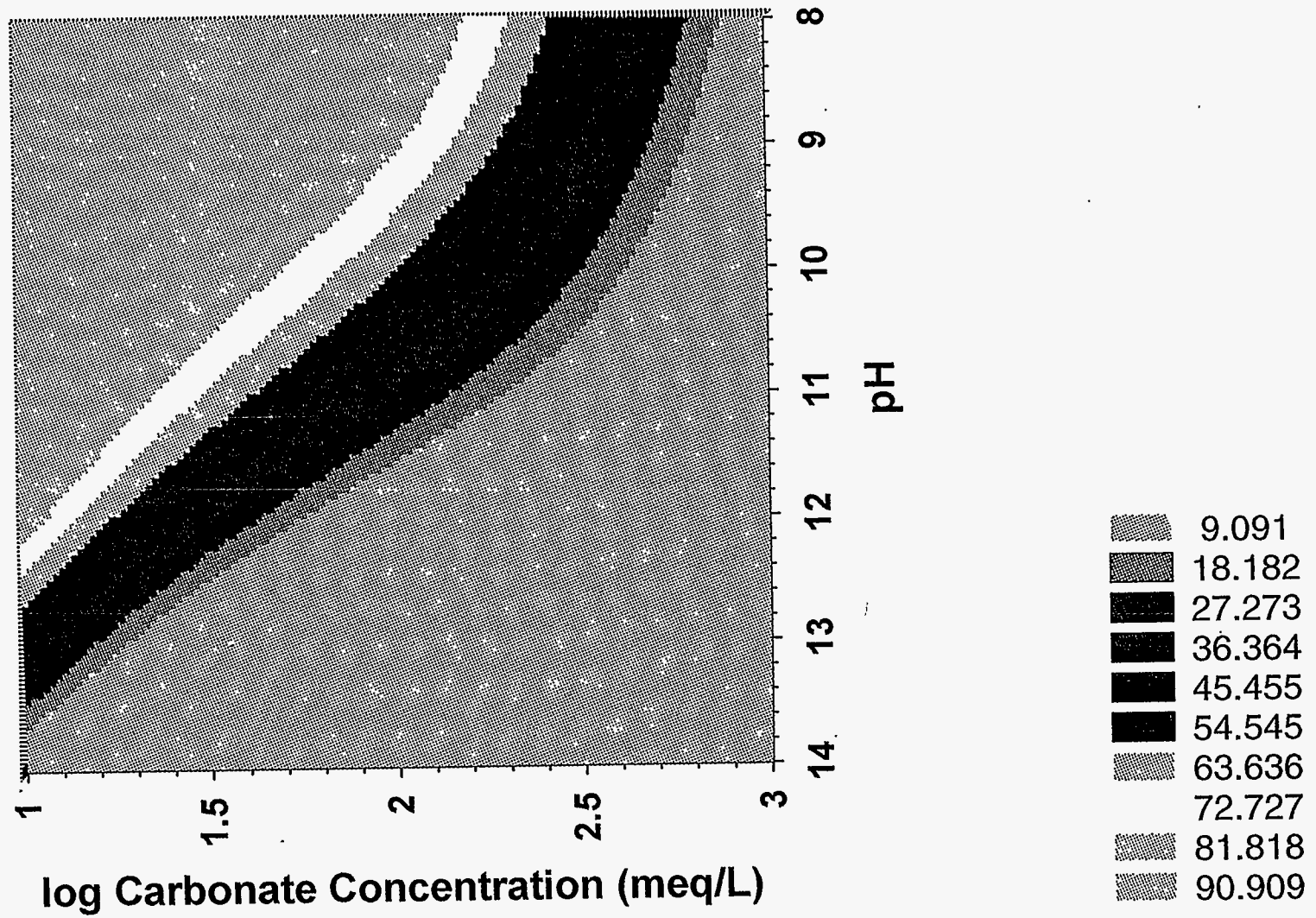

Figure 2.14. Estimated Pu(IV) Adsorption Isopeths with pH and Total Dissolved Carbonate as Variables

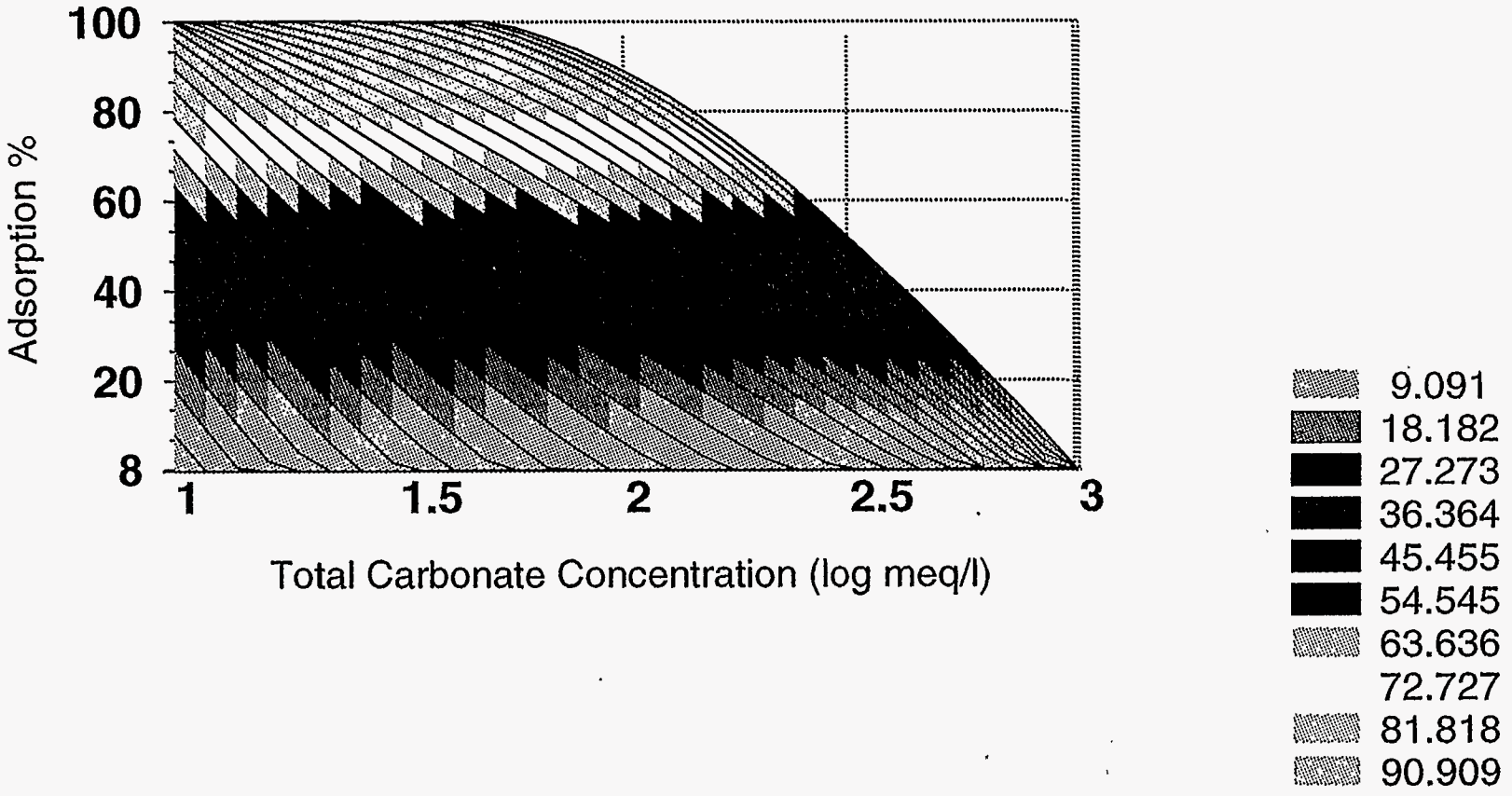

Figure 2.15. Estimated Pu(IV) Adsorption Isopeths as a Function of Total Dissolved Carbonate Concentration and at Various Fixed pH Values

Although empirical data do not exist regarding adsorption of Pu(IV) species on iron- and aluminum-oxide/hydroxide substrates under typical HLW tank conditions (very high pH, significant carbonate concentrations, presence of other complex-forming organic and inorganic ligands, high ionic strengths, high temperatures) the existing experimental data can be used to draw some conclusions regarding the adsorption of Pu(IV) on precipitated substrates.

- The tank supernatants are typically very highly alkaline and contain significant concentrations of dissolved carbonate.

- Pu(IV) in aqueous phase is likely to be present as anionic plutonium hydroxy or plutonium-hydroxy-carbonate species.

- Tank supernatants also contain other ligands that are known to retard or block the adsorption of Pu(IV) species.

These conditions led some chemists on the review team to conclude that plutonium adsorption onto hydrous oxides in waste tanks may not be a significant factor in plutonium partitioning between liquid and solid phases. Other members of the team believe the extraordinarily high pH, the large amount of iron and aluminum adsorbtion substrates present, the intimate mixing of fresh precipitates at the time of neutralization, and the hydroxyl bridging of mixed oxides during aging will result in strong adsorption of the plutonium to the more common hydrous oxide tank sludge.

3.0 Flocculation of Waste Particles

Sludge in the Hanford waste tanks will be retrieved by a variety of methods, which include sluicing and mixer pump operation. During some portions of the retrieval operations, particle settling may result in the segregation of particles according to their settling velocities. Plutonium particles within the sludge may have a density and settling velocity that could differentiate them from other particles during transport and settling and, thereby, result in the concentration of plutonium and segregation of plutonium from neutron absorbers.

The analysis described in this section was performed in an effort to determine whether flocculation of solid particles will prevent the segregation of discrete waste solids according to their individual settling velocities. If a plutonium particle flocculates with other sludge particles, the unique density and settling velocity of the plutonium particle will be masked by the properties of the floc. In this way, particle flocculation eliminates the driving force to achieve segregation. If it can be shown that rapid flocculation of the particles causes the plutonium-containing solids to be effectively bonded to the other waste solids, then the criticality concerns associated with particle segregation can be dismissed.

Calculations were performed to predict whether the waste solids will agglomerate under the conditions expected during waste retrieval. These calculations required that certain properties of the waste solids and supernate be quantified. When the needed data were not available, conservative assumptions were made. The calculations predict that particles in the size range of about 1 to 10 microns will be weakly flocculated, provided the salt concentration in the retrieval fluid is maintained at or greater than about 0.10 molar and the pH exceeds 10.0. The calculations do not predict that the smaller particles (≤ 1 μm) will form sufficiently strong flocs, but this prediction is not consistent with the observed behavior of sludge solids during hot-cell settling tests. The settling rate data imply the small particles undergo flocculation along with the larger particles. The conservatism in the values assumed for the effective Hamaker constant and particle surface charge are apparently the source of the discrepancy between the predicted and observed flocculation behaviors for the sub-micron particles.

Most importantly, TEM studies of sludge solids demonstrate the sludge is composed principally of sub-micron particles. This fact, along with the results of the hot-cell settling tests and the flocculation calculations, leads to the conclusion that the particles are flocculated under normal tank conditions. Thus, segregation of individual waste particles is not expected to occur during retrieval operations, provided the salt concentration is at least 0.1 molar in the supernate and the mixing intensity is low enough to permit flocculation.

The TEM particle size and composition analyses are described in Section 3.1. The flocculation calculations and hot-cell settling tests are described in Section 3.2.

3.1 TEM Evidence for Particle Flocculation

Pacific Northwest National Laboratory (PNNL) previously performed studies of tank waste in support of the Tank Waste Remediation System (TWRS). Within the TWRS project is the Pretreatment Technology Development activity, which focuses on understanding the nature of tank sludge and its leaching characteristics to help develop process flow sheets for sludge dissolution and further processing before final vitrification.

Several analytical tools have been used to characterize the particle size, mineralogy, and speciation of selected elements in the sludge. These data were gathered to support the on-going sludge leaching studies. The tools used include TEM, x-ray absorption spectroscopy (XAS) using two techniques: x-ray absorption near-edge spectroscopy (XANES) and x-ray absorption fine structure spectroscopy (EXAFS), Raman spectroscopy, and nuclear magnetic resonance spectroscopy (NMR).

In addition to the chemical characterization analyzers, particle size analyzers have been employed sparingly to measure the sizes of sludge particles and agglomerates. The particle/agglomerate size data are needed to improve the understanding of sludge settling and sedimentation properties. Several techniques have been used to measure the sludge particle size distributions. These include electron microscopy, laser light chopping, light scattering, and photon correlation spectroscopy.

The TEM data are the most relevant to the analysis of potential criticality scenarios. Analysis of the TEM data permits an assessment of sludge particle size, tendency to agglomerate, crystallinity, and mineralogy, all of which can influence the criticality analyses. TEM is a useful tool for characterizing tank sludge because it provides data on size, morphology, chemical composition, and mineralogy for solids down to a size on the order of 5 nm (0.005 μm).

TEM characterization data for sludge samples from 10 tanks have been reported thus far: AW-105, B-111, BX-107, C-109, C-112, S-104, SY-101, SY-103, T-104, and T-111. Further, several tank sludge simulants and pure phases of aluminum hydroxide, iron hydroxide and calcium phosphate have been studied. The results of these studies are summarized below. Pertinent references from which the following observations were taken include Virden et al. (1994a,b), LaFemina et al. (1994a,b), LaFemina et al. (1995a,b,c), Liu et al. (1995), Liu (1995), and Bunker et al. (1995).

In general, Hanford tank sludge consists of very small primary particles, both amorphous and crystalline, that readily agglomerate under present conditions to form flocs. The individual primary particles range in particle size from a few nanometers to perhaps as large as a few microns, but in general the primary particles are sub-micron in size with most probable sizes between 0.010 and 0.050 μm. Over 90% of the particles characterized are smaller than about 1 μm. Most of the individual crystallites (primary particles) are smaller than 0.05 μm.

The largest primary particles found thus far are usually crystalline salt particles such as $NaNO_3$, $NaOH \cdot 4H_2O$, or gibbsite. The more common sub-micron primary particles are usually agglomerated to form clusters with sizes from sub-micron to a few microns. The clusters can continue to grow in

size and occasionally reach sizes of tens of microns to a few hundred microns. The larger-sized aggregates can readily be broken down into smaller aggregates using mechanical energy (such as mixing).

The agglomerates appear somewhat non-selective regarding which other primary particles become incorporated into the aggregate. That is, agglomerates usually contain several chemically diverse or mineralogically distinct primary particles and take on irregular fractal shapes. These findings suggest that it is quite rare for crystalline particles of fixed composition to be found with sizes as large as a few microns. Much more common are random-composition aggregates of many sub-micron sized primary crystallites in a primary agglomerate which can attach with other agglomerates to form clusters that can reach tens to hundreds of microns in size. Such clusters readily break apart with the application of mechanical energy into the smaller primary agglomerates with sizes from tens of nanometers to as large as a few microns.

That sludge particles aggregate to form micron-sized (and larger) flocs containing a diverse mix of chemical species is an important finding. The implication is that plutonium-laden particles will be distributed throughout the flocs and, therefore, unable to concentrate via any of the various hypothesized mechanisms. On the basis of the TEM results, it is inferred that the segregation of any given chemical specie from the remainder of the sludge, due to hydrodynamic action, is highly unlikely.

This conclusion is based on the assumption that plutonium-laden particles undergo flocculation in a manner similar to that of the other particles in the sludge. Studies of plutonium-laden particle flocculation have apparently not been conducted, so it is not certain whether this assumption is valid. There are indications, however, that it is a reasonable assumption. First, studies of plutonium solids by Grebenshchikova and Davydov (1965) show that plutonium (IV) hydroxide particles undergo a change from positive to negative surface charge at about pH = 8.5. This change is similar to the behavior observed for the metal oxide and hydroxide solids in the Hanford tank waste (Virden et al. 1994b). Second, the flocculation calculations described in Section 3.2 indicate that the sludge particles should be at least weakly flocculated at moderate to high salt concentrations (>0.1 molar). Conservative assumptions were used in these calculations (which applied to all the sludge particles regardless of chemical composition), so the waste solids are probably more strongly flocculated than predicted by the calculations.

The TEM analyses have not identified plutonium-laden particles within any of the flocs examined. This result is expected, as the TEM detection limit is not low enough to detect most radionuclides present in the sludge, unless the radionuclides are highly concentrated in specific phases. Thus, the lack of identified plutonium-laden particles is evidence that plutonium is not present at high concentrations in any of the sludge particles, but is instead dispersed among particles containing other species.

In the sections that follow, the TEM data obtained for sludge samples from specific tanks are summarized. This information is provided to illustrate the range of particle types and compositions that have been identified and to show that the primary sludge particle size is generally submicron.

3.1.1 TEM Data from AW-105 Sludge

Upon drying in preparation for TEM measurements, the sludge from tank AW-105 was found to consist of two different materials, one a pure white powder and the other an orange-brown sludge. The white powder contains two highly crystalline materials. The primary aggregates of the first crystalline material have a bi-modal size distribution with some particles between 0.1 and 0.5 μm and the remaining particles between 1 and 2 μm. These particles are composed of alkali salts, which are probably $NaNO_3$ and KNO_3. The smaller particles may represent fresh precipitate that occurs upon drying the sample to perform the TEM analysis; the larger particles are assumed to be *native* in the sludge.

The second crystalline phase observed in the white powder has primary particles of <0.01 μm and agglomerates up to about 1 μm. These particles are ZrO_2 and represent about 20 vol% of the aggregates in the sample.

The orange-brown sludge material contains five types of very small aggregates with primary particles all being nanometer-sized. The various particles were 50 vol% boehmite [AlOOH], 30 vol% zirconia [ZrO_2], 15 vol% goethite [Fe_2O_3], and smaller amounts of a ferric-chromic oxide and sheet-like alumino-silicate clay-like material. A trace of calcium carbonate [calcite] appears in the sample also.

3.1.2 TEM Data from C-109 and C-112 Sludge

TEM analyses of sludge from tank C-112 showed most of the particles are fine grained (<0.01 μm), but many agglomerates and a very few crystalline aluminum-bearing and uranium-bearing particles reach 5 to 10 μm. The fine-grained particles are primarily calcium phosphate, iron/nickel hydrous oxides, aluminum hydroxide, and iron hydroxide. Crystalline boehmite [AlOOH] and gibbsite [$Al(OH)_3$] were positively identified in this sludge sample.

An EXAFS characterization of sludge from tanks C-109 and C-112 shows that stable strontium (and by inference ^{90}Sr) in the sludge is incorporated into calcium carbonate crystals, mainly the aragonite form (70%) and calcite (10%), and hydroxyapatite [$Ca_5(OH)(PO_4)_3$].

3.1.3 TEM Data from T-111 Sludge

Sludge characterization of material from T-111, a tank which contains two types of bismuth phosphate waste, shows a large amount of crystalline sodium hydrogen phosphate. The material is agglomerated to sizes up to 100 microns that break apart upon washing in a sodium nitrite/hydroxide solution into smaller agglomerates of about 5 μm. These smaller agglomerates, in turn, are made up of primary particles with mean sizes of 0.05 μm. Other particles consist of iron, bismuth, and silicon in a

fairly fixed ratio, although no x-ray diffraction patterns were observed that would suggest the compound was crystalline. The compound is inferred to be amorphous bismuth ferrite [$Fe_2Bi(SiO_4)_2OH$]. Less common particles that appear to be crystalline and present in the sludge include hydroxyapatite [$Ca_5(OH)(PO_4)_3$] with rod-like particles and 0.1 μm size; Jacobsite [Fe_2MnO_4] with plate-like particles and 0.5 μm size; goethite [FeOOH] with rod-like particles with 0.5 μm size; and lanthanum pyrophosphate [$La_4(P_2O_7)_3$] with irregularly shaped particles and crystallite size of 0.5 μm.

3.1.4 TEM Data for SY-103, BX-107, and T-104 Sludge

Some other tank sludges that were examined using TEM include sludges from tank SY-103 with amorphous alumino-silicate phases predominating; tanks BX-107 and T-104 with amorphous aluminum hydroxide and amorphous aluminum phosphates predominating with some sodium-alumino-silicates present. In these tanks, agglomerates with a primary particle size of 0.01 μm predominate.

TEM and its accessory EDS (energy dispersive spectroscopy) to identify elements and XRD (x-ray diffraction) to identify crystal structure and thus mineralogy in combination with XANES (which can determine valence state of elements) were used to determine the chemical speciation of Cr in several sludges. X-ray absorption spectroscopy which includes both EXAFS and XANES is very sensitive and can monitor many elements when they are present at 10 ppm or higher. TEM requires an element be present at about 1000 ppm to obtain quantitative analyses. Interestingly, the Cr found in sludges from tanks with bismuth phosphate waste is generally found to be about 75 $\pm$ 5% in the trivalent state and 25 $\pm$ 8% in the hexavalent state. Cr found in sludge from REDOX wastes (one tank analyzed) was found to be 100% hexavalent and readily leached during sludge washing.

3.1.5 Implications of TEM Results for Criticality Analyses

Although TEM analyses show that most of the primary particles (both by number and volume fraction) in tank sludges are smaller than 0.1 μm in diameter, measurements of particle size based on indirect techniques, such as sedimentation and light scattering, indicate most of the particles are larger than 1 μm. This apparent discrepancy between reported particle sizes from the two measurement techniques demonstrates that sludge particles are heavily agglomerated under typical waste conditions (for example, high pH and salt concentration). The significance of particle agglomeration is it prevents the segregation of different chemical species according to their individual settling velocities. Thus, separation of plutonium-laden particles from other waste solids is prevented.

The primary sludge particles agglomerate to form large flocs that range from 10 μm to about 1 mm in diameter. The size of these flocs is determined by the intensity of shear and Brownian motion present in the supporting solution. More intense fluid motion increases the tendency for the flocs to break apart into smaller agglomerates. Retrieval operations (such as, sluicing and mixer pump jets) induce sufficiently intense fluid motion to break up large flocs, but these are expected to re-form once mixing is stopped. Very intense shear can break up agglomerates into discrete primary particles, but under typical tank supernate conditions (salt concentration greater than 0.1 molar) these particles will rapidly agglomerate when the mixing intensity is sufficiently reduced.

3.2 DLVO Theory Predictions of Sludge Flocculation

Calculations were performed to predict whether flocculation is expected to occur under the expected conditions during waste retrieval. The results of these calculations are consistent with the conclusions drawn from the TEM results presented in Section 3.1. At a minimum, the micron-sized sludge particles are predicted to be weakly flocculated when the supernate salt concentration is in excess of 0.10 molar. This prediction is based on conservative assumptions for certain key sludge properties, so the solids are likely to be more strongly flocculated than is predicted by the calculations. Consideration of hot-cell settling rate data for sludge solids also indicates the sludge particles are flocculated. These analyses are discussed in the following sections.

3.2.1 Background

A quantitative theory describing colloidal flocculation was developed by Derjaguin, Landau, Verwey, and Overbeek. Their theory is described by Hiemenz (1986) and by other authors in most standard colloid science texts. Known as the DLVO theory, it represents the standard approach for predicting the tendency of colloidal systems to undergo flocculation. The theory is conceptually simple. The magnitude of the repulsive forces between particles is compared to the magnitude of the interparticle attractive forces. If the attractive forces exceed the repulsive forces, the particles are expected to flocculate.[a]

Particles dispersed in a liquid often develop a surface charge. The surface charge can arise through the adsorption of ions onto the particle surface or through the addition or removal of protons from molecules at the particle surface.[b] Metal hydroxide and oxide particles are often found to have a positive surface charge at low pH, zero charge at a pH between about 6 and 9, and a negative charge at higher pH (Hunter 1981). At the pH range of interest for tank waste applications ($pH \geq 10$), the hydrous metal oxide sludge solids will be negatively charged. Higher liquid pH results in particles that are more strongly negatively charged. Particle agglomeration tends to be inhibited by the negative charges.

As two negatively charged particles approach each other, their respective electric fields interact and a repulsive force develops. The magnitude of this repulsive force can be estimated using Coulomb's law and classical electrostatics. However, the nature of the interaction between particles is more complicated than that described by Coulomb's law, which assumes point charges separated by a distance. Each charged solid particle submerged in a liquid is surrounded by a cloud of oppositely charged ions. Negatively charged particles are surrounded by a diffuse cloud of cations (positively charged). As two

---

(a) Some texts differentiate between the terms flocculation and coagulation according to the nature of the net interparticle attractions. In this report, the term flocculation is used to describe all types of particle interactions where aggregation of particles occurs.

(b) Other mechanisms can result in the development of particle surface charge, but these are not described here.

particles approach each other, these ion clouds interact and generate a force of repulsion. The work done by moving two spherical particles of radii a_1 and a_2 together from an initial large separation distance to a separation of h is given by the following equation (Shaw 1980):

$$\phi_R(h) = \frac{64\pi\varepsilon a_1 a_2 k^2 T^2 \Upsilon_1 \Upsilon_2}{(a_1 + a_2)e^2 z^2} \exp(-\kappa h) \tag{3.1}$$

where ε = permittivity of the interparticle medium, C^2/Nm^2
κ = Debye parameter as given by Equation (3.2), m^{-1}
T = absolute temperature, K
Υ_i = charge-dependent parameter for particle I as given by Equation (3.3)
e = electron charge = 1.6×10^{-19} C
z = valence of the salt ions in solution, 1.0 is used here
k = Boltzmann's constant = 1.38×10^{-23} J/K.

The measurement unit for ϕ_R as given in Equation 3.1 is joules. The value of the Debye parameter, which is also called the inverse double-layer thickness, is given by

$$\kappa = \left(\frac{2e^2 N_A c z^2}{\varepsilon k T} \right)^{\frac{1}{2}} \tag{3.2}$$

where N_A = Avogadro's number = 6.02×10^{23} molecules/mole
c = concentration of z:z electrolyte, moles/m^3
k = Boltzmann's constant = 1.38×10^{-23} J/K

The value of the charge-dependent parameter used in Equation 3.1 is given by:

$$\Upsilon_i = \tanh\left(\frac{ze\psi_i}{4kT} \right) \tag{3.3}$$

In Equation 3.3, the term ψ_i is the surface charge (in volts) of particle number I.

Equations 3.1, 3.2, and 3.3 were used to estimate the repulsive force between particles of various sizes. A temperature of about 300K (roughly 80°F) was used for all calculations. The DLVO predictions were found to be relatively insensitive to variations in temperature over the range of 290K to 380K (63 to 225°F), which covers the range of temperatures expected during waste retrieval.

Attractive forces arise between particles due to a combination of dipole-dipole and induced dipole-dipole interactions at the molecular level (Hiemenz 1986). The magnitude of the attractive force is a function of the particle sizes, shapes, compositions, and the properties of the fluid medium between the particles. For spheres, the attractive potential (in joules) is given by Equation 3.4. In this equation, the term A, which is called the Hamaker constant, accounts for the dependence of the attractive force

on the composition of the particles. The Hamaker constant is a complicated function of the dielectric and polarization properties of the particles and the surrounding fluid medium.

$$\phi_A(h) = -\frac{A}{6}\left[\frac{2a_1\bar{a}_2}{h^2+2a_1h+2a_2h} + \frac{2a_1\bar{a}_2}{h^2+2a_1h+2a_2h+4a_1a_2} + \ln\left(\frac{h^2+2a_1h+2a_2h}{h^2+2a_1h+2a_2h+4a_1a_2}\right)\right] \quad (3.4)$$

The net interaction potential, Φ_{net}, is given by summing the repulsive potential, which has a positive magnitude, with the attractive potential, which has a negative magnitude. The resulting formula describes the nature of the resultant interaction. If the net potential is negative, the particles attract. If the net potential is positive, the particles repel. The net interaction potential is given by:

$$\phi_{net}(h) = \phi_R(h) + \phi_A(h) \quad (3.5)$$

The net interaction potential function is usually plotted in units of kT versus particle separation distance (h) as measured between the nearest particle surfaces (as opposed to the center-to-center distance). Units of kT, which is Boltzmann's constant times absolute temperature, are used to provide a direct comparison of the magnitude of the net force with the forces generated by molecular vibrations.[a] A typical plot of three different net interaction potentials is shown in Figure 3.1. Curve (a) shows a positive net interaction at essentially all interparticle distances. No flocculation is predicted for this case. Curve (b) shows a positive net interaction potential at separations of about 5 to 20 nm, but the net force is attractive (negative potential) at distances greater than about 20 nm. Flocculation is predicted for this case. Curve (c) shows a net negative interaction for all separations. Rapid, irreversible flocculation is predicted.

The curves in Figure 3.1 were generated by selecting different surface charge values for particles 0.5 microns in diameter surrounded by a 0.01 molar monovalent salt solution. The parameters used to model the net interaction potentials expected during waste retrieval are described in the next section.

3.2.2 Assumptions Used for DLVO Calculations

To perform the DLVO calculations for the tank waste conditions during retrieval, it was necessary to make two key assumptions. First, the magnitude of the Hamaker constant had to be determined. Second, the magnitude of the particle surface charge had to be estimated. The temperature and salt concentrations expected during retrieval were also estimated, but there is a sound basis for the selection of specific values for both of these parameters. Insufficient data are available to accurately estimate the

(a) Thermally induced molecular vibration forces are the source of Brownian motion in particles suspensions.

waste surface charge and effective Hamaker constant; so conservative assumptions were made. The justification for the Hamaker constant and particle charge values used in the calculations is given in this section.

The Hamaker constant used for the following DLVO calculations was 0.8×10^{-20} J. This value was selected, based on an examination of the range of reported Hamaker constants for inorganic compounds. No Hamaker constant data were found for plutonium compounds. Russel et al. (1989) reports effective Hamaker constants (for particles in water) for a variety of substances (such as silica, calcite, and calcium fluoride). The reported Hamaker constants range from 0.83×10^{-20} to 5.32×10^{-20} J. A lower Hamaker constant implies a smaller attractive force, so it is conservative to select a Hamaker constant at the low end of typical values. The actual effective Hamaker constants for the waste solids are likely to be larger than 0.8×10^{-20} J, but in the absence of relevant data, the use of the lower Hamaker constant is justified.

The particle surface charges were all assumed to be -200 mV. It is known that many metal oxides and hydroxides are negatively charged at high pH (Hunter 1981). The predominant neutron absorber particles (iron and aluminum oxides and hydroxides) are expected to have a negative surface charge. It is expected that any plutonium oxide or hydroxide particles would also be negatively charged at high pH, but surface charge data for plutonium compounds are not available. Grebenshchikova and Davydov (1965) report the charge on plutonium (IV) hydroxide particles is negative at pH values higher than about 8.5.

A surface charge magnitude of -200 mV was selected based on the known typical range of particle zeta-potentials. Zeta-potential is a quantity that is related to the particle surface charge, but they are not the same. The zeta-potential is smaller than the particle surface charge by an amount dependent on the salt concentration in the liquid (Hiemenz 1986). Zeta-potential is defined as the electrostatic potential at the surface of shear. The surface of shear exists at the distance from the particle surface where the ions are not bound so tightly as to prevent viscous flow. Hunter (1981) states the absolute magnitude of zeta-potential is usually less than about 150 mV.

Fortunately, the DLVO calculations are relatively insensitive to the magnitude of the surface charge when the absolute magnitude is in excess of 100 mV. Because the typical range of zeta-potentials at high pH implied the surface charge on the waste particles could possibly be more negative than -150 mV, a value of -200 mV was chosen and used for the DLVO calculations. The difference between the DLVO predictions for an assumed -100 mV surface charge and a -200 mV surface charge is minimal, so this assumption is not overly conservative.

Zeta-potential measurements have been made on waste simulant solids (Virden et al. 1994b). At high pH (11.8), it was reported the zeta-potential was about -50 mV. The salt concentration in the liquid was not measured, so the magnitude of the particle surface potential cannot be reliably estimated. However, it seems reasonable that the surface potential was less than (more negative) -60 mV. The

zeta-potential measurements on waste simulants, which contained the same chemical species as expected in NCAW, indicate the assumed -200 mV surface potential for the DLVO calculations is reasonable, yet conservative.

The biggest uncertainty in the input parameters for the DLVO calculations is clearly the estimated Hamaker constant. The assumed value of 0.8×10^{-20} J could credibly be about an order of magnitude too low. The effect of a larger Hamaker constant on the calculations is to make flocculation more likely. Because a conservatively low Hamaker constant has been assumed, flocculation may occur, even though the DLVO calculations predicted no flocculation. In fact, this is the case; the TEM results imply the sludge particles aggregate (see Section 3.1) in cases where the DLVO calculations predict only very weak net interparticle attractions.

3.2.3 Analysis of Flocculation Modeling Results

The results of the DLVO calculations are discussed in this section. The DLVO suspension stability calculations imply the concentration of salt expected in the liquid during retrieval is high enough to ensure rapid particle flocculation. This conclusion applies, provided the supernate salt concentration exceeds about 0.1 molar. If a more dilute supernate is assumed, the resulting flocs will either be weaker or not form at all, depending on how low the salt concentration is assumed to be. If corrosion-inhibiting water (dilute sodium-hydroxide-nitrite) is assumed to represent the supernate, flocs will form, but the flocs will be weaker and it is not clear whether the weak flocculation will be sufficient to prevent particle segregation. Based on the TEM data presented in Section 3.1, however, adequate flocculation is expected.

Rapid flocculation of particles is expected to prevent the separation of plutonium-laden particles from the rest of the sludge/waste solids, that act as neutron absorbers. Differences in density and settling velocities between the plutonium-laden solids and the other waste solids (primarily metal hydroxides and oxides) may allow plutonium to become concentrated either near the bottom or near the top of a settled solids layer. The position depends on whether the Pu-particle settling velocity is greater than or less than that of the non-Pu particles. This situation is unlikely to occur because all the particles in the slurry are expected to participate in rapid flocculation, which will inhibit segregation of waste solids. The resulting flocs, which may contain Pu and non-Pu solids, will have similar settling properties, preventing the segregation of Pu from non-Pu solids.

This conclusion assumes the mixing intensity applied to the slurry during settling is relatively low. More intense mixing may inhibit floc formation and permit some degree of particle segregation. The justification for this conclusion follows.

Salt Effects on the Electrostatic Double-Layer

The concentration of salt in the tank supernatant liquid influences whether flocculation will occur. At high pH, the waste solids are expected to be negatively charged. In the absence of significant dissolved salts, the particles repel each other electrostatically and no flocculation takes place. When

salt is added, the resulting ions reduce the influence of the electrostatically repulsive particles. The interparticle attractive forces (van der Waals and London dispersion forces) can overcome the electrostatic repulsion, if enough salt is added. When this happens, the particles can flocculate.

Figure 3.2 shows the net interaction potential plotted as a function of interparticle separation for four different particle sizes. The interaction potential is the sum of the interparticle attractive and electrostatic repulsive forces. Attractive forces are assigned a negative sign, so a negative net interaction potential indicates a net attractive force between the particles. The units used to express the interaction potential are in terms of kT, which is the product of Boltzmann's constant (1.38E-23 J/K) and absolute temperature (300K). Units of kT are used because they allow the magnitude of the interparticle forces to be compared to the magnitude of thermal forces (from molecular vibrations). If the magnitude of a net attractive or repulsive force is on the order of a few kT or less, it is unlikely to have a significant influence on the interparticle behavior because the force will be masked by thermal forces.

The net interaction potentials shown in Figure 3.2 indicate that flocculation is predicted for particles larger than about 2 microns in diameter when the salt concentration is 0.021 molar (equal to that of inhibited water). The curve for 2-micron particles shows the minimum interaction potential is about -7 kT. In practice, colloidal systems with net interaction potentials between about -15 kT and -3 kT form very weak flocs, which are easily disturbed by the combination of thermal and applied shear forces (Hiemenz 1986). When the interaction potential is lower than -15 kT, however, the attractive forces are stronger and the flocs more resistant to disturbance.

The attractive forces are predicted to be dominant for 10 micron particles as shown in Figure 3.2 (minimum net interaction potential of -35 kT). However, body-type forces (gravity and inertia) become important when compared to colloidal forces for particles larger than 5 microns, so DLVO calculations for particles larger than 5 microns should be applied cautiously. The buoyed weight of a 10-micron diameter sludge particle (assumed spherical) is on the order of 10^{-11} N. For comparison to the colloidal forces, the maximum net attractive force indicated in Figure 3.2 is used. The maximum attraction is given by the maximum positive slope of the net interaction potential curve. In Figure 3.2, the maximum attractive force between 10-micron particles is estimated to be 0.5×10^{-11} N. In Figure 3.3, the maximum force for the 10-micron particles is about 1.2×10^{-11} N. Thus, for 10-micron particles, the gravitational force is approximately equal to that of the net attractive force.

Sensitivity to Surface Charge Assumption

The net interaction potential plots for particles in a 0.1 molar salt solution are shown in Figure 3.3. A salt concentration of 0.1 molar was selected because this figure represents the current salt concentration in the AY-102 supernate.[a] Provided that AY-102 supernate is used as the retrieval fluid for C-106

(a) The sodium cation concentration in the Tank AY-102 supernate is reported by Castaing (1994) to be 2150 mg/L, which is 0.093 M.

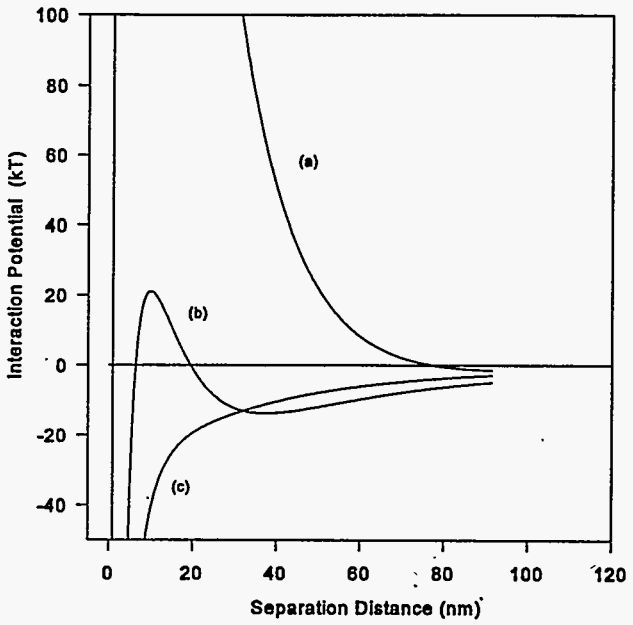

Figure 3.1. Example DLVO Interaction Plot

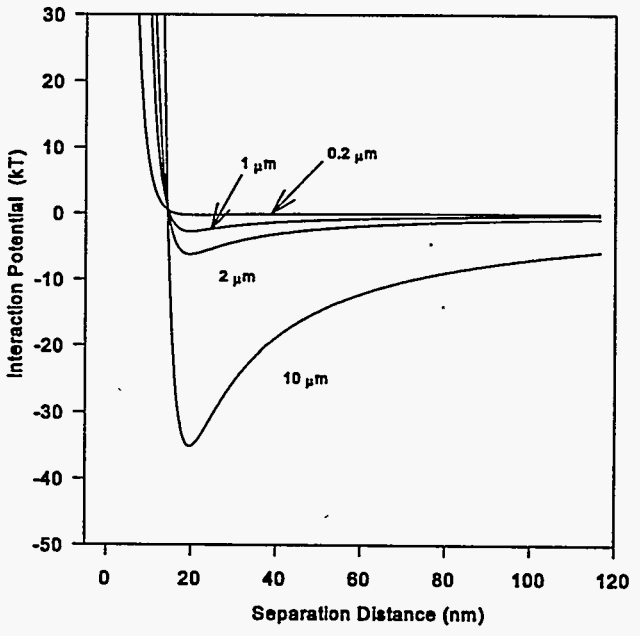

Figure 3.2. 0.021 M Salt and -200 mV DLVO Calc.

sluicing, the particles will be exposed to salt concentrations of 0.1 molar or greater.[a] Figure 3.3 shows that particles on the order of 1 micron and larger are expected to flocculate together. Smaller particles will be bound less strongly together.

The net interaction potential for a 0.10 M salt concentration and a -100 mV assumed surface charge is shown in Figure 3.4. The curves in Figures 3.3 and 3.4 are essentially identical. This indicates the DLVO calculations are relatively insensitive to the assumed surface charge when the surface charge is less than -100 mV and the salt concentration is 0.1 molar.

Flocculation Rate

The flocculation rate at 0.10 M salt concentration is expected to be rapid. Because the interaction potentials are all predicted to be negative (net attraction), no potential energy barrier exists to slow the flocculation of particles. The flocculation rate will be controlled by the rate at which the particles encounter one another, which is a function of both mixture agitation and particle diffusion. Hunter (1993) states the rate of flocculation in the absence of an appreciable potential energy barrier is on the order of seconds to minutes. Thus, the waste solids are expected to flocculate rapidly after the mixing intensity is sufficiently reduced to avoid destroying the flocs as they form.

Further evidence for rapid flocculation comes from hot-cell settling tests in which the initial (quantified over the first 0.5 h) particle/floc settling rate is high. This behavior indicates the flocs are forming over time-scales of minutes rather than hours or days. Flocculation at this rate is fast compared to the time required for particle/floc settling in the waste tanks. For the purpose of addressing particle segregation, the flocculation rate is rapid. Because the flocculation is expected to be rapid, it is unlikely that any appreciable particle-size segregation will occur before flocculation occurs.

Selective Agglomeration

In some colloidal systems, selective agglomeration of particles can occur. Selective agglomeration would be of concern for criticality analyses if, for example, the plutonium-containing particles preferentially flocculated with each other rather than with the neutron absorbers. Selective agglomeration can occur when one or more species of particles in a suspension either have no significant surface charge or are oppositely charged compared to the other particles in the suspension. If, for example, all the neutron absorber particles possess a large negative charge while the plutonium-containing particles have only a weak negative charge, it is possible the plutonium-containing particles will selectively agglomerate with each other, rather than with the neutron absorbers. Alternatively, if the plutonium-containing particles have a positive charge, they will agglomerate preferentially with the negatively charged absorber particles, rather than with other plutonium-containing particles.

(a) As sludge is retrieved from C-106, the salt concentration in the liquid is expected to increase as the soluble fraction of C-106 solids dissolves.

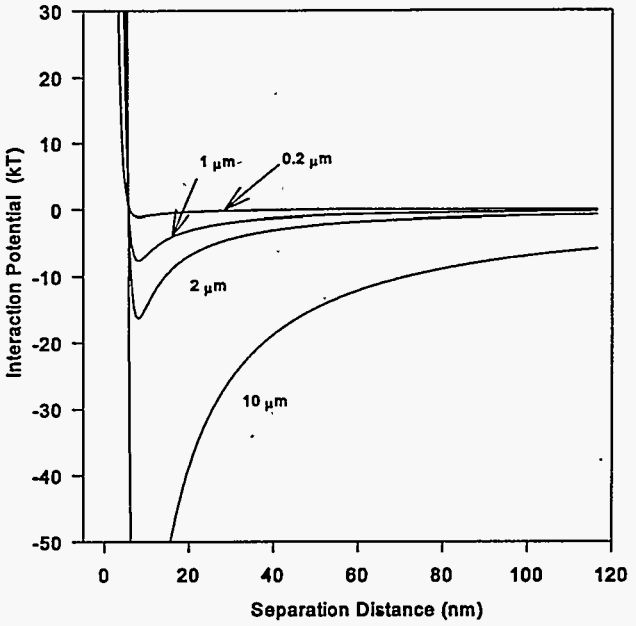

Figure 3.3. 0.10 M Salt and -200 mV DLVO Calc.

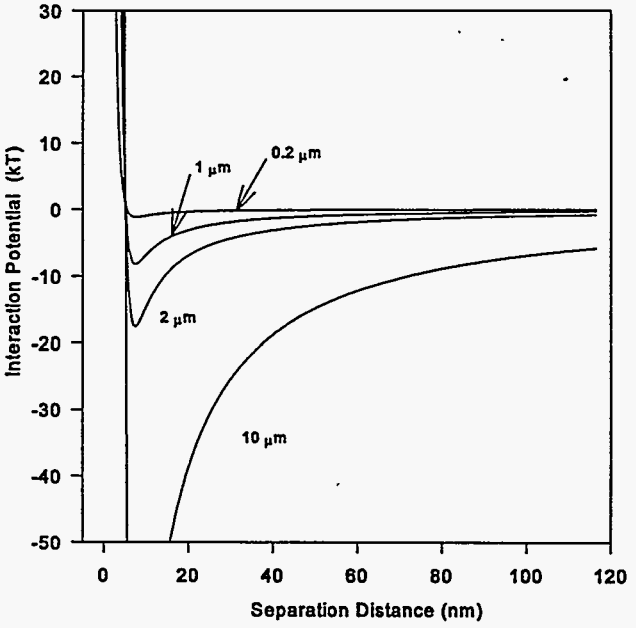

Figure 3.4. 0.10 M Salt and -100 mV DLVO Calc.

Selective agglomeration should not occur in suspensions of tank waste solids provided the solution pH is maintained above about 10. At pH >10, the neutron absorber particles and the plutonium-containing particles should all possess a significant negative surface charge, which will prevent selective agglomeration. Zeta-potential measurements made on simulated waste solids (primarily neutron absorbing oxides and hydroxides of iron and aluminum) demonstrate the neutron absorbing particles possess a surface charge more negative than about -22 mV at a pH of 10.0. Zeta-potential data for plutonium compounds have not been found, but tests conducted on Pu^{4+} solutions by Grebenshchikova and Davydov (1965) indicate the resulting $Pu(OH)_4$ particles are negatively charged at a pH greater than about 8.5. Transition from a positive charge to a negative charge at a pH of about 8 to 9 is similar to that reported for the neutron-absorbing solids.

Retrieval operations conducted at lower solution pH may be vulnerable to selective agglomeration effects. If operations are to be conducted where the solution pH is expected to decrease to below 10, a more thorough analysis of the potential for selective agglomeration must be conducted.

Floc Destruction by Viscous Shear

The DLVO calculations conservatively predict that some degree of particle flocculation should be observed at 0.1 M salt (and higher). Because the predicted flocs are relatively weakly bonded particle aggregations, vigorous mixing may effectively prevent the formation of flocs. Under conditions of moderate to intense mixing, localized particle segregation may be achieved by applying enough shear to inhibit flocculation, but not enough mixing intensity to prevent the largest particles from settling to the tank floor.

A spherical particle subjected to a uniform shear field will experience shearing and extensional forces on the order of F_{shear}, which is given by:

$$F_{shear} = \mu \gamma \pi d^2 \tag{3.6}$$

where μ = liquid viscosity, Pascal-sec
γ = shear rate, s^{-1}
d = particle diameter, m

The maximum attractive force for 2-micron particles in a 0.1 M salt solution (for the assumed surface potential and Hamaker constant) is estimated from Figure 3.3 to be about 7×10^{-12} N. Equation 3.6 predicts that 2-micron particles in a moderately intense 100 s^{-1} shear field will experience about 1.2×10^{-12} N of force. A more intense shear field of 500 s^{-1} will apply a force approximately equal to that of the interparticle attractive force. Thus, flocculation may be inhibited if the slurry is exposed to moderately intense mixing.

This comparison of shear and interparticle attractive forces is over-simplified. A more rigorous treatment of the problem would be required to determine what level of mixing intensity will permit sufficient flocculation to occur. Unless this further analysis is completed, the conclusion that

flocculation will prevent particle segregation should be applied specifically to weakly-mixed sludge settling scenarios. The TEMPEST simulations shown in Section 4.2.3 suggest the AY-102 receiver tank is a weakly-mixed settling scenario.

Implications of Hot-Cell Sludge Settling Tests

Samples of waste solids have been withdrawn from many of the Hanford waste tanks. Some samples have been subjected to settling rate tests. Of great interest to the criticality issue resolution work is the fate of plutonium-containing particles during settling. If the settling velocities of the plutonium-containing particles are appreciably higher or lower than those of the neutron absorbing particles the potential may be present to reach plutonium concentrations of concern during waste retrieval and handling operations.

A direct test of the fate of plutonium-containing particles has apparently not been conducted. Such a test would involve settling waste slurries from an initially well-mixed condition either under gentle or no agitation. The resulting sediment bed would be analyzed to determine if any significant enrichment of plutonium concentration occurs in any portion of the bed.

Even though direct measurements of plutonium segregation by settling have not been made, the existing waste solid settling velocity data provide information relevant to the particle flocculation analysis presented.

The DLVO calculations presented in Figures 3.2 through 3.4 indicate that particles larger than roughly 1 microns are expected to flocculate in a 0.10 M retrieval fluid. Particles smaller than about 1 micron will be very weakly bonded to any particles with which they might happen to flocculate, depending on the validity of the surface charge and Hamaker constant assumptions used for the DLVO calculations.[a] It is important to determine the fate of the particles smaller than 1 micron. Do they remain dispersed and subsequently settle upon the layer of flocculated larger particles or do they participate in the flocculation?

It appears the answer to this question is the smaller particles participate in the flocculation process and settle along with the larger particles. This conclusion is based on the observed settling behavior of waste solids.

Waste solids settling tests are conducted by first diluting the solids with either water or tank supernate to the desired level, mixing well, and then watching the rate at which the interface between the

---

(a) The DLVO calculations presented in Figures 3.2 through 3.4 apply to equal particle sizes. That is, $a_1 = a_2$. Calculations were also done to examine the interaction potentials between particles of different sizes. The magnitude of the interaction potential is determined largely by the size of the smaller particle, so statements made based on $a_1 = a_2$ DLVO calculations are expected to apply equally well to $a_1 <> a_2$ particle interactions.

settling solids and the clear supernate progresses downward. In settling tests of solids from Tank SY-102 (Winters 1995) and C-107[9],[(a)] the supernate above the settling slurry is relatively clear. The maximum rate at which the supernate/slurry interface moves downward provides an indication of the settling velocities of the smallest particles, or smallest flocs within the slurry. The unhindered settling velocity for a sphere in a viscous liquid is given by Stokes' law:

$$v = \frac{2}{9} \frac{R^2(\Delta\rho)g}{\mu} \qquad (3.7)$$

where v = particle settling velocity, m/s
R = particle radius, m
$\Delta\rho$ = density difference between particle and fluid, kg/m^3
g = gravitational acceleration, 9.8 m/s^2
μ = fluid viscosity, Pa-sec

Winters (1995) reports the maximum settling velocity for a 2:1 dilution of SY-102 solids with water was 0.42 cm/h. Assuming an effective settling particle density of roughly 2500 kg/m^3 [2.5 g/cm^3], ($\Delta\rho$ = 1500 kg/m^3), and a fluid viscosity of 1.1 cP (based on supernate salt concentration measurements provided by Winters), the particle diameter corresponding to a settling velocity of 0.42 cm/h is about 1.3 microns.

However, Equation 3.7 applies only to relatively dilute particle suspensions in which the settling rate is controlled by the interaction between the particle and the surrounding fluid. In more concentrated suspensions, the interactions between particles can significantly decrease the observed settling rate. This is relevant because the SY-102 settling velocity data presented by Winters were obtained from a concentrated suspension. The 2:1 dilution of SY-102 solids had a density of 1290 kg/m^3, 36.5 wt% solids, and an apparent viscosity at low shear rates of about 10 to 15 cP. At such a high solids concentration the settling is expected to be much slower than that observed in more dilute suspensions. It has been observed that settling velocities for C-107 solids exhibit unhindered settling only for slurry concentrations less than about 15 wt%. Thus, the SY-102 settling velocity data are not expected to be representative of unhindered settling and the Stokes' law equation does not apply. Because of this conclusion, the 1.3 micron particle/floc size estimated by Stokes' law may be much smaller than the actual particle/floc size.

The maximum settling velocities for C-107 solids thus far observed have been on the order of 5-15 cm/h, which is much faster than the SY-102 solids in hindered settling. The C-107 solids were settled at much lower concentrations ranging from 4.5 wt% to about 10 wt%. The solids were washed with inhibited water and allowed to settle, so the salt concentration used was relatively low (about

---

(a) Brooks, K.P., J.R. Phillips, R.L. Myers, K.G. Rappe, D.R. Rector, and P.A. Smith. "Sludge Pretreatment Studies Using Hanford Tank C-107." Letter Report to WHC, September 1996, Pacific Northwest National Laboratory, Richland, Washington.

0.021 M). Under these conditions the initial interface settling rate was about 15 cm/h when the initial solids concentration was 4.5 wt%. Using a particle density of 2500 kg/m^3 and a supernate viscosity of 0.55 cP (the test was run at 50°C), Stokes' law (Eq. 3.7) implies an effective particle/floc diameter of about 5.3 microns.

The interface settling rate provides an estimate of the settling velocities of the *smallest* particles/flocs in the suspension. Thus, the particles/flocs of the C-107 solids settling in inhibited water are expected to be *larger* than about 5 microns. Because the number-average particle size of the C-107 solids has been measured at about 0.6 microns,[a] it is clear that flocculation is occurring in the C-107 slurry even at the relatively low salt concentration of inhibited water.

Because the settling velocity data imply that even the smallest of the settling particles/flocs are considerably larger than 1 micron, it is reasonable to conclude the sub-micron particles are flocculating along with the larger particles and settling as flocs with an effective (aerodynamic) diameter of 5 to 10 microns or more.

It is possible the small particles flocculate with both each other and the larger particles, and are protected from disrupting forces by the structure of the larger particles in the floc. Alternatively, the Hamaker constant and surface charge used to develop the DLVO interaction potential curves may be overly conservative. Regardless, it appears reasonable to conclude that particle flocculation takes place at salt concentrations on the order of 0.1 M and higher. If slurries containing sufficient salt are allowed to settle, rapid flocculation is expected to prevent the segregation of particles, according to their individual settling velocities.

(a) Brooks, K.P., J.R. Phillips, R.L. Myers, K.G. Rappe, D.R. Rector, and P.A. Smith. "Sludge Pretreatment Studies Using Hanford Tank C-107." Letter Report to WHC, September 1996, Pacific Northwest National Laboratory, Richland, Washington.

4.0 Segregation Processes

This chapter evaluates processes that could potentially segregate and concentrate fissile material within sludge during retrieval. Although strong evidence presented in Chapter 3 indicated the primary sludge particles are submicron, this chapter begins with an assumption that the primary sludge particle size distributions are accurately represented by light scattering measurements. Section 4.1 describes the results of simple 1-dimensional calculations of settling. Section 4.2 provides the results of 3-dimensional fluid dynamic models using the TEMPEST code. Section 4.3 reports the observations of segregation which occurred during testing of a 1/12-scale mixer pump using a waste simulant. Finally, Section 4.4 examines literature related to segregations achieved in the mineral processing industry and evaluates the applicability of the mechanisms to tank waste during retrieval.

4.1 Scoping Results for Stagnant Settling Case

This section provides results based on a simplified 1-dimensional analytical model. The conceptual model is based on a double-shell tank (DST) that initially contains a uniformly mixed slurry and is then allowed to settle under stagnant conditions. It is assumed the fissile material exists as discrete particles rather than within particles of mixed composition. If the fissile material can be shown to exist within particles of mixed composition that include large amounts of neutron absorbers, fluid dynamic segregation calculations may be unnecessary.

The stagnant settling scenario could not result in a criticality because it results in a uniform distribution across the floor of the tank. No single tank has sufficient fissile content to exceed an areal concentration of 2583 g/m^2 (240 g/ft^2) Pu-239 which is the minimum areal concentration required to achieve criticality (Bratzel et al.1996 and Waltar et al. 1996). Formation of a uniform layer within a 75-ft diameter DST would require 1060 kg of Pu-239. The total inventory in SY-102 is estimated at <42 kg (Tusler 1995) while the inventory of C-106 may be as high as 100 kg (WHC 1995).

However, the results provide some insight into the extent of segregation that might occur under differential settling (segregation) conditions. For example, while the larger particles settle faster and would be expected to be more concentrated near the bottom of a settled layer, each layer deposited has a distribution of particles which include a variety of sizes and densities. This distribution of sizes and densities in the settled layer will tend to limit the degree to which fissile material may concentrate.

4.1.1 Simplified Sedimentation Model

Conceptually, a DST containing a uniform slurry is allowed to settle under stagnant conditions and the compositions of the layers deposited are determined. The particles settle at their terminal settling

velocity as calculated based on Stokes' Law (see Appendix B, Equation B.5). If the particle Reynolds number exceeds 2, the friction factor is set equal to the following (Bird et al. 1960):

$$f = \frac{18.5}{N_{Re}^{\frac{3}{5}}} = \frac{18.5\mu^{\frac{3}{5}}}{(\rho D_p w)^{\frac{3}{5}}} \qquad (4.1)$$

where N_{re} = particle Reynolds number
μ = dynamic viscosity
ρ = fluid density
D_p = particle diameter
w = settling velocity.

Equation 4.1 is needed only for calculation of the settling velocities of the largest particulates in the SY-102 particle size distribution and for bounding sensitivity cases where the PuO_2 is set at the largest size. Thus, the calculated results are not sensitive to the selection of viscosity because within the Stokes' Law regime, the velocity of all particles is inversely proportional to the viscosity.

The individual particles within the model settle until they reach the tank floor. The particles striking the floor over a given time increment are determined and the composition of the material is taken to represent the composition of a settled layer of sediment. The model does not calculate the accumulation of sediment but rather determines when various particles reach the floor over time. The maximum fissile content of any layer of deposited sediment (expressed as mass fraction of solids) is then divided by the initial fissile content of the uniform slurry (also expressed as mass fraction of solids) to determine a factor increase in fissile concentration. Only the composition of the settled sludge is considered, not the degree of consolidation of the sludge layer.

Initially, no hindered settling effects are considered. However, calculations including hindered settling effects are included in Section 4.1.2.2. Particle agglomeration is not explicitly considered in the model although the agglomeration behavior discussed in Chapter 3 is important for interpreting the results.

The uniform slurry is assigned a particle size distribution based on analysis of SY-102 or C-106 sludge samples as documented by DiCenso et al. (1995), Castaing (1994), or Weiss (WHC 1993a). Core samples of Tank SY-102 were taken in 1988 (Scheele and Petersen 1989) and 1990, and a supernatant sample was taken in 1994. No particle size distribution data were obtained from the 1990 core. Thus, the particle size distribution was taken from the 1988 sample. The particle size distribution was measured on the lower core segment (segment 102-SY-4B) which does not include the region of the core containing solids high in Pu-239. Therefore, the particle size distribution does not include the high

Pu-239 solids; it is not known whether the particle size distribution of the solids high in Pu-239 is similar to that measured. However, the particle size distribution was used for the current calculation.

The C-106 particle size distributions used for this analysis were taken from measurements made in 1977 as reported by Castaing (1994) and subsequent data collected by Weiss on a 1986 core (WHC 1993a). The 1986 sample was a composite sample of the entire core. Little is known about the specifics of the measurement technique and sample preparation. It is suspected the larger particles in the distribution may actually be agglomerates of smaller particles. However, the measured size distributions are used for the current calculations. The particle size distributions used for the modeling are provided in Table 4.1.

In all cases, the fluid density was set to 1.0 g/cm^3 with a viscosity of 1.0 cP. Iron was assumed to exist as hematite with a density of 5.26 g/cm^3 and aluminum was assumed to exist as gibbsite with a density of 2.4 g/cm^3. The amount of iron and aluminum in the sludge was based on waste characterization data (Castaing 1994, DiCenso et al. 1995). All other sludge components were arbitrarily assigned a

Table 4.1 Particle Size Volume Distributions Used in Modeling

C-106 (Castaing 1994)		C-106 (WHC 1993a)		SY-102 (DiCenso et al. 1995)	
Size, µm	Volume %	Size, µm	Volume %	Size, µm	Volume %
52.5	6.1	90	0.49	137.5	2.5
47.5	7.4	80	0.68	80	25
42.5	10.8	67	0.49	55	31
37.5	8	58	0.00	45	18
32.5	0.8	49	0.49	35	7
27.5	4	41	0.98	25	9
22.5	12	35	1.96	15	8
17.5	5	29	4.01	7.5	0.5
12.5	11	26	5.87		
7.5	36	21	8.31		
		18	11.24		
		15	13.49		
		13	18.87		
		11	14.37		
		9	10.26		
		7.8	3.42		
		6.5	2.54		
		5.5	2.54		

density of 2.0 g/cm^3, believed to be conservatively on the low side. The PuO_2 was assigned a density of either 11.4 or 6.0 g/cm^3. The density of 11.4 corresponds to crystalline PuO_2. In an aqueous environment, the density of hydrous, less crystalline PuO_2 may be lower than 11.4 due to waters of hydration and some crystal disordering. Although definitive data are not available, it is the opinion of chemists who have worked with freshly-precipitated PuO_2 that the particle density is about 6 g/cm^3. The amount of plutonium assumed for C-106 simulations was set at 0.132 g/l sludge in C-106, corresponding to a conservative 100 kg inventory. For SY-102, a concentration of 0.154 g/l is taken based on an inventory of 41.4 kg plutonium and 71000 gallons of sludge (WHC 1995). These initial concentrations have little effect on the calculation of the degree of segregation but do influence the impact of a given degree of segregation.

The particle volume within the distributions in Table 4.1 were assigned identities based on sludge composition. No data on variations of sludge composition with particle size are available. Therefore, except where noted, the iron, aluminum, and *other* components were assumed to exist uniformly through out the entire size distribution. The plutonium was distributed uniformly across the size distribution for some cases and given a fixed size in other cases. Iron, aluminum and PuO_2 were explicitly tracked with their own densities within the calculation with all other sludge components being grouped into the category *other*. Thus, using the Weiss particle size distribution, the problem becomes one of tracking (18 sizes)(4 densities) = 72 different types of particles, each with its own concentration determined from characterization data, as they settle to the floor of the tank.

4.1.2 Simulation Results

The results of the simulations are summarized in Table 4.2. The factor increase represents the maximum increase in mass fraction PuO_2 (based on solids only) for any sediment layer within the sludge solids for the conditions shown. A value of "5.7" in Table 4.2 indicates the mass fraction of PuO_2 has increased by a factor of 5.7 compared to the initially uniform slurry.

4.1.2.1 Bounding Sensitivity Analysis

Additional bounding cases were calculated in which the PuO_2 is assigned the largest particle size within the sludge distribution. This case provides the greatest potential for segregation to the bottom of the sediment layer. These cases are not considered to be realistic in that plutonium oxide particulate would be expected to be small with an upper bounding size in the <2 to 8 micron range (see Section 2.2.5). These bounding cases are provided to indicate the sensitivity of the results to the establishment of the upper bound of <2 to 8 microns on the plutonium particulate. Table 4.3 presents the results for each of the three particle size distributions.

For the C-106 particle size distribution in Castaing (1994), the calculated enrichment factors indicate that even under bounding assumptions the fissile concentration just reaches the conservative waste model limit of 2.6 g/l of Pu needed to attain criticality (see Rogers 1993 for derivation of this value). In the case of the Weiss (WHC 1993a) particle size distribution though, the enrichment factor of 93.9 indicates

Table 4.2. Maximum Factor Increases in PuO_2 Mass Fraction in Sediment Layer

	Maximum Increase in Sediment PuO_2 Mass Fraction	
Plutonium Distribution	PuO_2 density = 11.4 g/cm^3	PuO_2 density = 6.0 g/cm^3
C-106 (particle size distribution from Castaing 1994)		
Uniform over all sizes	5.7	2.7
Monodisperse, 17.5 μm	4.1	6.6
Monodisperse, 7.5 μm	6.5	5.3
C-106 (particle size distribution by Weiss WHC 1993a)		
Uniform over all sizes	5.5	2.7
Monodisperse, 21.5 μm	9.3	5.5
Monodisperse, 5.5 μm	3.4	8.0
SY-102 (particle size distribution from DiCenso et al. 1995).		
Uniform over all sizes	7.5	3.9
Monodisperse, 15 μm	5.2	14.4
Monodisperse, 7.5 μm	32.1	19.3

Table 4.3. Bounding Sensitivity Cases for Maximum PuO_2 Particle Size

	Maximum Increase in Sediment PuO_2 Mass Fraction	
Plutonium Distribution	PuO_2 density = 11.4 g/cm^3	PuO_2 density = 6.0 g/cm^3
C-106 (52.5 μm PuO_2, particle size distribution from Castaing 1994)		
Monodisperse, 52.5 μm	19.8	9.6
C-106 (90.0 μm PuO_2, particle size distribution by Weiss WHC 1993a)		
Monodisperse, 21.5 μm	93.9	55.3
SY-102 (137.5 μm PuO_2, particle size distribution from DiCenso et al. 1995)		
Monodisperse, 15 μm	25.7	15.2

a Pu concentration in the settled sludge bottom layer of 12.4 g/l. This concentration would be worrisome, if it actually were to occur. Although it is not considered likely that PuO_2 particles would reach 90 μm, let alone be exclusively 90 μm, the case points out the importance of establishing a 10-20 micron upper bound on PuO_2 size or smaller as argued in Section 2.2.5. In the case of SY-102, the degree of concentration is less severe, due to the greater quantity of larger particle sizes (the assumed neutron absorbers) within the sludge particle-size distribution.

4.1.2.2 Hindered Settling Effect

In the modeling described up to this point, the settling velocity of particles is not dependent on the local concentration of suspended solids. However, at high solids concentrations the settling velocities of particles are slowed (see Appendix B for more discussion). Calculations were performed to determine if hindered settling could have a significant effect on the degree of segregation described in Section 4.1.2.1. The results indicate that a hindered settling model has very little impact on the degree of segregation predicted. The hindered settling model (see Appendix B):

$$w = w_0 (1-C)^{4.7} \tag{4.2}$$

where w = hindered fall velocity
w_0 = non-hindered fall velocity
C = volume fraction solids.

Due to the dependence on local concentration, the problem requires more highly intensive calculations than for the non-hindered settling case discussed in Section 4.1.2.1. The problem differs slightly in configuration from the earlier model in that it does simulate the formation and consolidation of the settled layer of solids. Thus, the distances of fall are slightly different for different particles, depending on where in the bed they settle. Because of this difference, it is not expected that the hindered and non-hindered cases would agree exactly, even with no effect of hindering on segregation. However, the models are sufficiently similar to determine if the hindered settling model has a significant effect on the degree of segregation.

The model described in Section 4.1.1 was applied and compared to results obtained using the hindered settling model. Both simulations used the C-106, Castaing particle size distribution. Instead of placing all materials uniformly across the distribution, the material identities of the particle size distribution were assigned as follows:

PuO_2 was assigned a particle size of 10 μm.
Hematite was assigned particle size of 7.5 μm.
Gibbsite was assigned particle sizes of 7.5, 12.5, 17.5, and 22.5 μm.
Other was assigned particle sizes of 22.5 μm through 52.5 μm.

This method of assigning compositions reduces the number of different particle types to be tracked. Although this distribution of composition may not accurately represent the sludge, the importance of this model is to look for differences between the results calculated for the hindered and non-hindered models. The results were calculated not only for the PuO_2 particle, but also for each of the other particles in the problem. As seen in Table 4.4, the degree of segregation does not appear greatly influenced by the presence of the hindered settling effect. The degree of difference between results may be due to differences in the model configurations or to a very small effect of the hindered settling on the results. However, it is clear the hindered settling does not have a significant effect on segregation.

4.1.2.3 Interpretation of Results from 1-Dimensional Settling Calculations

The conservative waste model developed by Rogers (1993) describes a sludge that is at least as neutronically reactive as any known tank sludge composition. A safe Pu concentration of 2.6 g/l has been established for the conservative waste model sludge for a sludge of infinite extent and optimal water moderation. Thus, for Tank C-106, the initial concentration of 0.132 g/l must be concentrated by a factor of 20 to reach 2.6 g/l Pu content. For any factor less than 20, the plutonium-concentrated sludge could not be made critical even if collected in large masses. In all of the cases evaluated, no sediment layer exceeded an increase in concentration of a factor of 10. This increase leaves a safety factor of 2 and indicates it would be extremely difficult to reach a Pu concentration sufficient to reach criticality.

Table 4.4. Factor Increase in Mass Fraction Solids Concentration for Various Particles With and Without the Effect of Hindered Settling

Composition	Size, μm	Non-Hindered	Hindered
Other[a]	52.5	3.9	4.2
Other	47.5	3.9	3.0
Other	42.5	4.1	3.4
Other	37.5	4.7	4.7
Other	32.5	5.4	6.7
Other	27.5	4.0	5.5
Other	22.5	3.8	5.1
$Al(OH)_3$	22.5	3.3	3.7
$Al(OH)_3$	17.5	3.8	4.0
$Al(OH)_3$	12.5	3.0	3.5
PuO2	10	5.3	6.7
$Al(OH)_3$	7.5	2.6	3.7
Fe_2O_3	7.5	4.0	3.9

(a) Other represents all sludge components except iron, aluminum, and plutonium compounds and is calculated with a particle density of 2.0 g/cm^3.

The SY-102 model assumes a concentration of 0.154 g/l initially so that concentration by a factor of 17 is needed to reach the 2.6 g/l level. If Pu is assumed to be evenly distributed over all size ranges, this waste also has a safety factor of 2 between the minimum safe concentration and the maximum calculated Pu sediment concentration after preferential settling. However, the particle size distribution of SY-102 is much different than C-106 in that 83.5% of the solids volume is associated with particles 35 μm or greater in diameter. Thus, when the plutonium is assumed to be 15 or 7.5 microns, the calculations indicate the fissile material concentrates substantially in the upper levels of the sludge. For the monodisperse 15 μm PuO_2 particle, the concentration reaches 2.2 g/l which is close to the safe limit for an infinite mass of sludge. This concentrated layer contains 7.7% of the plutonium with only 0.5 wt% of the sludge. About 9.9% of the solids settle on top of this layer.

For a PuO_2 particle of 7.5 μm (the smallest SY-102 particulate in the measured distribution), the concentration factors are sufficient to exceed the 2.6 g/l safe level for infinite geometry, providing Pu concentrations of 4.9 and 3.0 g/l for PuO_2 densities of 11.4 and 6 g/cm^3, respectively. In the case of the 11.4 g/cm^3 PuO_2 material, the high concentration sediment layer contains 3% of the PuO_2 along with 0.1 wt% of the sludge. About 4.9% of the solids settle on top of this layer. In the case of the 6 g/cm^3 PuO_2 material, the high concentration sediment layer contains 7.7% of the PuO_2, along with 0.4 wt% of the sludge. Thus, it is possible to exceed the infinite safe limit in thin layers within the sediment. However, the 2583 g/m^2 (240 g/ft^2) areal limit still applies, so that regardless of the degree of concentration in any layer of sediment, criticality is not possible as long as the sludge settles into flat, uniform layers. This type of settling is expected for the slow settling materials that concentrate in the upper regions of the sludge. Also, the regions that exceed the safe limit for the 7.5 μm PuO_2 particles contain only 3%, or 7.7% of the PuO_2, dependent upon the assumed particle density of PuO_2 material, which corresponds to only 1.24 kg Pu at 4.9 g/l and 3.19 kg Pu at 3.0 g/l, respectively. The critical mass of Pu needed for 4 g/l and 10 g/l Pu concentrations in the conservative waste (sludge) model are 108 kg and 3.0 kg, respectively. Thus, even if the highest concentration layer were selectively collected from around the tank and dried to optimal water content, the layer still would not be sufficient to reach criticality.

Finally, particle flocculation is expected to interfere with segregation due to settling. If PuO_2 particles flocculate, the fluid dynamic properties of the flocs will not be significantly different than other flocs around them and the settling will not favor any particular material. Calculations indicate that 10 μm particles would be agglomerated at the conditions expected within the tanks. Sludge settling tests indicate that no particles settle at velocities representative of submicron-sized particles, indicating that flocculation is occurring among submicron particles (see Chapter 3). Thus, for particles of 10 μm or less flocculation is expected. The maximum plutonium particle size is expected to be on the order of <2 to 8 microns (Section 2.2.5).

The results of the 1-D models indicate that if the upper bound for Pu particle size is 10-20 μm or less, it is extremely unlikely that segregation sufficient to achieve criticality will occur. However, this 1-D model is not sufficient by itself because it cannot address 3-dimensional concerns that material might be selectively deposited in a localized area by fluid movements within the tank. This selective deposition is addressed by TEMPEST modeling presented in Section 4.2. Also, the 1-D model cannot

address processes where the transient settling behavior is important. These issues are addressed by examining mineral separation processes from the mining industry (see Section 4.4).

4.2 Three-Dimensional Fluid Dynamic Modeling with the TEMPEST Code

This section describes the 3-dimensional modeling efforts with the TEMPEST code (Trent and Eyler 1993, and Onishi et al. 1995). The modeling is an attempt to bound the magnitude of particle segregation that might occur when the contents in Hanford tanks are disturbed by input of kinetic energy during sludge retrieval.

The TEMPEST code was used to investigate the potential extent of particle segregation that might occur during operation of mixer pumps or during sluicing retrieval. The TEMPEST code and our conceptual model account for various physical properties and rheology correlations for non-Newtonian flow and hindered particle settling to reproduce the potential behavior of Hanford tank wastes. Model parameters for the tank waste transport modeling include viscosity, particle settling velocities, and yield/shear stress. The way the current version of TEMPEST handles the yield stress has a limitation: it cannot keep sludge that should not move stationary for an extended time.

The particle size distribution in each TEMPEST simulation is represented by either 7 or 9 discrete particle sizes. These sizes were selected to match the particle size distributions, based on available light scattering data for solids in Tanks SY-102 (DiCenso et al. 1995) and C-106 (see Castaing 1994 for available data). As discussed in Chapter 3, these particle size distributions actually represent heterogeneous agglomerates; plutonium probably does not exist as pure discrete particles. However, evaluation of the modeling results, as if the plutonium exists at a given size and density, enhances the defense in depth approach. All of the reported progress represents the first 10s of minutes to 1.5 hours for sluicing of Tank C-106, settling of the sluiced solids into the receiver Tank AY-102, and solids mixing with the jet-pump in Tank SY-102. The degree of solids segregation in these three computer exercises may not be at steady-state, so the final results may differ from these preliminary results. However, it is expected additional calculations would not dramatically change the conclusions presented. Modeling for long time periods is difficult because up to 24 hours of computer CPU time to model just 1 to 3 minutes of real time in the tanks where complicated fluid dynamics are occurring.

4.2.1 Summary of TEMPEST Features

A general literature review into the fluid dynamic processes that could promote segregation is presented in Appendix B. This section describes the features contained within the TEMPEST fluid dynamic model (Section 4.2.1.1) and provides a comparison of input data to actual tank waste properties (Section 4.2.1.2).

4.2.1.1 TEMPEST Fluid Dynamic Model

The TEMPEST code has a variety of options for simulating fluid dynamic problems. The TEMPEST code (Version T.2.10c) as implemented for the simulations described in Section 4.2 provides a simulation of an isothermal, incompressible flow in which the density and viscosity are influenced by the concentration of suspended particulates. Implicit within the TEMPEST model is the assumption the Boussinesq condition is applicable. The assumptions and complete equations for conservation of mass and momentum and for treatment of turbulence are documented in Trent and Eyler (1989). This section provides an overview of the fluid dynamic model as implemented in TEMPEST.

Turbulent flow Reynolds stresses are modeled through an effective viscosity. The Prandtl-Kolmogrov hypothesis is used to relate the effective viscosity to a velocity and a length scale. In this approach, transport equations for the turbulent kinetic energy (k) and the dissipation of turbulent kinetic energy (ϵ) are solved by the k-ϵ model to determine the effective turbulent (eddy) viscosity as:

$$\mu_T = C_\mu \rho k^2/\epsilon \tag{4.3}$$

where C_μ = constant equal to 0.09
ρ = fluid density
k = turbulent kinetic energy
ϵ = dissipation of turbulent kinetic energy.

The base fluid density and molecular viscosity are the same as those of water at 37°C for all TEMPEST code calculations for Tanks C-106 and AY-102. For the TEMPEST calculations for Tank SY-102, a measured value for the fluid density (1.03 g/cm^3 from DiCenso et al. 1995) and the estimated molecular viscosity of the supernate of 1 cp (see Onishi and Hudson 1996) were used for the base fluid.

The slurry molecular viscosity is then calculated by multiplying the molecular viscosity of the base fluid by a factor of a raised to the power β:

$$\mu = \mu_o a^\beta \tag{4.4}$$

where μ_o = base fluid viscosity = 0.69 cP (C-106, AY-102) or 1.0 cP (SY-102)
a = 105,000 (4,500,000 in some cases)
β = C_v/C_{vmax}
C_v = volume fraction solids in slurry
C_{vmax} = 0.46 (0.53 in some cases).

For some SY-102 tank simulations, values of a and C_{vmax} were selected to be 4,500,000 and 0.53, respectively, based on limited SY-102 sludge data (DiCenso et al. 1995). The a value of 4,500,000 was obtained as the ratio of the largest recently measured SY-102 sludge viscosity of approximately 4,500 Pa-s to the supernate viscosity of 1 cP. The variations of viscosity with the solid fraction for these two cases

is shown in Figures 4.1 and 4.2. The form of this equation was selected in a previous effort to model the periodic rollover and gas release processes in Tank SY-101 (Trent and Michener 1993). The value of a is determined by dividing a high viscosity intended to represent a very high solids concentration by a viscosity typical of a more dilute slurry or supernatant. Reliable data on which to base the value of C_{vmax} are not available. To reliably set this parameter, accurate data are needed for the particle, bulk, and fluid densities for sludge. Although a significant amount of data of this type is available, its accuracy is in question. For example, Bratzel (1980) examined four analyses of C-106 tank sludge to assure measurements were using a consistent basis. The resulting (bulk density, particle density) data pairs in g/cm^3 were (1.22, 0.727), (1.324, 1.082), (1.579, 1.495), and (1.485, 1.140). In all cases, the particle density was less than the bulk density, [a physical impossibility for Hanford sludge], which casts serious doubt on the validity of the data. Due to the difficulty of obtaining a direct data basis for the value of C_{vmax}, the value of C_{vmax} was selected to be a reasonable value within the same range as values selected previously to model SY-101. Values of 0.46 and 0.53 were used for C_{vmax}. The previous SY-101 modeling effort produced results similar to observed tank phenomenon. Comparisons between TEMPEST model predictions and tank waste characterization data is provided in Section 4.2.1.2.

The calculated slurry molecular viscosity is used to calculate the fluid transport, but is not used to adjust the input settling velocity for each particle size used in the model. The impact of high solids concentrations on particle settling velocities is accounted for separately as follows.

The molecular viscosity of the slurry is added to the turbulent viscosity and the sum is used in fluid dynamic calculations.

Particle size distributions are represented using discrete particle sizes to represent portions of particle size distributions obtained from characterization of sludge samples using light scattering techniques. Currently, data from only two Hanford tanks is utilized; C-106 and SY-102 (Castaing 1994, DiCenso et al. 1995). As discussed in Chapter 3, these particle size distributions represent flocs of primarily submicron particulates. However, analyzing the segregation, assuming they represent discrete particles, is conservative and provides a defense in depth when determining the potential for criticality occurring during retrieval. Due to the lack of specific information on the density of different sized particles, all TEMPEST calculations for cases dealing with Tanks C-106 and AY-102 initially assume the particles have a uniform density of 2.44 g/cm^3, based on C-106 solids properties (DiCenso et al. 1995). For the TEMPEST calculations on Tank SY-102, a particle density of 1.80 g/cm^3 is used, based on DiCenso et al. (1995). However, the density of approximately 2.18 g/cm^3 is needed to match the measured bulk sludge density of 1.56 g/cm^3 with the solid fraction value reported by DiCenso et al. 1995, which is equivalent to C_{vmax} of 0.53. Thus, particle densities of 1.80 and 2.18 g/cm^3 are used for SY-102. Information is not available on the shape of different materials, so all particulates are assumed to be spherical. To some extent, the results for different assumptions for the particle size, density, and shape of a minor component can be evaluated by calculating the settling velocity and determining an equivalent diameter for that particle.

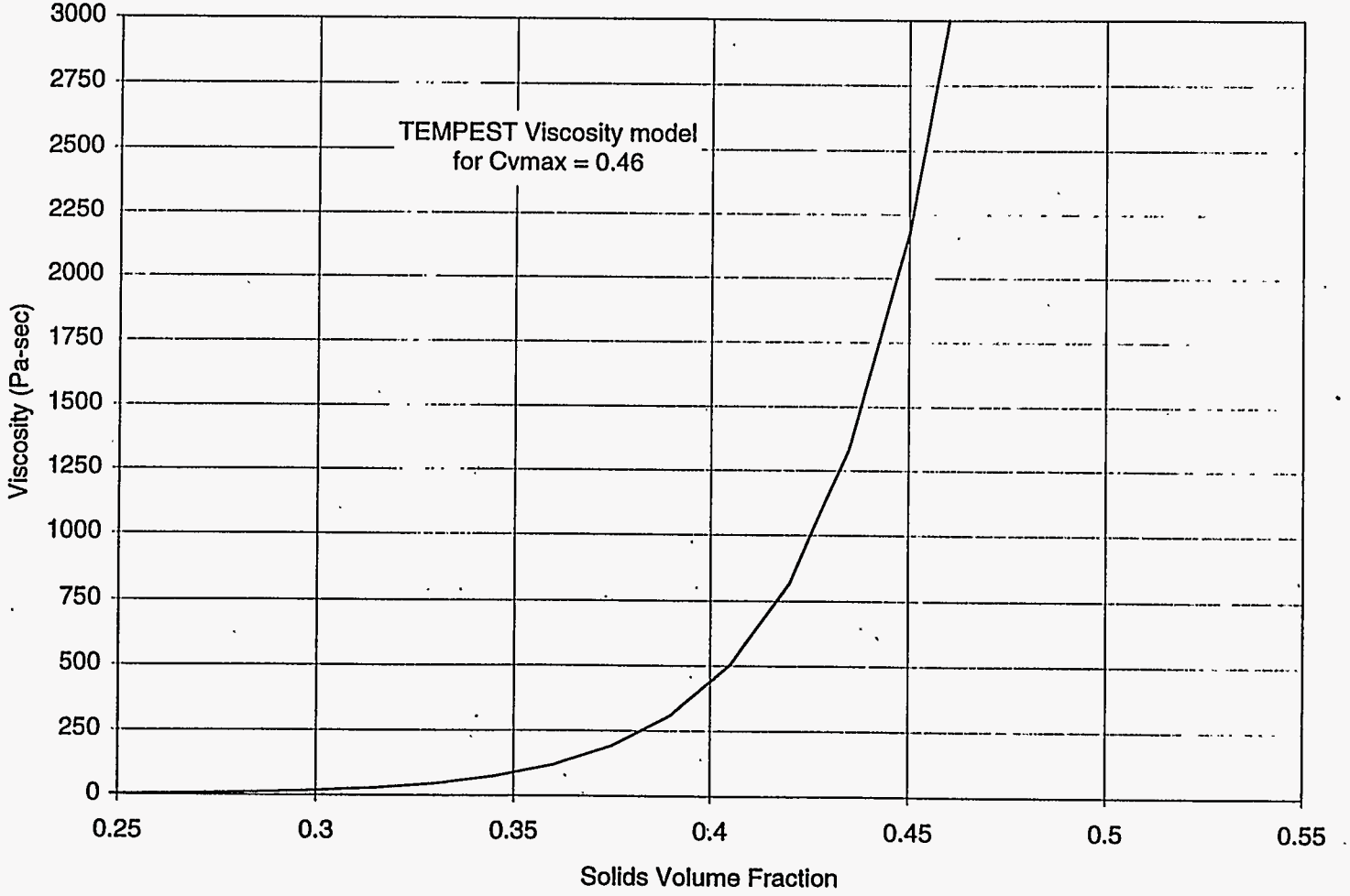

Figure 4.1. Variation of Viscosity with Solid Concentrations (C_{vmax} of 0.46)

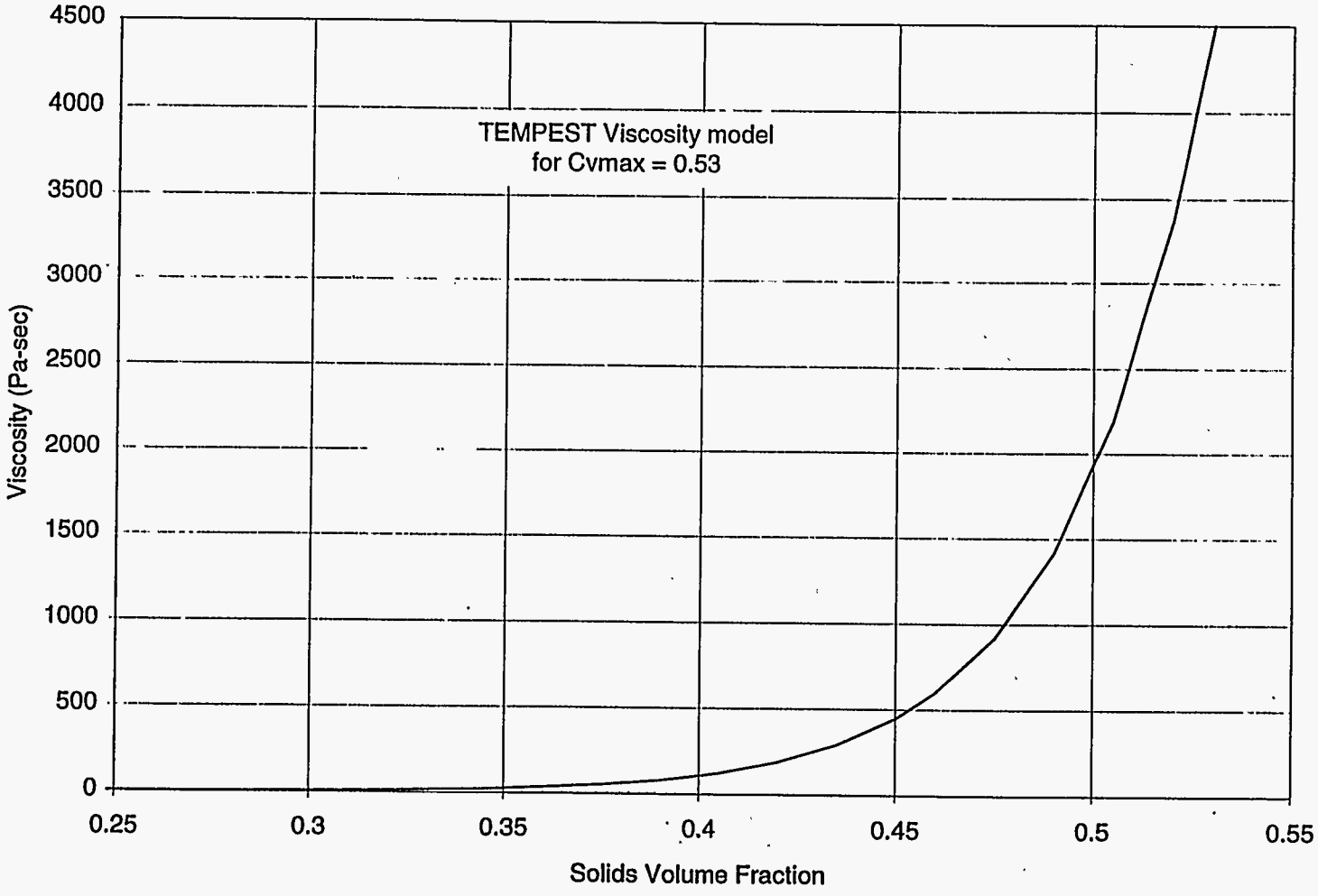

Figure 4.2. Variation of Viscosity with Solid Concentrations (C_{vmax} of 0.53)

The settling velocity of each particle is provided to the code in the form of a velocity that is calculated assuming spherical particles using Stokes' Law (Equation B.5). These input settling velocities do not include the effects of particle interaction, such as particle flocculation or agglomeration. Particle agglomeration is expected to occur and is discussed in some detail in Chapter 3. The TEMPEST model includes the effect of hindered settling. The input settling velocity of each particle is adjusted for the effects of hindered settling, based on an equation of the form

$$V_s = V_{so}(1-\beta)^b \tag{4.5}$$

where V_s = hindered settling velocity
V_{so} = input settling velocity (unhindered settling velocity)
β = C_v/C_{vmax}, with C_{vmax}=0.46 or 0.53
C_v = volume fraction solids in slurry
b = 6.0.

This correlation is discussed in Appendix B as Equation B.6. The value of b for the Stokes' Law settling region was provided in Table B.2 as 4.65. However, using this value resulted in unrealistic settling occurring on top of the existing settled sludge layers in the bottom of the tank in the AY-102 simulation. Therefore, a modification of Equation 4.5 was required. Because the value of C_{vmax} impacts the viscosity calculation (see Equation 4.4), it was decided to change the value of b instead to avoid affecting the viscosity. Setting b to a value of 6.0 increased the hindering effect and prevented the unrealistic settling within the sludge layer. This value of 6.0 was used for all simulations reported in Section 4.2. A check was made to ensure that the potential error introduced into the settling results would not be unacceptable. This check is discussed in Section 4.2.4.

In some, but not all, TEMPEST simulations, a yield stress was introduced into the rheology model. The inclusion of the yield stress model is identified where applicable when results are presented in Section 4.2. The expression used to calculate the yield stress is:

$$\tau_{yield} = b_1\beta^{b_3}\left(\frac{1 - e^{-b_2\dot{\gamma}}}{b_2\dot{\gamma} + \epsilon}\right)(1-\alpha) \tag{4.6}$$

where τ_{yield} = calculated yield stress
b_1 = yield stress = 1.5 psi
b_2 = strain coefficient = 50, dimensionless
b_3 = moisture exponent = 25, dimensionless
β = C_v/C_{vmax}
$\dot{\gamma}$ = strain rate of fluid
ϵ = a small constant set at 1E-30
α = volume fraction gas which is set to zero for all simulations.

The calculated yield stress is added to the stress imparted by the viscosity in response to fluid shear. This yield stress formulation has been implemented with only limited success in the past and the validity of the results it produces is uncertain. However, simulations were performed with and without the presence of the yield stress to evaluate the effect on results. The comparison of the simulation results with and without yield stress indicated the inclusion of yield stress in the model did not have a large effect on particle segregation.

While TEMPEST has the capability to model diffusive effects on solutes and particles, the input was intentionally selected to eliminate diffusive effects.

4.2.1.1.2 Limitations of the TEMPEST Model. Within TEMPEST, the suspended particles settle relative to the base fluid due to gravity. The particle settling velocity is adjusted to account for hindered settling but otherwise the particles neither accelerate nor decelerate relative to the base fluid, so the velocity remains constant. The momentum of the particles is not included in the model. As a result, if settling velocities were neglected, particles will tend to follow the streamlines even through sudden changes in direction. Several mechanisms that are useful in mineral processing cannot be simulated using TEMPEST. These mechanisms include film concentration, differential acceleration, Bagnold forces, flotation, and interstitial trickling. A discussion of mechanisms which are exploited in the mineral processing industry to achieve separations is included in Section 4.4.

4.2.1.2 Comparison of Input Data and Tank Waste Characterization Data

In many cases, no rheological information exists for a tank sludge of interest. The slurried tank sludge viscosity data that do exist typically include information for one or two solids concentrations. Therefore, a fluid dynamic model, as was described in Section 4.2.1.1, is needed to estimate properties in a continuous manner for sludge concentrations for which data do not exist. However, it is important to assure the predictions of physical properties used within the model are comparable to tank waste data, where data exist. This section explores the degree to which the fluid property values within the model agree with measurements on actual tank waste.

4.2.1.2.1 Viscosity. For the majority of the regions within the TEMPEST simulations that have been calculated, the turbulent viscosity is much greater than the molecular viscosity after adjustment for the solids content. Thus, after these two values are added together within the model, the molecular viscosity has little effect on the calculated results for these regions. The molecular viscosity input values and viscosity model predictions become important in the areas of the simulation where velocities are low and solids concentrations are high. The low velocities reduce the magnitude of the turbulent viscosity and the high solids content increases the fluid molecular viscosity.

The value of a in Equation 4.4 (105,000) was arrived at by dividing a viscosity of 2500 Pa-s, taken to be a value for a very high solids content slurry, by the viscosity of 0.024 Pa-s which is representative of a relatively dilute slurry. Willingham (1994) surveyed data on tank sludges, slurries, and supernatants and found sludge viscosities in the range of 30 to 1,800 Pa-s with occasional high values exceeding this

range. Thus, the high end viscosity of 2500 Pa-s appears a reasonable value for a consolidated sludge. Similarly, values for slurries typically range from 0.010 to 0.070 Pa-s, which is consistent with the lower value of 0.024 Pa-s. Near the end of this study, viscosity of the SY-102 sludge was measured. The measured viscosity of the sludge, which is estimated to have a volume fraction of 0.53, varies widely from about 10 Pa-s to 4500 Pa-s, depending on the strain rate. The SY-102 supernate viscosity was estimated at approximately 1 cP (Onishi and Hudson 1996). Thus, as stated previously, values of a and C_{vmax} were selected to be 4,500,000 and 0.53, respectively, in some SY-102 modeling.

The predictions of the viscosity model can be checked against characterization data for sludge from SY-102. The TEMPEST SY-102 mixer pump model simulates an approximate 3:1 dilution of the settled sludge with supernatant liquid (3 parts supernatant liquid to 1 part sludge). Actual characterization data for a 1:1 and 2:1 dilutions of SY-102 sludge with water indicate the slurry exhibits no yield stress and fits a pseudoplastic model (DiCenso et al. 1995). The viscosity model used in TEMPEST is not pseudo-plastic, so the viscosity is not shear dependent (as long as a yield stress is not specified). Comparison between the data and the model is made by using the data-derived model to calculate the apparent viscosity for a range of observed shear rates from the TEMPEST model for 1 mixer pump operating in the center of the tank. The solids content for the TEMPEST model was determined by assuming the initial sludge layer had a volume fraction solids of 0.45, just below the maximum value of 0.46. This concentration is then diluted 3:1 with supernatant as the model executes. The comparison is shown graphically in Figure 4.3. The range of shear rates observed within a single cross section of the tank, which does not include the jet, was 0.06 to 0.84 s^{-1}. Because the mixer pump problem includes relatively high shear rates, values for lower shear rates are also included in Figure 4.3.

Comparison of the TEMPEST predictions for the 1:1 dilution indicate the TEMPEST model appears somewhat more sensitive to increasing concentration than the available 102-SY characterization data indicates. The discrepancy is larger at high shear rates and less at lower shear rates. The data for the 2:1 dilution appear to be fairly well approximated with the model slightly over-predicting at high shear and under-predicting at low shear. Thus, while the viscosities of the fully mixed tank may be very close to data based predictions, the viscosity in high concentration, high shear regions would be higher than would be indicated by data for SY-102. The differences in viscosity, between TEMPEST predictions and actual data, in high shear regions has little impact on the particle segregation predictions in Section 4.2 because the turbulent viscosity tends to dominate in these regions.

4.2.1.2.2 Yield Stress. The yield stress model within TEMPEST contains several parameters. The parameter b_2 (strain coefficient) is primarily concerned with allowing an exponential to function in place of the discontinuous Bingham model (see Section B.1.2.1). Thus, its value is not selected based on fluid dynamic properties. The parameters b_1 and b_3 (yield stress and moisture exponent, respectively) are not based on waste characterization data. They are taken directly from efforts to model the periodic rollover and gas release phenomenon occurring within the SY-101 sludge.

The yield stress model was implemented for a run of the AY-102 model. Examining the calculated yield stresses within the TEMPEST model, it appears the yield stress only becomes important within the

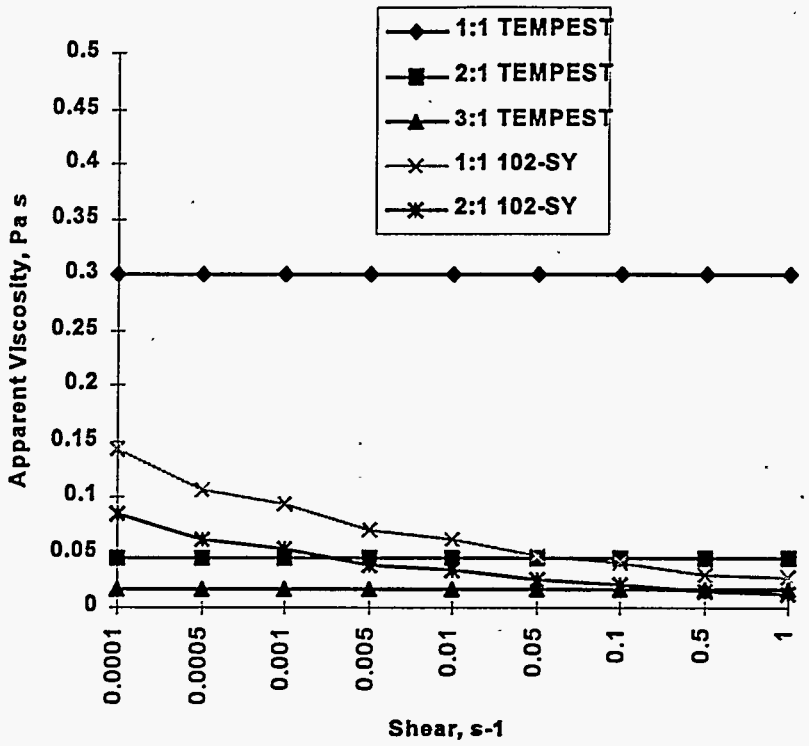

Figure 4.3. Comparison of TEMPEST Model Predictions and SY-102 Characterization Data for Various Water:Sludge Dilutions

bottom two cells of the problem containing the initial sludge layers where the solids concentrations are highest. In these areas, the yield stress that is added to the viscous stress reaches about 0.07 Pa at a volume fraction solids of 0.29. This total is somewhat smaller than the 4.7 Pa yield stress measured for a 1:1 dilution of AY-102 solids with a volume fraction solids estimated at 0.12. However, the measured value is uncertain because the characterization report does not provide any units on the yield stress, and it must be assumed the units are the commonly used Pa (WHC 1993b).

The validity of the TEMPEST yield model is uncertain. The users manual for the TEMPEST code notes, "The Bingham yield model is in development and testing and should be used with caution in the present version" (Eyler et al. 1993). The difficulty in modeling a yield stress using a Bingham yield model is the viscosity is predicted to go to infinity when the shear rate drops to zero. Also, a discontinuity appears at the point where the shear stress is equal to the yield stress (Mahoney and Trent 1995). The approach taken within TEMPEST to avoid these problems is to substitute a stiff exponential for the yield stress. In addition, the yield stress model used in TEMPEST incorporates a dependency on the solids concentration. The particulates in the colloidal size range have the greatest effect on yield stress, so that a simple correlation to volume fraction solids may not be sufficient to predict the yield stresses between different waste slurries.

The yield model was implemented for the AY-102 TEMPEST calculations presented in Section 4.2.4 in order to determine if unexpected behaviors might influence the segregation behavior. However, the yield model itself should not be considered an accurate representation of the yield behavior of the sludge. Although the cases have been calculated for investigative purposes, the development and validation of the TEMPEST yield model is beyond the scope of the current activity.

The conceptual model described here was implemented to calculate several specific problems that are described in this section (4.2).

4.2.2 Retrieval of Sluiced Solids from Tank C-106

The fate of sludge particles during these types of operations is being evaluated using TEMPEST runs on the C-106 sludge pump-out operation. The physical properties of the sludge waste used in the modeling are taken from Castaing (1994). Input data taken from this document include bulk density of the sludge at approximately 1.45 g/ml and a void volume of approximately 40% filled with interstitial solution. The particle density of the sludge was estimated at approximately 2.4 g/ml. The particle size distribution is shown in Table 4.5.

Table 4.5. Particle Size Distributions of Tank C-106 Sludge

Solid Size Fractions	Particle Sizes (μm)	Percent weight	Fall Velocity* (mm/s)
1	5 - 10	35	0.076
2	10 - 15	11	0.19
3	15 - 20	5	0.36
4	20 - 25	12	0.58
5	25 - 30	4	0.88
5	30 - 35	0.8	0.88
6	35 - 40	8	1.6
7	40 - 45	10.8	2.0
8	45 - 50	7.4	2.5
9	50 - 55	6	3.1
	Total	100	

*Unhindered fall velocity is input to the model assuming the fluid is pure water at 37°C. TEMPEST internally calculates hindered fall velocity for each particle size for the appropriate slurry conditions calculated at each node and time step.

The average particle size for this sludge sample, based on weight, is about 16 μm. The overlying supernate has a density of 1.03 g/ml. As discussed elsewhere in this report, a conservative estimate is that Pu-oxide particles have a particle density of 11.46 g/ml. Some chemists on the team have argued that the amorphous/hydrous Pu oxide has a particle density closer to 6 g/ml, although referenceable data have not been located. The settling velocity of the 11.46 g/ml (a conservative case) density particles with a conservative particle size of 10 μm is 0.83 mm/s in pure water at 37°C, which corresponds to the falling velocity of solid particles of Size Fraction 5 (see Table 4.5). The 6 g/ml particle density (perhaps a more realistic case) with a realistic particle size of 2 μm diameter has a fall velocity of 0.014 mm/s in pure water at 37°C. This realistic falling velocity is much smaller than those of solid particles of Size Fraction 1 in Table 4.5. Thus, the TEMPEST model results for Solids 5 and 1 can be regarded as representative of conservative and more realistic discrete Pu-bearing solid behavior in Hanford sludge. This viewpoint will be continued through the remaining discussion of the TEMPEST results.

A retrieval pump will withdraw the slurry generated by the sluicing operation at the rate of 300 gpm. The current plan is to dig a 3 feet deep and 5 feet diameter excavation or hole (well point) in Tank C-106 sludge, from which the slurry pump will extract the material and transfer it to Tank AY-102. The well point is simulated as a right-circular cylinder with a diameter of 5 feet and a height of 3 feet. The well point for the withdrawal of sludge provides a location where larger, more dense sludge particles could selectively segregate from the flow and collect at the bottom of the well point. The TEMPEST code is applied to this case as a full 3-D representation. The inlet slurry stream to the hole is assumed to contain 30 wt% solids, which is the maximum capacity of the pump that will withdraw material from the hole. The slurry will be removed by a suction pump 4 inches in diameter that is located, for these calculations, at the top center of the cylindrical well point. The actual location of the retrieval pump will be at some elevation within the pit. Moving the suction point to the top of the cylinder is a simplification and probably increases the potential for settling in the bottom of the well point. Thus, our analysis will be conservative regarding the particle segregation issue. The solids are divided into nine size fractions by combining the 25-30 μm and the 30-35 μm sizes as the fifth of the nine size fractions. (Table 4.5). TEMPEST can only handle 9 discrete size categories, as opposed to the 10 discrete sizes available from the actual data. All solids are assumed to have particle densities of 2.4 g/ml for the TEMPEST calculations, but based on a real particle's falling velocity it can be determined which of the nine particle bins would be equivalent. After specific particle size and density information becomes available for actual sludge species, it is easy to determine which bin should be used to estimate particle segregation potential without rerunning the code.

Although it is likely that some solids entering the pump out point will be in the form of chunks of aggregated sludge, chunks are not included in the model. Chunks would tend to settle very fast, relative to individual particles, and would include both fissile material and neutron absorbers. Because of this situation, the degree of segregation of discrete Pu-rich particles would be reduced by the presence of mixed-particle chunks settling into the pump out point.

In the model, the slurry is forced by the sluicing into this hole from a 10-cm-wide by 5-cm-deep channel at one edge (the 9 o'clock position on the figures) of the top of the cylindrical hole. The slurry is

withdrawn from the top center of the hole through a 4-inch diameter pipe. With the sluicing rate of 300 gpm, the hole is filled in about 1.5 minutes and steady-state flow is established fairly quickly.

The TEMPEST code was used (Trent and Eyler 1993, and Onishi et al. 1995) to examine the possibility of particle segregation in the bottom of the 3 by 5 foot cylinder, dug out by the sluice jet for the pump-out operation. As discussed in Section 4.2.1, the TEMPEST code and the conceptual model account for various physical properties and rheology correlations for non-Newtonian flow and hindered particle settling needed for simulation of Hanford tank wastes.

Main model parameters for the tank waste transport modeling are those determining viscosity, particle settling velocities, and yield/shear stress. Specific formulas and values selected for the modeling are shown in Equations 4.3, 4.4, and 4.5 (see Section 4.2.1). The current TEMPEST version's handling of the yield stress has a limitation in that it cannot keep sludge that should not move stationary for an extended time. As no measured rheology values are available for the Tank C-106 wastes, rheology values were selected that were constrained by measured values for Tank SY-101 wastes and the rheology values that were used in previous TEMPEST modeling for mixing in SY-101 tank wastes (Trent and Michener 1993). Furthermore, because no tank waste retrieval operations are being performed yet, no model calibration specific to Tanks C-106, AY-102, and SY-102 or other tanks is possible. However, the same rheology parameter values are used that were successfully used by the TEMPEST SY-101 modeling, and it is expected the calculated overall behavior presented here is valid. Moreover, as will be discussed in Section 4.2.4, the predicted values of viscosity (approximately 17 cp) for fully mixed wastes in Tank SY-102, that relied on the Tank SY-101 rheology, matched reasonably well with the measured consistency factor of 0.013-0.014 Pa-s for the mixed SY-102 wastes (with the volume ratio of sludge to supernate of 0.5), confirming the general validity of the chosen model parameters (DiCenso et al. 1995).

The simulation time step used for the sluicing-pump out modeling was approximately 2 milliseconds. Early simulation results (up to seven minutes) show that concentrations of each of the nine particle-size solids are relatively uniformly distributed within the entire hole. Solid 1 (the finest size at 5-10 μm, see Table 4.5) is the most uniformly distributed and Solid 9 particles (the coarsest sized at 50-55 μm diameter) show some non-uniformity.

Figure 4.4 shows predicted distributions of flow (m/s) and Solid 9 concentrations (kg/m^3) in a vertical plane extending from the top to the bottom of the hole and from the slurry inlet channel (shown at the right of the figure) to the center of the hole after seven minutes from the start of the sluicing. Figure 4.5 shows the horizontal distribution of Solid 9 concentration for the circular plane at the bottom of the hole. As indicated in these figures, predicted concentrations of the Solid 9 after 50 minutes vary from 22.1 kg/m^3 near the surface to 105 kg/m^3 near the bottom, revealing some differential particle settling effects (an increase in coarse particle concentration at the bottom of the hole of 475% over the incoming well-mixed sludge slurry). This value is not the total enrichment factor for Solid 9 particles versus the total sludge. Such a calculation requires a sum of the concentration of all nine particle sizes to get the bulk sludge concentration. The major portion of the hole from top to bottom has a Solid 9 particle concentration of

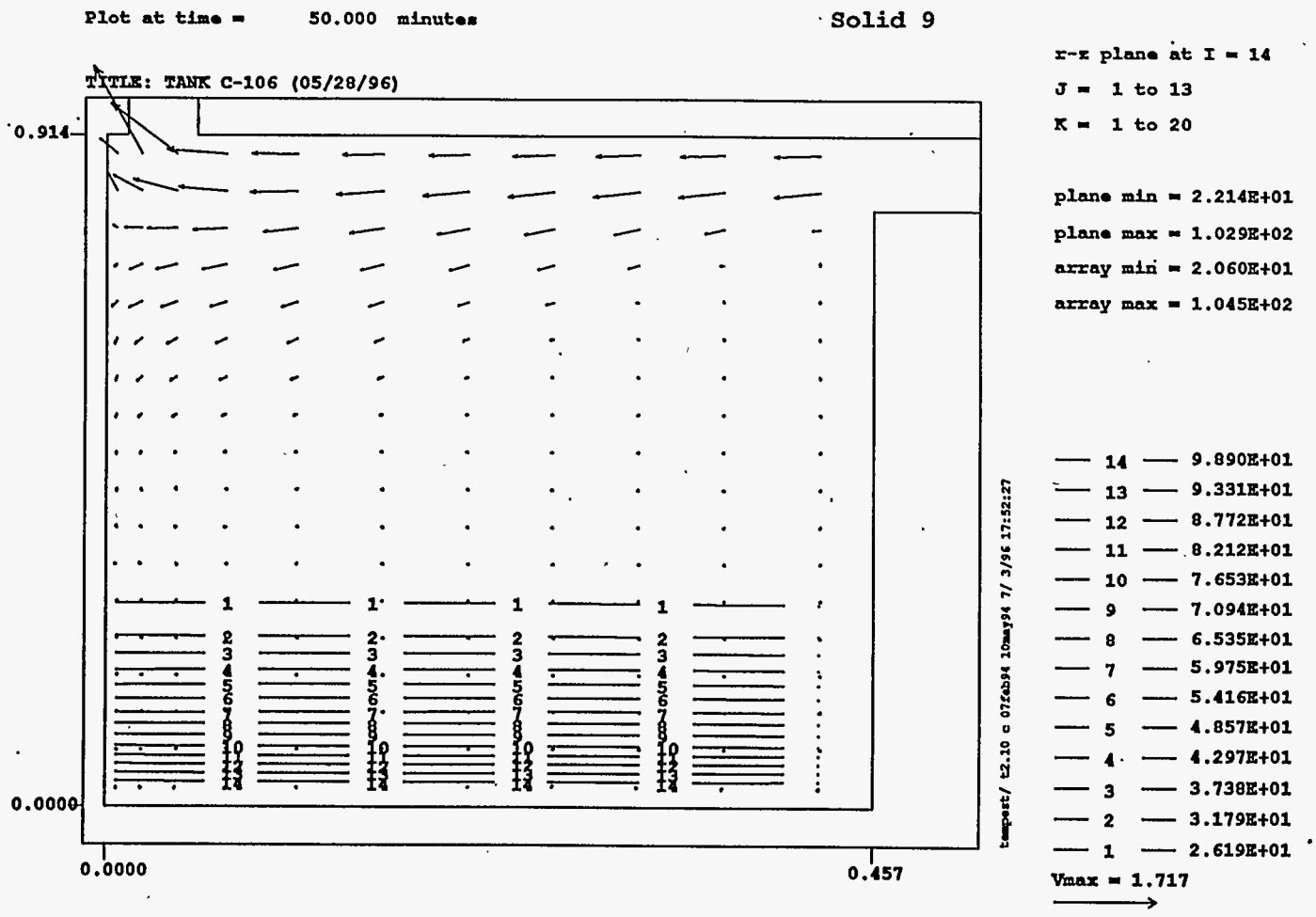

Figure 4.4. Predicted Vertical Distributions of Flow (m/s) and Solid 9 Concentration (kg/m³) on Vertical Plane 14 (9 o'clock Position) of the Hole at 50 Simulation Minutes

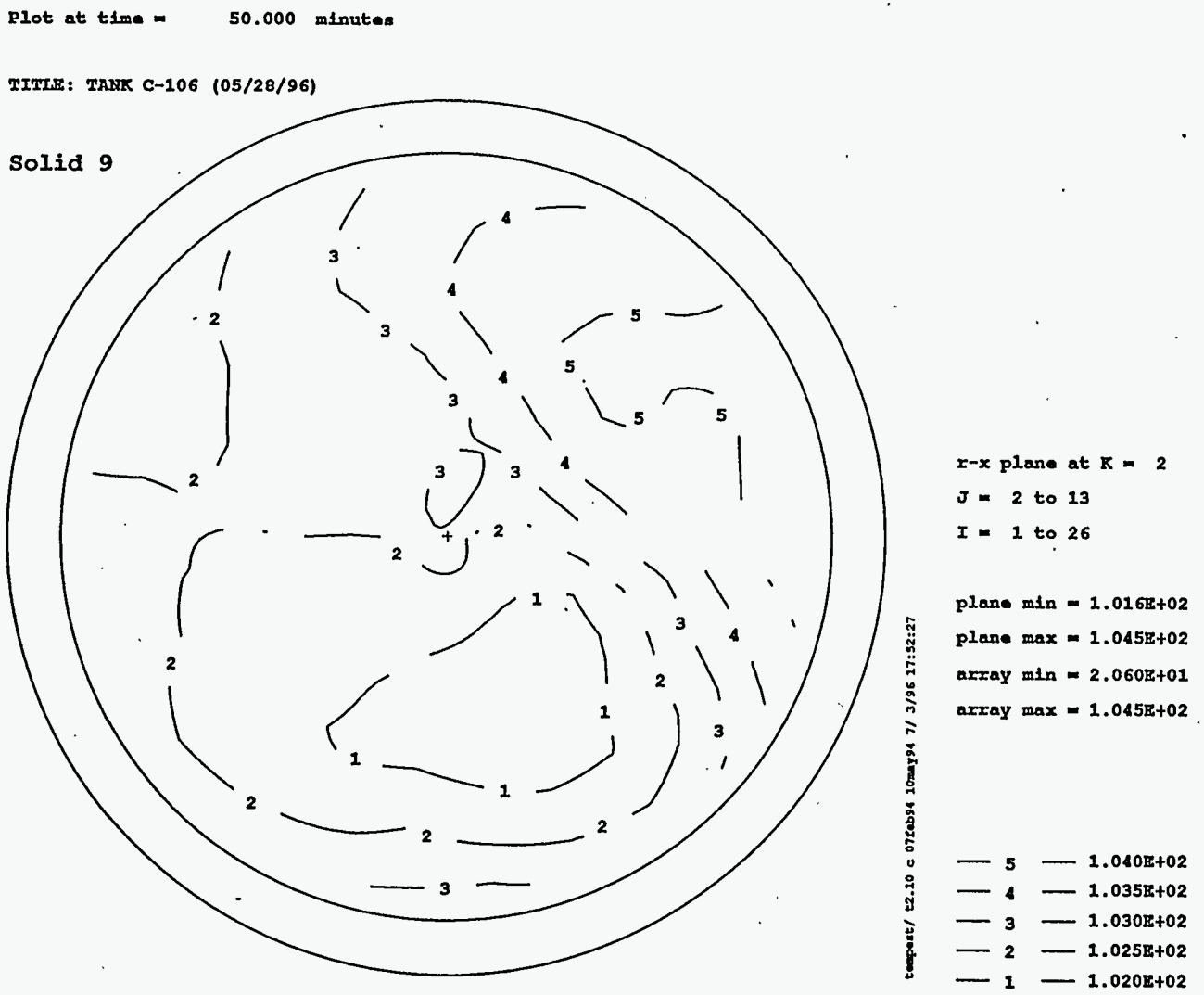

Figure 4.5. Predicted Horizontal Distributions of Flow (m/s) and Solid 9 Concentration (kg/m³) at Bottom of the Hole at 50 Simulation Minutes

approximately 24 kg/m^3. Note the incoming slurry has a Solid 9 concentration of 22.2 kg/m^3. Thus, very little change is found within the bulk of the excavated hole from which the slurry is pumped out of the tank.

As compared to Solid 9, Solid 5 (a medium-sized particle or the conservative representation of Pu-bearing solids) particle concentrations are even more uniformly distributed than the biggest particles within the hole. Near the bottom of the well point excavation, Solid 5 particle concentrations vary only from 30.4 to 30.7 kg/m^3; however, they vary only from 17.1 to 17.5 kg/m^3 near the top of the hole, as shown in Figures 4.6 through 4.8. The incoming concentration of Solid 5 is 17.5 kg/m^3. Thus, only a small increase in concentration is present near the bottom of the excavation.

For Solid 1 (the more realistic representation of the Pu-bearing solids), the particle concentration distribution is uniform throughout the hole, ranging 136.3 to 136.5 kg/m^3, with an incoming concentration of 130 kg/m^3. The predicted Solid 1 distribution near the bottom of the excavation is shown in Figure 4.9.

To test the sensitivity of the predictions to the yield stress of the sludge (and the limitation in the TEMPEST code), the sluicing-pump out operation with no yield stress was also modeled. This model is equivalent to allowing all the sludge to be moved with no threshold velocity needed to create solid movement. Figure 4.10 shows the predicted Solid 9 particle concentrations after 20 minutes of sluicing. The predictions with the no yield stress condition show particle concentrations that vary from 22.1 to 60.2 kg/m^3. Corresponding simulation results with the yield stress at 20 minutes are shown in Figure 4.11. The comparison between Figures 4.10 and 4.11 (showing Solid 9 concentrations varying from 22.1 to 72.5 kg/m^3) shows these results are similar to each other, thus indicating the solid movement is not very sensitive to the selection of yield stress values in these calculations.

Predicted maximum solid segregation for Solids 1, 5, and 9 over the incoming slurry concentrations that account for the total sludge settled at various positions near the bottom of the well point excavation are shown in Figure 4.12. This figure shows the relative concentrations of the Pu-bearing solids for the realistic case and conservative case (Solids 1 or 5, respectively) are actually reduced within the pump-out hole, due to a slight concentration increase of coarser solids (for example, Solid 9 with an assumed particle density of 2.4 g/ml) under the model test conditions and durations stated. Thus, for the model results obtained to date under the conditions and duration simulated, the sluice/pump-out operation does not segregate Pu-bearing solids to any measurable degree. Apparently the advective fluid flow patterns created by the sluice jet and suction pump completely dominate over the tendency of individual particles to settle with differing velocities.

These predictions indicate little segregation of the particles in the horizontal direction (across the cross-section at any depth when looking down from above the hole). Some concentration of larger particles is found near the bottom, but the smaller particles (Solid 1) will still be occupying a major share of the bulk solids, even at the bottom of the hole, if they have the same particle density as the bulk sludge. As mentioned, when actual data are obtained for the particle density of sludge as a function of

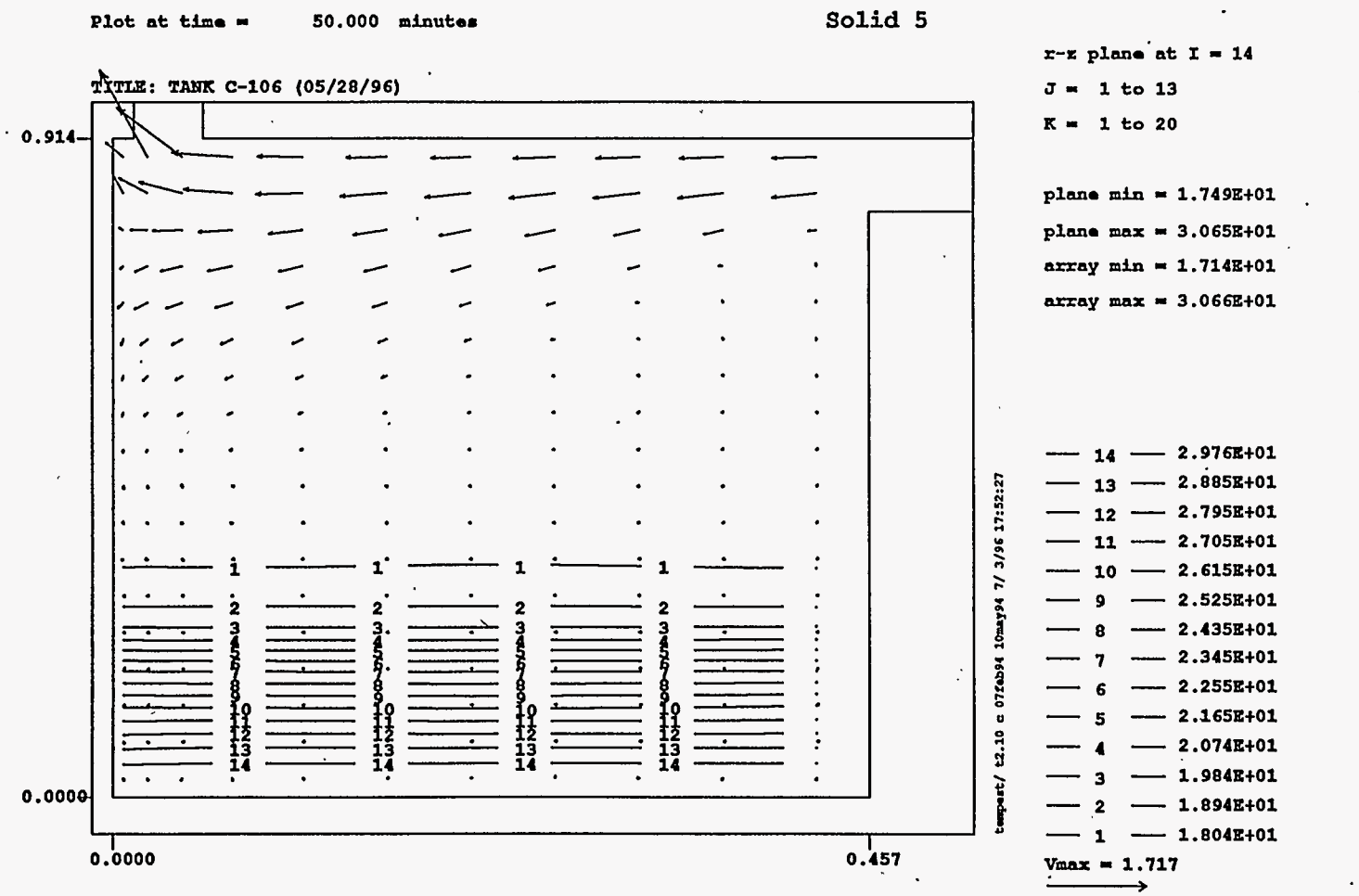

Figure 4.6. Predicted Vertical Distributions of Flow (m/s) and Solid 5 Concentration (kg/m³) on Vertical Plane 14 (9 o'clock Position) of the Hole at 50 Simulation Minutes

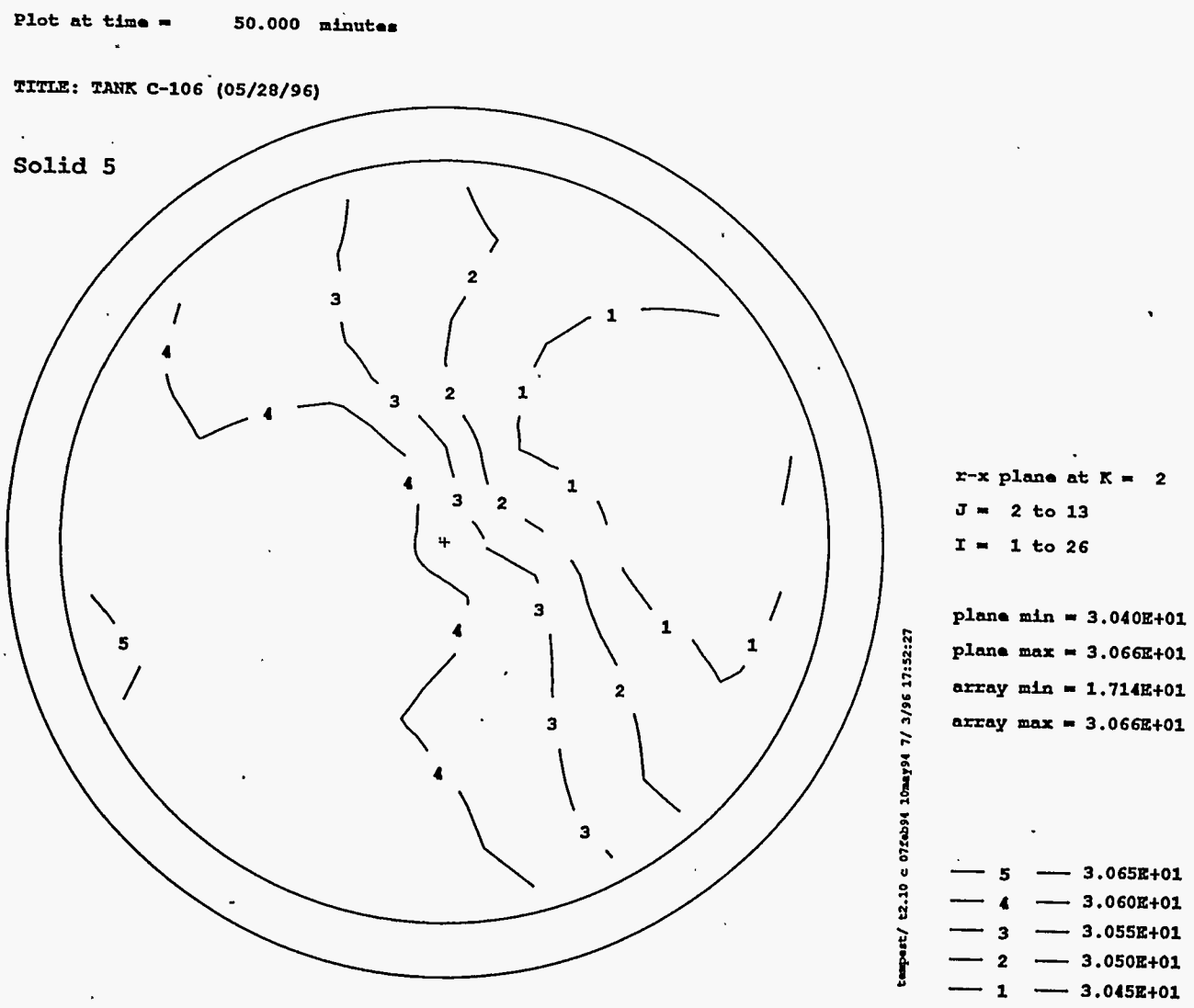

Figure 4.7. Predicted Horizontal Distributions of Flow (m/s) and Solid 5 Concentration (kg/m^3) at Bottom of the Hole at Seven Simulation Minutes

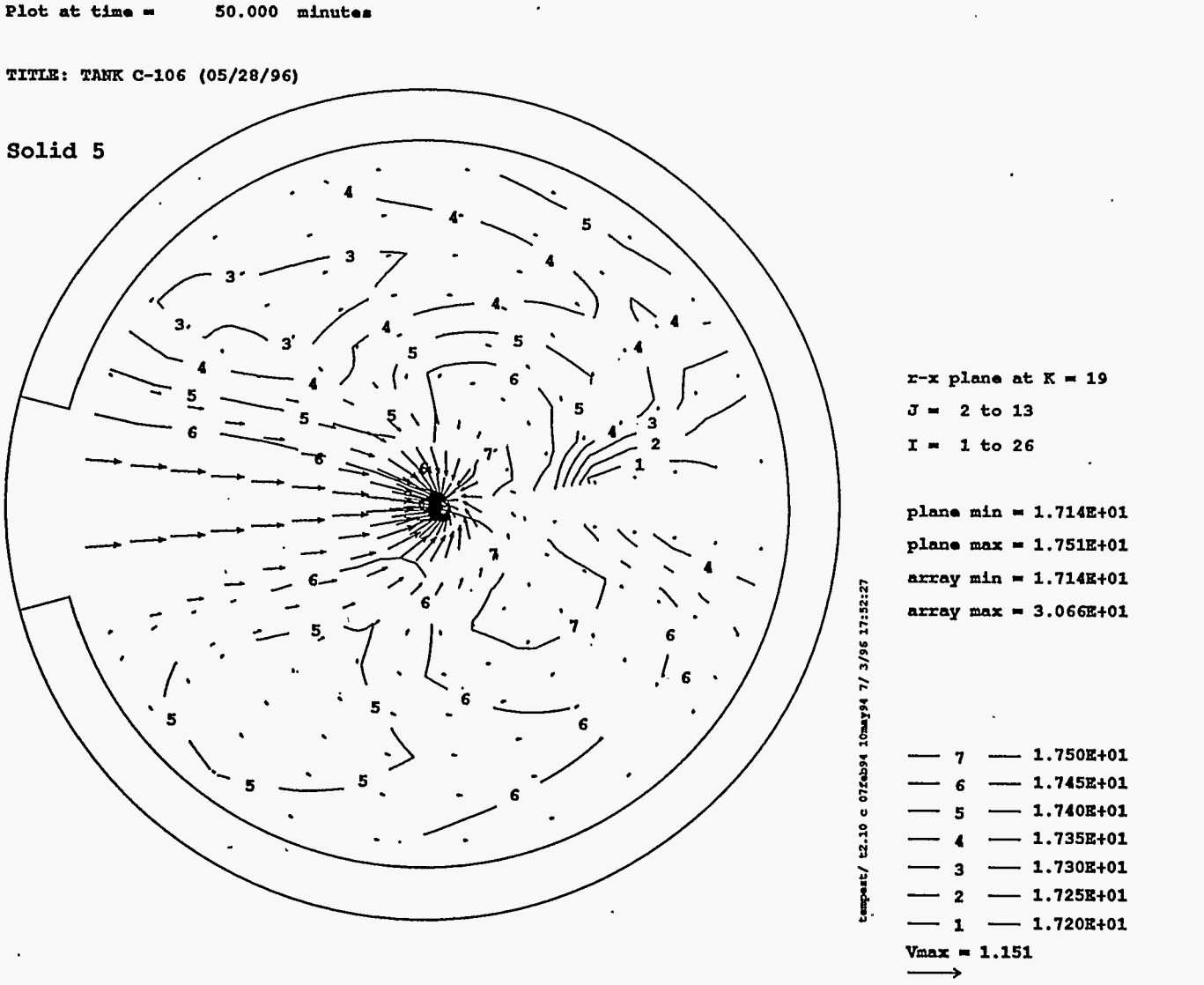

Figure 4.8. Predicted Horizontal Distributions of Flow (m/s) and Solid 5 Concentrations (kg/m^3) at Top of the Hole at 50 Simulation Minutes

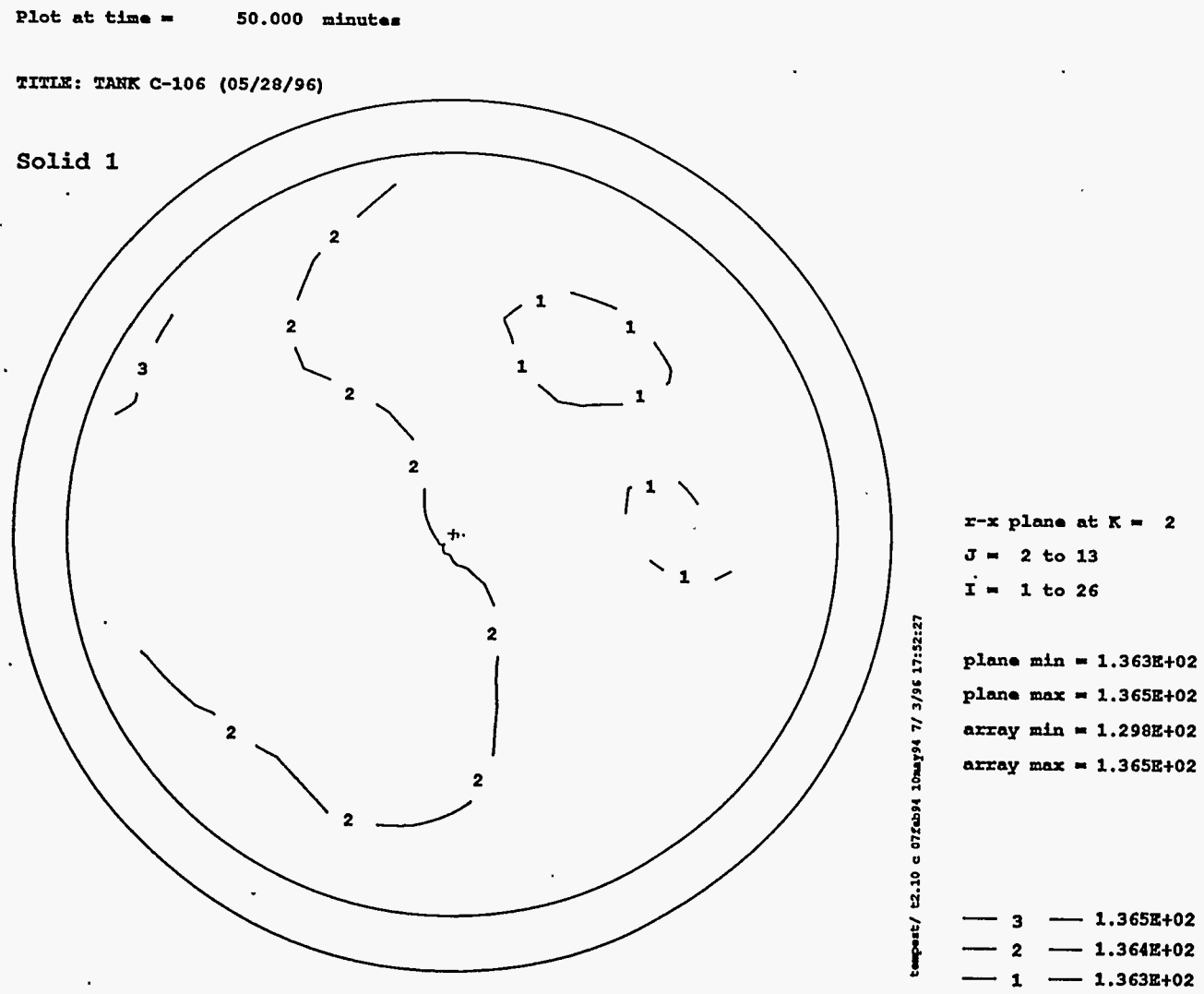

Figure 4.9. Predicted Horizontal Distributions of Flow (m/s) and Solid 1 Concentration (kg/m^3) at Bottom of the Hole at 50 Simulation Minutes

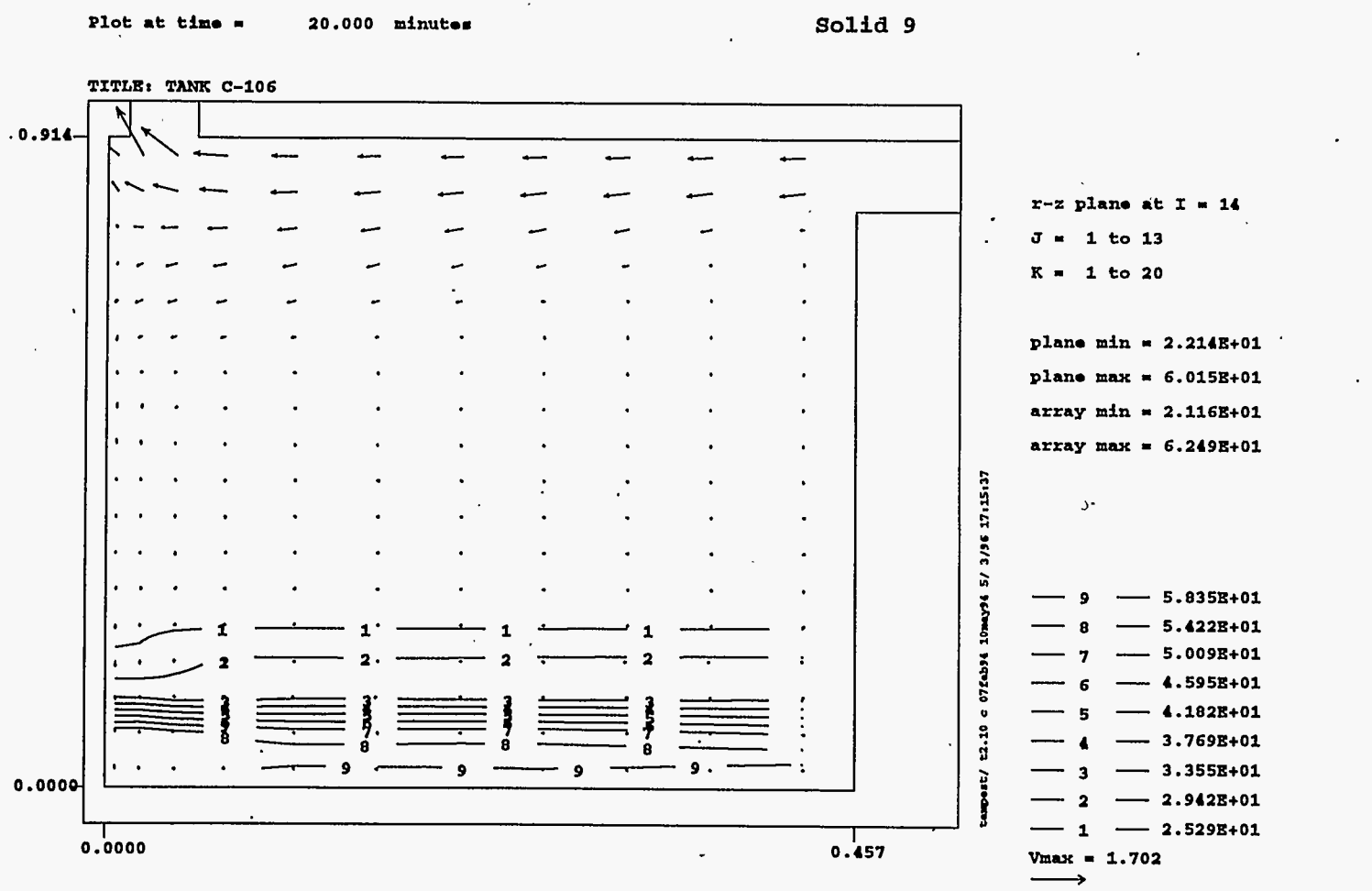

Figure 4.10. Predicted Vertical Distributions of Flow (m/s) and Solid 9 Concentration (kg/m^3) on Vertical Plane 14 (9 o'clock Position) of the Hole Without Yield Stress at 20 Simulation Minutes

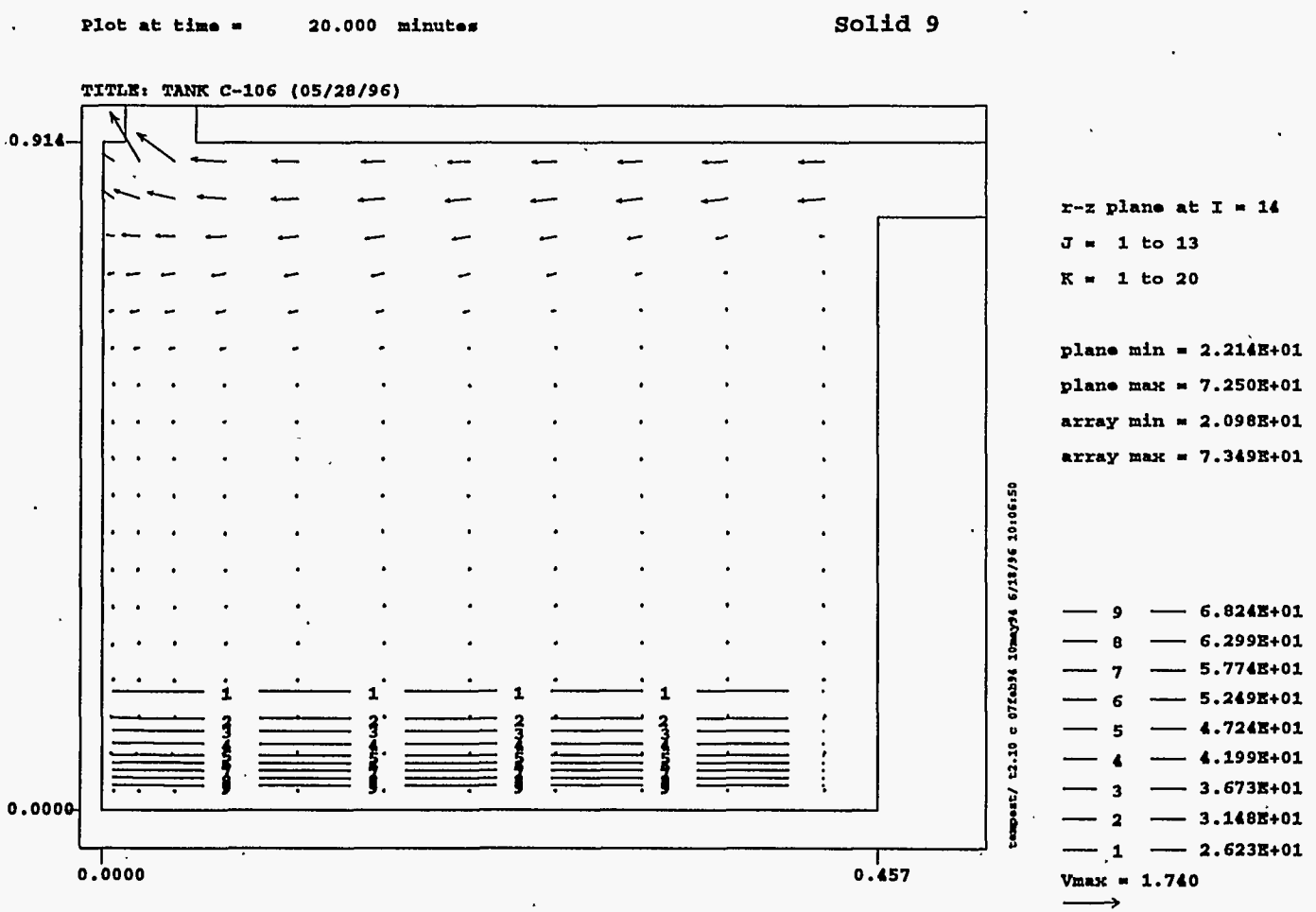

Figure 4.11. Predicted Vertical Distributions of Flow (m/s) and Solid 9 Concentration (kg/m^3) on Vertical Plane 14 (9 o'clock Position) of the Hole with the Yield Stress at 20 Simulation Minutes

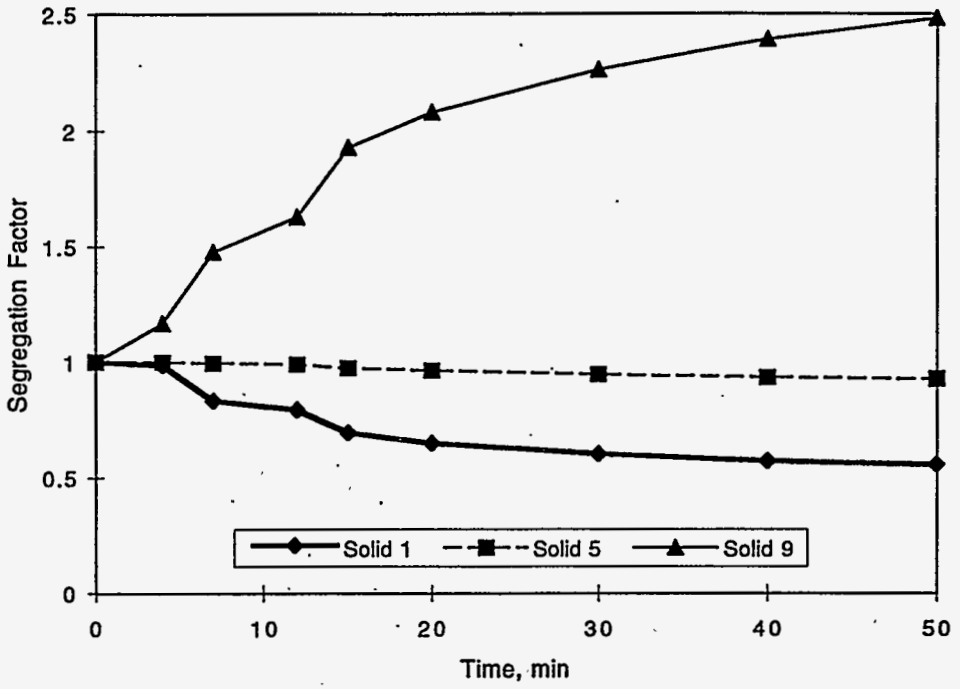

Figure 4.12. Predicted Maximum Segregation Over the Initial Conditions Near the C-106 Tank Bottom

particle size, the individual settling velocities can be calculated and the appropriate bin number chosen to reinterpret the TEMPEST code predictions. This reinterpretation can be made without rerunning the code, unless a large portion of the sludge particle density-size values leads to falling velocities outside the range shown in Table 4.5. Thus, the sluice pump-out operation appears unlikely to segregate solid particles in any significant degree, under the simulation test assumptions and conditions.

4.2.3 Addition of Sluiced C-106 Solids to Tank AY-102

This section examines the potential for solid segregation occurring when sluiced solids from Tank C-106 are introduced into Tank AY-102. After removal from Tank C-106, a slurry containing up to 30 wt% solids will be pumped at a rate of 300 gpm through a slurry distributor in Tank AY-102. The solids in the slurry were assumed to have the same size distribution as the Tank C-106 sludge (Table 4.5). This assumption presupposes the sluice stream and centrifugal pumps used for transfer do not destroy the original particle size distribution of the sludge. Waste Tank AY-102 initially contained 1.5 feet of the sludge and 15 feet of supernate above the sludge layer. The sludge in waste Tank AY-102 has a bulk density of 1.4 g/ml (Castaing 1994), and is assumed to have the same particle size distribution as that of Tank C-106.

The inlet pipe at Tank AY-102 has a distributor consisting of four 1-inch diameter nozzles, oriented at right angles to each other to form a cross in the horizontal plane. The distributor is located 6 feet off

the tank center and 13 feet above the tank bottom. A 4-inch suction pipe to recirculate the Tank AY-102 supernate back to Tank C-106 for continued feed to the sluice jet is located at 22 feet from the center (or 28 feet from the slurry inlet distributor) at the surface of the supernate (16.5 feet above the tank bottom). The suction pipe is located at 45° between two of the four injection nozzles. The suction pipe volumetric flow rate for outgoing supernate liquid is set to 300 gpm to match the incoming slurry discharge. To simplify the simulation and still maintain some conservativeness regarding potential solid setting in the tank, the slurry distributor inlet was moved to the center of Tank AY-102, and the tank diameter was increased from the actual 75 feet to 81 feet (to account for the 6 foot off center actual location). Symmetry was thus allowed in the calculation which cuts down the run times significantly, but still provides the right geometry to the walls and distance between the inlet and supernate outlet suction pump.

The TEMPEST code was used to calculate a full 3-D simulation case (with yield stress, but without simulating chemical reactions) with approximately 20 ms time steps. Figure 4.13 shows the predicted vertical distribution of Solid 5 (the conservative Pu-bearing solid) concentration after one simulation hour. The figure depicts the slurry plume descending from one of the four nozzles toward the tank bottom and the slurry density current spreading over the original 1.5-ft deep Tank AY-102 sludge layer with a little mixing with the original tank sludge. Near the surface of the tank in the supernate, very little Solid 5 is present. Figures 4.14 and 4.15 show the predicted Solid 5 concentrations on a horizontal plane just above the original AY-102 sludge layer after 25-minute and 1-hour simulation times, respectively. The fan shaped isoconcentration contours reflect the density current movement. These figures show the jets cause the slurry plume to break into four discrete fingers that hit the tank wall and swivel back toward the tank center. Solid 5 concentration profiles, thus, show accumulation between the 4 distributor nozzles after 25 minutes. After 60 minutes, the Solid 5 concentrations are increased between the 4 jet pathways and along the tank periphery. Variations of Solid 5 concentrations within this horizontal plane near the original sludge interface vary approximately 30% (from 5.6 to 7.3 kg/m^3 at one hour) across the tank cross section. Due to the steady accumulation of all particles sizes of solids in this layer just above the original AY-102 sludge, all solids (including Solid 5) are expected to increase their concentrations to eventually reach a total volume fraction of solids of 0.46 (C_{vmax}), the value chosen to represent a completely settled sludge layer. When a layer (grid spacing in the numerical computer calculation) reaches this volume fraction of settled solids, additional solids that settle at later times must accumulate in the next higher grid layer, just above the layer that has just reached Cvmax = 0.46. This layer-by-layer accumulation sequence is expected to continue until all of the Tank 106-C sluiced slurry has been placed in and settles in Tank AY-102.

The stream of slurried sludge sinks very rapidly to the tank bottom, immediately after being expelled from the 1-inch nozzles, toward the tank bottom. [See Figures 4.16 and 4.17, depicting velocity and Solid 5 distributions on the horizontal plane containing the four slurry jet nozzles (near the liquid surface)]. Figure 4.17 covers an expanded radial distance (1.9 m) equivalent to the distances shown by velocity arrows in Figure 4.16. The closely bunched contours reveal very rapid initial mixing. Because the four slurry jets distribute the sludge so it slides on the original Tank AY-102 sludge surface as a density current, hardly any solids move toward the pump suction inlet at the surface. This process also prevents solids from being recirculated back to Tank C-106 during the initial sluicing period, a favorable

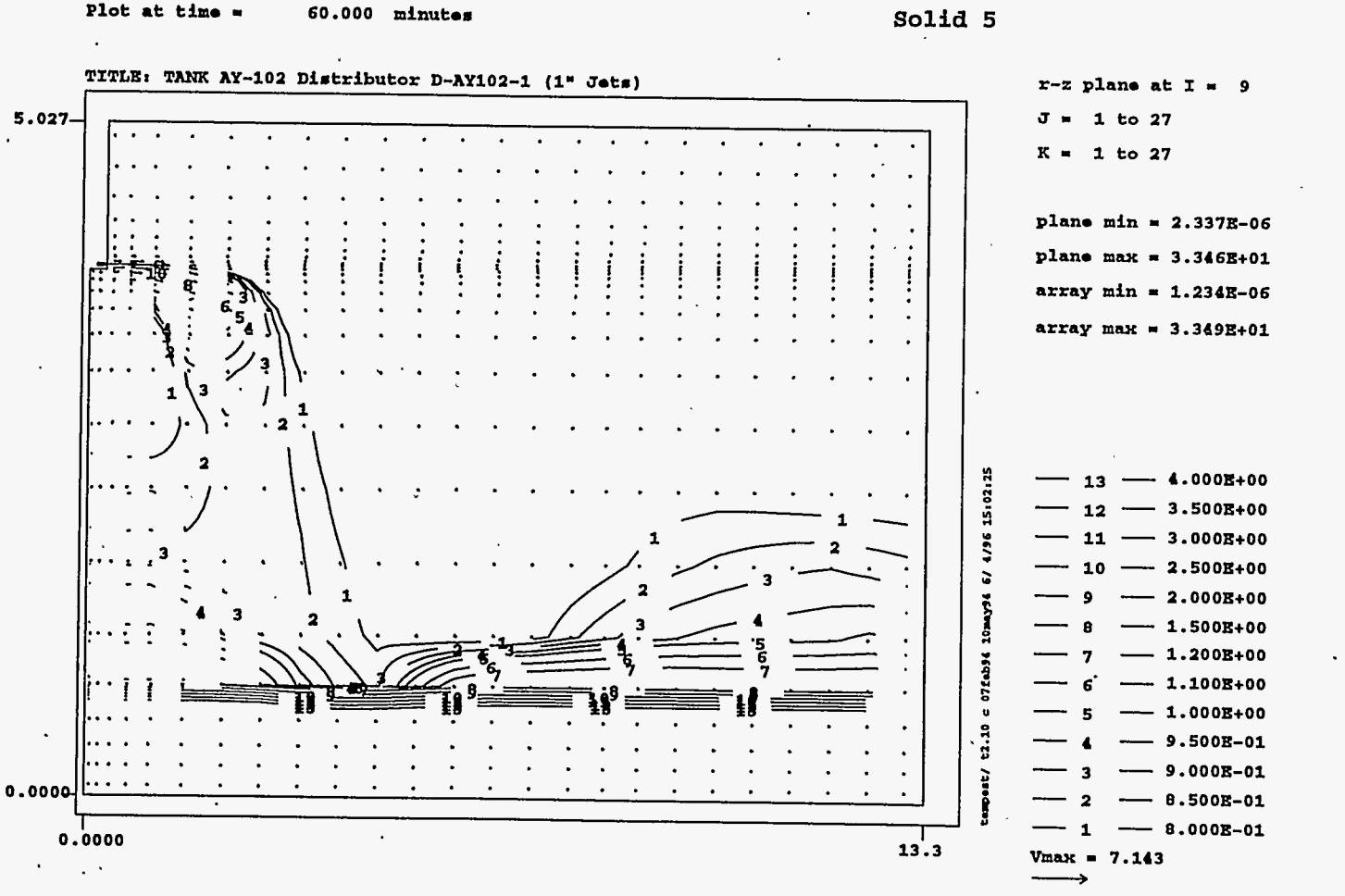

Figure 4.13. Predicted Vertical Distributions of Flow (m/s) and Solid 5 Concentration (kg/m³) on Vertical Plane 9 Containing One of the 1-Inch Nozzles in Tank AY-102 at One Simulation Hour

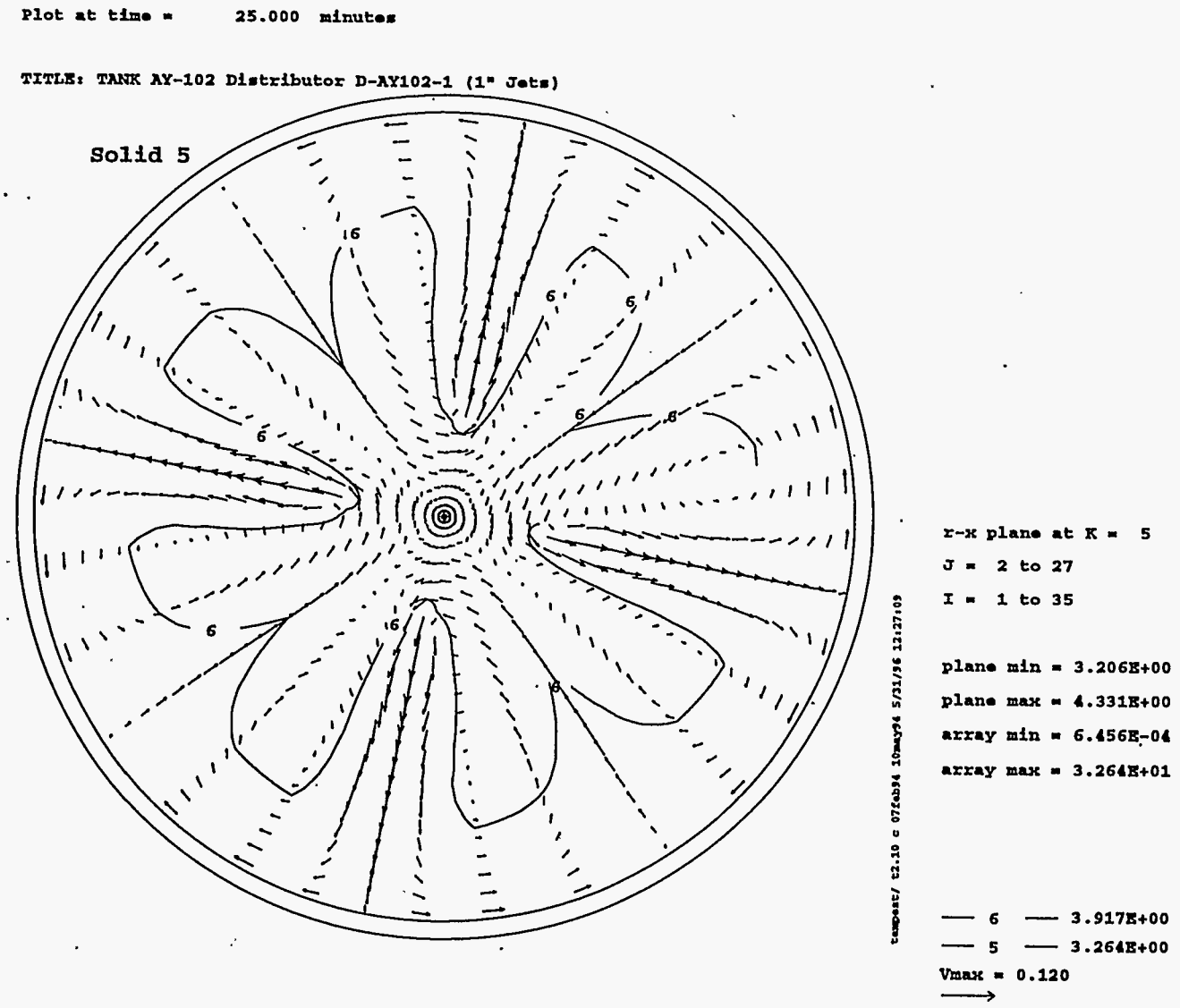

Figure 4.14. Predicted Horizontal Distributions of Flow (m/s) and Solid 5 Concentration (kg/m³) at 15 Inches Above the Bottom of Tank AY-102 at 25 Simulation Minutes

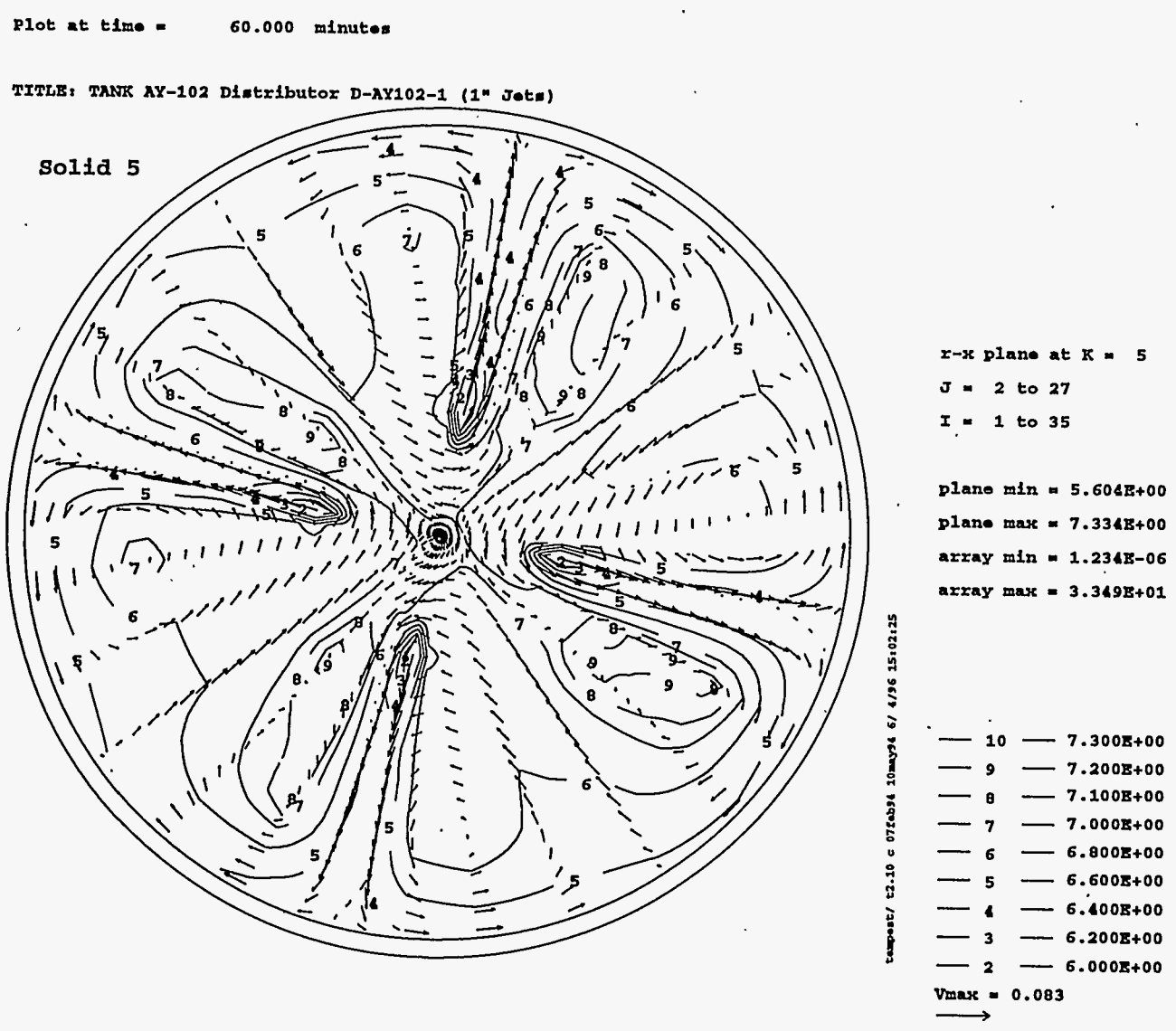

Figure 4.15. Predicted Horizontal Distributions of Flow (m/s) and Solid 5 Concentration (kg/m^3) at 23 Inches Above the Bottom of Tank AY-102 at One Simulation Hour

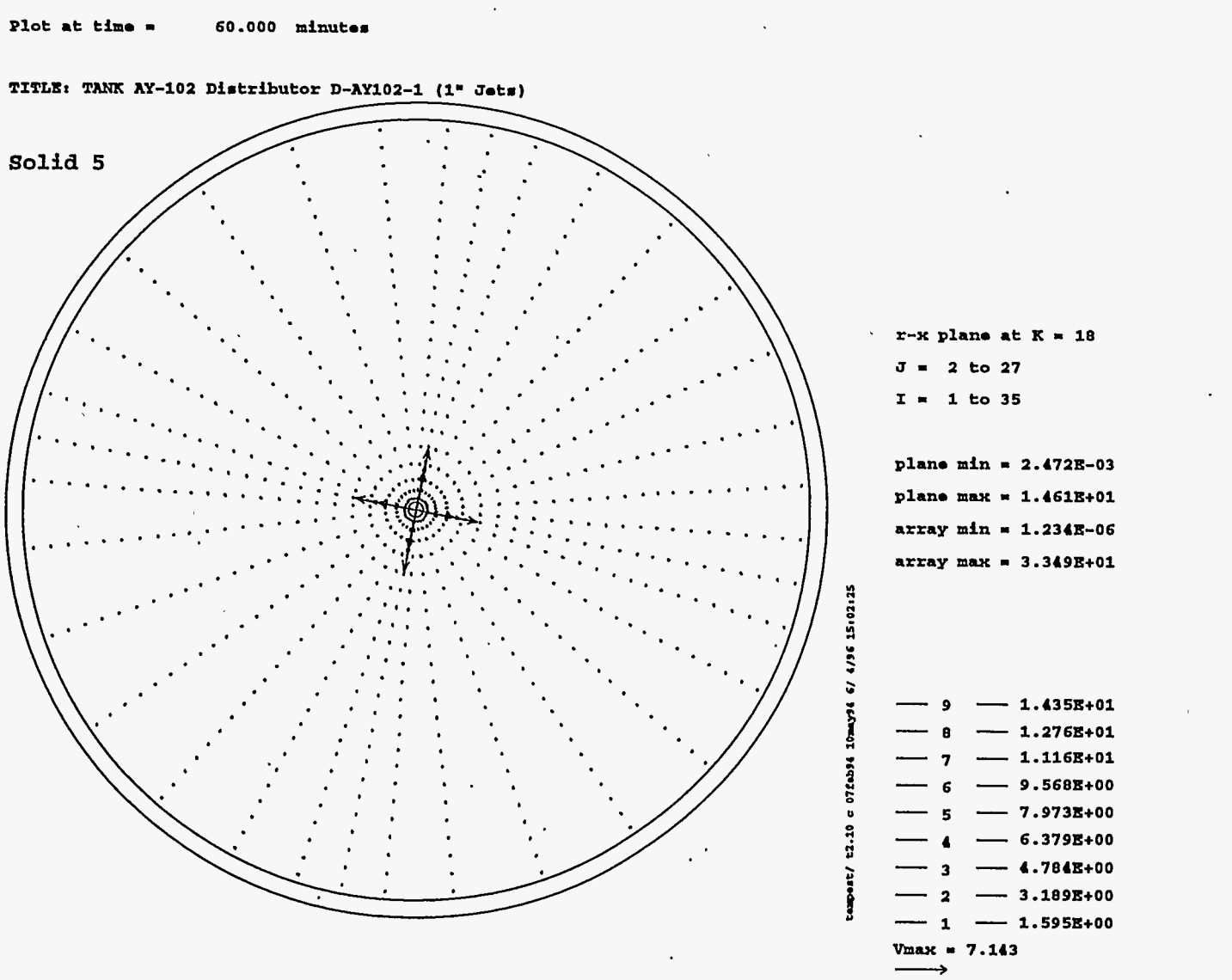

Figure 4.16. Predicted Horizontal Distributions of Flow (m/s) and Solid 5 Concentration (kg/m³) on the Plane Containing Four 1-Inch Nozzles in Tank AY-102 at One Simulation Hour

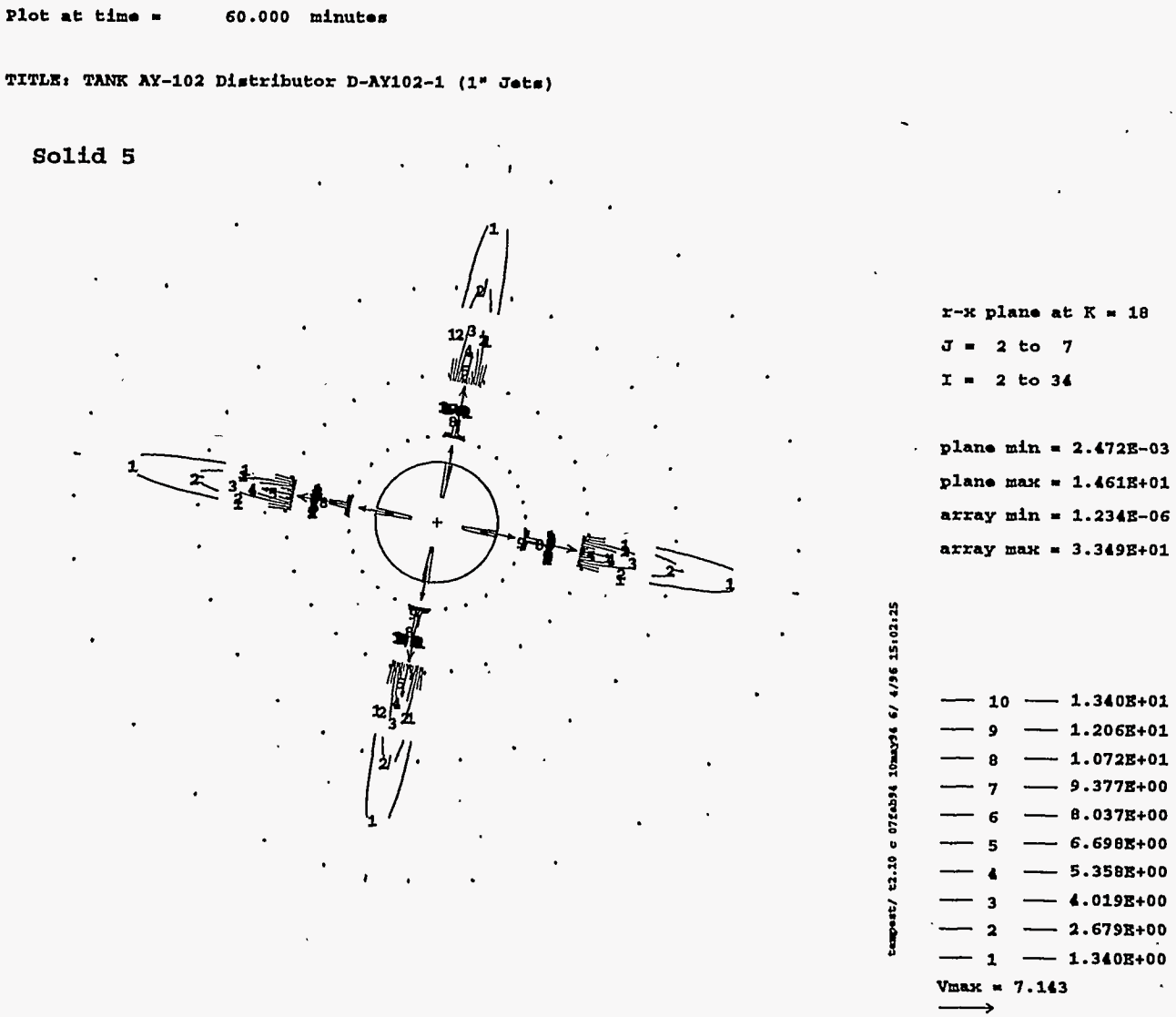

Figure 4.17. Close-up (within 1.9 m from the Tank Center) of Predicted Horizontal Distributions of Flow (m/s) and Solid 5 Concentration (kg/m^3) on the Plane Containing Four 1-Inch Nozzles in Tank AY-102 at One Simulation Hour

circumstance. Figure 4.18 clearly indicates where very small Solid 5 concentrations (ranging from $1.2x10^{-6}$ to $2.7x10^{-5}$ kg/m^3) are found in this surface plane.

Other particle size solids show similar patterns to that of Solid 5. Solid 1 (more realistic representation of Pu-bearing solids) shows an even more uniform distribution (Figures 4.19 and 4.20). Solid 9, the largest particles in the sludge, have somewhat less uniform distribution patterns (Figures 4.21 and 4.22). These simulation results are for one hour of simulation time (one hour of sludge entering Tank AY-102 after initiation of sluicing Tank C-102). The predictions indicate that most of the slurry introduced into Tank AY-102 will be accumulated over the original Tank AY-102 sludge layer at the tank bottom.

The predicted maximum segregation, for three of the particle sizes over the initial slurry concentrations, on the horizontal layer just above the original Tank AY-102 sludge after one-simulation hour is shown in Figure 4.23. As shown in this figure, Solid 5 gradually increases its relative concentrations by up to 1.5, while Solid 1 shows practically no segregation. Assuming these two particle bins represent the conservative and most representative estimates for Pu-bearing solids, the predictions indicate the slurry receiving operation does not significantly segregate Pu-bearing solids in the receiving tank. At this stage, any detailed discussion is not viable without collecting more detailed data on the slurry characteristics (such as slurry rheology), knowledge on the individual particle densities, and chemical makeup of different particle sized sludge.

4.2.4 Mixer Pump Operation in SY-102

Potential particle segregation during the jet mixer operation in DST SY-102 is being evaluated. Tank SY-102 has a sludge layer with a bulk density of 1.56 g/mL; the overlying supernate has a density of 1.03 g/mL (DiCenso et al. 1995). The particle density of the average bulk sludge is 1.80 g/mL, and it contains $NaNO_3$(s), $Al(OH)_3$(s), $Na_3PO_4 \cdot 12H_2O$(s), and iron solids (Onishi and Hudson 1996). The particle distribution and calculated unhindered settling (fall) velocity are shown in Table 4.6 (DiCenso et al. 1995). These setting velocities were calculated by assigning fluid viscosity of 1.0 cp.

The average particle size based on the volume is about 53 μm (DiCenso et al. 1995). In Tank SY-102 modeling, all seven of these solid fractions are included. A conservative estimate is that Pu-solids have a particle density of 11.46 g/mL. Some chemists on the team have argued the amorphous/hydrous Pu oxide has a particle density closer to 6 g/mL. The unhindered settling velocity of the conservative density particles with a particle size of 10 μm is 0.57 mm/s, which (moving to the next highest velocity) corresponds to the falling velocity of solid particles of Size Fraction 4 (Table 4.6). While the latter particle density (perhaps a more realistic case) with a particle size of 2 μm diameter has a unhindered fall velocity of 0.011 mm/s. This realistic falling velocity is much smaller than those of solid particles of Size Fraction 1 in Table 4.6. Thus, the predicted model results for Solids 4 and 1 can be regarded as conservative and as more realistic representatives of Pu-bearing solid behavior.

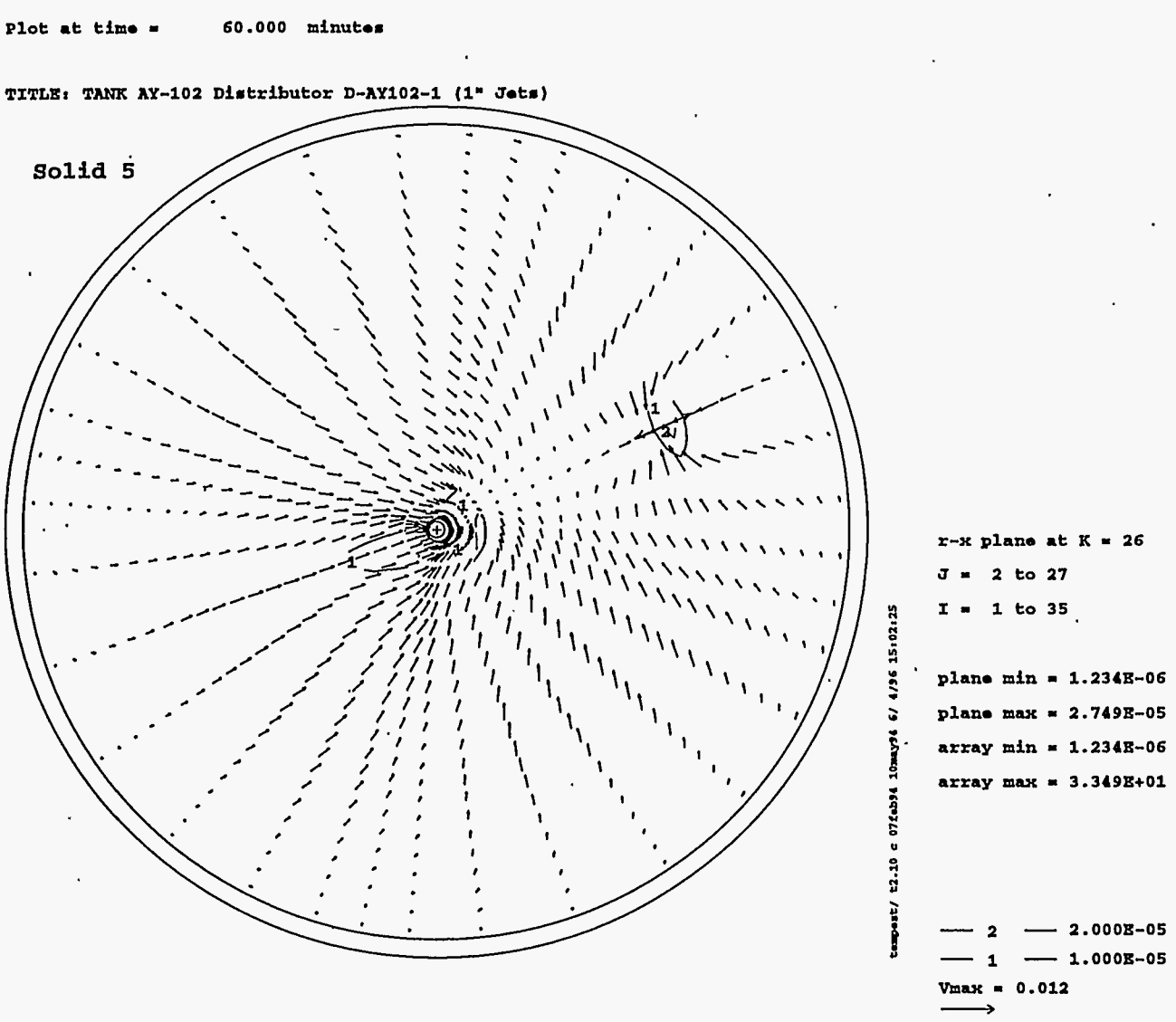

Figure 4.18. Predicted Horizontal Distributions of Flow (m/s) and Solid 5 Concentration (kg/m^3) at the Top of Tank AY-102 at One Simulation Hour

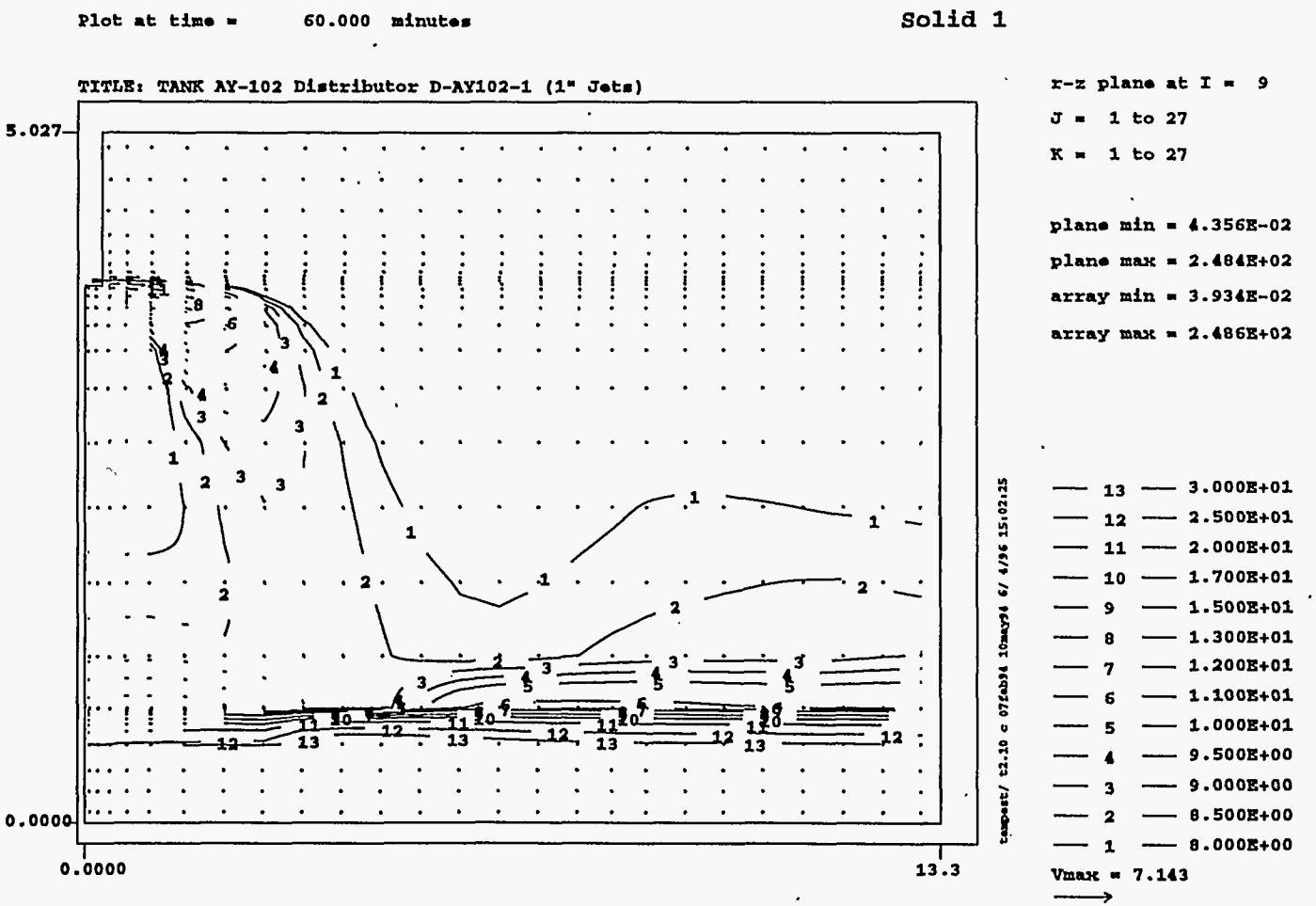

Figure 4.19. Predicted Vertical Distribution of Flow (m/s) and Solid 1 Concentration (kg/m^3) on Vertical Plane 9 Containing One of the 1-Inch Nozzles in Tank AY-102 at One Simulation Hour

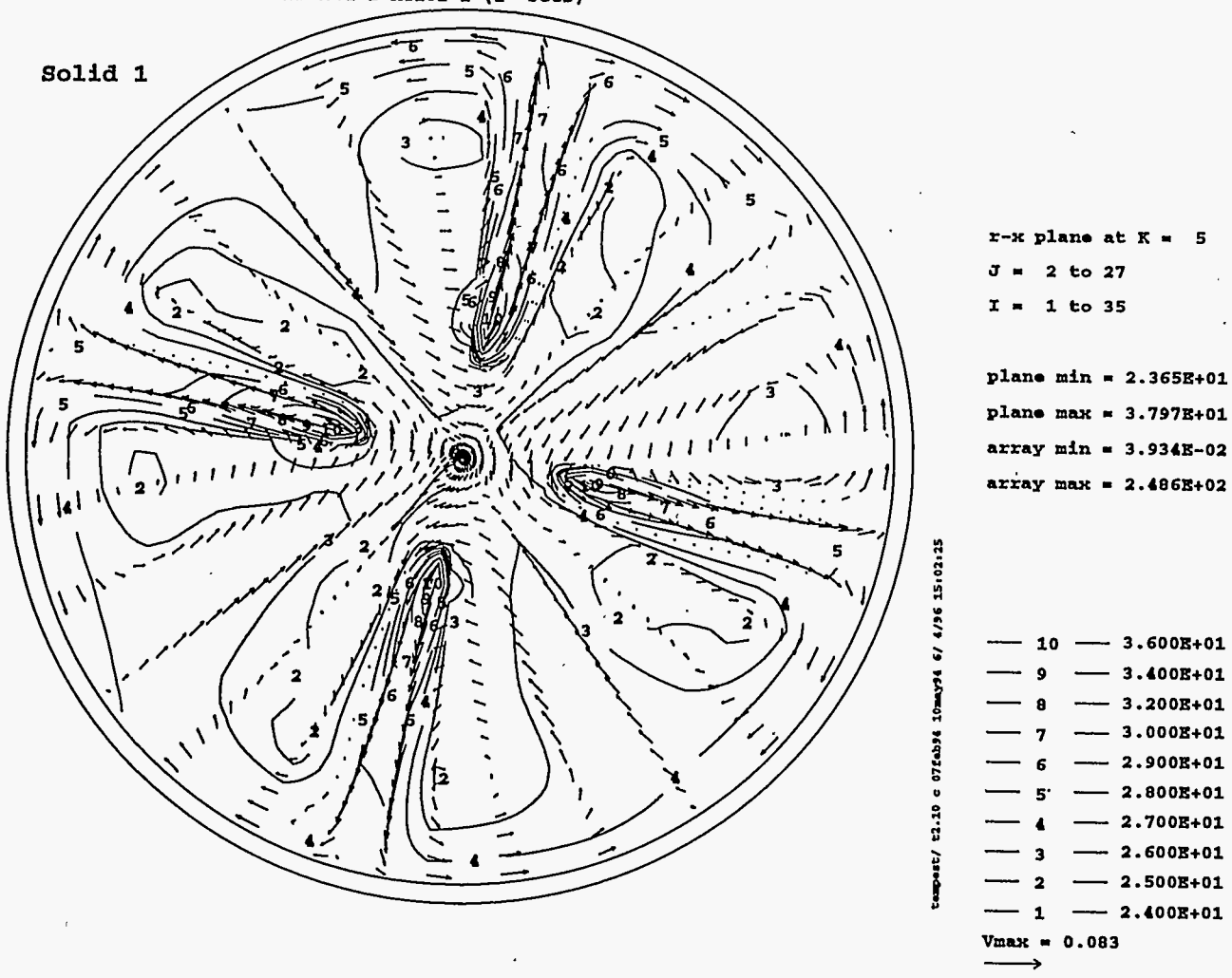

Figure 4.20. Predicted Horizontal Distributions of Flow (m/s) and Solid 1 Concentration (kg/m³) at 23 Inches Above the Bottom of Tank AY-102 at One Simulation Hour

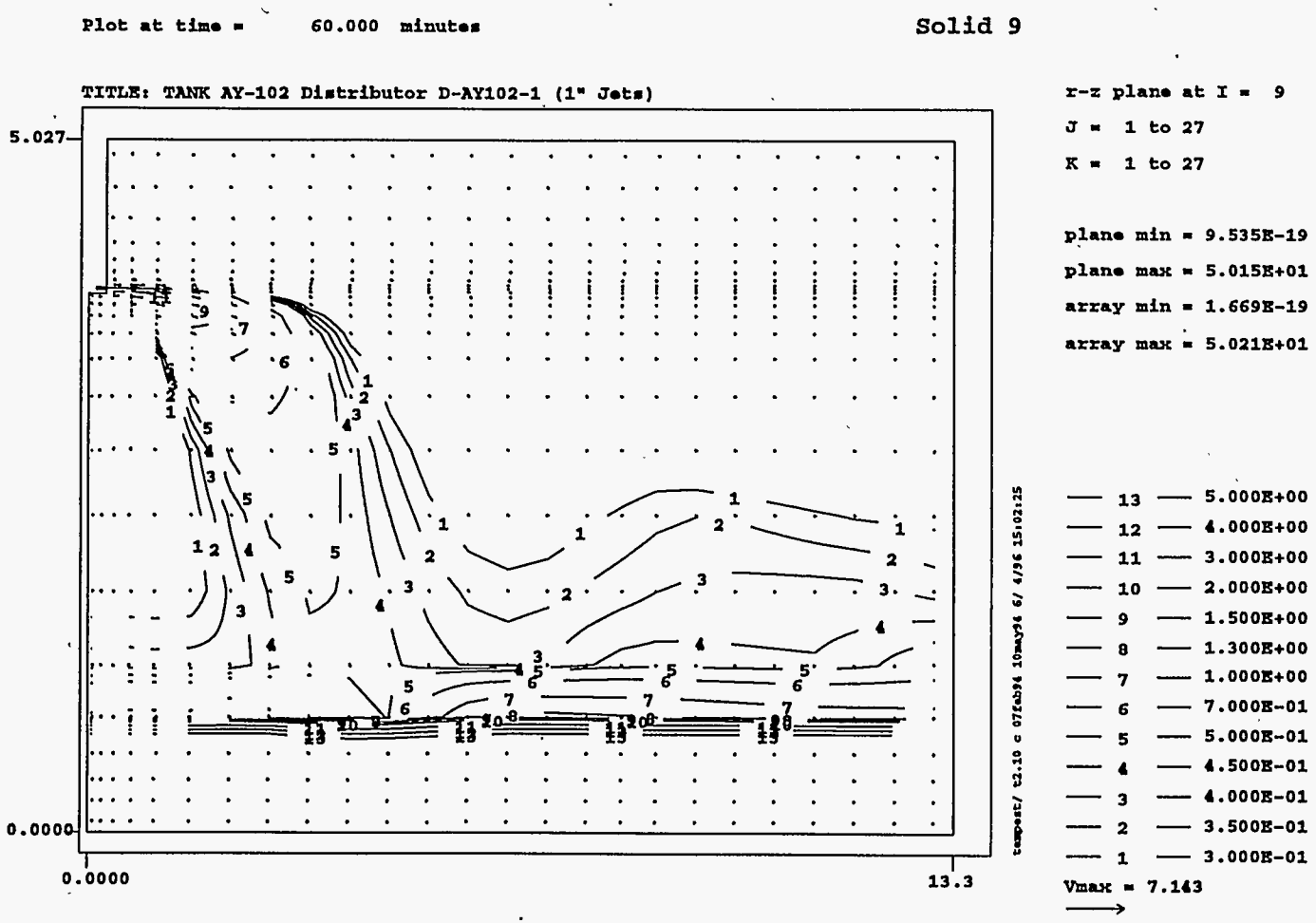

Figure 4.21. Predicted Vertical Distributions of Flow (m/s) and Solid 9 Concentration (kg/m^3) on Vertical Plane 9 Containing One of the 1-Inch Nozzles in Tank AY-102 at One Simulation Hour

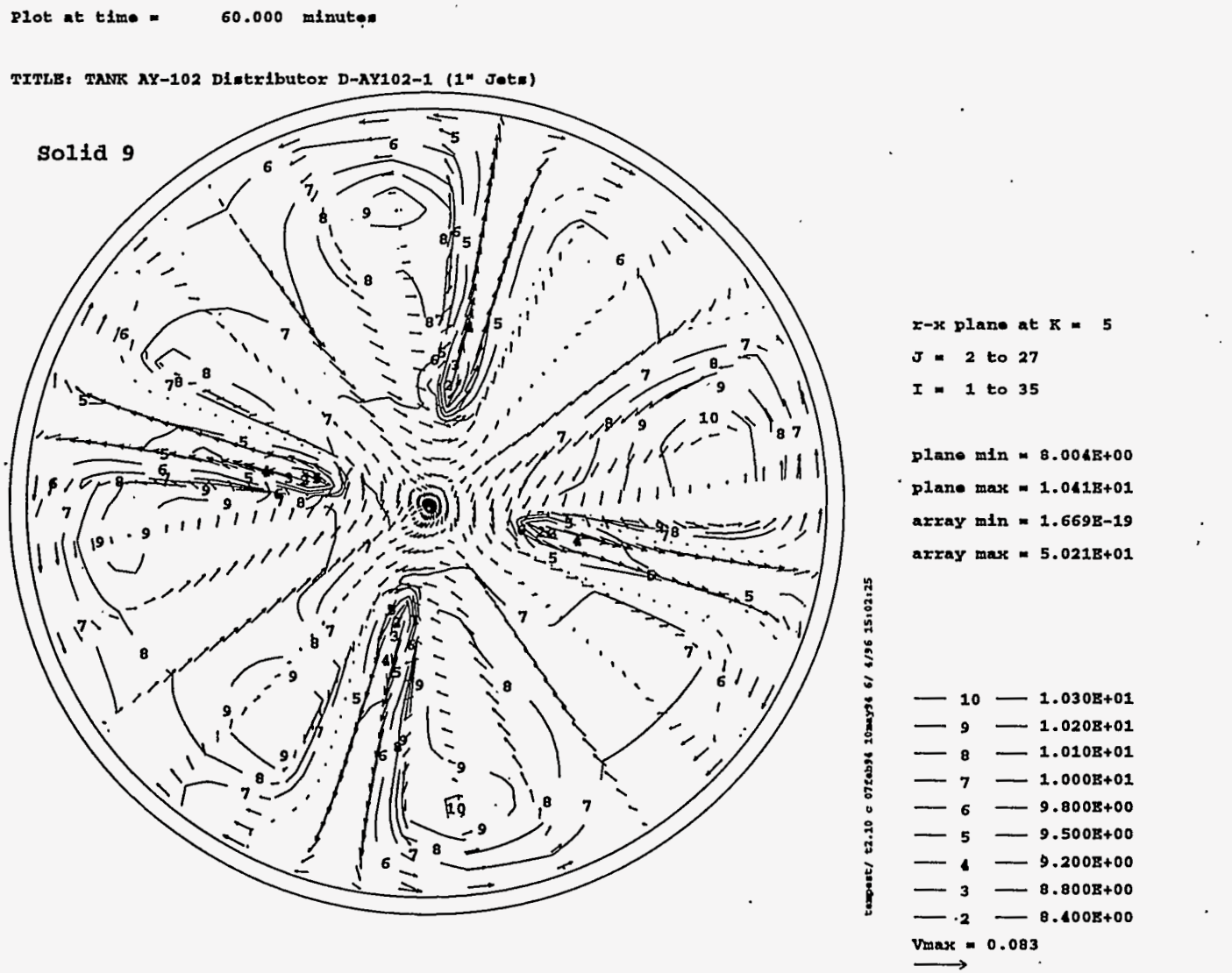

Figure 4.22. Predicted Horizontal Distributions of Flow (m/s) and Solid 9 Concentration (kg/m^3) at 23 Inches Above the Bottom of Tank AY-102 at One Simulation Hour

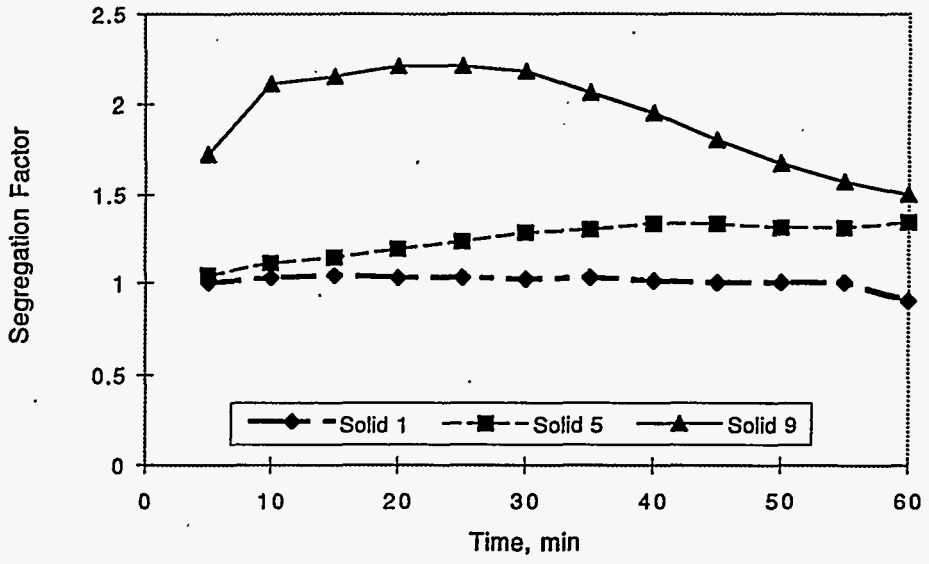

Figure 4.23. Predicted Maximum Solid Segregation for Solids 1, 5, and 9 at 23 Inches Above the Bottom of Tank AY-102 Over One Simulation Hour

Table 4.6. Particle Size Distributions of Tank SY-102 Sludge

Size Fractions	Particle Sizes, μm	Percent Volume	Fall Velocity (mm/s)
1	10 - 20	7	0.081
2	20 - 30	8	0.24
3	30 - 40	8	0.49
4	40 - 50	19	0.81
5	50 - 60	30	1.2
6	60 - 100	25	2.5
7	100 - 175	3	7.1
	Total	100	

The Tank SY-102 conceptual model used in TEMPEST simulates the operation of two mixer pumps, each with two jet nozzles. The four outlets have 6-inch diameter nozzles and are placed 17 inches above the tank bottom; the pump suction line has a 15-inch diameter and is positioned 7 inches above the tank bottom. The jet nozzles inject fluid into the tank at a velocity of 60 ft/s. These two mixer pumps are located 20 feet from the tank center on opposite ends of a diagonal line through the tank center. Each jet rotates over a half circle at the speed of 0.5 rpm.

The 102-SY tank represents the most challenging modeling problem of those currently being performed. Tank SY-102 TEMPEST runs are 3-dimensional, but are reduced through symmetry so that only one quadrant of the tank must be modeled. The reduction of the problem via symmetry arguments assumes the jets of the two mixer pumps are synchronized and counter-rotating. In one case, sludge movement is simulated in a half tank with two opposed rotating jets.

Five TEMPEST test cases were selected for Tank SY-102 modeling. The first three cases used one set of sludge and rheology conditions (C_{vmax} = 0.43, sludge viscosity = 3000 Pa-s), and the fourth and fifth cases assumed C_{vmax} = 0.53, and sludge viscosity of 4500 Pa-s). The latter cases were included in the study, because near the end of this project, PNNL measured the SY-102 sludge rheology under a separate study, indicating the measured maximum viscosity was approximately 4500 Pa-s with the sludge volume fraction of approximately 0.53.

In the first two test cases, the rotating jet is located at the center of the tank. One of these cases has the tank sludge initially sitting at the bottom (static sludge case); the second case starts with the tank sludge fully mixed within the tank supernate, assumed to have three times the volume of the sludge. This 3 to 1 ratio for supernate liquid to sludge is common to all three test cases. For the fourth and fifth cases, the sludge to supernate volume ratio was 1:2 to reflect the current (July 1996) condition. The third test case has a jet located 20 feet off center. However, the rotation of the jet is represented by discrete 90-degree changes in mixer pump discharge direction at 30-second intervals to simulate a rotation rate of 0.5 rpm. The first two test cases were performed because of concern about the flow patterns of the jet. Rotating the jet in 90° increments under the third test case may not sufficiently agitate the overall sludge so that significant differences might be observed in particle deposition patterns.

The first three test cases were simulated without a threshold yield stress for the settled sludge. In the other two cases, a small yield stress was included. For the first test case, which has a 6-inch jet nozzle located at the tank center with sludge initially static at the tank bottom, the model ran for 1.5 hours. As the jet mixed the sludge and supernate, all the solid concentrations kept changing with time. However, instead of changing the solid concentrations in the jet at every time step, the jet solid concentrations were only changed several times during the entire simulation. Thus, the model results at this time are a qualitative representation of the pump mixer operation. The 3-dimensional distributions of predicted volume fractions of Solid 9 after the first 2 minutes, 30 minutes, and 1.5 hours are shown in Figures 4.24 through 4.26 with the volume fractions color coded. These figures indicate that as the sludge-mixing time progresses, the jet containing the sludge slurry is mixing the sludge and supernate, but it takes about 1.5 hours to mix them fully within most of the tank. Also, the stream of slurry exiting the jet eventually almost reaches the tank wall. Because the current TEMPEST has limited success with handling yield stress (especially for the sludge to resist initial movement induced by the flow), no yield stress for the current simulation was used. Thus, the TEMPEST results indicating almost all the bottom sludge is eventually mixed may not be valid. A significant yield stress actually exists in the sludge prior to initiating the jet pump mixing, more resistance to sludge movement may be present than currently modeled.

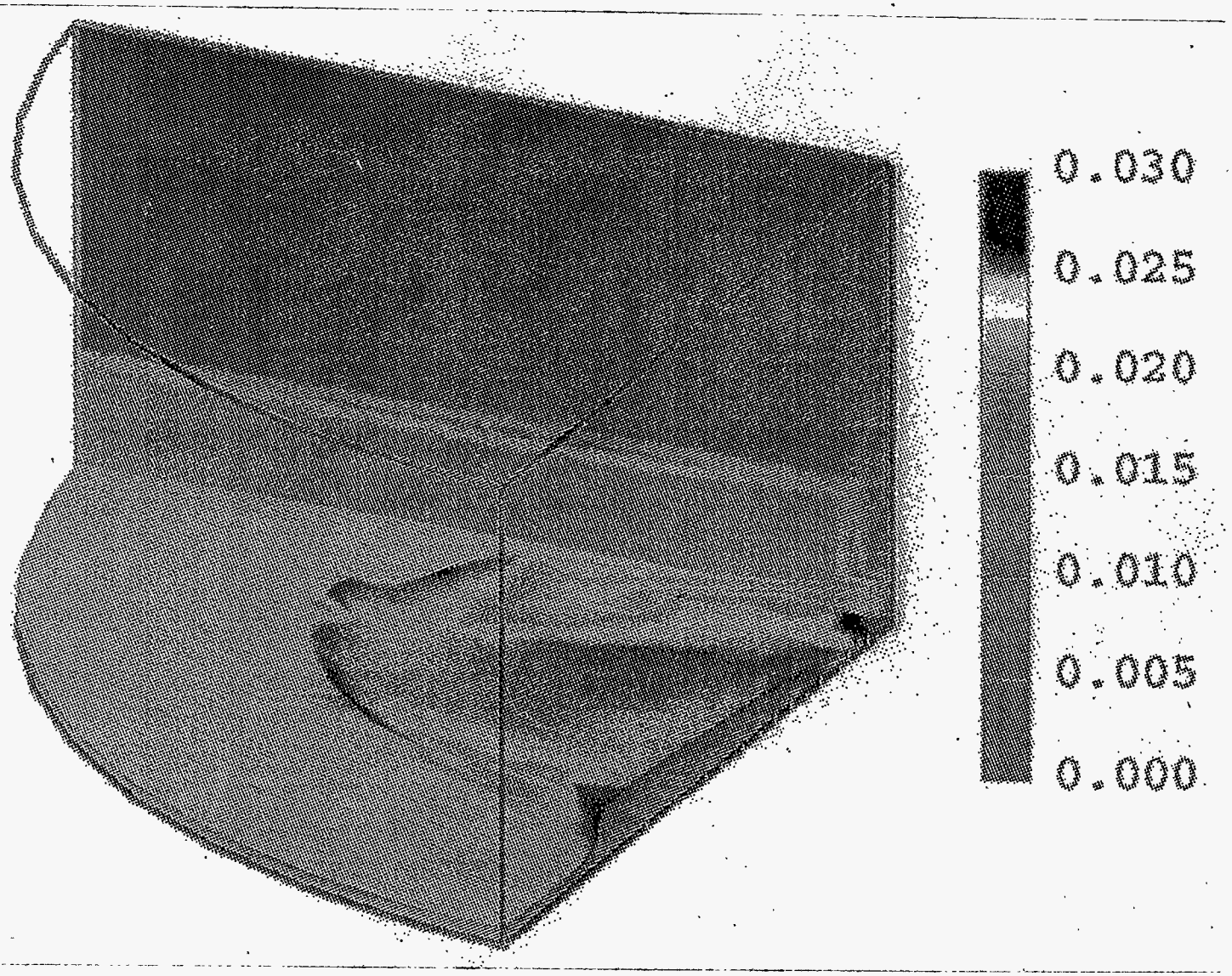

Figure 4.24. Predicted Three-Dimensional Distribution of Solid 9 Volume Fractions After Two Minutes of Mixer Pump Operation for Initially Settled Sludge in SY-102 Tank Case 1

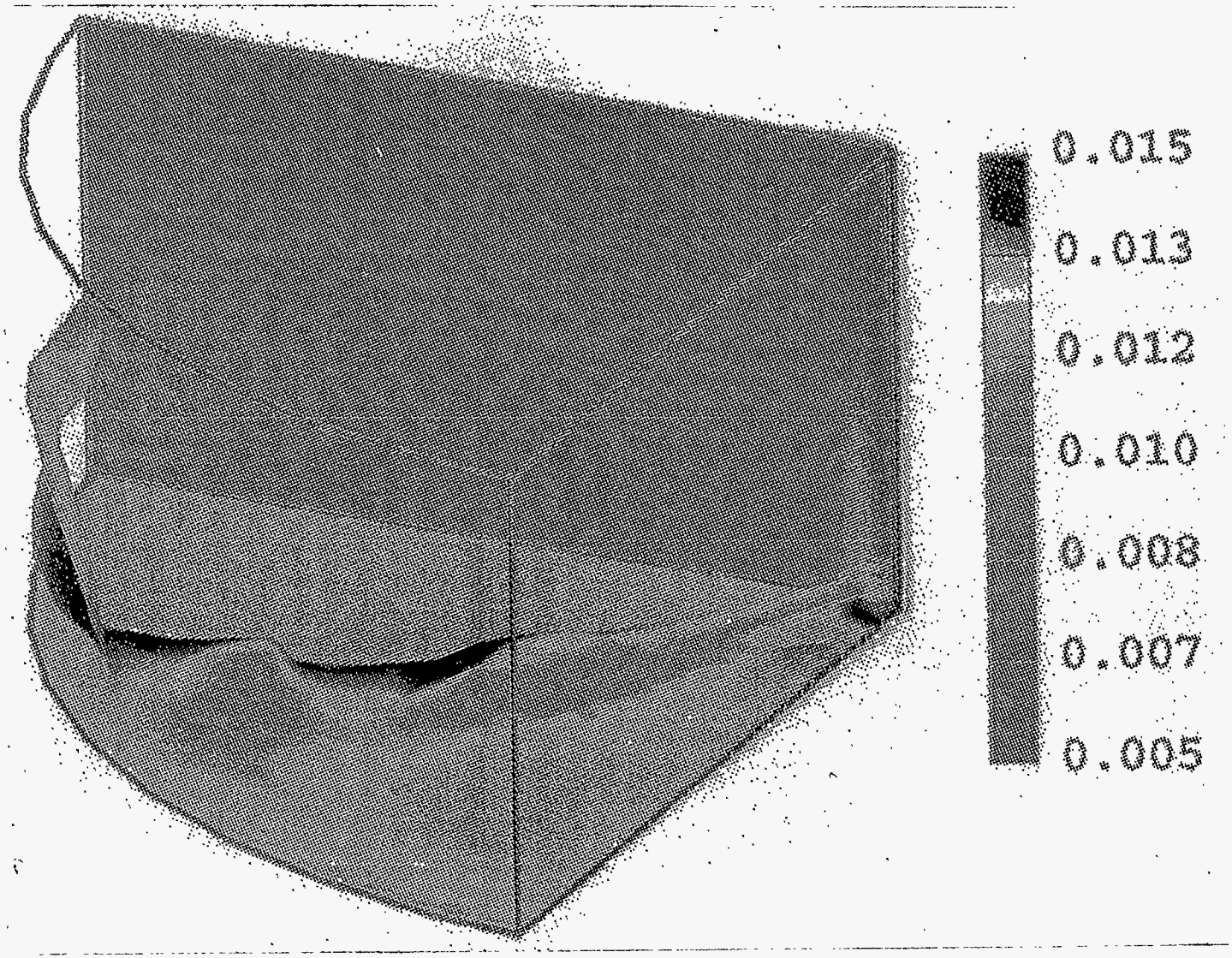

Figure 4.25. Predicted Three-Dimensional Distribution of Solid 9 Volume Fractions After 30 Minutes of Mixer Pump Operation for Initially Settled Sludge in SY-102 Tank Case 1

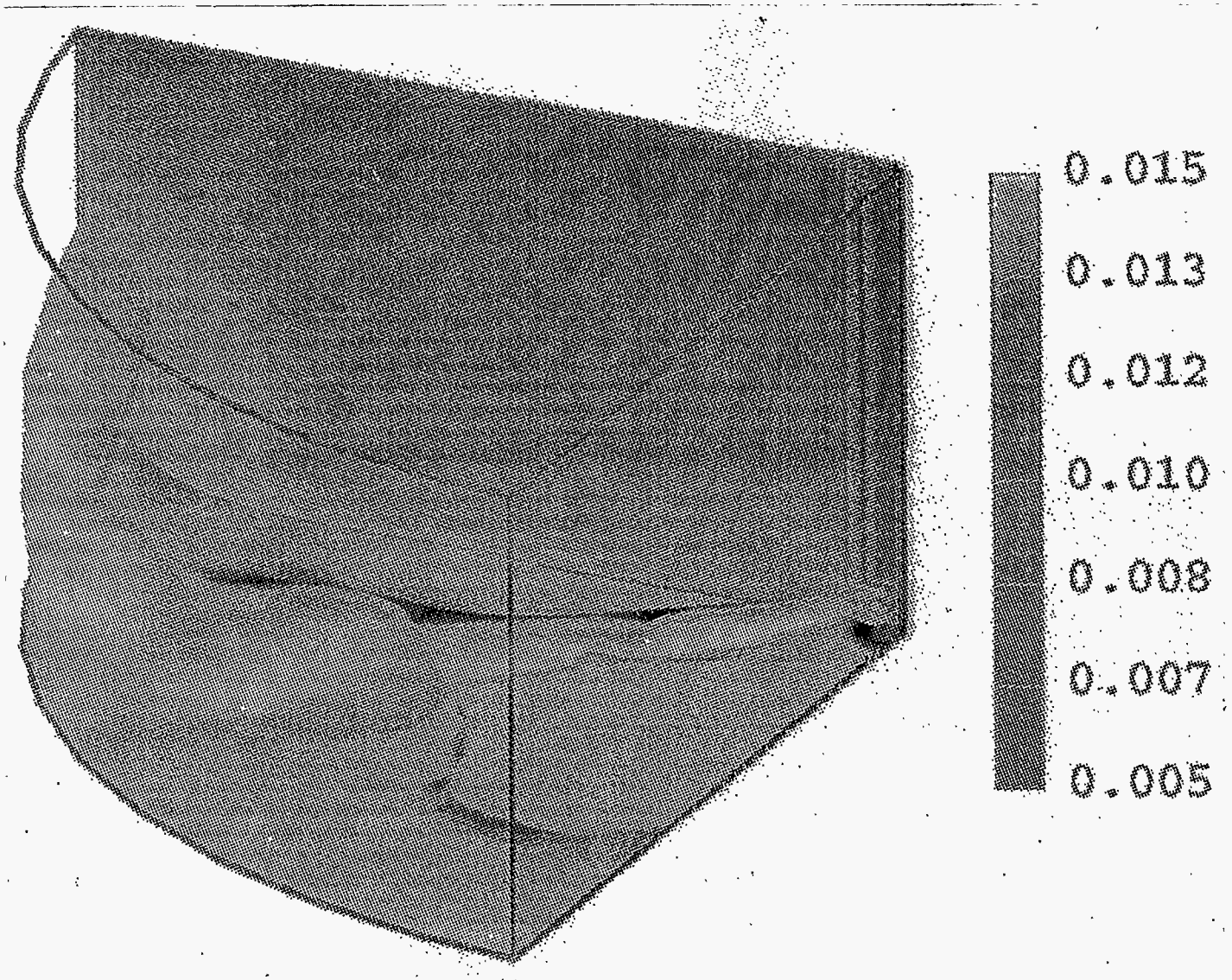

Figure 4.26. Predicted Three-Dimensional Distribution of Solid 9 Volume Fractions After 1.5 Hours of Mixer Pump Operations for Initially Settled Sludge in SY-102 Tank Case 1

Potential particle segregation was evaluated during continuous pump operation after the sludge and supernate were fully mixed, as the second test case. Internally (TEMPEST-generated) calculated viscosity varies from 0.016 to 0.022 Pa-s. Although these values are not directly comparable to available measured rheology data, these internally calculated viscosity values are nonetheless similar to measured consistency factors of 0.013-0.014 Pa-s for fully mixed SY-102 tank waste obtained in the lab by mixing Tank SY-102 sludge with twice the volume of its supernate, as shown in Table 4.7 (DiCenso et al. 1995). A more detailed discussion on rheology was presented in Section 4.2.1.

The model predicted some settling of Solid 7 (the coarsest solid with 100-175 μm diameter) and hardly any settling of Solid 1 (the finest solid with 10-20 μm diameter), as expected. (See Figures 4.27 and 4.28 showing the Solid 7 and 1 distributions at 1.5 simulation hours.) Fully mixed concentrations for Solids 1 and 7 are 16.6 and 9.0 kg/m^3, respectively. The distribution of all other solids (changes from the initial solids concentrations), including Solid 4, falls between these two patterns. As indicated in Figures 4.29 and 4.30, accumulation patterns for Solids 7 and 1 on the bottom of the tank also reflect these patterns, showing Solid 7 varying its concentration from 9.1 kg/m^3 near the tank center to 14.2 kg/m^3 along the tank wall; Solid 1 varies only from 16.6 to 16.7 kg/m^3, showing no position sensitive variable accumulation.

Predicted maximum solid segregation (the factor change over the initially assumed well-mixed state) for Solids 1, 4, and 7 is shown in Table 4.8. This table indicates the relative concentrations of the two presumed Pu-bearing solids (Solids 1 or 4) are actually reduced near the tank bottom, due to the slight concentration increase of coarser solids (Solid 7) under the model test conditions and durations tested. Thus, under Case 2 conditions and duration simulated, the mixer pump operation does not segregate the Pu-bearing solids in any measurable amount after the sludge and supernate are fully mixed and the pump is continuously run.

The third test case with the off-center jet requires very small simulation time-steps. At the early stage of the simulation (at five simulation minutes), the model predicted a large portion of the sludge was not mixed by the jet, as shown in Figures 4.31 and 4.32 depicting a vertical slice through the tank (at 2 o'clock position) and a horizontal plane at the tank bottom, respectively. The two figures show the particle concentration distributions of Solid 4 (the conservative presumed case for Pu-rich solids). The particle concentrations shown in Figure 4.31 (vertical slice through the tank) vary from 0.131 to 21.0 kg/m^3. This result indicates that even though no yield stress was imposed in this case, sludge has not appreciably been resuspended yet, due mostly to TEMPEST calculating a very large viscosity for

Table 4.7. Power Law Curve Fit Parameters for Tank SY-102 Wastes (DiCenso et al. 1995)

SY-102 Waste	Consistency Pa-s	Flow Behavior Index
Sample 1	0.013	0.808
Sample 2	0.014	0.791

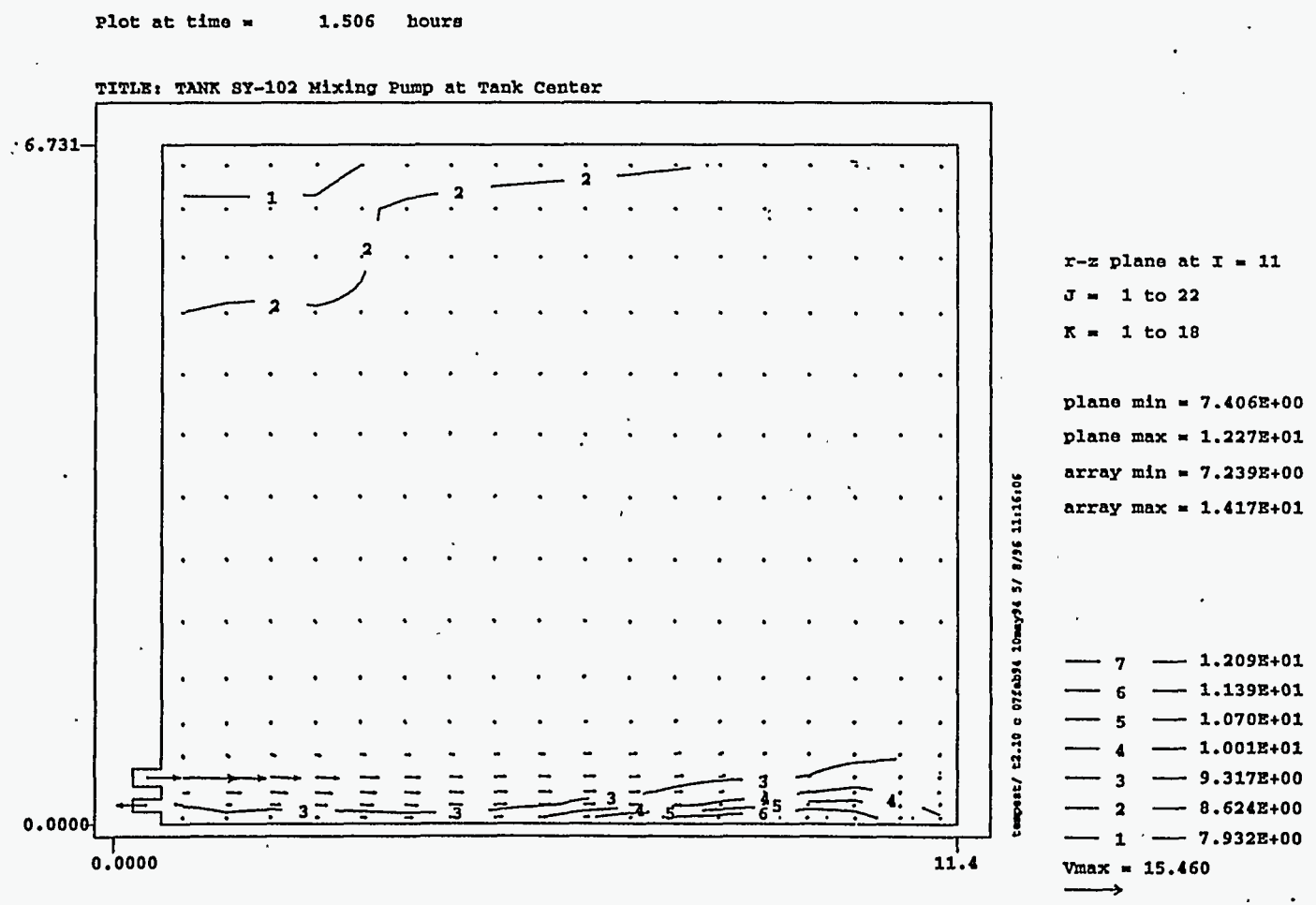

Figure 4.27. Predicted Vertical Distributions of Flow (m/s) and Solid 7 Concentrations (kg/m^3) on Vertical Plane 11 (12:30 Clock Position) With Sludge Initially Fully Mixed with Supernate at 1.5 Simulation Hours for SY-102 Tank Case 2

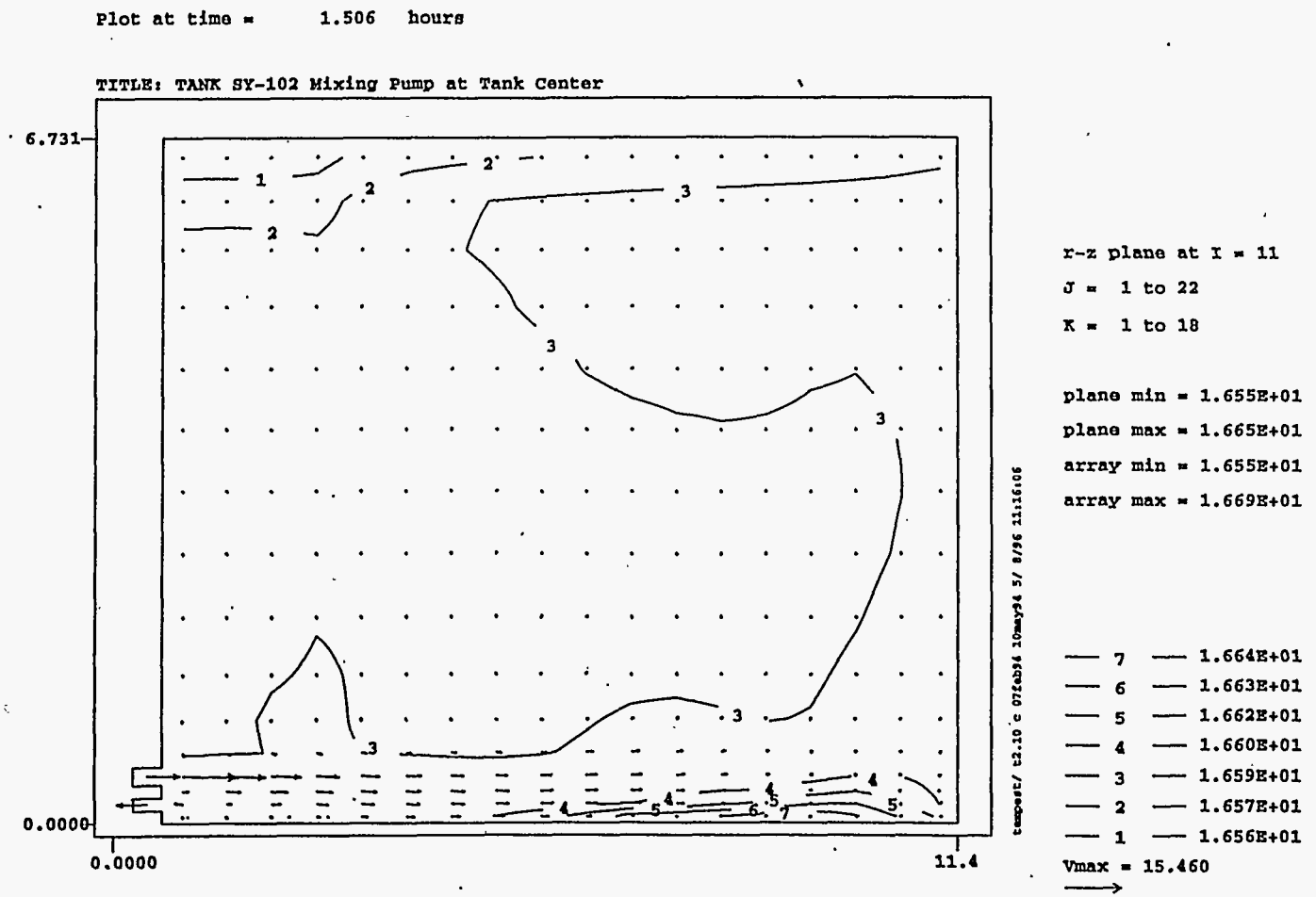

Figure 4.28. Predicted Vertical Distributions of Flow (m/s) and Solid 1 Concentration (kg/m^3) on Vertical Plane 11 (12:30 Clock Position) With Sludge Initially Fully Mixed with Supernate at 1.5 Simulation Hours for SY-102 Tank Case 2

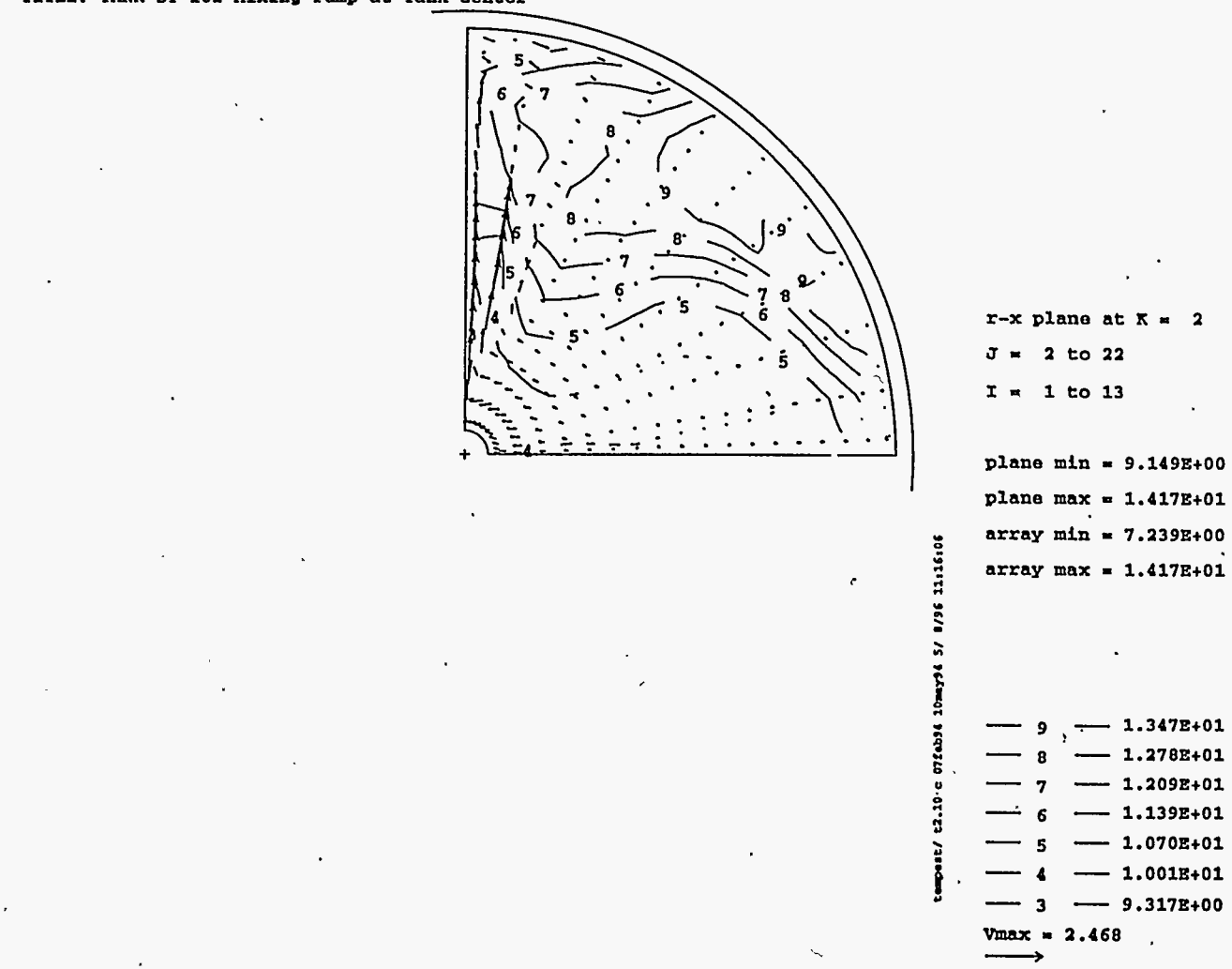

Figure 4.29. Predicted Horizontal Distributions of Flow (m/s) and Solid 7 Concentration (kg/m^3) at the Bottom of Tank With Sludge Initially Fully Mixed With Supernate at 1.5 Simulation Hours for SY-102 Tank Case 2

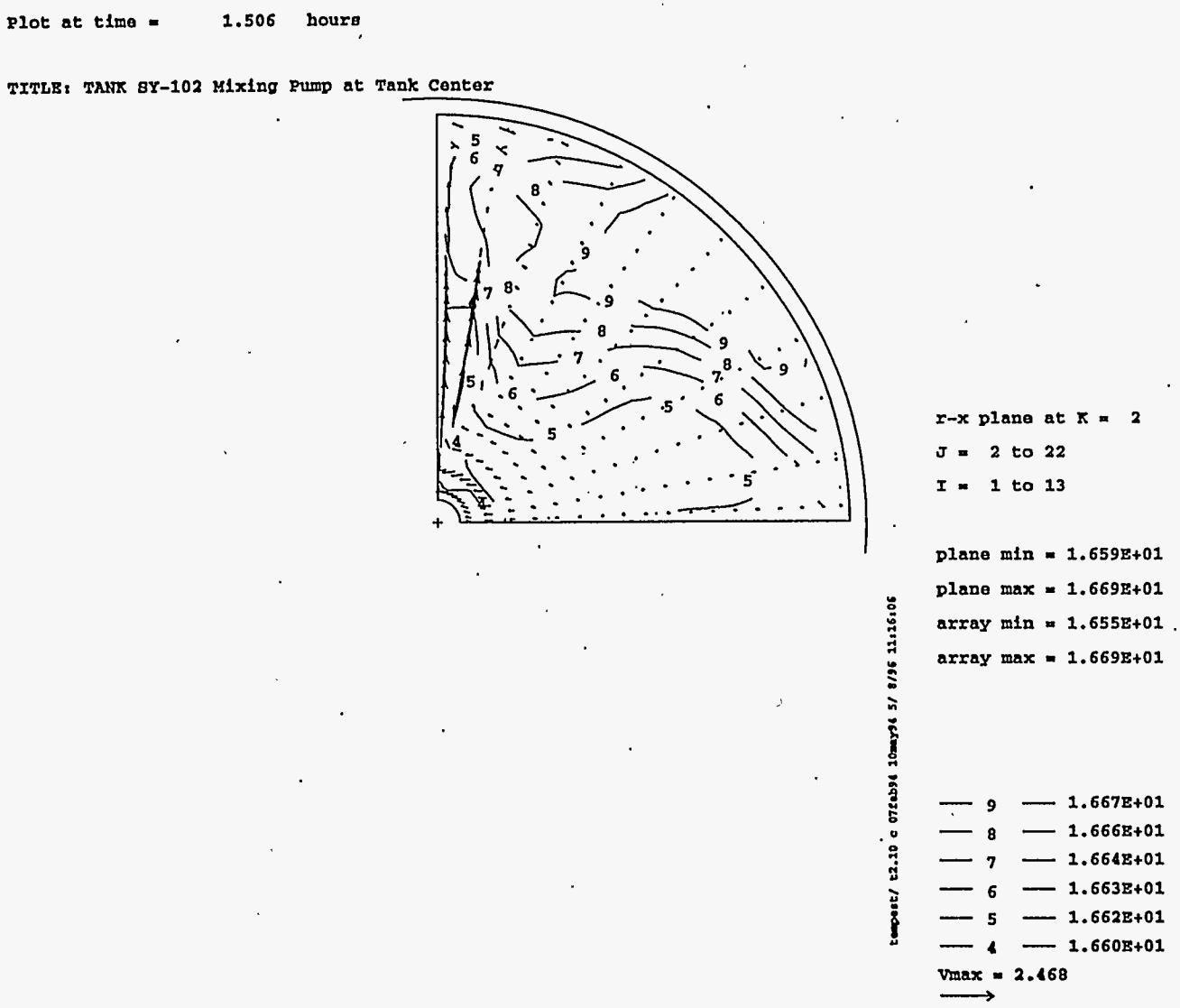

Figure 4.30. Predicted Horizontal Distributions of Flow (m/s) and Solid 1 Concentrations (kg/m³) at the Bottom of Tank With Sludge Initially Fully Mixed With Supernate at 1.5 Simulation Hours for SY-102 Tank Case 2

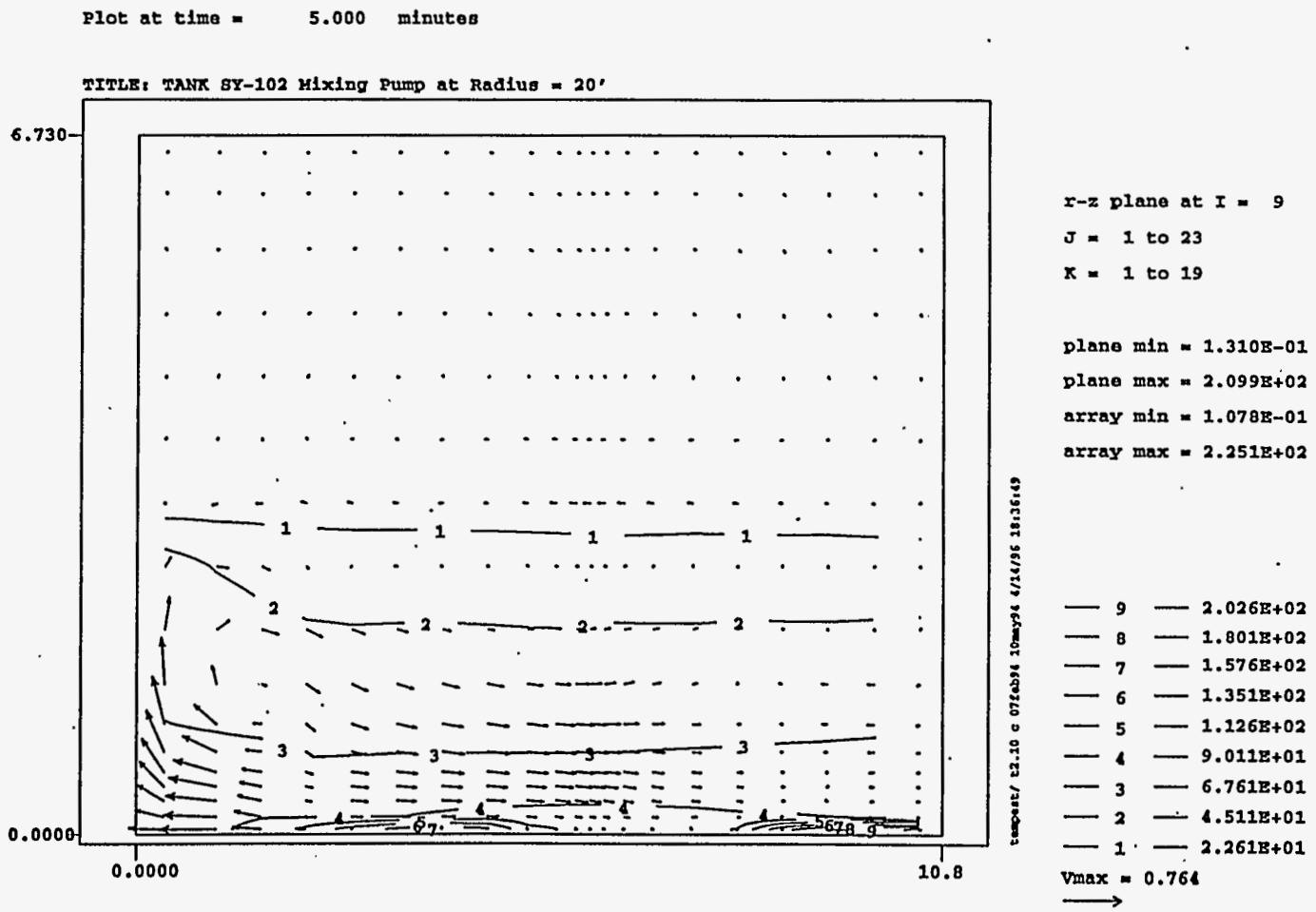

Figure 4.31. Predicted Vertical Distributions of Flow (m/s) and Solid 4 Concentration (kg/m3) on Vertical Plane 9 (2 o'clock Position) in with Off-Center Jet at Five Simulation Minutes for SY-102 Tank Case 3

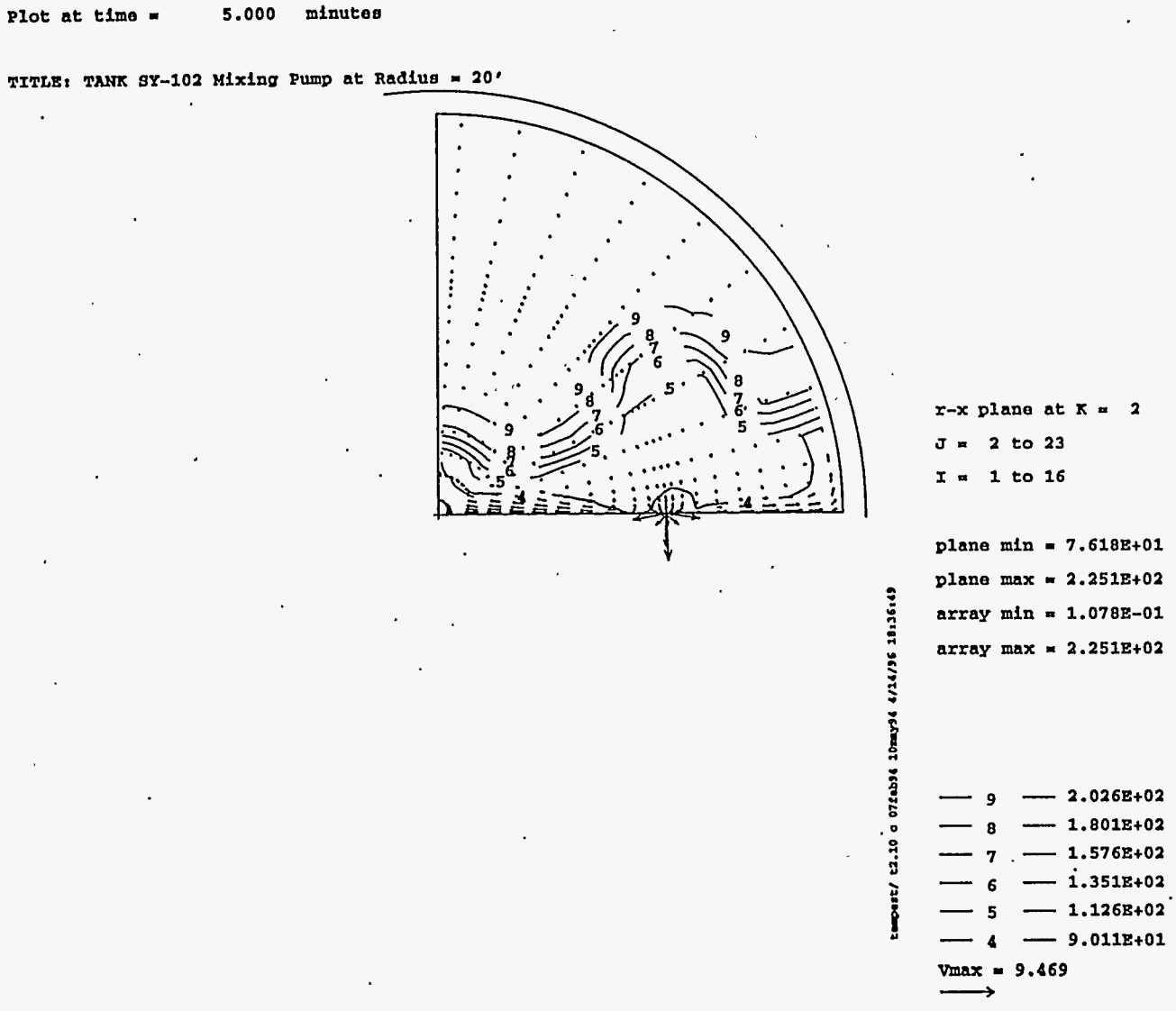

Figure 4.32. Predicted Horizontal Distributions of Flow (m/s) and Solid 4 Concentrations (kg/m^3) at the Bottom of Tank with Off-Center Jet at Five Simulation Minutes for SY-102 Tank Case 3

Table 4.8. Maximum Segregation Over the Initial Conditions Near the SY-102 Tank Bottom for Case 2

Solid Types	Initial Condition	30 Minutes	60 Minutes	90 Minutes
Solid 1	1	0.91	0.91	0.93
Solid 4	1	0.96	0.96	0.97
Solid 7	1	1.4	1.4	1.3

the slurry because of the high concentrations of suspended solids. TEMPEST, at least for this early simulation time, shows the bulk of the sludge has not resuspended and is hardly moving.

To test the sensitivity of predictions to the particle settling velocity, the unhindered settling velocity of Solid 4 was increased by 10 times above the actual value of 0.81 mm/s shown in Table 4.6. As before, TEMPEST then internally calculated a hindered settling velocity, as affected by the suspended solids concentration. All other solid fall velocities (unhindered) were kept the same as those shown in Table 4.6. The predicted distributions of Solid 4 for this increased fall velocity case are shown in Figures 4.33 and 4.34. The particle concentration for the vertical slice through the tank (at 2 o'clock position) varies from 0.126 to 21.3 kg/m^3 (see Figure 4.33). The comparison of Figures 4.33 and 4.34 with Figures 4.31 and 4.32 clearly reveals that although some additional settling for the increased settling velocity case is present, the large increase (10-fold increase) in the fall velocity for Solid 4 did not significantly change the particle concentration distribution and accumulation patterns for this particle size in the tank. Approximately a 100-fold difference on settling velocity, as seen between Solids 1 and 7, is needed before significantly measurable segregation differences occur between the various sludge particles. This sensitivity analysis thus, gives some guidance on how much difference it will take in particle size and particle density (as they relate to hydrodynamic settling velocity [see Appendix B for the relationship]) to lead to significant differences to settling trends between various types of sludge components, such as Pu-rich particles and hydrous iron and aluminum oxides (common neutron absorbers). This analysis also leads to the conclusion that adjustments in the hindered settling model (Equation 4.3) does not introduce unacceptable errors in segregation.

The fourth simulation case is similar to Case 2 to determine potential solid segregation during the continuous pump jet mixing operation after the sludge is fully mixed with supernate. Unlike the second case, this case reflects more closely the current SY-102 tank condition by having the sludge to supernate volume ratio of 1:2, sludge viscosity of 4500 Pa-s, and C_{vmax} of 0.53, as discussed previously. This case was simulated for 1.5 hours. Although specific solid concentrations at a given location are different, the predicted solid distribution patterns are similar to those of Case 2. Figures 4.35 and 4.36 show predicted Solid 7 distributions of the fourth case after 1.5 simulation hours. These figures indicate that Solid 7 (the coarsest solid) has relatively uniform concentrations in the bulk of the tank, but its concentrations are higher along the tank wall near the bottom. Solids 4 (a conservative representation of Pu solid) and

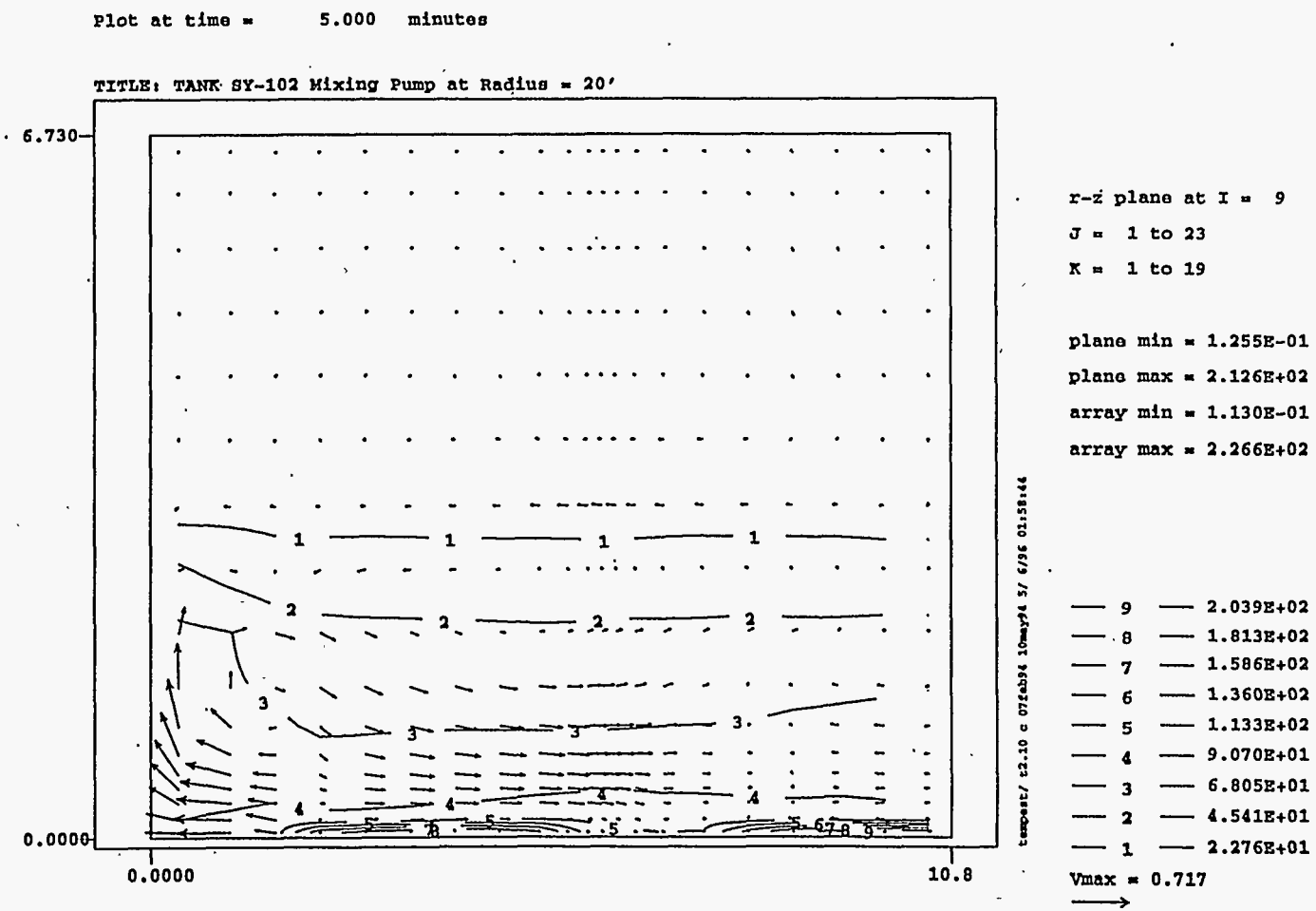

Figure 4.33. Predicted Vertical Distributions of Flow (m/s) and Solid 4 (with 10 Times Greater Fall Velocity) Concentration (kg/m^3) on Vertical Plane 9 (2 o'clock Position) with Off-Center Jet at Five Simulation Minutes for SY-102 Tank Case 3

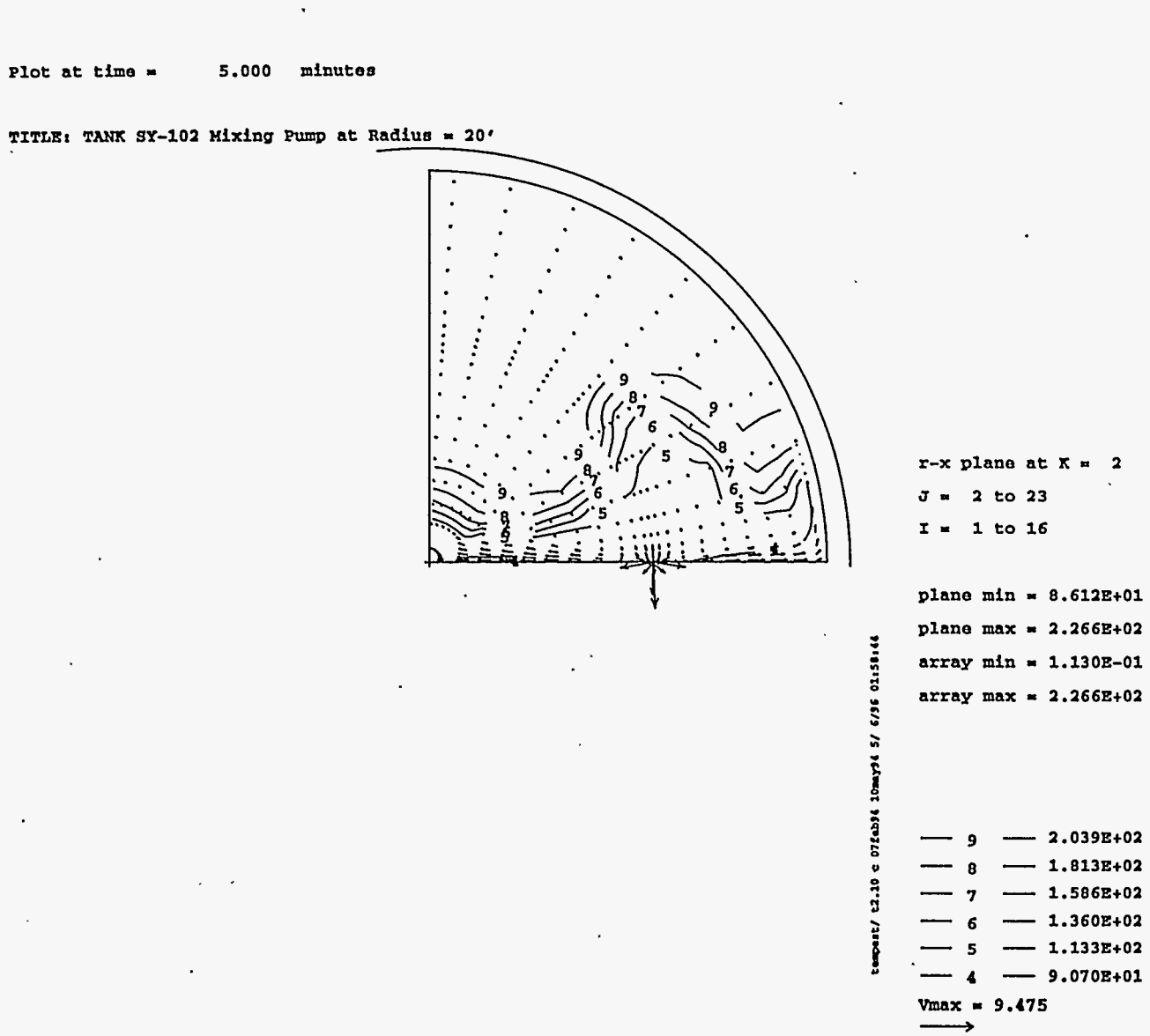

Figure 4.34. Predicted Horizontal Distributions of Flow (m/s) and Solid 4 (with 10 Times Greater Fall Velocity) Concentrations (kg/m^3) at the Bottom of Tank with Off-Center Jet at Five Simulation Minutes for SY-102 Tank Case 3

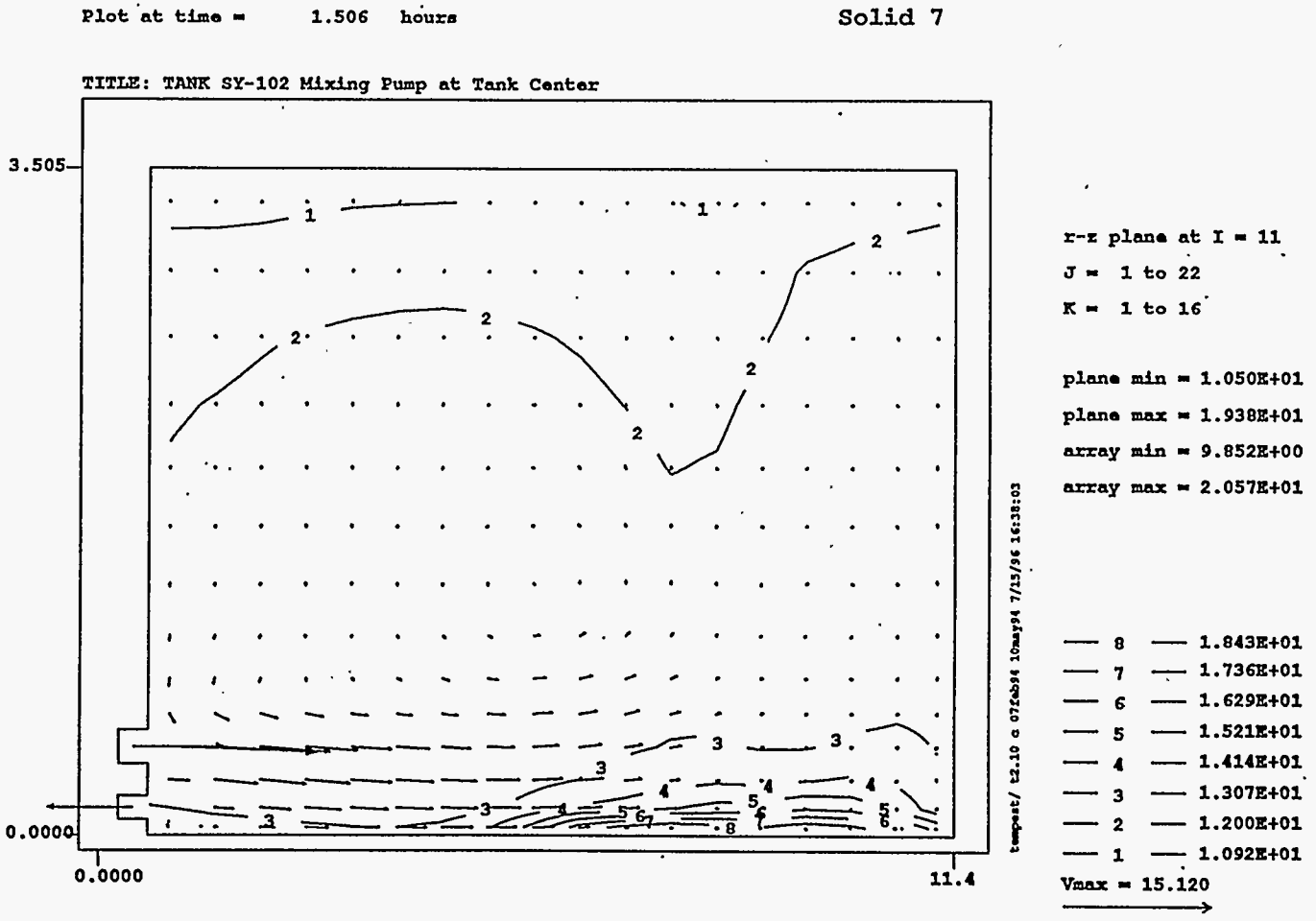

Figure 4.35. Predicted Vertical Distributions of Flow (m/s) and Solid 1 Concentration (kg/m^3) on Vertical Plane 11 (12:30 Clock Position) With Sludge Initially Fully Mixed with Supernate at 1.5 Simulation Hours for SY-102 Tank Case 4

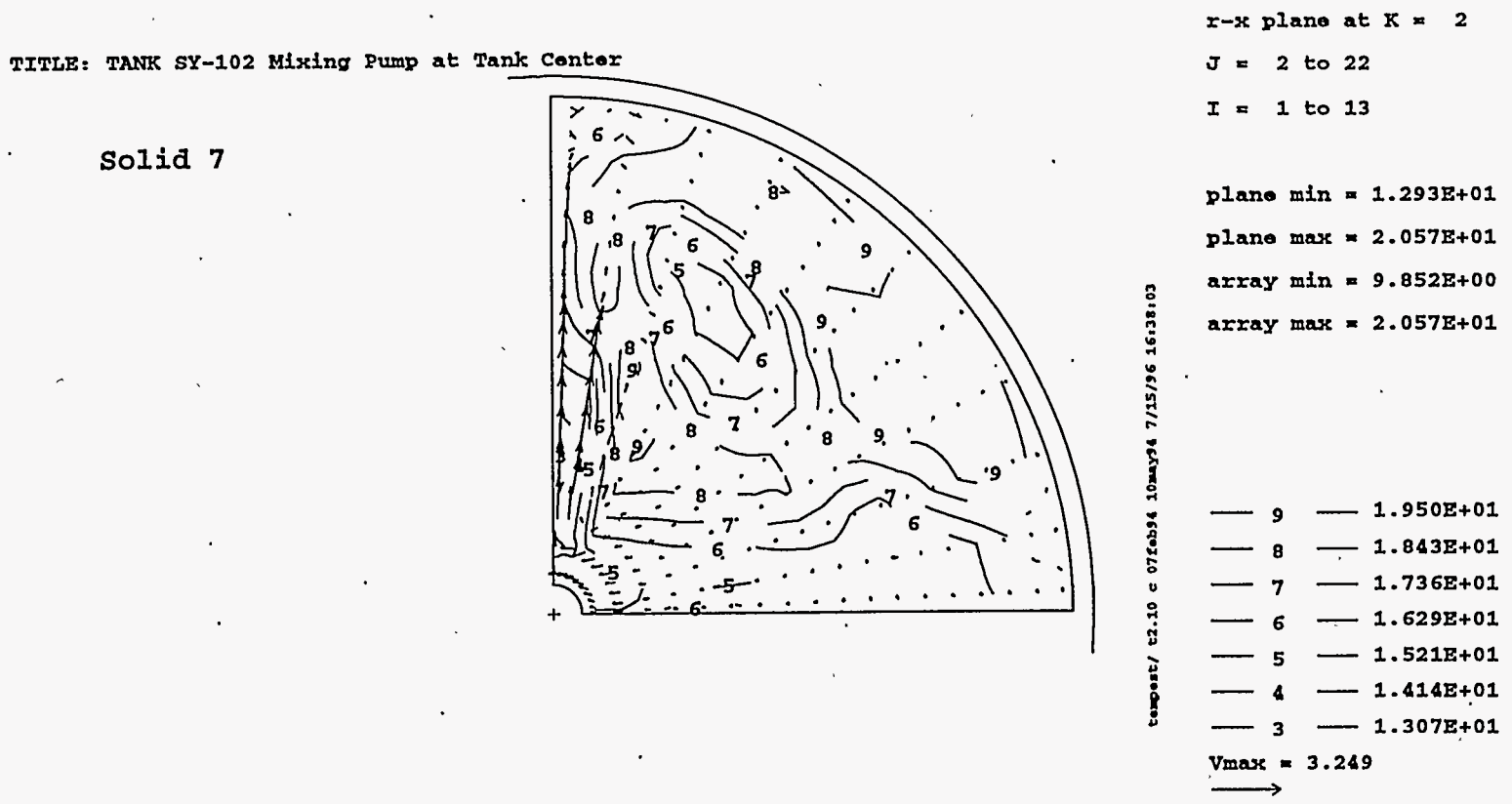

Figure 4.36. Predicted Vertical Distributions of Flow (m/s) and Solid 7 Concentrations (kg/m³) on Vertical Plane 11 (12:30 Clock Position) with Sludge Initially Fully Mixed with Supernate at 1.5 Simulation Hours for SY-102 Tank Case 4

Solid 1 (more realistic representation of Pu solid) are more uniformly distributed throughout the tank, with slightly higher concentrations still showing along the wall near the bottom, as shown in Figures 4.37 and 4.38, respectively.

Predicted maximum solid segregations for Solids 1, 4, and 7 for this case are shown in Table 4.9. This table indicates the relative concentrations of the two presumed Pu-bearing solids (Solids 1 or 4) are actually reduced near the tank bottom, due to the slight concentration increase of coarser solids (Solid 7). These segregation values are very similar to those of Case 2 (see Table 4.8). Thus, according to the model results obtained under these conditions and duration simulated, the mixer pump operation does not segregate the Pu-bearing solids in any measurable amount after the sludge and supernate are fully mixed and the pump is continuously run.

TEMPEST Case 5 was run to simulate two opposing rotating jets located 20 feet off center to reflect recently obtained SY-102 characterization data, as indicated above. Since a half tank was modeled in this case, the computational time was significantly increased compared to other cases. The recent SY-102 data have not been available long enough to allow long-term simulations to be completed. Thus, the simulation time for Case 5 was short. Predicted Solid 7 concentrations on the tank bottom and 17 inches above the bottom tank at 3.56 minutes are shown in Figures 4.39 and 4.40. At that time, the jets are shooting out at 2 and 8 o'clock directions. The Solid 7 concentration in 2 o'clock vertical plane is shown in Figure 4.41. These figures shows that jets are not penetrating further into the sludge yet at this time and the most of the sludge is not yet moved.

4.2.5 Air-Lift Circulator Operation

The air-lift circulator (ALC) consists of a long, vertical, open-ended cylinder with an air supply at the lower end. The air rises due to buoyancy, and in the process entrains some liquid into the bottom of the pipe. The total flow rate of entrained liquid depends on the air supply rate, the geometry of the cylinder, and the physical properties of the liquid.

In the Hanford tanks, the ALC system's performance is complicated by the fact the liquid is actually a slurry which contains suspended solids. No specific correlations in the literature explicitly consider the characteristics for sparging of solid-liquid suspension. So, it will be assumed the slurry is a liquid with a density and viscosity equal to those of the slurry.

This assumption is justified if the suspended particles are relatively small which is the case in most (if not all) of the Hanford waste tanks. The goal of this section is to determine whether the entrained liquid flow rate used in a past TEMPEST prediction documented by Eyler (1983) is reasonable. The TEMPEST analysis made a similar assumption regarding flow of the mixed slurry. So, any uncertainty resulting from treating the slurry mixture as a liquid is also embedded in the final results of the past TEMPEST simulation for ALCs.

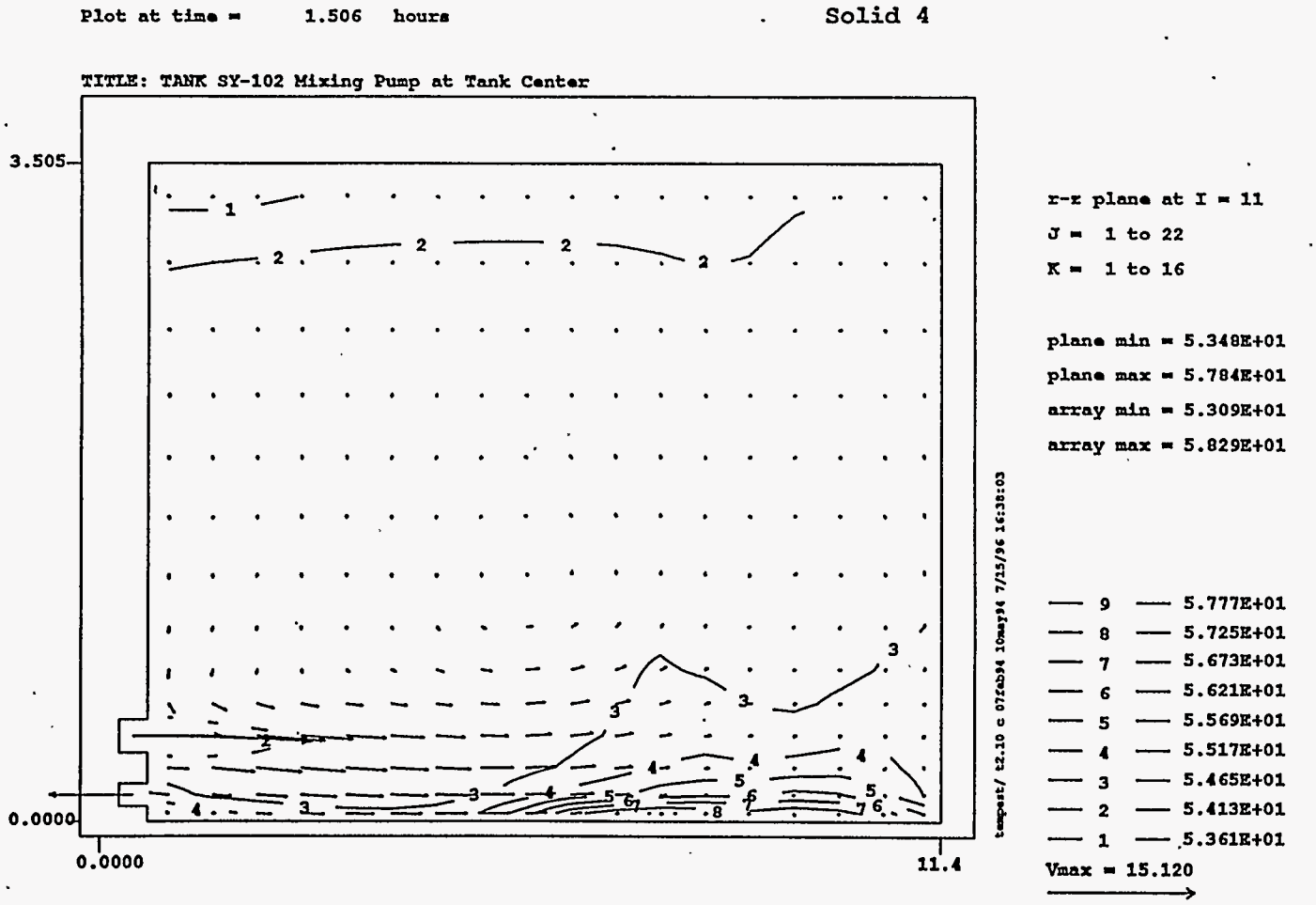

Figure 4.37. Predicted Vertical Distributions of Flow (m/s) and Solid 7 Concentrations (kg/m³) on Vertical Plane 11 (12:30 Clock Position) With Sludge Initially Fully Mixed with Supernate at 1.5 Simulation Hours for SY-102 Tank Case 4

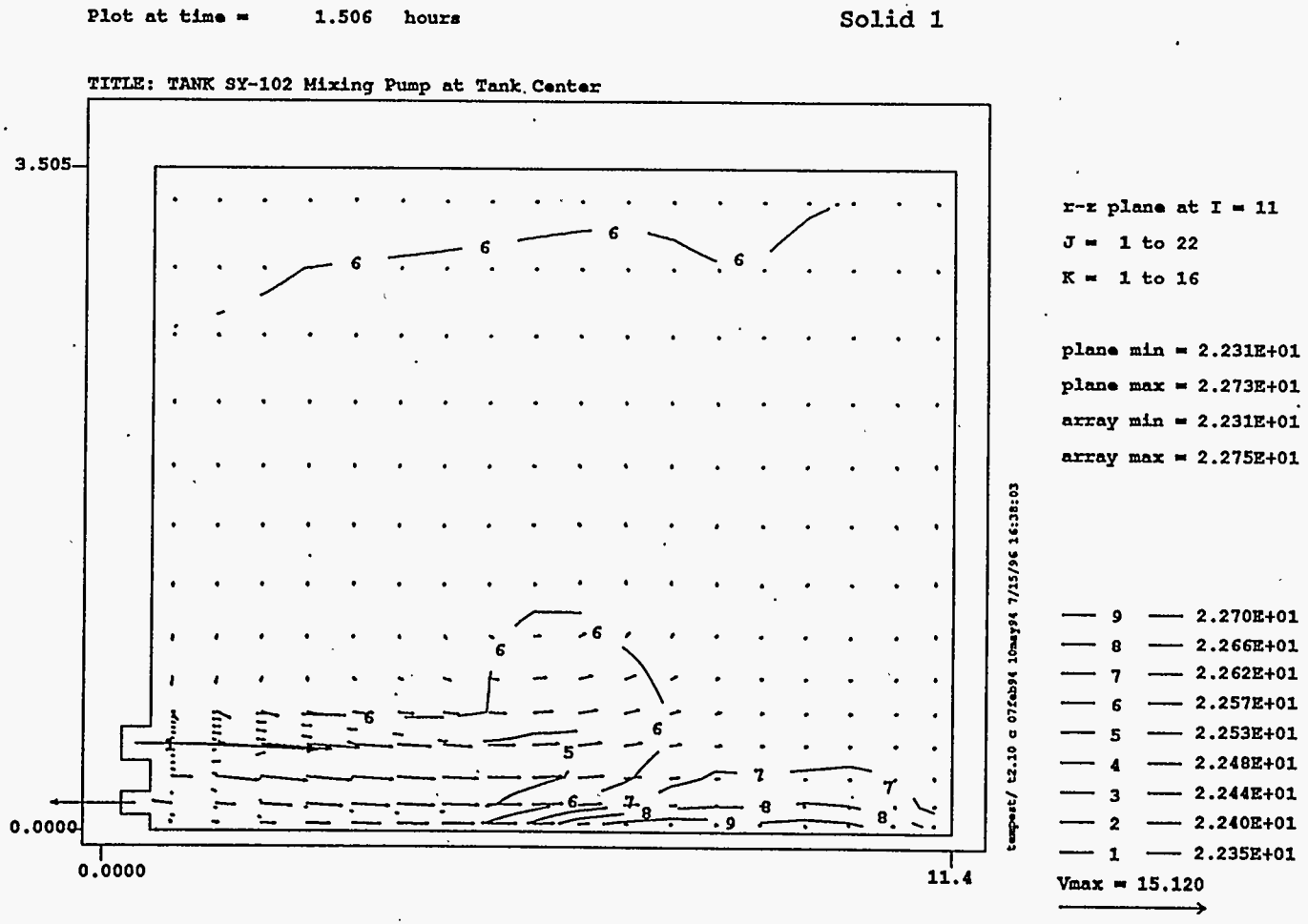

Figure 4.38. Predicted Vertical Distributions of Flow (m/s) and Solid 1 Concentrations (kg/m^3) on Vertical Plane 11 (12:30 Clock Position) With Sludge Initially Fully Mixed with Supernate at 1.5 Simulation Hours for SY-102 Tank Case 4

Table 4.9. Maximum Segregation Over the Initial Conditions Near the SY-102 Tank Bottom for Case 4

Solid Types	Initial Condition	30 Minutes	60 Minutes	90 Minutes
Solid 1	1	0.91	0.90	0.91
Solid 4	1	0.96	0.96	0.97
Solid 7	1	1.4	1.5	1.4

Figure 4.42 is a schematic of an ALC. Air is forced through the inner pipe and escapes out the bottom where it creates bubbles and entrains liquid and fine particles that rise with the bubbles within the cylinder. The buoyancy created by the rising bubbles moves the entrained slurry and creates convection cells that pull sludge/slurry from the neighboring volume. Hanford waste tanks that contain ALCs usually have about 22 such dual pipe systems spread in two concentric circles around the tank with the intent of completely mixing the slurry content within the tank.

The flow rate inside the cylinder may be predicted by recognizing the pressure drop calculated for flow outside the cylinder must be equal to the pressure drop calculated inside the cylinder. The pressure drop inside the cylinder is related to the flow of entrained slurry.

Appendix C presents the details of the analyses to determine whether the velocity of the entrained tank slurry, caused by the rising bubbles that Eyler (1983) used, is reasonable.

For a minimum air flow rate of 50 scfm in each of 22 ALCs in a Hanford tank, the total flow rate for entrained slurry of 2100 gpm in each ALC is justified. Therefore, the liquid entrainment assumed in past TEMPEST calculations appear valid.

An older version of the TEMPEST code was used by Eyler (1983) to simulate liquid flow and solid movement in a DST by imposing the induced liquid velocity of 0.961 ft/s in each circulator. The older version of TEMPEST assumed that viscosity was independent of solid concentrations and that the flow was Newtonian.

The TEMPEST 1/7 tank modeling is based on the symmetry afforded by the location of the 22 ALCs which are spaced evenly around the tank in two concentric circles. Solids with a settling velocity of 0.03 m/s were placed at the bottom of the tank (Eyler 1983). As the air-induced liquid flow rises through the outer 30-inch tubes of the ALC, the flow around the tube bottoms (0.76 m above the tank bottom) will entrain sludge into the tubes. This erodes solids around the bottom of the tubes. However, the velocity decreases with the distance away from the tube bottom perimeter, and the velocity near the tank bottom is probably about 0.05 m/s or less more than 1 m away from each ALC, as also predicted by the past TEMPEST run (see Figure 4.43). As discussed in Appendix B, the critical velocity is about 0.2 m/s for the most easily erodible medium sand (diameter of 0.3 mm), 0.4 m/s for coarse sand (diameter of

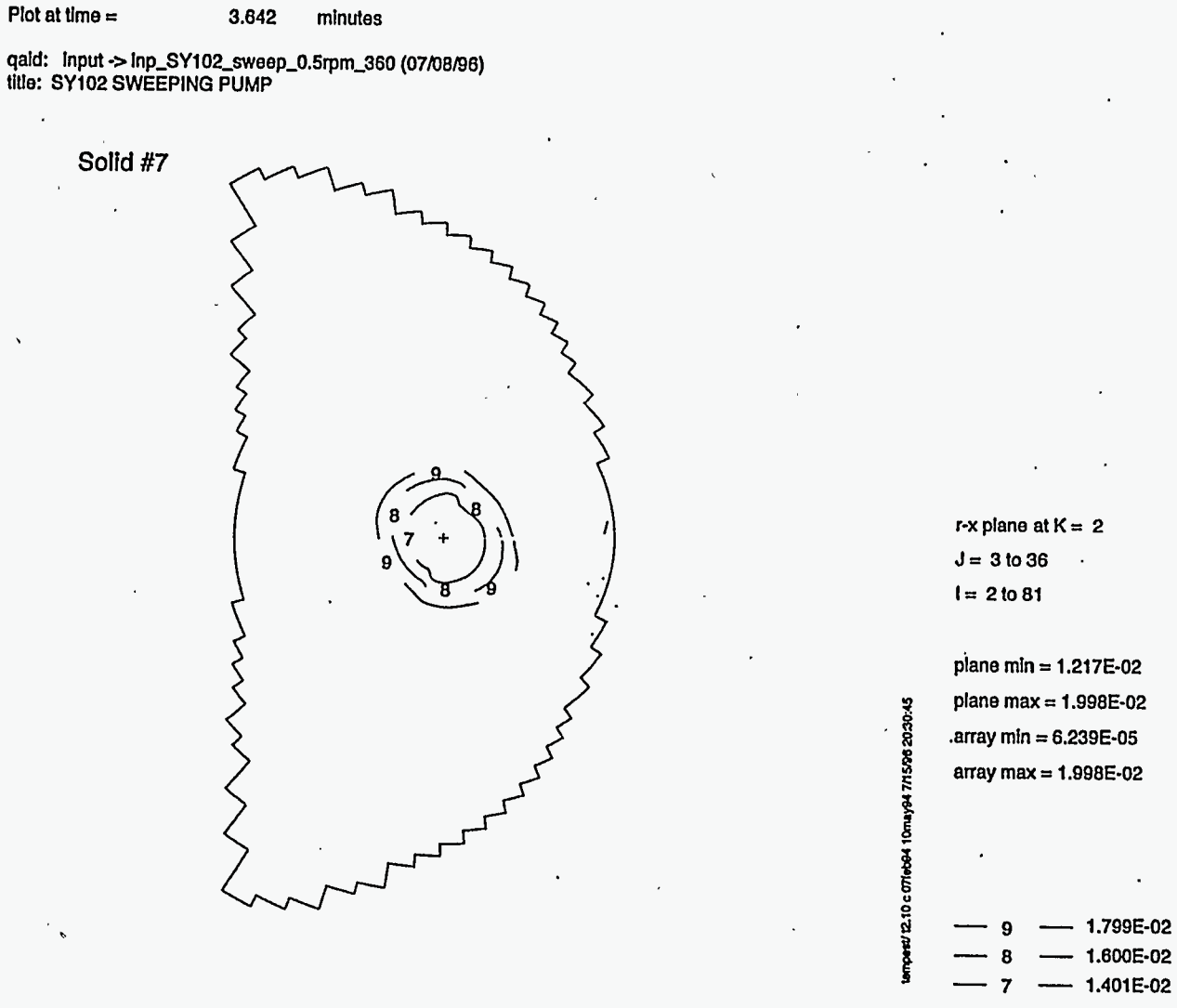

Figure 4.39. Predicted Horizontal Distribution of Solid 7 Volume Fraction at the Bottom of Tank with Off-Center Jet at 3.6 Simulation Minutes for SY-102 Tank Case 5

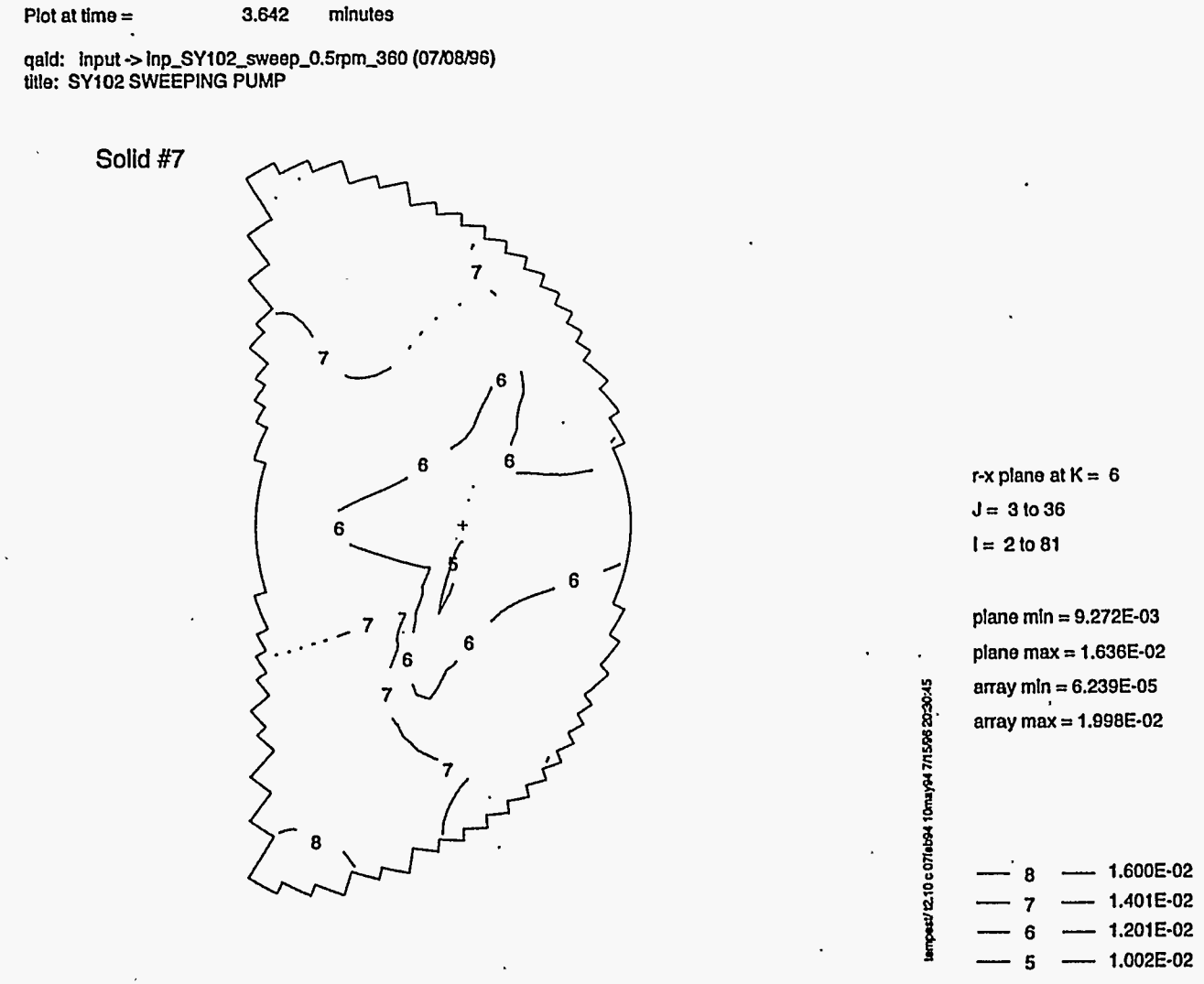

Figure 4.40. Predicted Horizontal Distribution of Solid 7 Volume Fraction at 17 Feet Above the Tank Bottom with Off-Center Jet at 3.6 Simulation Minutes for SY-102 Tank Case 5

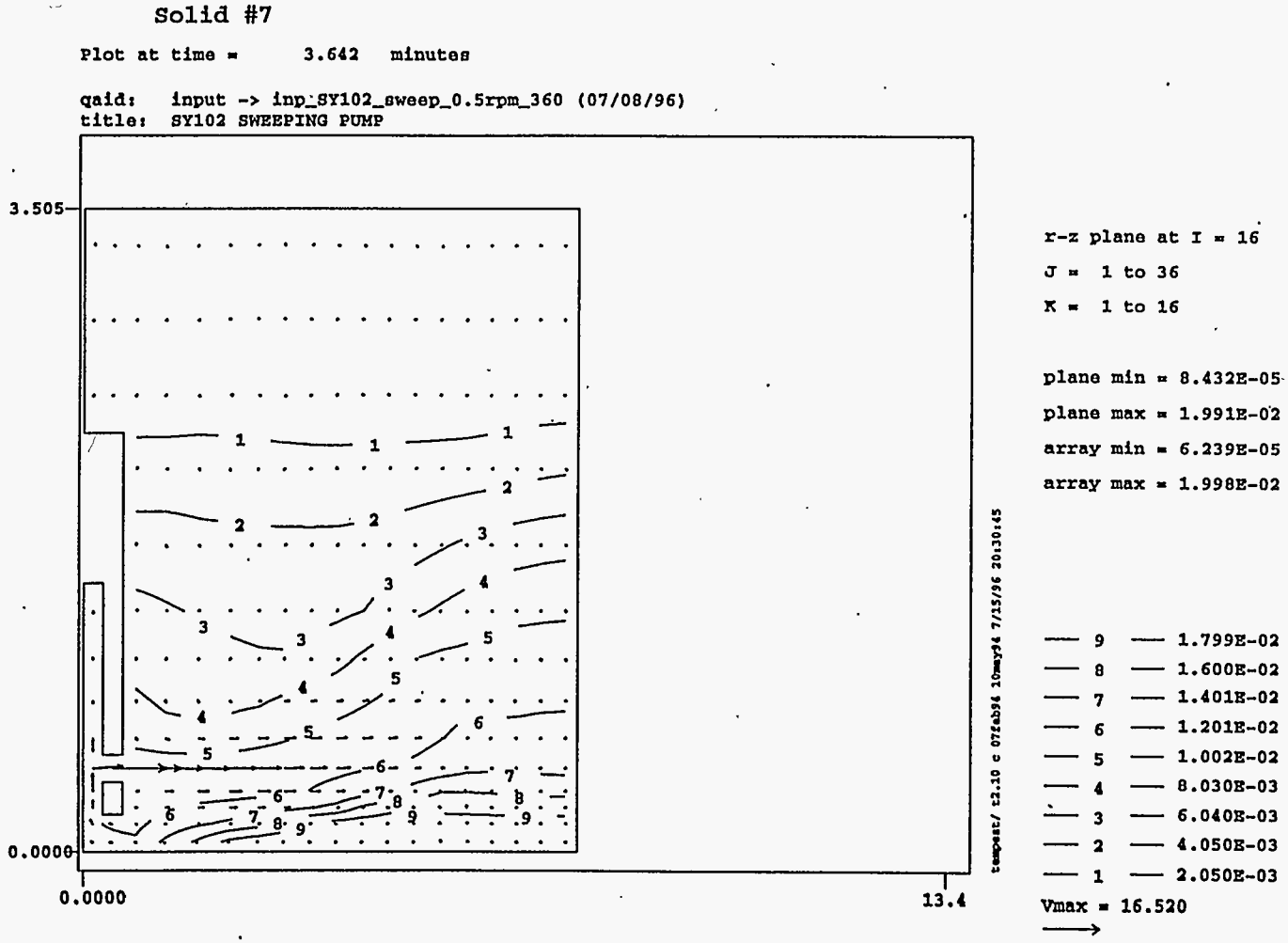

Figure 4.41. Predicted Vertical Distributions of Flow (m/s) and Solid 7 Volume Fraction on Vertical Plane 9 (2 o'clock Position) with Off-Center Jet at 3.6 Simulation Minutes for SY-102 Tank Case 5

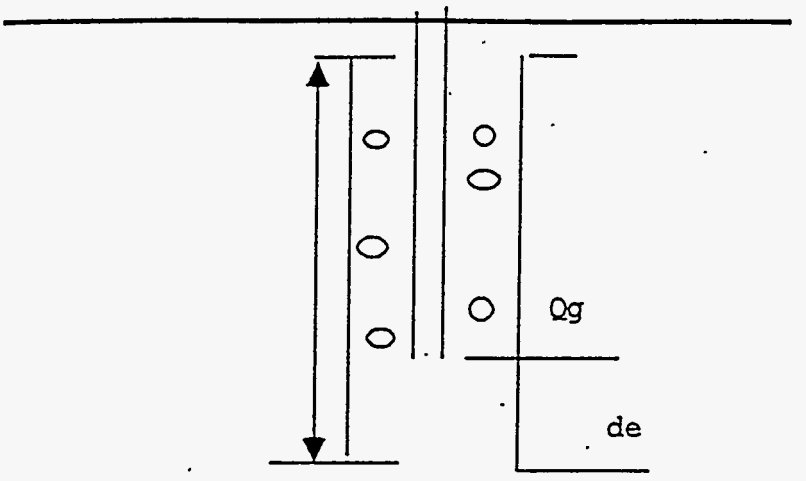

Figure 4.42. Schematic of an Air-Lift Circulator

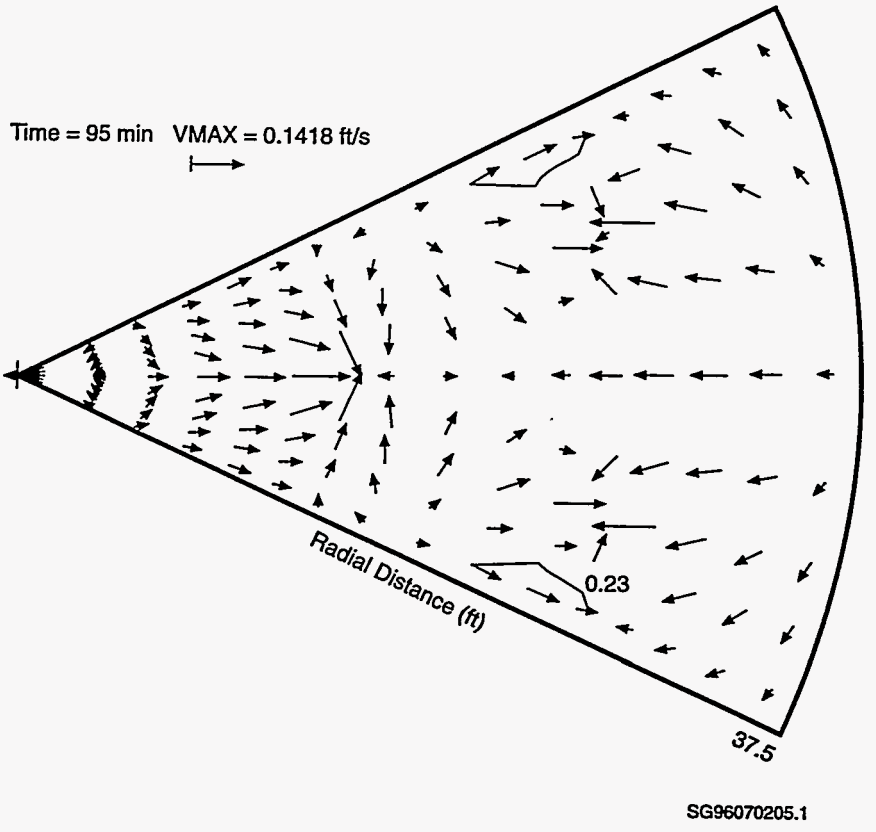

Figure 4.43. TEMPEST Predicted Velocity Field for Sludge Slurry at Bottom of Tank While Air-Lift Circulators are Running

2 mm), 1.3 m/s for medium gravel (diameter of 1 cm), and 2.5 m/s for 1 μm clay (Vanoni 1975, Simons and Senturk 1977). Thus, although the older TEMPEST model predicted that uniform mixing and complete sludge resuspension were achieved throughout the tank after 15 simulation minutes, the actual scouring is probably limited to local areas around the ALCs, and many solids located beyond 1 m or so from the air-circulators will not be resuspended by the induced flow. However, most of the solids resuspended by the induced flow will probably follow a local recirculating flow pattern around the tubes, with some small amount of the resuspended solids settling on top of solids that do not move during the operation of the ALCs. The probability that this selective settling in zones between and away from each ALC could lead to concentration of much sludge material and Pu-rich sludge, in particular, is remote. Neutronic criticality calculations suggest that a rather large volume of material would need to settle (even assuming spherical geometry) for criticality to occur. There will be 22 zones in the tank (approximately concentric circles around each ALC for which there will be complete resuspension and uniform settling in thin layers when the air is shut off and many interconnected zones just outside of the 22 concentric circles where little or no sludge will be resuspended. What little resuspended sludge that settles out over these zones would be dispersed around the 22 active zones and not preferentially settle in any select dead zone. Rather, the sludge which settles out during ALC operation will be distributed among all the areas which are too far from the ALC bottoms to be entrained and suspended.

Furthermore, because the fine solid particles considered to represent Pu solids in this study are not very easily floated by attaching to air bubbles, as discussed in Section 4.4, the flotation technique used in mining industry (ALC itself) is not very likely to significantly segregate Pu-solids.

4.3 Evaluation of 1/12-Scale Data from Mixing Uniformity Tests

Experimental evidence that particles segregate by size during operation of mixer pumps appears in Bamberger et al.[a] That document describes a series of scaled mixing experiments that were performed to determine the power required to maintain particles in suspension using mixer pumps. Although the potential for separation was not specifically studied, a small amount of data were collected that can be used to assess the potential for separation during operation of mixer pumps. This section provides a brief description of the experiments, a synopsis of some data relevant to separation and criticality, and a discussion of the implications with respect to separation during actual operation of mixer pumps.

Section 4.3.1 provides a general description of the scaled experiments. Section 4.3.2 describes the test procedure. Section 4.3.3 provides a description of the simulants used during testing. Section 4.3.4 describes the average particle size distribution remaining in solution at several pump speeds, and Section 4.3.5 describes the variation of particle size in the settled layer.

(a) Unpublished. *1/12-Scale Mixing Experiments to Characterize Double-Shell Tank Slurry Uniformity*. Pacific Northwest National Laboratory, Richland Washington.

4.3.1 Scaled Experiments

Experiments were conducted in a 1/12-scale system for testing DST retrieval technologies. The 1/12-scale tank is installed in the 336 Building in the 300 Area of the Hanford Site. The system included a 1/12-scale model of a Hanford DST, one simulated 1/12-scale mixer pump which was mounted in the center of the tank and simulant preparation equipment and instrumentation. A detailed description of the facility is available in Bamberger et al.[a]

Fourteen experiments were conducted to determine the power required to suspend particulate materials using one centrally located mixer pump. The test matrix included four simulants and several flow rates. This matrix provided data to determine the influence of three separate factors on mixing behavior. The factors were average particle diameter, pump power, and mixture viscosity. Based on the data, the influence of these factors on separation can be partially assessed.

The specific properties of the simulants were selected based on a scaling methodology described in Bamberger et al.[a] and Liljegren (1993). This scaling methodology is based on the principle of similarity, as described in Fox and McDonald (1973). When applied to mixing of solids-liquid mixtures using mixer pumps, the analysis indicates that eight dimensionless parameters must match to achieve similarity. If all dimensionless parameters match, the theory states that mixing will be similar in two vessels. The full theory was tested experimentally and found to apply to mixing of solid materials when all eight dimensionless parameters match (Johnson 1994).

However, it is not possible to match all parameters when modeling a full-scale tank problem. For this reason, tests were conducted in a manner that matched seven of the dimensionless parameters, but did not match the Reynolds number. This compromise was based on literature information that indicated the Reynolds number has a negligible effect above $Re = 10^4$. However, all tests were performed in the fully turbulent region, which is expected to apply during mixing in DSTs.

Because flow was turbulent and all dimensionless parameters, other than Reynolds number, match those in the range anticipated for DSTs, the experiments are expected to mimic full-scale mixing behavior well. Consequently, the data should be useful for determining the degree of segregation of solids during mixing.

4.3.2 Test Procedure

The 1/12-scale tests involved five major steps. The first three were: 1) preparing simulant, 2) running the mixer pump at the desired power until steady conditions were achieved, and 3) collecting bottle samples, which were analyzed to determined the degree of suspension at steady state. After bottle samples were collected the pump power was lowered to a new value. When the new steady state was achieved, more samples were collected. This procedure was repeated until data was collected at three power levels for each simulant. The final two steps were performed after the test at the third power level was collected.

(a) Unpublished. *1/12-Scale Mixing Experiments to Characterize Double-Shell Tank Slurry Uniformity*. Pacific Northwest National Laboratory, Richland Washington.

These two steps were: 4) the mixer pump was turned off; 5) after solids settled completely, solids at a number of locations in the settled layer were collected, and sizes were analyzed.

Bottle samples were analyzed to characterize the solids concentration, viscosity, and average diameter of solids in the suspension. The data of greatest relevance to criticality are: the particle size distributions in the suspended slurry and the particle size distributions in settled solids. More details related to the test procedure and data collected are provided in Bamberger et al.[a]

4.3.3 Properties of Well-Mixed Simulants

The settling behavior of tank wastes were studied using slurry simulants. The solids used to manufacture the simulants were either Minusil-10[b] or Minusil-40. The supernatant consisted of water or a sugar-water mixture. The solids in the simulant were selected to be fairly monodisperse. However, settling behavior indicated the simulants behaved as polydisperse mixtures.

Unlike tank waste, all particulate material in the simulant is expected to have the same specific gravity, which is approximately 2.6 g/cm^3; all particles are roughly similar in shape. Therefore, all major differences in settling behavior during the experiments are due to size variations. In DSTs, settling behavior will vary depending on particle diameter, shape, and specific gravity of the waste particles.

Table 4.10 describes the mean diameter of particles in the simulants used during experiments. These sizes were measured from bottle samples collected during the final stage of simulant preparation. During this step, the scaled mixer pump was run at a speed that allowed particles to be maintained in suspension; the purpose was to achieve good mixing and suspension. Bottle samples were drawn and the samples were analyzed to determine the average particle size and the viscosity of the mixture. Different numbers of bottle samples were drawn, depending on the specific test.

Table 4.10. Particle Sizes and Viscosity of Simulants Used in Experiments

Simulant	Volume Mean Particle Size (micron)	Standard Deviation (micron)	Viscosity of Mixture (cP)
S1	5.85	3.19	1.50
S2	22.14	13.59	1.75
	22.21	13.90	1.75
	22.08	13.61	1.40
S3[a]	6.59	5.02	3.46
	6.41	4.09	3.55
	5.96	3.59	3.59
S4[a]	20.78	12.44	2.85
	20.46	13.82	2.73
	17.33	12.74	not measured

(a) From first runs for bottles B3H, B3M, and B3L.

(a) Unpublished. *1/12-Scale Mixing Experiments to Characterize Double-Shell Tank Slurry Uniformity*. Pacific Northwest National Laboratory, Richland Washington.
(b) Minusil is a trademark name for Pennsylvania Glass Sand Corporation.

4.3.4 Effect of Pump Power on the Diameter of Suspended Particles

After complete mixing, the pump power was lowered to model behavior that will occur in DSTs during retrieval. During this phase of testing, some particle settling occurred and the concentration of suspended solids decreased. Additional settling occurred as power was lowered further during testing. In addition, the average size of particles in the suspended slurry decreased for all cases. The average diameters from a selected group of bottle samples are provided in Table 4.11. The selected bottles are the first set of bottle samples collected after the tank had reached a steady degree of settling at the target pump power. Additional bottles were taken and analyzed, but are not reported here.

Before proceeding with interpretation of this data, it must be stated the data is not fully analyzed. The magnitudes for the pump flow rates are taken directly from laboratory notebooks. The actual flow rate varied slightly around a steady state value, so more exact values require averaging the complete data stream, which was not reported in Bamberger et al.[a] In addition, the particle size data were often clipped, as a result of the choice of bin increments selected for the purpose of measurement. The best selection of bin increments can only be made after one size histogram is obtained. Because the original experiment did not focus on particle segregation effects, this histogram was not obtained. Some further analysis is required to evaluate the effect of this clipping on the diameter averages and standard deviations reported here. Because the effect of clipping on the precision of the data has not been assessed, all calculated numerical values will be stated in approximate terms, with only one significant figure. Further analysis would allow more precise statement of the numerical values; however, the approximate values are sufficient to describe trends.

The following trends appear in the data. The mean diameter of suspended particles decreases when the pump power is lowered. The mean particle diameter for simulant S1 decreased from 5.85 microns measured when fully mixed to roughly 5 microns when the pump operated at 20.8 gpm. The mean particle diameter decreased further to roughly 2.5 when the pump flow rate was cut in half, and decreased to roughly 1.1 when the pump flow rate was cut to 5.4 gpm. Similar behavior is seen for all four simulants. The greatest amount of segregation is seen for simulant S1, probably because flow rates varied by a factor of four for this case. Flow rates varied by a factor of two for the others.

Equally important, the standard deviation of the particle distributions also decreased as particles settled. For example, the standard deviation of the particle size distribution for the S1 simulant at the lowest power is 0.28 microns. This number is approximately one-fourth of the mean particle diameter. In contrast, the ratio of the standard deviation of the particle size to the average particle diameter in the original fully mixed simulant exceeded one-half. This decrease in the standard deviation of the particle diameter always occurs with selective settling, and is a mathematical requirement. However, it is useful to examine the ratio of the standard deviation to mean particle diameter. This ratio decreases along with the mean particle diameter, indicating the suspended solids are becoming very monodisperse.

The fact that the suspended material is monodisperse is an important observation for criticality because remaining suspended material would settle if the pumps were turned off after segregation of this

---

(a) Unpublished. *1/12-Scale Mixing Experiments to Characterize Double-Shell Tank Slurry Uniformity*. Pacific Northwest National Laboratory, Richland Washington.

Table 4.11. The Effect of Pump Power on the Size of Suspended Particles[a]

Simulant	Pump Flow Rate (gpm)	Volume Mean Particle Size (micron)	Standard Deviation (micron)
S1	20.8	4.88	2.25
		5.37	2.66
	10.5	2.35	1.08
		2.64	2.64
		2.92	2.92
	5.4	1.03	0.26
		1.05	0.28
		1.12	0.29
S2	18.79	12.22	9.58
		9.22	7.44
		9.07	6.82
	15.46	9.30	10.00
		7.04	4.66
		6.28	3.80
	10.6	4.82	3.02
		4.84	2.94
		4.52	2.39
S3	20.66	5.88[b]	3.49
		5.95	3.49
		6.03	3.54
	15.7	5.84	3.52
		5.18	2.74
		5.36	2.92
	10.5	4.77	2.45
		6.06	5.37
		4.62	2.26
S4	16.5	8.70	7.37
		8.51	6.72
		7.87	5.88
	15.7	7.49	5.89
		7.59	5.64
		7.49	5.19
	10.6	3.37	1.63
		3.14	1.65
		3.26	1.58

(a) Data Bamberger et al. from unpublished report.
(b) Taken from the first analysis for each bottle sample.

type was allowed. If this situation occurred, the top layer of settled material would consist of small particles only. However, the thickness of this layer will be very small, because the monodisperse particles are observed only for cases where severe settling has already occurred. This fact will be reflected in the measured size distributions in the settled bed presented later; these distributions did not exhibit a distinct layer of very small particles. After the agitation is stopped, the remaining fine particulate would tend to form a uniform layer of sediment. Insufficient plutonium is present to achieve criticality in a uniform sludge layer within a DST, regardless of the degree of segregation achieved.

4.3.5 Settled Solids

After all tests with an individual simulant were completed, samples were collected from the settled bed of solids that formed on the bottom of the tank. Data are available for Simulants S2, S3, and S4. No data were collected for S1. Results for Simulant S2 are described here. This simulant was selected because it is a low viscosity simulant, and, therefore, tests were run at a higher Reynolds number than S3 and S4. S3 is a small diameter simulant, and is more representative of the particle size in the tanks, but this test has not been examined in detail. The most ideal typical case for a tank would be S1, which is both the lowest viscosity test case and the smallest particle size. Unfortunately, no settled solids data for that case were collected in those tests.

The volume mean and standard deviations at three radial locations are provided in Table 4.12. The flow rates, when the reported measurement points were first observed to fall in the settled layer, are provided in the table. The data were taken by syringe from the settled solids layer after the liquid had been drained from the tank.

The general trend is for the diameter of the settled solids to decrease with elevation from the tank bottom. This trend is consistent with the size decreasing as pump power was turned down. The particles

Table 4.12. Particle Diameters in Settled Solids for Simulant S2

Radial Location (inches)	Elevation Above Tank Bottom (inches)	Volume Mean Particle Size (micron)	Standard Deviation (micron)	Mixer Pump Flow During Deposition (gpm)
28	3.125	9.08	7.90	15.56 gpm
	1.125	26.28	12.99	18.79 gpm
	0.25	36.01	20.09	18.79 gpm
34	6.25	11.06	7.90	10.6 gpm
	5.375	19.02	10.88	15.56 gpm
	0.25	33.39	12.60	18.79 gpm
37.5	6.75	16.58	10.47	10.6 gpm
	5.00	18.55	10.55	15.56 gpm
	0.25	35.35	17.29	18.79 gpm

at the lower layers settled during the first series of tests when the pump power was relatively high; the particles in the upper layers settled in the later tests, or after the pump was turned off.

The diameter of the settled solids also appears to vary with radial location. The largest mean particle diameters are found at the smallest radial location of 28 inches. This pattern may occur because the solids settle preferentially near the outside wall. So, only very large particles can settle near the pump nozzle when the pump is operating at high speed.

When fully mixed, the volume average diameter of this simulant was roughly 22 microns, with a standard deviation near 13 microns. So, the settling pattern indicates the large particles settled first, while the small particles settled last. However, the standard deviations of the particle sizes remain relatively large. For example, the measured sample taken from a radial location of 28 inches and an elevation of 0.25 inch has a mean diameter of 36 microns. However, the standard deviation is 20 microns, or nearly two-thirds the mean diameter. This standard deviation exceeds that of the original batch. While large particles settled preferentially, many small particles also settled. In all cases, the standard deviation is at least one-half the mean particle size. It is unlikely that segregation by size is very strong in the settled layer. This statement is true despite the very strong segregations observed in the suspended solids. The apparent contradiction arises because the extremely monodisperse populations of particles consist of very small populations of fines that remain suspended at low pump powers. When these fines settle, they form a very thin layer of solids that was not detectable using the simple sampling methods applied to the settled layer of solids.

4.3.6 Implications

The data presented in this section have a number of implications that are relevant to criticality. The most important is that segregation by size and chemical species, if chemical species are shown to favor specific sizes, may occur in the tank. However, in no case were monodisperse populations (all material is one specific size) of particles achieved anywhere in a settled layer of particles. The data suggest that segregation is noticeable, but it is not extremely strong. In all cases, large particles settle preferentially, but some small particles always settle with them. The degree of segregation will likely be greater with an initially broader size distribution than used in these specific tests.

Although not performed to date, it may be possible to use the existing 1/12-scale data to predict the degree of segregation that may occur during mixing of tank waste. This would require knowledge of the distribution of settling velocities and corresponding compositions for the tank waste. While this information is not available, it still may be possible to extend bounding settling calculations described in Sections 4.1 and 4.2. Full particle population density histograms for our 1/12-scale tests exist to support this task.

4.4 Gravity Concentration

This section provides a review of mining literature concerning particle segregation using gravity concentration and examines the implications of each of the various separation methods to the potential for criticality. Gravity concentration is one of the earliest known methods for separating heavy minerals such as gold and tin oxide from their lighter ore components. The mining literature was reviewed to determine if the mechanisms that achieve the gravity separations are applicable to separating plutonium-rich particles from neutron absorber-sludge particles in the tanks.

Gravity concentration achieves separation of minerals according to their relative density or particle size. At least four approaches to gravity concentration have been identified: density, stratification, flowing film, and shaking (Burt 1986), as shown in Figure 4.44. In density separations, a fluid with an apparent density between those of the materials to be separated is selected so the lighter component(s) will float while the heavier component(s) will settle. In stratification separations, the materials to be separated are subjected to repeated vertical pulsation of the carrier fluid so the heavier materials segregate beneath the lighter components. Jigs and jigging are typical of stratification equipment. In flowing film separations, the separations are achieved by the relative movement of the particles in a slurry flowing down an inclined plane. Sluices, pinched sluices, Reichert Cones, palongs, and spiral separators represent types of flowing film separators. In shaking separations, the mineral components separate in a flowing film with an imposed oscillating or orbital horizontal shear force. Shaking tables, the Bartles-Mozley concentrator, and Crossbelt concentrator are typical shaking separators.

Particles can also be separated by centrifugal methods, including centrifuges and cyclones. Flotation is also used to recover fine particle size minerals from their ores. Flotation separations are achieved by introducing fine bubbles into the fluid. The ore particles attach to the bubbles and rise to the surface, where they are removed.

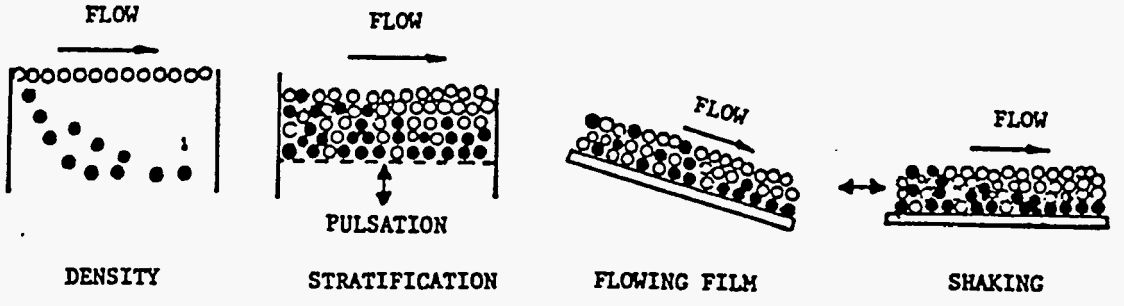

Figure 4.44. Gravity Concentration Methods (from Burt 1986)

4.4.1 Density Separations

Density separations are achieved by introducing the materials to be separated into a fluid with a density falling between the two materials to be separated. The lower density materials will float and the higher density materials will settle. Density segregation, as applied in the ore processing industry, is not applicable to plutonium segregation in the tanks because all of the particles of concern have densities greater than supernatants and would have a tendency to settle. Only in situations where a particle was induced to float in an aqueous solution would density segregation become a possible concern. Flotation is discussed in Section 4.4.5.

4.4.2 Stratification

In stratification processes such as jigging, particles are sorted based on the movement of the particles in a bed through which a fluid is passed vertically. The bed is dilated by the upward movement of the fluid and is contracted by the downward movement. In typical mining applications, the cycle frequency would be in the range of 100 to 300 cycles per minute for millimeter-sized particles. Lower frequencies are used for larger particles (Burt and Mills 1984). Four mechanisms have been proposed for describing the stratification process: 1) differential acceleration at the beginning of fall, 2) hindered settling, 3) attainment of the minimum potential energy level, and 4) interstitial trickling (Burt and Mills 1984).

At the top of the upward, dilation pulse, the particles have zero velocity and begin to fall with the accelerations and velocities that are functions of the particle density and are independent of the particle size. The heavier particles will have a larger initial acceleration and will therefore travel farther than a lighter particle over a finite time before terminal velocities are attained. Thus, if the cycle frequency is high enough for the fall time to be short and the number of falls large, the separations can be achieved, based on the relative accelerations of the particles.

With hindered settling, higher particle concentrations result in increased particle interactions. The apparent density of the slurry increases due to these increased interactions so that individual particles settle as if they were in a more dense fluid than the actual slurry fluid. Thus the apparent ratio of settling velocities for particles of different sizes changes and stratification occurs. This theory is not universally accepted.

Another mechanism for stratification is that a bed of particles will seek its minimum potential energy level. A uniform mixture of light and heavy particles with a center of gravity at its center will rearrange to a condition with the heavier particles on the bottom, thereby lowering the center of gravity and reducing the potential energy of the system. The jigging operation serves to fluidize the bed so the potential energy can be released.

Interstitial trickling can contribute to the stratification achieved by jigging operations. Because the particles do not travel the same distance during a bed dilation cycle, they will come to rest at different

instants. Coarse particles may remain in suspension for a shorter time, so they bridge together. Finer particles can still settle through the interstices between the larger particles during the bed settling phase of the cycle.

4.4.3 Flowing Film Separations

Flowing film separations include several mechanisms for achieving separations (Burt and Mills 1984). These include:

- thin film separations where the film thickness and particle size are similar and the rate of shear on the fluid is small
- flowing film concentration where the particle slurry experiences continuous shear
- flowing film concentration enhanced with riffles to form mini-centrifugal concentrators.

Thin film separations require laminar flow down a smooth inclined plate. Under these conditions, a parabolic velocity profile is created in the fluid with the fluid velocity at zero on the plate surface and highest at the film/air interface (Burt and Mills 1984). Particles in contact with the plate surface are forced to slide or roll down the incline by the fluid action. The fluid must provide the force necessary to overcome any sliding or rolling resistances. Because of the fluid velocity profile, the larger and lighter particles will tend to move farther than smaller and heavier particles. Mineral particles typically distribute in the general down slope sequence of fine heavy, coarse heavy and fine light, and coarse light particles. Thin film separations work with film thicknesses up to about 10 particle diameters.

When a slurry of sufficient particle concentration is subjected to flow, particle collisions and interactions result in a stress normal to the direction of fluid flow. This is known as the Bagnold force. The significance of the resulting force on the particles can be shown to decrease with increasing particle density and increase with increasing particle size. Under such conditions, larger particles tend to move to the fluid surface where the shear strain is less and the smaller particles tend to move to the bottom of the particle bed where the shear strain is greatest (Holtham 1992). The resulting sorting of particles is coarse light particles on top, followed by fine light and coarse heavy particles, and fine heavy particles on the bottom.

Sluice boxes may incorporate riffles perpendicular to the flow path to enhance the recovery of heavy particles. The riffles form eddies or vortexes in the fluid between the riffles so the heavier particles are ejected from the vortex while lighter particles are swept away. The riffles also allow the heavier particles to settle and prevent them from being carried away by the bulk fluid flow. To be effective, the fluid flow must be high enough to create the vortices between riffles yet slow enough that the particles do not remain in suspension (Clarkson 1994).

For all flowing film separations, fluid velocities must be low enough that particles are not simply maintained in suspension due to the fluid turbulence.

4.4.4 Shaking Devices

The mechanisms by which shaking tables achieve particle segregation are complex and not clearly understood (Burt 1986). The shaking induces shear in the bed, similar to the flowing film concentrators, so that Bagnold forces become important. Thin fluid films are typically used so that particle rolling and sliding become important. Shaking tables typically include riffles to improve recovery. The resulting separating mechanisms can oppose one another with the dominant mechanism determined by operating parameters. Operating experience indicates that for a feed material with fine particles, the best approach is to use less water, less feed, higher frequencies at lower amplitudes, and low riffles. These conditions are similar to those for the Bartles-Mozley concentrator described in the following paragraph.

Most gravity separation devices used in the mining industry are effective in recovering minerals with particle sizes down to approximately 100 μm. Figure 4.45, from Burt (1986), shows typical operating ranges for gravity concentration equipment. Smaller-particle (<100 μm) slurries are referred to as slimes and require low capacity approaches, such as the Bartles-Mozley concentrator, Crossbelt concentrator, or centrifuges to achieve significant separations of the finer particles down to approximately 5 μm in size. Recoveries of cassiterite (tin ore, SnO_2, $\rho = 6.99$) particles in excess of 50% at 5 μm and 80% at 10 μm have been achieved with the Bartles-Mozley devices. The Bartles-Mozley concentrator uses smooth decks inclined to less than two degrees to minimize the slurry velocity (Mills and Burt 1979). The device operates with a slurry film thickness of between 0.5 and 1 mm. An orbital shear is imposed on the film via the deck. A typical shear rate would be on the order of 4.5 to 5 m/min. Recovery is highest when the velocity ratio, defined as the fluid film velocity divided by the shear rate, is less than 1.0 (Mills and Burt 1979). The roughness profile of the deck has an important effect on the recovery of the fines (Sivamohan and Forssberg 1986). For example, a wood deck with a roughness profile of 30 to 40 μm demonstrated significantly greater retention of fines compared to a stainless steel deck with a roughness profile of 0.25 to 0.50 μm.

4.4.5 Flotation

Flotation is used extensively for the recovery of fine-sized minerals from their ores. In flotation processes, the particulates in the carrier fluid are induced to attach to air bubbles and to float to the surface due to the buoyant force acting on the combined bubble/particle. Flotation is very sensitive to the chemistry of the particles and the fluid because the attachment of the particles to the bubbles is dependent on surface tension and zeta potential which are also dependent on the chemistry of the system. Perry and Chilton (1973) describe the flotation process as follows:

> "In flotation machines, the ore is suspended in water ... by means of mechanical or air agitation. The surfaces of specific mineral particles are treated with chemicals

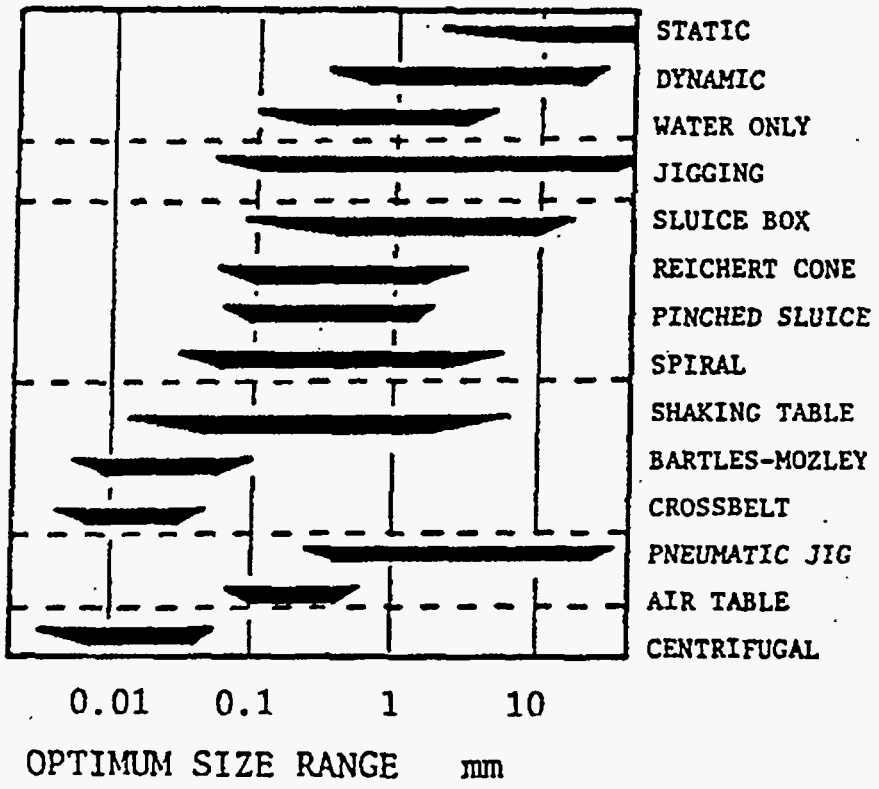

Figure 4.45. Typical Particle Sizes Recovered for Various Gravity Concentration Devices

of froth or foam forms at the top of the flotation machine. The air-avid minerals become attached to air bubbles and rise to the surface where they collect in the froth and are skimmed off. Undesired minerals are depressed or rendered non-floatable either by leaving their surfaces unaltered or by collector adsorption or through the use of modifying agents. The valuable concentrates from froth flotation may be either the froth product which collects at the top or the underflow product."

Flotation can be induced by 1) injection of air while the slurry is under pressure and then releasing the pressure such that small air bubbles form, 2) direct bubbling of air into the slurry, or 3) saturating the slurry with air and then applying a vacuum (Tchobanoglous and Burton 1991). Aeration flows are typically in the range of 1 to 3 m^3 air/min per m^2 of froth surface area. Flotation can be enhanced by the addition of chemicals to alter the surface or structure of the particles so that air bubbles are more easily trapped or adsorbed. Collectors are typically organic chemicals added to the minerals to make their surfaces more hydrophobic. Depressants are added to make a particular material less likely to float. Other organic materials can be added as a frother to stabilize the froth or foam on the surface of the fluid until the froth can be skimmed away. A carrier such as calcium carbonate, which can be easily floated,

may be added, if the particles to be separated do not readily attach to the bubbles, but do attach to the carrier. These modifying chemicals can be added in relatively small quantities ranging from 0.02 to 2 kg per tonne.

Flotation has been used to separate plutonium and cerium from sands and soils. To separate plutonium and coral sands from Johnston Atoll, a fatty acid was added to make the plutonium-enriched particles hydrophobic; flurosilicic acid and sodium silicate were added to make the clean coral hydrophilic (Mishra et al. 1996). The authors recommended using a 2-stage flotation process for cleaning the minus 100-mesh (149-micron) contaminated coral. Mechanical flotation would be used for the larger particles and column flotation would be used for the sludge fraction smaller than 38 microns. Treatability tests showed recoveries of 85% of the activity in the sludge fraction in the column flotation, but with 45% of the coral captured also. Higher concentrations of the depressant would be required to reduce the coral carryover.

Mechanical flotation methods have generally not been successful in the recovery of fine radionuclides from contaminated soils. However, laboratory work reported by Cho et al. (1996) showed that cerium dioxide, used as a surrogate for plutonium dioxide, could be recovered successfully from soils using 10^{-3} molar oleic acid at pHs of 4 and 9. The cerium dioxide was a minus 200-mesh (74-micron) size fraction with a median particle size of approximately 35 microns. Recovery was enhanced by the addition of 0.5 to 10% of minus 150-mesh calcium carbonate as a carrier, yielding recoveries of 65 and 95%, respectively. Maximum recoveries with oleic acid alone were 73%.

4.4.6 Comparison to Tank Waste Conditions

The only waste phase for which criticality could potentially be an issue is tank sludge. Tank sludge particulates are fine with sizes ranging from less than 1 μm up to about 100 μm. It is also quite likely that much of the material classified as >10 μm actually consists of agglomerates of smaller particles. Plutonium, the most important fissile material in the tanks, is believed to exist as very fine particulate and in any case should be less than about 10 microns.

As seen in Figure 4.45, many of the devices used commercially to achieve segregation by gravity separation methods would fail to achieve significant segregation for tank sludge. The devices that could potentially achieve segregation fall into the categories of centrifugal devices and shaking devices including shaking tables, Bartles-Mozley Concentrators, and Bartles-Mozley Crossbelt Concentrators. As Figure 4.46 shows, the recovery of <10 μm particles decreased significantly even for these fine-particle recovery devices (Burt and Mills 1984). Separations of tin ore (cassiterite, density = 6.99 g/cm^3) and tungsten ores (wolframite, density = ~7.1g/cm^3 and scheelite, density = 6.1 g/cm^3) are shown in the figure for orbital shear devices (Bartles-Mozley and Crossbelt), discontinuous shear devices (shaking table and rocking vanner), and the Denver Buckman Tilting Concentrator that relies on thin-film separations.

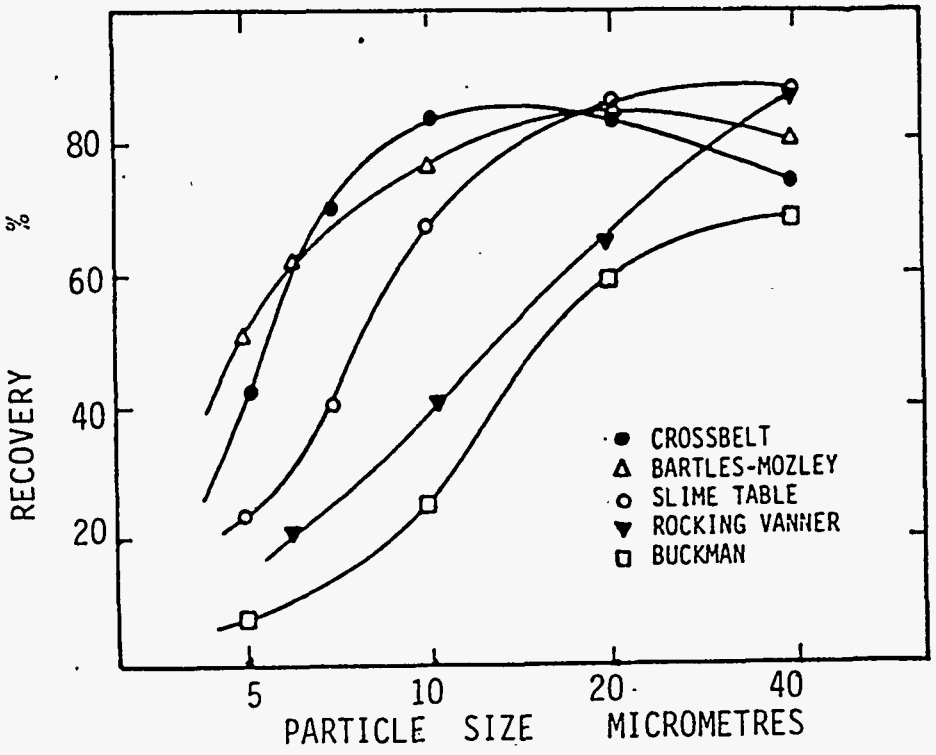

Figure 4.46. Fine-Particle Recovery Using Various Technologies

Centrifugal devices include centrifuges and cyclones. Both devices rely on creating centrifugal forces to separate the heavy particles and, therefore, require specialized equipment configurations that are not considered applicable to any known tank operating activity or pieces of equipment in tanks (risers, ALCs, liquid level wells).

Density separations are not expected under current tank operating conditions. The densities of the fissile material particles and neutron poisons are greater than the density of the supernatants. However, as discussed in the preceding sections of this chapter, some segregation is possible in the settled solids.

Slime concentrators typically rely on a shaking mechanism to achieve segregation of the particles in a thin flowing film. Different-sized particles and different density particles are segregated, due to the different velocity at which they traverse the surface. This phenomenon is not expected to occur to any great degree in the tank for several reasons. First, although segregation could occur in the layer of fluid moving across the tank floor, no collection device would selectively collect the slower moving particles. In the separator, selective collection is achieved by shaking the surface in an eccentric manner to force particles on the surface to exit preferentially to one side of the device. Turbulence would also interfere with the segregation. In the separator, the film is kept very thin to assure laminar flow conditions. Turbulence would tend to lift particles from the surface, and result in mixing that would disrupt the segregation process. Therefore, while some segregation from this mechanism is conceptually possible,

no apparent mechanism is apparent to allow it to achieve the degree of segregation needed or to continuously segregate material in such a way to collect it into a critical configuration.

It is unlikely that any significant segregation of plutonium will occur due to the mechanisms used to achieve gravity separations in the minerals processing industry. Though devices are available to achieve separations of small particles less than 10 μm size, the effectiveness of the separation decreases rapidly below 10 μm. Furthermore, the separation processes typically require thin fluid films or particulate movement with specific geometries or frequencies that are not likely to occur within a tank for the sustained times required to achieve the separations.

Segregation due to flotation is possible in the tanks, due to air sparging and pumping activities and the possible presence of organic chemicals in the waste slurry that could act as collectors or frothers. However, some evidence appears in the literature that flotation may not be an effective separation technique for small particles in the same size range as considered for the tank wastes (Wells 1991, Cho et al. 1996). Also, at pH 11 and above, it is likely the plutonium and iron will be present as hydroxides which are hydrophilic and therefore much less likely to floatable. If flotation were to become an issue for a particular waste stream, relatively simple tests can be conducted using 100 ml samples to determine if a particular waste would segregate plutonium due to flotation.

5.0 Benchmarks for Assessment of Criticality

In order to determine if the degree of segregation in a given scenario will result in a criticality, it is necessary perform criticality calculations. Because it would be very time consuming to perform specific calculations for each scenario, conservative benchmarks have been established through which a given scenario can be shown to be subcritical. This section provides a brief summary of concepts related to criticality and useful criticality benchmarks for the convenience of the reader. For a more in-depth discussion, refer to information compiled by Rogers et al. (1996) and by Braun et al. (1994).

Neutrons produced by fissions may be lost from a system (leakage), be absorbed by a nuclear reaction other than fission (absorption), or cause additional fissions. Fission interactions with the fissile materials of interest are more likely to occur with neutrons that are slowed to thermal energies. The neutrons may be slowed by scattering interactions with various materials present. The slowing process is referred to as moderation and materials which slow the neutrons effectively, while absorbing only a small fraction, are referred to as moderators. For a system of infinite size, the multiplication factor, k_∞, is defined as the ratio between the rate of neutron production and the rate of neutron absorption. When the ratio is equal to 1, the system is said to be critical. For a finite system, a similar term, k_{eff}, is defined as the ratio of neutron production to the rate of neutron loss to absorption and leakage. When k_{eff} is greater than 1, a criticality occurs, resulting in an exponential growth in the rate of fissions.

5.1 Fissile and Fissionable Materials in Tank Waste

Fissile materials may be fissioned by neutrons of any energy, including thermal neutrons. Fissionable materials may undergo fission only by fast (>1MeV) neutrons. The most important fissile material in the tank waste is ^{239}Pu (Pu). Quantities of ^{233}U, ^{238}Pu, ^{240}Pu, and ^{241}Pu are conservatively assumed to be Pu. The fissile nuclide ^{235}U generally occurs in nature at 0.72%, with the remainder being ^{238}U. In this case, the absorption from the ^{238}U more than offsets the contribution of ^{235}U to criticality. ^{235}U that is present in excess of 0.72 wt% is treated conservatively as Pu.

^{238}U, ^{238}Pu, and ^{240}Pu are fissionable but not fissile. Thus, small amounts of moderators such as water drastically reduce the ability of these nuclides to contribute to criticality. In fact, in the tank environment, ^{240}Pu increases the amount of Pu required to achieve criticality. Other fissionable radionuclides include ^{237}Np and ^{241}Am. Due to their small concentrations and their fissionable nature, ^{237}Np and ^{241}Am are generally not important to criticality in tank waste.

5.2 Safe Neutron Absorber Ratios

Each nuclide has a specific ability to absorb neutrons, which is expressed as an absorption cross section. The absorption cross section varies widely between different nuclides. In a particular region of sludge, the absorption cross sections of all the nuclides contribute to the neutron absorption capability of

the sludge. If the absorption cross section in any region is sufficiently large, relative to the content of fissile material, criticality becomes impossible, regardless of other factors, such as geometry or degree of moderation.

Safe ratios of neutron absorbers to Pu have been determined and are provided in Table 5.1, expressed as the mass of absorber to mass of Pu. If a homogeneous sludge contains an absorber in a mass ratio as high as shown in Table 5.1, no criticality is possible. Boron and cadmium are particularly effective neutron absorbers and may be referred to as poisons. The presence of boron and cadmium would tend to dominate the absorption in a criticality analysis. However, it is difficult to ensure that the boron and cadmium remain associated with the Pu. Therefore, boron and cadmium are conservatively neglected in analysis of tank waste criticality. In a large system from which leakage is small, k_{eff} is largely determined by the absorption cross section and Pu content and is nearly independent of neutron scattering. Therefore, a sum-of-fractions rule may be applied to multiple absorbers that are present. For example, if two nuclides are each present at half of their safe ratio, then criticality is impossible. Most waste streams transferred to tanks contain absorber concentrations well in excess of that required to assure subcriticality. Data on characterization of specific waste streams transferred to tanks have been compiled as Appendix A.

Table 5.1. Safe Mass Ratios of Neutron Absorbers to Pu-239

Element or Compound	Safe Ratio (Mass Absorber/Mass Pu-239)
Aluminum (Al)	910
Bismuth (Bi)	48000
Boron (B)	0.095
Cadmium (Cd)	0.235
Calcium (Ca)	770
Carbon (C)	28000
Chromium (Cr)	135
Copper (Cu)	130
Hydrogen (H)	15
Iron (Fe)	160
Lanthanum (La)	121
Manganese (Mn)	32
Mercury (Hg)	5
Nickel (Ni)	105
Nitrogen (N)	61
Nitrate (NO_3)	270*
Phosphorous (P)	1300
Sodium (Na)	360
Silicon (Si)	1400
Thorium (Th)	243
Uranium (natural)	770
Water (H_2O)	150*
Zirconium	4000
* Nitrate and water given for convenience. N and H are sources of absorption.	

5.3 Conservative Waste Model

Rogers (1993) examined 28 different single-shell tank sludges and formulated a conservative model for tank sludge for use in criticality evaluations. The goal was to define a sludge composition for use in analyses that would be at least as neutronically reactive as any real waste sludge. Thus, a composition was selected where the absorption cross section was less, and the ratio of scattering cross section to absorption cross section was higher than any known sludge.

The model assumes 1200 g/l of dry solids within the sludge. A low mass number is conservative because more mass increases the absorption cross section for a given chemical composition of sludge. For any calculations, the water content is selected for optimal moderation. The fissile content is varied independently within the model.

This conservative waste model is then used in criticality calculations; it is assumed that application of the result to any real tank sludge will be conservative. For the conservative waste model, the minimum concentration of plutonium required to achieve criticality assuming an infinite geometry is 2.6 g/l[a]. By comparison, the concentration required in pure water is 7.2 g/l[b]. The large difference is because the conservative waste model uses optimal water moderation, which is very low for low plutonium concentrations.

5.4 Geometric Factors

Due to leakage of neutrons out of the system, geometry is an important limitation in achieving criticality. Several benchmarks have been developed that incorporate the geometric factor.

5.4.1 Slab Geometry

Fine particulates generally settle into thin layers across a tank. For plutonium with water in an infinite slab geometry, a minimum of 2583 g Pu per m^2 of areal slab area (240 g/ft^2) is required to achieve criticality. This limit is conservative when applied to the conservative waste model. If plutonium is assumed to be evenly distributed across the area of a 22.9 m (75-ft) storage tank, a total of 1063 kg of plutonium is required to achieve criticality. This quantity is roughly equal to a conservative (high) estimate of the total inventory of all waste storage tanks combined and is an order of magnitude greater than the inventory that exists in any single storage tank at the present time. Below a Pu concentration of 5 g/l, the slab thickness required to achieve criticality increases rapidly from 1 m. At 4 g/l, a slab with thickness of 1.7 m is required.

(a) To determine this value, a k_∞ of 0.935 was used instead of 1.0 in order to account for uncertainty in the models used in the calculation.

(b) Actual calculated estimate is 7.8±0.3. A value of 7.2 is two standard deviations to the low side to ensure the value selected remains conservative.

5.4.2 Sphere Geometry

The optimum shape for promotion of criticality is a sphere, due to the minimum surface-area-to-volume ratio which reduces neutron losses due to leakage. While the conservative waste model provided a 2.6 g/l minimum concentration required for criticality, the volume containing high Pu concentrations will not be infinite. Table 5.2 provides a summary of results of calculations for spheres that indicate the sphere diameter and critical mass required, as a function of concentration within the conservative waste sludge.

Table 5.2. Requirement for Spheres to Attain Criticality in Conservative Waste Model

Pu Concentration, g/l	Sphere Diameter, cm (ft)	Sphere Volume, l	Critical Mass (g)
30	31.9 cm (1.05 ft)	17	520[a]
10	83.1 cm (2.73 ft)	300	3000
4	372 cm (12.2 ft)	27000	108000
3.6	510 cm (16.7 ft)	69400	250000
(a) This value is for pure water. The optimal water content is all water such that waste solids are displaced. If 1200 g/l of solids are assumed to be present the minimum critical mass is 750 g.			

The data in Table 5.2 indicates that at concentrations near the 2.6 g/l, the amount of Pu required to form a critical mass is excessive. In fact, even at 4 g/l, more Pu is required than is believed to exist in any one tank. Only at concentrations greater than 4 g/l is sufficient plutonium present in a tank to possibly form a critical mass. At concentrations above 4 g/l, the minimum critical mass requirement drops rapidly with increasing concentration.

6.0 Conclusions

This evaluation found no credible mechanism through which a criticality could be achieved during sluicing retrieval of Tank C-106 to AY-102 or through mixer pump operation in SY-102. While numerical probabilities of a criticality have not been calculated, the possibility of a criticality occurring during retrieval of these tanks is clearly remote. Although the study has focused on specific tanks, the information developed allows qualitative conclusions to be drawn for other tanks as well. The supporting conclusions of this study include the following:

- An in-depth literature review determined that while sorption to iron or formation of a solid solution with a good neutron absorber is possible, discrete $PuO_2 \cdot xH_2O$ particles (either existing free or physically trapped by other precipitates) or Pu in solid solution with a poor neutron absorber are also possibilities. Thus, segregation sufficient for criticality cannot be ruled out, based on plutonium chemistry.

- The calculated upper bound for $PuO_2 \cdot xH_2O$ crystal size is about 8 μm. Thus, it is considered unlikely that wastes contain discrete $PuO_2 \cdot xH_2O$ crystals exceeding 10 to 20 microns.

- Very strong evidence indicates the waste particles are, and will continue to be, agglomerated. The most direct evidence is a comparison of transmission electron microscopy (TEM) data with measured sedimentation velocities and particle size data generated using light scattering techniques. TEM measurements show the primary particles of the sludge are submicron; sedimentation and particle sizing information based on light scattering indicates much larger particles. In addition, conservative calculations lead to the conclusion that rapid formation of flocs will prevent segregation of the fissile material provided the salt concentration is at least 0.1 molar in the supernatant, the pH is at least 10, and the mixing intensity is sufficiently low to permit flocculation.

- While agglomerates within the waste are likely to be broken up by the pumps and possibly fluid jets associated with retrieval operations, they are expected to reform under conditions suitable for settling of solids.

- Selective agglomeration due solely to electrostatic interactions (where a single type of particle preferentially agglomerates with itself) should not occur under the pH and saline conditions existing within the tanks.

The remainder of the conclusions make the enabling assumptions that particles do not flocculate and that the light-scattering particle size distribution represents actual primary particle sizes. However, these assumptions are not believed to be accurate and are adopted only to provide a defense-in-depth.

- Pu will not concentrate in the lower regions of the sludge to the extent that it would exceed the 2.6 g/l safe concentration for infinite geometry in the conservative waste model. If small $PuO_2 \cdot xH_2O$ particles are assumed, the potential exists for segregation to the slowest settling layer to exceed

2.6 g/l although these solids will settle uniformly in a thin layer and be far below the 240 g/ft^2 level for a uniform slab.

- Full 3-dimensional models of solids being pumped out of C-106, of those same solids settling in AY-102, and of mixer pump operation in SY-102 show no indication of unusual segregation in any area of the tank. The greatest degree of solids enrichment in all simulations was about a factor of 2.5 for the largest solids in the distribution. Although the simulation times were limited due to the computational requirements, nothing indicates the level of segregation will reach the 17 to 20 needed to exceed the 2.6 g/l safe level in the conservative waste model.

- The upper bound on Pu particle size is below the normal particle size for mineral processing separations by gravity separation. Gravity separation would be difficult even in equipment designed for that purpose and accidental segregation sufficient to create large segregated masses needed to cause criticality does not appear credible.

- Segregation of plutonium by selective flotation of the plutonium appears highly unlikely. If the proper organic molecules were present to allow flotation, they would be expected to float other metal hydroxides along with the plutonium at the pH conditions typical of waste storage tanks. However, even if selective flotation were assumed to occur, the material would spread out in a foam layer across the tank and the 240 g/ft^2 areal limit for criticality would apply to the foam layer, so the entire plutonium content of a waste tank could be concentrated into a foam layer without resulting in a criticality.

7.0 References

Ackers, P. And W.R. White. 1973. Sediment Transport: New Approach and Analysis, *J. Hydr. Div.* ASCE, 99:2041-2060.

Agnew, S.F. 1995. *Hanford Defined Wastes: Chemical and Radionuclide Compositions.* LA-UR-94-2657, Rev. 2. Los Alamos National Laboratory, Los Alamos, New Mexico.

Agnew, S.F. 1996. *Hanford Tank Chemical and Radionuclide Inventories: HDW Model Rev. 3.* LA-UR-96-858, Rev. 2. Los Alamos National Laboratory, Los Alamos, New Mexico.

Allard, B. 1982. Solubilities of Actinides in Neutral or Basic Solutions, In *Actinides in Perspective,* N.M. Edelstein, Ed., Pergamon Press.

Amonette, J.A., and L.W. Zelazny. 1994. *Quantitative Methods in Soil Mineralogy.* SSSA Miscellaneous Pub. Soil Science Society of America, Inc., Madison, Wisconsin.

Anderson, J.D. 1990. *A History of the 200 Area Tank Farms.* WHC-MR-0132. Westinghouse Hanford Company, Richland, Washington.

Baes, C.F., and R.E. Mesmer. 1976. *The Hydrolysis of Cations.* John Wiley and Sons. New York. p 489.

Barney, G.S. 1992a. *Adsorption of Plutonium on Shallow Sediments at the Hanford Site,* WHC-SA-1516-FP, Westinghouse Hanford Company, Richland, Washington.

Barnhisel, R.I., and C.I. Rich. 1963. Gibbsite Formation from Aluminum Interlayers in Montmorillonite. *Soil Sci. Soc. Am. Proc.* 27:632-635.

Barrow N.J. and J.W. Bowden. 1987. A Comparison of Models for describing the Adsorption of Anions on a Variable Charge Mineral Surface. *J. Coll. Interfac. Sci.* 119:236-250.

Bartram, S.F. 1967. Crystallite-size Determination infrom line Broadening and Spotty Patterns. In *Handbook of X-Rays.* E.F. Kaelble, Ed. pp 17-1 to 17-18. McGraw Hill, New York.

Benjamin M.M., and J.O. Leckie. 1981. *Conceptual Model for Metal-Ligand-Surface Interactions during Adsorption.* Env. Sci. Tech. 15:1050-1056.

Bird, R.B., W.E. Stewart, and E.N. Lightfoot. 1960. *Transport Phenomena.* John Wiley and Sons, New York, New York.

Bish, D.L. and J.E. Post. 1989. *Modern Powder Diffraction.* Reviews in Mineralogy volume 20, Mineralogical Society of America, Washington, D.C.

Bratzel, D.R., W.W. Schulz, R. Vornehm, A.E. Waltar, H. Babad, G.S. Barney, J. Schwinkendorf, T.S. Vail, R.J. Serne, and G.W. Whatt. 1996. *Tank Farm Nuclear Criticality Review.* WHC-SD-WM-TI-725, Rev. 0., Westinghouse Hanford Company, Richland, Washington.

Braun, D.J., L.D. Muhlestein, T.B. Powers, and M.D. Zentner. 1994. *High Level Waste Tank Subcriticality Safety Assessment.* WHC-EP-0687, Westinghouse Hanford Company, Richland, Washington.

Brown, C.B. 1950. Sediment Transportation, In: *Engr. Hydr.*, H. Rouse, Ed., John Wiley and Sons, New York, New York.

Brownlie, W.L. 1981a. *Prediction of Flow Depth and Sediment Discharge in Open Channels.* Report KH-R-43A, W. M. Keck Laboratory of Hydraulics and water Resources, California Institute of Technology, Pasadena, California.

Brownlie, W.L. 1981b. *Compilation of Alluvial Channel Data: Laboratory and Field.* Report KH-R-43B, W. M. Keck Laboratory of Hydraulics and water Resources, California Institute of Technology, Pasadena, California.

Bunker, B.C., P.J. Bruinsma, G.L. Graff, C.R. Hymas, X.S. Li, J.R. Phillips, D.R. Rector, P.A. Smith, L. Song, J.M. Tingey, and Y. Wang. 1995. *Colloidal Studies for Solid/Liquid Separation.* TWRSPP-95-045, Pacific Northwest Laboratory, Richland, Washington.

Burt, R.O. 1986. "Selection of Gravity Concentration Equipment" In: *Design and Installation of Concentration and Dewatering Circuits.* Society of Mining Engineers, Littleton, Colorado.

Burt, R.O. and C. Mills. 1984. *Gravity Concentration Technology.* Elsevier, New York.

Camaioni, D.M., W.D. Samuels, B.D. Lenihan, S.A. Clauss, K.L. Wahl, and J.A. Campbell. 1994. *Organic Waste Tank Safety Program Waste Aging Studies.* PNL-10161, Pacific Northwest Laboratory, Richland, Washington.

Campbell, J.A., S. Clauss, R. Lucke, K. Grant, G. Mong, V. Hoopes, J. Rau, B. Lerner, and R. Steele. 1994a. *Flammable Gas Safety Program Analytical Methods Development: FY 1993 Progress Report.* PNL-9062, Pacific Northwest Laboratory, Richland, Washington.

Campbell, J.A., R.B. Lucke, S.A. Clauss, G.M. Mong, K.E. Grant, J.K. Rau, F.V. Hoopes, R.K. Steele, B.D. Lerner, and K.L. Wahl. 1994b. *Waste Tank Organic Safety Program Analytical Methods Development: FY 1994 Progress Report.* PNL-10128, Pacific Northwest Laboratory, Richland, Washington.

Campbell, J.A., R.B. Lucke, S.A. Clauss, G.M. Mong, K.E. Grant, J.K. Rau, F.V. Hoopes, K.L. Wahl, B.D. Lerner, and R.K. Steele. 1994c. *Flammable Gas Safety Program Analytical Methods Development: FY 1994 Progress Report.* PNL-10127, Pacific Northwest Laboratory, Richland, Washington.

Campbell, J.A., R.M. Bean, K.L. Wahl, G.M. Mong, K.E. Bell, K.B. Wehner, A.D. Rick, R.J. Ray, D.B. Bechtold, B.R. Wels, R.W. Schroeder, J.W. Ball, B.D. Valenzuela, J.M. Frye, S.L. Fitzgerald, P.P. Bachelor, B. Griffin, R.K. Fuller, A.B. Banally, and S.M. Parong. 1995a. *Analysis of Samples from Hanford Waste Tank 241-C-103.* PNL-10531, Pacific Northwest Laboratory, Richland, Washington.

Campbell, J.A., S.A. Clauss, K.E. Grant, F.V. Hoopes, G.M. Mong, J.K. Rau, R. Scheele, and K.L. Wahl. 1995. *Flammable Gas Safety Program Organic Analysis and Analytical Methods Development: FY 1995 Progress Report.* PNL-10776, Pacific Northwest Laboratory, Richland, Washington.

Castaing, B.A. 1994. *101-AY, 102-AY, & 106-C Data Compendium.* WHC-SD-TI-578 Rev. 1, Westinghouse Hanford Company, Richland, Washington.

Charyulu, M.M., I.C. Pius, A. Kadam, M. Ray, C.K. Sivaramakrishnan, and S.K. Patil. 1991. The Behavior of Plutonium in Aqueous Basic Media, *J. Radioanal. and Nucl. Chem.,* 152, (2), p. 479-485.

Chesworth, W. 1972. The Stability of gibbsite and Boehmite at the Surface of the earth. *Clays and Clay Miner.* 20:369-374.

Chisholm-Brause, C., S.D. Conradson, C.T. Buscher, P.G. Eller, and D.E. Morris. 1994. Speciation of Uranyl Sorbed at Multiple Binding Sites on Montmorillonite, *Geochim. Cosmochim. Acta,* 58, (17), p. 3625-3631.

Cho, E.H., G. Yanief, D.C. Yang, and F.F. Peng. 1996. "Carrier Flotation for the Removal of Radionuclides from Contaminated Soils." SME Annual Meeting 1996.

Choppin, G.R. 1983. Aspects of Plutonium Solution Chemistry. In *Plutonium Chemistry.* Ed W.T. Carnall and G.R. Choppin. pp 213-230. ACS Sym. Ser. 216. Washington D.C.

Clark, R.M. 1990. Water Supply. In: *Standard Handbook of Environmental Engineering.*, pp5.1 to 5.225. Ed. R.A. Corbitt. McGraw Hill, New York.

Clarkson, R. 1994. "The Use of Nuclear Tracers to Evaluate the Gold Recovery Efficiency of Sluiceboxes." *CIM Bulletin* Vol 87, No. 979, pp 29-37.

Cleveland, J.M. 1979. *The Chemistry of Plutonium.* Am. Nucl. Soc. LaGrange Park, Illinois. 653p.

Colby, B.R. 1964a. Practical Computation of Bed-Material Discharge. *J.of Hydr. Div.* ASCE, 90:217-246.

Colby, B.R. 1964b. *Discharge of Sands and Mean Velocity Relationships in Sand-Bed Streams,* Prof. Paper 462-A, United Sates Geological Survey, Washington D.C.

Coleman, G.H. 1965. *The Radiochemistry of Plutonium.* NAS-NS 3058. National Academy of Sciences-National Research Council, U.S. Atomic Energy Commission, Washington, D.C.

Colton, N.G. 1994. *Estimated Bulk Compositions for SST Sludges.* TWRSPP-94-086. Tank Waste Treatment science: Report for the Fourth Quarter FY 1994. Pacific Northwest Laboratory, Richland, Washington.

Corey R.B. 1981. Adsorption vs Precipitation. In: *Adsorption of Inorganics at Solid-Liquid Interfaces.* pp 161-182. M.A. Anderson and A.J. Rubin. Eds. Ann Arbor Science, Ann Arbor, Michigan.

Cornell, R.M. and U. Schwetmann. 1979. Influence of Organic Anions on the Crystallization of Ferrihydrite. *Clays and Clay Minerals.* 27:402-410.

Cross, M.M. 1965. Rheology of Non-Newtonian Fluids: A New Flow Equation for Systems, *J. Colloid Sci.* 20:417-437.

Dabak, T., and O. Yucel. 1987. Modeling of the Concentration and Particle Size Distribution Effects of the Rheology of Highly Concentrated Suspensions. *Powder Tech.* 52:193-206.

Davis J.A. and K.F. Hays. 1986. *Geochemical Processes at Mineral Surfaces: An Overview.* Pp 2-19. In *Geochemical Processes at Mineral Surfaces.* Davis J. A. and K. F. Hays. Eds., ACS Symp Ser. 323. Am. Chem. Soc., Washington, D.C.

Davis J.A. and D.B. Kent. 1990. *Surface Complexation Modeling in Aqueous Geochemistry.* Pp 177-260. In *Mineral-Water Interface Geochemistry.* M.F. Hochella, Jr. and A.F. White. Eds., Rev in Miner. Ser. V23, Min. Soc. Am., Washington, D.C.

Davis, J.A., R.O. James, and J.O. Leckie. 1978. Surface Ionization and Complexation at the Oxide/Water Interface, *J. Coll. Inter. Sci.* 63:480-499.

Delegard, C.H. 1995. Carbonate Complexes of Plutonium in Alkaline Solution. In *Calcination/ Dissolution Chemistry Development Fiscal Year 1995.* WHC-EP-0882, pp.4-25 to 4-31, Westinghouse Hanford Company, Richland, Washington.

Delegard, C.H. 1987. Solubility of $PuO_2 \cdot xH_2O$ in Alkaline Hanford High-Level Waste Solution, *Radiochim. Acta* 41:11-21. Also published as RHO-RE-SA-75 P, Rockwell Hanford Company, Richland, Washington.

Delegard, C.H., G.S. Barney, and S.A. Gallagher. 1984. *Effects of Hanford High-Level Waste Components on the Solubility and Sorption of Cobalt, Strontium, Neptunium, Plutonium, and Americium.* ACS Symp. Ser. *246*: 95-112. American Chemical Society, Washington, D.C. (This report was also published as RHO-RE-SA-18 P, Rockwell Hanford Company, Richland, Washington in 1983.)

Delegard, C.H., and S.A. Gallagher. 1983. *Effects of Hanford High-Level Waste Components on the Solubility of Cobalt, Strontium, Neptunium, Plutonium, and Americium.* RHO-RE-ST-3P, Rockwell HanfordCompany, Richland, Washington.

DiCenso, A.T., L.C. Amato, W.I. Winters. June 1995. *Tank Characterization Report for Double-Shell Tank 241-SY-102.* WHC-SD-WM-ER-366, Rev. 0. Westinghouse Hanford Company, Richland, Washington.

Dran, J.C., G.D. Mea, V. Noulin, J.-C. Petit, and V. Rigato. 1994. Interaction of Pseudocolliods with Mineral Surfaces: The Fate of the Scavenged Cation. *Radiochim. Acta,* 66/67:221-227.

DuBoys, P. 1879. Le Rohne et les Rivieres a Lit Affoullable, *Anneles des et Chausses*, Series 5, 18:141-195.

Dunn, I.S. 1959. Tractive Resistance of Cohesive Channels, *J. Soil Mech. Foun. Div.*, ASCE, NO. SMC, Proc. Paper 2062, 1-24.

Duns, H., and R.C.J. Ros. 1963. Sixth\Morld Petroleum Congress, Section 2, Paper No. 22. FranLafurt

Einstein, H.A. 1950. *The Bed Load Function for Sediment Transportation in Open Channels,* Technical Bulletin 1026, United Sates Department of Agriculture, Soil Conservation Service, Washington D.C.

Einstein, H.A., and N. Barbarossa. 1952. River Channel Roughness, *Trans.* ASCE, 117:1112-1146.

Edwards, A.B. 1952. The Ore Minerals and Their Textures, *J. Proc. Royal Soc. New South Wales.* 85:26-46.

Ellwood, K.R.J., G.C. Georgiou, T.C. Papanatasiou, and J.O. Wilkes. 1990. Laminar Jets of Bingham-Plastic Liquids, *J. Rheology.* 34:787-813.

Engelund, F. 1966. Hydraulic Resistance if Alluvial Streams, *J. Hydr. Div.* ASCE. 92:315-327.

Engelund, F., and E. Hansen. 1967. *A Monograph on Sediment Transport in Alluvial Streams,* Teknisk Vorlab, Copenhagen, Denmark.

Engelund, F., and J. Fredsoe. 1976. A Sediment Transport Model for Straight Alluvial channels, *Nordic Hydrology*, 7, pp. 293-306.

Eyler, L.L. 1983. *Sediment Settling and Resuspension in Waste Storage Tanks with Air Injection Circulators.* Letter Report FATE-83-109, Pacific Northwest Laboratory, Richland, Washington.

Eyler, L.L. 1984. Three-Dimensional Numerical Simulation of Settling and Resuspension of Solids in Storage Tanks with Air Injection Circulators. PNL-SA-11586, Pacific Northwest Laboratories, Richland, Washington. Presented at the Slurry Transport Association Ninth International Technical Conference on Slurry Transportation March 1984.

Eyler, L.L., D.S. Trent, J.A. Fort, December 1993. *TEMPEST: A Computer Program for Three-Dimensional Time-Dependent Computational Fluid Dynamics.* Volume 2: User's Manual, Version T, Mod 2. PNL-8857, Vol 2. Rev. 1. Battelle Memorial Institute.

Fan, Shou-Shan, ed. 1988. *Twelve Selected Computer Stream Sedimentation Models Developed in the United States.* Subcommittee on Sedimentation Interagency Advisory Committee on Water Data. Federal Energy Regulatory Commission, Washington, D.C.

Felmy, A.R. 1995. GMIN, A Computerized Chemical Equilibrium Program Using a Constrained Minimization of the Gibbs Free Energy: Summary Report. In *Chemical Equilibrium and Reaction Models.* ed. by R.H. Loeppert, A.P. Schwab, and S. Goldberg, pp. 377-407, SSSA Special Publication Number 42, American Society of Agronomy, Inc. Madison, Wisconsin.

Fox and McDonald. 1973. *Introduction to Fluid Dynamics.* John Wiley and Sons, New York, New York.

Frankel, N.A., and A. Acrivos. 1967. On the Viscosity of A Concentrated Suspension of Solid Spheres, *Chem. Eng. Sci.*, 22:847-853.

George, K., R.P. Raven, M. Tiffany, and L.E. Ross. 1996. Tank Farm Plant Operating Procedure. TO-200-030 Rev. E-7.

Glasstone S., and A Sesonske. 1981. *Nuclear Reactor Engineering,* Third Edition, Krieger Publishing Company, Malabar, Florida.

Govier G.W., and K. Aziz. 1972. *The Flow of Complex Mixture in Pipes,* Robert E. Krieger Publishing Company, Malabar, Florida.

Graf, W.H. 1971. *Hydraulics of Sediment Transport.* McGraw-Hill Book Co., Inc., New York, New York.

Grebenshchikova, V.I., R.V. Bryzgalova, and I.V. Chernitskaya. 1967a. The Coprecipitation of Plutonium with Lanthanum Oxalate. In: *Coprecipitation and Adsorption of Radioactive Elements.* pp 25-29. V.M. Vdovenko, Ed. Israel Program of Scientific Translations, Jerusalem.

Grebenshchikova, V.I., R.V. Bryzgalova, and I.V. Chernitskaya. 1967b. The Coprecipitation of Plutonium with Lanthanum Oxalate. In: *Coprecipitation and Adsorption of Radioactive Elements.* pp 30-33. V.M. Vdovenko, Ed. Israel Program of Scientific Translations, Jerusalem.

Grebenshchikova, V.I., and Y.P. Davydov. 1965. "State of Pu(IV) in the Region of pH = 1.0 to 12.0 at a Plutonium Concentration of 2×10^{-5} M." *Soviet Radiochemistry.* 7:2 191-195.

Hanson, H.D. 1980. *Transuranics in the Environment.* DOE/TIC-22800. U.S. Department of Energy, Washington, D.C.

Hiemenz, P.C. 1986. *Principles of Colloid and Surface Chemistry.* 2nd Ed., Marcel Dekker, Inc., New York, New York.

Hill, J.G., G.S. Anderson, and B.C. Simpson. 1995. *The Sort on Radioactive Waste Type Model: A Method to Sort Single-Shell Tanks into Characteristic Groups.* PNL-9814 Rev. 2. Pacific Northwest Laboratory, Richland, Washington.

Hobbs, D.T., and T.B. Edwards. 1993. *Solubility of Plutonium in Alkaline Salt Solutions.* WSRC-TR-93-131, Westinghouse Savannah River Company, Aiken, South Carolina.

Hobbs, D.T., T.B. Edwards, and S.D. Fleischman. 1993. *Solubility of Plutonium and Uranium in Alkaline Salt Solutions.* WSRC-TR-93-056, Westinghouse Savannah River Company, Aiken, South Carolina.

Hobbs, D.T. 1995. *Effects of Coprecipitation on the Concentrations of Uranium and Plutonium in Alkaline Salt Solutions.* WSRC-TR-95-0462, Westinghouse Savannah River Company, Aiken, South Carolina.

Hodgson, K.M., D.L. Herting, W.W. Schulz, L.A. Bray, and J.L. Swanson. 1985. *Content and Removal of TRU Elements from Aqueous Zirconium Cladding Waste.* In Proc. Intl. Symp. Actinide/Lanthanide Separations. G.R. Choppin, J.D. Navratil, and W.W. Schulz. Eds., World Scientific. Philadelphia.

Holtham, P.N. 1992. "Particle Transport in Gravity Concentrators and the Bagnold Effect." *Minerals Engineering*, Vol. 5, No. 2, pp 205-221.

Hsi, C.K.D. and D. Langmuir. 1985. Adsorption of Uranyl onto Ferric Oxyhydroxides: Application of the Surface Complexation Sit-Binding Model. *Geochim. Cosmochim. Acta* 49:1931-1941.

Hsu, P.H. 1966. Formation of Gibbsite from Aging Hydroxy-Aluminum Solutions. *Soil Sci. Soc. Am. Proc.* 30:173-176.

Hsu, P.H. 1977. Aluminum Hydroxides and Oxyhydroxides. I *Minerals in Soil Environments.* Pp 99-143, Soil Science Society of America, Madison, Wisconsin.

Hunter, R.J. 1981. *Zeta Potential in Colloid Science.* Academic Press, New York, New York.

Hunter, R.J. 1993. *Foundations of Colloid Science, Volume 1.* Clarendon Press, Oxford, England.

Inglis, C.C. 1968. Discussion of Systematic Evaluation of River Regime, by C.R. Neill and V.J. Galey, *J. Of Waterways and Harbors Division*, ASCE, 94:109-114.

Jansen, P. Ph., L. Van Bendegom, J. Van Den Berg, M. De Vries, and A. Zanen (eds.). 1979. *Principles of River Engineering—The Non-Tidal Alluvial River.* Pitman Publishing Limited, London, San Francisco, Melbourne.

Johnson. J.S. 1994. *Experiments to Demonstrate the Application of Similitude to the Design of Scaled Mixing Tests*, Master's Thesis, Washington State University, Pullman, Washington.

Karim, M.F. and J.F. Kennedy. 1981. *Computer-Based Predictions for Sediment Discharge and Friction Factor of Alluvial Streams,* IIHR Report No. 242, Iowa Institute of Hydraulic research, University of Iowa, Iowa City, Iowa.

Karraker, D.G. 1994. *Radiation Effects on the Solubility of Plutonium in Alkaline High Level Waste.* WSRC-MS-94-0278X (Rev. 2), Westinghouse Savannah River Company, Aiken, South Carolina.

Karraker, D.G. 1995. *Plutonium (VI) Solubility Studies in Savannah River Site High-Level Waste Supernate.* WSRC-TR-95-0244, Westinghouse Savannah River Company, Aiken, South Carolina. 1995).

Kennedy, J.F. 1963. The Mechanics of Dunes and Antidunes in Erodible-Bed Channels, *J. Fluid Mech. Vol.* 16, Part 4, pp. 521-544.

Kepak, F. 1971. *Adsorption and Colloidal Properties of Radioactive Elements in Trace Concentrations.* Chem. Rev. 71:357-370.

Kim, J.I. and B. Kanellakopulos. 1989. Solubility Products of Plutonium(IV) Oxide and Hydroxide. *Radiochim. Acta 48*:145-150.

Kinniburgh D.G. and M.L. Jackson 1981. Cation Adsorption by Hydrous Metal Oxides. Chap 3. In *Adsorption of Inorganics at Solid-Liquid Interfaces.* pp 161-182. Eds. M.A. Anderson and A.J. Rubin. Ann Arbor Science, Ann Arbor, Michigan.

Kodama, H., and M. Schnitzer. 1980. Effect of Fulvic Acid on the Crystallization of Aluminum Hydroxide. *Geoderma.* 24:195-205.

Koehler M., E.Wieland, and J.O. Leckie. 1992. *Metal-Ligand Interactions during adsorption of Uranyl and Neptunyl on Oxides and Silicates.* Proc. Of 7th Int. Symp. On Water-Rock Interaction -WRI7. V1: Low Temp. Env. Eds. Y.K. Kharaka and A.S. Maest. A.A. Balkema, Rotterdam, Netherlands.

Krone, R.B. 1962. *Flume Studies of the Transport of Sediment in Estuarial Shoaling Processes,* Hydraulic Engineering Laboratory and Sanitary Engineering Research Laboratory, University of California at Berkeley, California.

Kwong, N.G. and P.M. Huang. 1975. Influence of Citric Acid on the Chrystallization of Aluminum Hydroxides. *Clays and Clay Minerals.* 23:164-165.

Kwong K.F., and P.M. Huang. 1981. Comparison of the Influence of Tannic Acid and Selected Low-molecular Organic Acids on Precipitation Products of Aluminum. *Geoderma.* 26:179-193.

LaFemina, J.P., J.W. Virden, J. Liu, L. Song, A.R. Felmy, N.G. Colton, J.A. Franz, J.C. Linehan, D.L. Blanchard, B.C. Bunker, and M.L. Balmer. 1994a. *Tank Waste Treatment Science: Report for the Second Quarter FY 1994.* TWRSPP-94-027, Pacific Northwest Laboratory, Richland, Washington.

LaFemina, J.P., J.W. Virden, J. Liu, L. Song, V.S. Stenkamp, A.R. Felmy, E.A. Jenne, D. Rai, R.W. Fulton, N.G. Colton, J.G. Hill, G.S. Anderson, S.E. Faulk, J.A. Franz, J.C. Linehan, W.J. Shaw, C.D. Carlson, D.L. Balanchard, J.A. Campbell, S. Conradson, R.L. Gordon, N.J. Hess, J.C. Hutton, M.M. Lamourex, R.W. Stromatt, D.L. Styris, K.L. Wahl, B.C. Bunker, and M.L. Balmer. 1994b. *Tank Waste Treatment Science: Report for the Third Quarter FY 1994.* TWRSPP-94-086, Pacific Northwest Laboratory, Richland, Washington.

LaFemina, J.P., G.S. Anderson, D.L. Blanchard, P.J. Bruinsma, B.C. Bunker, N.G. Colton, S.D. Conradson, J.L. Cox, J.C. Hutton, A.R. Felmy, R.L. Gordon, G.L. Graff, N.J. Hess, J.G. Hill, E.A. Jenne, M.M. Lamourex, J. Liu, B.M. Rapko, D.R. Rector, P.A. Smith, L. Song, D.L. Styris, L.E. Thomas, A.J. Villegas, and Y. Wang. 1995a. *Tank Waste Treatment Science Task Quarterly Report for October-December 1994.* PNL-10762, Pacific Northwest Laboratory, Richland, Washington.

LaFemina, J.P., G.S. Anderson, D.L. Blanchard, P.J. Bruinsma, B.C. Bunker, I.E. Burgeson, Y.L. Chen, N.G. Colton, S.D. Conradson, A.R. Felmy, R.L. Gordon, G.L. Graff, N.J. Hess, J.G. Hill, J.C. Hutton, C.R. Hymas, E.A. Jenne, M.M. Lamourex, X.S. Li, J. Liu, G.J. Lumetta, L. Rao, B.M. Rapko, D.R. Rector, J.R. Rustad, P.A. Smith, L. Song, S.M. Sterner, D.L. Styris, L.E. Thomas, J.M. Tingey, S.M. Tingey, A.J. Villegas, and Y. Wang. 1995b. *Tank Waste Treatment Science Task Quarterly Report for January- March 1995.* PNL-10763, Pacific Northwest Laboratory, Richland, Washington.

LaFemina, J.P., D.L. Blanchard, P.J. Bruinsma, B.C. Bunker, I.E. Burgeson, Y.L. Chen, N.G. Colton, S.D. Conradson, A.R. Felmy, R.L. Gordon, N.G. Gotts, G.L. Graff, N.J. Hess, J.C. Hutton, C.R. Hymas, M.M. Lamourex, X.S. Li, J. Liu, G.J. Lumetta, J.R. Phillipos, B.M. Rapko, D.R. Rector, J.R. Rustad, P.A. Smith, L. Song, S.M. Sterner, L.E. Thomas, J.M. Tingey, S.M. Tingey, L.Q. Wang, and Y. Wang. 1995c. *Tank Waste Treatment Science Task Quarterly Report for April-June 1995*. PNL-10764, Pacific Northwest Laboratory, Richland, Washington.

LaFlamme B.D. and J.W. Murray. 1987. Solid/Solution Interaction: The Effect of Carbonate Alkalinity on Adsorbed Thorium. *Geochim. Cosmochim. Acta.* 332:351-357.

Lane, E.W. 1947. Report of the Subcommittee on Sediment Terminology, *Transactions, American Geophysical Union,* Vol. 28, No. 6, pp. 936-938, Washington, D.C.

Laursen, E.M. 1958. The Total Sediment Load of Streams, *J. Hydr. Div.*, ASCE, 54:1-36.

Leliavsky, S. 1966. *An Introduction to Fluvial Hydraulics*. Dover Publications, Inc., New York, New York.

Lemire R.J. and P.R. Tremaine. 1980. Uranium and Plutonium Equilibria in Aqueous Solutions to 200°C. *J. Chem. Eng. Data.* 25:361-370.

Lide, D.R. 1995. *CRC Handbook of Chemistry and Physics*, CRC Press, New York.

Lierse, Ch. 1985. Chemical behavior of plutonium in natural aquatic system: hydrolysis, carbonate complexation and redox reaction. Ph. D. Thesis, Technische Universitiat Munchen, Munchen, Germany.

Liljegren, L.M. 1993. *Similarity Analysis Applied to the Design of Scaled Tests of Hydraulic Mitigation Methods for Tank 241-SY-101.* PNL-8518, Pacific Northwest Laboratory, Richland, Washington.

Lindsay, W.L. 1979. *Chemical Equilibria in Soils*, John Wiley & Sons, New York, New York.

Liu, J. 1995. *TEM Characterization of Tank Sludge Simulants*. TWRSPP-95-033, Pacific Northwest Laboratory, Richland, Washington.

Liu, J, L.E. Thomas, Y.L. Chen, and L.Q. Wang. 1995. *Sludge Characterization Studies.* TWRSPP-95-019. Tank Waste Treatment science: Report for the Third Quarter FY 1995. Pacific Northwest Laboratory, Richland, Washington.

Liu, J., L.R. Pederson, and L. Q. Wang. 1995. *Solid-Phase Characterization in Flammable-Gas-Tank Sludges by Electron Microscopy.* PNL-10723. Pacific National Laboratory, Richland, Washington.

Lumetta, G.J., B.M. Rapko, M.J. Wagner, J. Liu, and Y.L. Chen. 1996. *Washing and Caustic Leaching of Hanford Tank Sludges: Results of FY 1996 Studies*. PNNL-11278, UC-721. Pacific Northwest National Laboratory, Richland, Washington.

Maddock, T., Jr. 1976. Equations for Resistance to Flow and Sediment Transport in Alluvial Channels, *Water Resour. Res.* 12:11-21.

Mahoney, L.A. and D.S. Trent. 1995. *Correlation Models for Waste Tank Sludge and Slurries*. PNL-10695, Pacific Northwest Laboratory, Richland, Washington.

McNown, J.S., J. Malaika, and R. Pramanik. 1951. Particle Shape and Settling Velocity, *Transactions*, pp. 511-522, 4th Meeting of the International Association for Hydraulic Research, Bombay, India.

Mehta, A.J., E.J. Hayter, W.R. Parker, R.B. Krone, A.M. Teeter. 1989. Cohesive Sediment Transport In: Process Description. *J Hydr. Div.*, ASCE. 115:1076-1093.

Meyer-Peter, E. and R. Muller. 1948. *Formulas for Bed-Load Transport, Report on Second Meeting of International Association for Hydraulic Research*, pp. 39-64, Stockholm, Sweden.

Mills, C. and C.R. Burt. 1979. "Thin Film Gravity Concentrating Devices and the Bartles-Mozley Concentrator." *Mining Magazine*, Vol 141(1), pp 32-39.

Mishra, M., R.K. Mehta, and S. Chen. 1996. "Selective Flotation of Ultra Fine Radionuclides from Johnston Atoll Coral Sand." SME Annual Meeting 1996.

Morel, F.M.M., J.G. Yeastad, and J.C. Westall. 1981. Adsorption Models: a Mathematical Analysis in the Framework pf General Equilibrium Calculations. In *Adsorption of Inorganics at Solid-Liquid Interfaces*. pp 262-294. Eds. M.A. Anderson and A.J. Rubin. Ann Arbor Science, Ann Arbor, Michigan.

Nakato, T. 1990. Tests of Selected Sediment-Transport Formulas. *J. Hydr. Div.*, ASCE. 116:362-379.

National Research Council. 1983. *An Evaluation of Flood-Level Prediction Using Alluvial-River Models*. National Academy Press, Washington, D.C.

Nitsche, H. 1991. Solubility Studies of Transuranium Elements for Nuclear Waste Disposal: Principles and Overview. *Radiochim. Acta 52/53*:3-8.

Nordin, C.F., Jr. 1989. River Meander Model I: Development. In: *J. Hydr. Div.*, ASCE, 115:1433-1450.

Onishi, Y. 1994a. Sediment Transport Models and Their Testing. In: *Computer Models of Free Surface and Pressurized Flow*, pp. 281-312, M.H., Chaudrey, and L.W. Mays ed., NATO ASI Series E, Applied Sciences-Vol. 274, Klumer Academic Publisher, The Netherlands.

Onishi, Y. 1994b. Contaminant Transport Models in Surface waters'., In: *Computer Models of Free Surface and Pressurized Flow,* pp. 313-341, M.H. Chaudrey and L.W. Mays, ed., NATO ASI Series E, Applied Sciences-Vol. 274, Klumer Academic Publisher, The Netherlands. Partheniades, E. 1962. A Study of Erosion and Deposition of Cohesive Soils in Salt Water, thesis Presented to the University of California at Berkeley, California.

Onishi, Y., H.C. Graber, and D.S. Trent. 1993. Preliminary Modeling of Wave-Enhanced Sediment and Contaminant Transport in New Bedford Harbor, In: *Nearshore and Estuarine Cohesive Sediment Transport.* A.J. Mehta, Ed. American Geophysical Union, pp. 541-557.

Onishi, Y. and J.D. Hudson. 1996. *Waste Mixing and Diluent Selection for the Planned Retrieval of Hanford Tank 241-SY-102: A Preliminary Assessment,* PNNL-10927, Pacific Northwest National Laboratory, Richland, Washington.

Onishi, Y., H.C. Reid, and D.S. Trent. 1995. *Dilution Physics Modeling: Dissolution/Precipitation Chemistry.* PNL-10815. Pacific Northwest Laboratory, Richland Washington.

Pabalan R.T. and D.R. Turner. 1992. *Sorption Modeling for HLW Performance Assessment. Re. On Res. Act. For Calender Year 1991.* Ed. W.C. Patrick. CNWRA 91-01A. San Antonio, TX. Cen. Nuc. Waste Reg. Analysis. 8-1 to 8-66.

Partheniades, E. 1962. A Study of Erosion and Deposition of Cohesive Soils in Salt Water, Ph. D. Thesis, Civil Engineering Department, University of California, Berkeley, California.

Payne T.E., K. Sekine, J.A. Davis, and T.D. Waite. 1992. *Modeling of Radionuclide Sorption Processes in the Weathered Zone of the Koongarra Ore Body*, pp 57-85. Alligator Rivers analogue Project annual Report, 1990-1991. Ed. P. Duerden. Aus. Nuc. Sci. Tech. Org.

Pennders, R.M.J., M. Prins, and M.J. Frissel. 1985. The Influence of Environmental Factors on the Solubility of Pu, Am, and Np in Soil-Water Systems. In: *Speciation of Fisson and Activation Products in the Environment.* Elsevier Science. Publishing Co. Inc., New York, pp 38-46.

Penneman, R.A., R.G. Haire, and M.H. Lloyd. 1988. Polymolybdates as Plutonium (IV) Hosts. In: *Actinide Separations,* Ed. J.D. Navratil, and W.W. Schulz. ACS Symp. Ser. 117. Am. Chem Soc., Washington, DC.

Perry, R.H., and C.H. Chilton. 1973. *Chemical Engineer's Handbook.* McGraw-Hill Book Company, San Francisco, California.

Pikaev, A. 1996. *Gamma Radiolysis of Alkaline Aqueous Solutions of Neptunium and Plutonium.* Poster at Chemistry of the Actinides and Technetium in Alkaline Media Meeting, Battelle Auditorium, April 2, 1996, Richland, Washington.

Pius, I.C., M.M. Charyulu, B. Venkataramani, C.K. Sivaramakrishnan, and S.K. Patil. 1995. Studies on Sorption of Plutonium on Inorganic Ion Exchangers from Sodium Carbonate Medium, *J. Radioanal. Nucl. Chem. Letters,* 199, (1), p. 1-7.

Pool, K.H. and R.M. Bean. 1994. *Waste Tank Organic Safety Project Analysis of Liquid Samples from Hanford Waste Tank 241-C-103.* PNL-9403, Pacific Northwest Laboratory, Richland, Washington.

Postma, A.K., D.B. Bechtold, G.L. Borsheim, J.M. Grigsby, R.L. Guthrie, M. Kummerer, M.G. Plys, and D.A. Turner. 1994. *Safety Analysis of Exothermic Reaction Hazards Associated With the Organic Liquid layer in Tank 241-C-103.* WHC-SD-WM-SARR-001, Westinghouse Hanford Commpany, Richland, Washington.

Pryke, D.C. and J.H. Rees. 1986. Understanding the Behaviour of the Actinides Under Disposal Conditions: A Comparison Between Calculated and Experimental Solubilities. *Radiochim. Acta 40*:27-32.

Pryke, D.C. 1985. A simple Model for the Calculation of Actinide Solubilities in a Repository for Nuclear Waste. In: *Speciation of Fisson and Activation Products in the Environment.* Elsevier Science. Publishing Co. Inc., New York, pp 157-161.

Rai D., A.R. Felmy, D.A. Moore, and M.J. Mason. 1995. *The solubility of Th(IV) and U(IV) Hydrous Oxides in concentrated $NaHCO_3$ and Na_2CO_3 Solutions.* Mat. Res. Soc. Symp. Proc. 353:1143-1150. Mat. Res. Soc. Philadepphia, Pennsylvania.

Rai, D. and J.L. Ryan. 1984. Solubility Constraint: An Important Consideration in Safety Assessment of Nuclear Waste Disposal. *Mat. Res. Soc. Symp. Proc. 26*:805-815.

Rai, D., R.J. Serne, and D.A. Moore. 1980. Solubility of Plutonium Compounds and Their Behavior in Soils. *Soil Sci. Soc. J. 44*:490-495.

Raudkivi, A.J. 1967. *Loose Boundary Hydraulics*, Pergamon Press, New York, New York.

Rees, J.H. 1985. The Theoretical Derivation of Solubilities of Long-Lived Radionuclides in Disposal. *J. Nucl. Mater. 130*:336-345.

Reynolds, D.A. and D.L. Herting. 1984. *Solubilities of Sodium Nitrate, Sodium Nitrite, and Sodium Aluminate in Simulated Nuclear Waste.* RHO-RE-ST-14P, Rockwell International, Richland, Washington.

Richards, K. 1982. *Rivers—Form and Process in Alluvial Channels*, Methuen and Co., Ltd., London and New York.

Richardson, J.F. and W.N. Zaki. 1954. Sedimentation and Fluidisation: Part I. *Trans. Instn. Chem. Engrs*, Vol. 32

Righetto, L., G. Bidoglio, B. Marcandalli, and I.R. Bellabono. 1988. Surface Interactions of Actinides with Alumina Colloids. 44/45:73-75.

Rijn, L. C. Van. 1984a. Sediment Transport, Part I: Bed Load Transport, *J. Hydr. Div.* ASCE. 110:1431-1456.

Rijn, L. and C. Van. 1984b. Sediment Transport, Part II: Suspended Load Transport, *J. Hydr. Div.* ASCE. 110:1613-1641.

Rogers, C.A. 1993. *An Analytical Model For Evaluating Subcritical Limits for Waste in Hanford Site Storage Tanks.* WHC-SD-SQA-CSA-20356, Rev. 0. Westinghouse Hanford Company, Richland Washington.

Rogers, C.A. 1996. *CSER 96-010: Criticality Parameters for Tank Waste Evaluation.* WHC-SD-SQA-CSA-507, Rev. 0, Westinghouse Hanford Company, Richland, Washington.

Ros, N.C. J.J. 1961. Petrol. Technology 13, 1037

Rouse, H. 1937a. Modern Conceptions of the Mechanics of Fluid Turbulence, *Trans.* ASCE. 102:463-543.

Rouse, H. 1937b. *Nomogram for the Settling Velocity of Spheres,* Division of Geology and Geography Exhibit D of the Report of the Commission on Sedimentation, 1936-37, pp. 57-64, National Research Council, Washington, D.C.

Russel, W.B., D.A. Saville, and W.R. Schowalter. 1989. *Colloidal Dispersions.* Cambridge University Press. Cambridge, Massachusetts.

Sanchez, A.L., J.W. Murray, and T.H. Sibley. 1985. The Adsorption of Pu (IV) and (V) of Goethite. *Geochim. Cosmochim. Acta.* 49:2297-2307.

Scheele, R.D., and M.E. Petersen. June 1989. *Results of the Characterization of Samples of Waste from Double-Shell Tank 102-SY.* Pacific Northwest Laboratory. Richland Washington.

Schindler, P., H. Althaus, F. Hofer, and W. Minder. 1965. "Loslichkeitsproduckte von Metalloxiden und - hydroxiden: Loslichkeitsprodukte von Zinkoxid, Kupferxide und Kupferoxid in Abhangigkeit von Teilchengrosse und molarer Oberflache. Ein Beitrag zur Thermodynamik von Grenzflachen fest-flussig." *Helv. Chim. Acta* 48:1204-1215.

Schindler, P. 1967. Heterogeneous Equilibria Involving Oxides, Hydroxides, Carbonates, and Hydroxide Carbonates. In *Equilibrium Concepts in Natural Water Systems*, Adv. Chem. Ser., No. 67, pp196-221, American Chemical Society, Washington, D.C.

Schindler, P. 1981. Surface Complexes at Oxide-Water Interfaces, In: *Adsorption of Inorganics at Solid-Liquid Interfaces,* M.A. Anderson and A.J. Rubin, Eds., Ann Arbor Science, Ann Arbor, Michigan, p. 1-50.

Schwertmann U. and R.M. Taylor. 1989. Iron Oxides. In: *Minerals in Soil Environments.* Soil Sci. Soc. Am. Madison, Wisconsin.

Schwertmann, U. and R.M. Cornell. 1991. *Iron Oxides in the Laboratory.* Verlagsgesellschaft mbH, VCH Publishing, New York, New York.

Sederburg, J.P. 1994. *Chemical Compatibility of Tank Wastes in Tanks 241-C-106, 241-AY-101, and 241-AY-102.* WHC-SD-WM-ES-290. Westinghouse Hanford Company, Richland, Washington.

Serne, R.J. 1989. Radiation Effects on Chemistry. *Engineering Geology.* 26:319-329.

Serne, R.J., G.A. Whyatt, S.V. Mattigod, Y. Onishi, P.G. Doctor, B.N. Bjornstad, M.R. Powell, L.M. Liljegren, J.H. Westsik, Jr., N.J. Aimo, K.P. Recknagle, G.R. Golcar, T.B. Miley, G.R. Holdren, D.W. Jeppson, R.K. Biyani, and G.S. Barney. 1996. *Fluid Dynamics, Particulate Segregation, Chemical Processes, Natural Ore Analog and Tank Inventory Discussions that Relate to the Potential for Criticality in Hanford Tanks.* WHC-SD-WM-TI-757, Rev. 0, Westinghouse Hanford Company, Richland, Washington 99352.

Shannon, R.D. 1976. Revised Effective Ionic Radii and Systematic Studies of Interatomic Distances in Halides and Chalcogenides. *Acta Cryst.* A32:751-767.

Shaw, D.J. 1980. *Introduction to Colloid and Surface Chemistry.* 3rd Ed., Butterworths, Boston, Massachusetts.

Shen, H.W., and C.S. Hung. 1972. An Engineering Approach to Total Bed Material Load by Regression Analysis, *Proc. Of the Sedimentation Syst.*, 14.1-14.17, Berkeley, California.

Shergold, F.A. 1946. The Effects of Sieve Loading on the Results of Sieve Analysis of Natural Sands, *J. Soc. Chem. Ind.*, London. 65:245-249.

Shields, A. 1936. Anwendung der Aenlichkeitsmechanik und der Turbulenzforschung auf die Geschiebebewegung, *Mitteilungen der Preussischen Versuchsanstalt fur Wasserbau und Schiffbau*, Berlin, Germany, Translated to English (Application of Similitude Mechanics and the Research on Turbulence to Bed-load Movement.) by W.P. Ott and J.C. van Uchelen, California Institute of Technology, Pasadena, California.

Shulits, S. 1935. The Schoklitsch Bed-Load Formula, Engineering, London, England, pp. 644-646, and pp. 687.

Simons, D.B., and F. Senturk. 1977. *Sediment Transport Technology*, Water Resource Publications, Denver, Colorado.

Sivamohan, R. and K.S.E. Forssberg. 1986. "Progress in Gravity Concentration - Theory and Practice." In: *Advances in Mineral Processing*. Society of Mining Engineers, Littleton, Colorado.

Smerdon, E.T., and R.P. Beasley. 1961. Critical Tractive Forces in Cohesive Soil, *Ag. Eng.*, St. Joseph, Michigan, pp. 26-29.

Smith, D.K. 1989. "Computer Analysis of Diffraction Data." In: *Modern Powder Diffraction,* Reviews in Mineralogy, Vol 20, pp 183-216, Mineralogical Society of America, Washington, D.C.

Sposito, G. 1986. *Distinguishing Adsorption from Surface Precipitation.* In Geochemical Processes at Mineral Surfaces. Eds Davis J. A. and K. F. Hays. ACS Symp Ser. 323. Am. Chem. Soc. Washington, DC.

Stumm, W. and J.J. Morgan. 1981. Aquatic Chemistry, 2nd. Edition. John Wiley and Sons Publishing, New York, New York.

Sullivan, J.C. 1983. Reaction of plutonium Ions with Products of Water Radiolysis. In *Plutonium Chemistry*. Eds: W.T. Carnall and G.R. Choppin. pp 241-249. ACS Sym. Ser. 216. Washington, D.C.

Sundborg, A. 1956. The River Klaralven, a Study of Fluvial Processes, *Geografiska Annaler*, pp. 127-316.

Tait, C.D., S.A. Ekberg, P.D. Palmer, and D.E. Morris. 1995. *Plutonium Carbonate Speciation Changes as Measured in Dilute Solutions with Photoacoustic Spectroscopy.* LA-12886-MS, Los Alamos National Laboratory, Los Alamos, New Mexico.

Tank Waste Science Panel. 1991. *Chemical and Physical Processes in Tank 241-SY-101: A Preliminary Report.* PNL-7595, Pacific Northwest Laboratory, Richland, Washington.

Tchobanoglous, G. and F.L. Burton. 1991. *Wastewater Engineering Treatment, Disposal, and Reuse.* McGraw Hill, Inc. pp 242-248.

Teeter, A.M. 1988. *New Bedford Harbor Project--Acushnet River Estuary Engineering Feasibility Study of Dredging and Dredged Material Disposal Alternatives--Report 2, Sediment and Contaminant Hydraulic Transport Investigations*, U.S. Army Corps of Engineers Waterways Experiment Station, Viscksburg, Mississippi.

Temer, D.J. and R. Villareal. 1995. *Sludge Washing and Alkaline Leaching Tests on actual Hanford Tank Sludge: A Draft Report on Samples TY-104 and C-107.* LAUR-95-3211. Los Alamos National Laboratory, Los Alamos, New Mexico.

Temer, D.J. and R. Villareal. 1996. *Sludge Washing and Alkaline Leaching Tests on actual Hanford Tank Sludge: A Draft Report on Samples B-104 and BX-109.* LAUR-96-1986. Los Alamos National Laboratory, Los Alamos, New Mexico.

Theis, C.V. 1935. The relation between the lowering of the piezometric surface and the rate and duration of discharge of a well using groundwater storage. *Trans. Amer. Geophys. Union,* 2, pp.519-524.

Thiyagarajan, P., H. Diamond, L. Soderholm, E.P. Horwitz, L.M. Toth, and L.K. Felker. 1990. Plutonium(IV) Polymers in Aqueous and Organic Media, *Inorg. Chem.* 29:1902-1907.

Ticknor, K.V., T.T. Vandergraaf, and D.G. Juhnke. 1986, *The Effect of Laboratory Time-Scale Hydrothermal Alteration on Igneous Rok Coupon Radionuclide Sorption/Desorption,* TR-376, Atomic Energy of Canada Limited Research Company, Chalk River, Ontario, Canada.

Ticknor, K.V. 1993. Actinide Sorption by Fracture-Filling Minerals. *Radiochim. Acta,* 60:33-42.

Toffaleti, F.B. 1969. Definitive Computations of Sand Discharge in Rivers, *J.of Hydraulic Division,* ASCE. 95:225-248.

Tole, M.P. 1984. SomeIimplications of the role of kinetics in enhancing element transport: *in Hydrochemical Balances in Freshwater Systems.* E. Ericksson, Ed. pp. 79-86. International Association of Hydrological Sciences, Publication No. 150.

Tole, M.P., A.C. Lasaga, C. Pantano, W.B. White. 1986. The Kinetics of Dissolution of Nepheline ($NaAlSiO_4$). *Geochim Cosmochim Acta,* 50:379-392.

Toste, A.P., R.B. Lucke, T.J. Lechner-Fish, D.J. Hendren, and R.B. Myers. 1987. Organic Analyses of Mixed Nuclear Wastes. *Waste Management '87, Volume 3:* 323-329, : R. G. Post, Ed. University of Arizona Press, Tucson, Arizona.

Toste, A.P., L.J. Kirby, and T.R. Pahl. 1984. Role of Organics in the Subsurface Migration of Radionuclides in Groundwater. *ACS Symp. Ser. 246*: 95-112. American Chemical Society, Washington, DC.

Toth, L.M., H.A. Friedman, and M.M. Osborne. 1981. Plymerization of Pu(IV) in Aquous Nitric Acid Solution, J. Inorg. Nucl. Chem. 43:2929-2934.

Toth, L.M., H.A. Friedman, G.M. Begun, and S.E. Doris. 1984. Raman Study of Uranyl Ion Attachment to Thorium(IV) Hydrous Polymer, *J. Phys. Chem.* 88: 5574-5577.

Trent, D.S. and L.L. Eyler. 1993. *TEMPEST: A Computer Program for Three-Dimensional Time Dependent Computational Fluid Dynamics*. PNL-8857 Vol. 1, Version T, Mod 2, Pacific Northwest Laboratory, Richland, Washington.

Trent, D.S. and L.L. Eyler. 1989. *TEMPEST: A Three Dimensional Time-Dependent Computer Program for Hydrothermal Analysis, Volume 1: Numerical Methods and Input Instructions.* PNL-4348, Vol 1, Rev. 2. Pacific Northwest Laboratory, Richland Washington.

Trent, D.S., and T.E. Michener. 1993. *Numerical Simulation of Jet Mixing Concepts in Tank 241-SY-101.* PNL-8559, Pacific Northwest Laboratory, Richland, Washington.

Tripathi, V.S. 1984. *Uranium(VI) Transport Modeling: Geochemical Data and Submodels.* Ph. D. Dissertation. Stanford University. Stanford, California.

Tusler, S.A. *Double-Shell Tanks Plutonium Inventory Assessment May 1995.* WHC-SD-WM-TI-640, Rev. 0 Westinhouse Hanford Company, Richland, Washington.

Van Vleet, R.J. 1993a. *Radionuclide and Chemical Inventories for the Double Shell Tanks.* WHC-SD-WM-TI-543, Rev 1. Westinghouse Hanford Company, Richland, Washington.

Van Vleet, R.J. 1993b. *Radionuclide and Chemical Inventories for the Single Shell Tanks.* WHC-SD-WM-TI-565, Rev 1. Westinghouse Hanford Company, Richland, Washington.

Vanoni, V.A., ed. 1975. *Sedimentation Engineering*, ASCE Manuals and Reports on Engineering Practice, ASCE, New York, New York.

Violante, A. and P. Violante. 1980. Influence of pH, Concentration and Chelatng Power of Organic Anions on the Synthesis of Aluminum Hydroxides and Oxyhydroxides. *Clays and Clay Miner.* 28:425-434.

Violante, A. and P.M. Huang. 1985. Influence of Inorganic and Organic Ligands on the Formation of Aluminum Hydroxides and Oxyhydroxides. *Clays and Clay Miner.* 33:181-192.

Virden , J.W., B.C. Bunker, and J. Lui. 1994a. *Solids Formation and Sludge Dissolution: Results of Transmission Electron Microscopy on Tank Sludge Simulant.* T WRS-PP-94-028, Pacific Northwest Laboratory, Richland, Washington.

Virden, J.W., J. Liu, B.C. Bunker, V.S. Stenkamp, and L. Song. 1994b. *Solids Formation and Sludge Dissolution: Final Report for FY1994.* TWRSPP-94-092, Pacific Northwest Laboratory, Richland, Washington.

Wadell, H. 1932. Volume, Shape, and Roundness of Rock Particles, *J. Geol.* 40: 443-451.

Wahl, K.L., J.A. Campbell, S.A. Clauss, K.E. Grant, B.D. Lerner, G.M. Mong, A.K. Sharma, C.E. Petersen, A.J. Saenz, S.A. Bryan, I.E. Burgeson, R.D. Scheele, and R.L. Sell. 1995. *Waste Tank Organic Safety Program Advanced Organic Analysis and Analytical Methods Development: FY 1995 Progress Report.* PNL- 10777, Pacific Northwest Laboratory, Richland, Washington.

Walsh, D.E. and P.D. Rao. 1986(?). *A Study of Factors Suspected of Influencing the Settling Velocity of Fine Gold Particles.* MIRL Report no. 76, Mineral Industry Research Laboratory, University of Alaska, Fairbanks, Alaska.

Waltar, A.E., H. Babad, G.S. Barney, R.E. Felt, J. Greenborg, L.H. Rogers, R.J. Serne, and G.A. Whyatt. 1996. *Project W-320 Tank 241-C-106: Criticality Review Team Report.* WHC-SD-W320-CSA-001, Rev. 0, Westinghouse Hanford Company, Richland, Washington.

Weigel, F., J.J. Katz, and G.T. Seaborg. 1986. Plutonium. In *The Chemistry of Actinide Elements.* Chapman and Hall, London.

Wells, A. 1991. "Some Experiences in the Design and Optimisation of Fine Gravity Concentration Circuits." *Minerals Engineering*, Vol 4(3/4), pp 383-398.

Westall, J. and H. Hohl 1980. A Comparison of Electrostatic Models for Oxide/Solution Interface. *Adv. Coll. Interfac. Sci.* 12:265-294.

WHC 1993a. Laboratory Reports for WHC-SD-WM-ES-244. WHC-MR-0419. Westinghouse Hanford Company, Richland Washington. Contains letter: Weiss, R.L. to T.R. Pauly, April 14, 1987. Additional Analyses on Core Samples from Tanks 241-C-105 and 241-C-106. Internal Letter No. 65453-87-050. Rockwell International.

WHC 1993b. Laboratory Reports for WHC-SD-WM-ES-244. WHC-MR-0419. Westinghouse Hanford Company, Richland Washington. See letter J.E. Horton of 222-S to W.R. Christensen, July 22, 1977, and Subreport: 102AY Data: Results of the Characterization of 102-AY Solids, Washed Solids and Supernatant R.D. Scheele, M.E. Petersen, J.M. Tingey, 1990. Pacific Northwest Laboratory, contained within.

(WHC 1995a. *90-Day Safety Screen Results for Tank 241-C-103, Push Mode Core Samples 63 and 66.* WHC-SD-WM-DP-099, Rev. 0B, Westinghouse Hanford Company, Richland, Washington.

WHC 1995b. *Tank Waste Source Term Inventory*, April 1995, WHC-SD-WM-ER-400. Westinghouse Hanford Company, Richland Washington.

White, M.D., and M. Oostrom. 1996. Subsurface Transport Over Multiple Phases (STOMP), Code Users Guide. PNNL-11217, Pacific Northwest National Laboratory, Richland, Washington.

White, C.M. 1940. The Equilibrium Grains on the Bed of a Stream, *Proc. Royal Soc.* London, Series A. 174:322-338.

White, M.D., and M. Oostrom. 1996. *STOMP: Subsurface Transport Over Multiple Phases. Theory Guide.* PNNL-11217. Pacific Northwest National Laboratory, Richland, Washington.

Willingham, C.E. 1994a. Thermophysical Properties of Hanford High-Level Tank Wastes - A Preliminary Survey of Recent Data. PNL-9419 Pacific Northwest Laboratory, Richland Washington.

Winters, W.I. 1995. *Tank Characterization Report for Double-Shell Tank 241-SY-102.* WHC-SD-WM-ER-366, Rev. 0. Westinghouse Hanford Company, Richland, Washington.

Yamaguchi, T., Y. Sakamoto and T. Ohnuki. 1994. Effect of the Complexation on Solubility of Pu(IV) in Aqueous Carbonate System. *Radiochim. Acta.*66/67:9-14.

Yang, C.T. and A. Molinas. 1982. Sediment Transport and Unit Stream Power Function. *J. Hydr. Div.*, ASCE. 108:774-793.

Yang, C.T. 1973. Incipient Motion and Sediment Transport, *J. Hydr. Div,* ASCE, 99:1679-1704.

Yang, C.T. 1979. Unit Stream Power Equations for Total Load, *J. Hydr. 40:*123-138.

Zakharova E.V. and V.M. Ermolaev. 1995. "Transformation of Solid Phases during Storage of Radioactive Sludge in Tanks." *Radioactive Waste Management and Environmental Remediation Session*, American Society of Mechanical Engineers Proceedings 1995 annual Meeting, pp 129-132.

Zandi, I., and G. Govatos. 1967. Heterogeneous Flow of Solids in Pipelines. *J. Hydr. Div. ASCE.* 93:145-159.

Znamenskaya, N.S. 1967. The Analysis of Estimating of Energy Losses by Instantaneous Velocity Distribution of Streams with Movable Bed, Proceedings, *Twelfth Congress of the International Association for Hydraulic Research.* 1:27-30.

Appendix A

Properties of Generated Waste Relevant to Criticality Hazard

Appendix A
Properties of Generated Waste Relevant to Criticality Hazard

A.1 Objective/Scope

This chapter characterizes the waste in the underground tanks using historical accounts of flows and compositions of waste stream inputs, waste treatment processes, and analytical results of recent waste samples from the tanks.

A.2 Background

This section describes the waste streams that were added to the waste tanks and subsequent operations conducted on the waste. It describes the plutonium/uranium processing facilities, cesium and strontium removal facilities, and evaporation facilities, and their waste streams that were discharged to the tank farms. It also reports the chemical composition of the streams including densities, pH, volumes, and estimated solids contents. We also characterize waste streams that were returned to the tank farms after being removed and treated and describe in-farm treatment of the waste and operations affecting changes of the waste, including estimates based on waste characterization.

A.2.1 Wastes from Plutonium Separations and Finishing Operations at Hanford

Plutonium separations processing began at the Hanford Site in 1944 at the bismuth phosphate plant and continued until 1990 when the PUREX plant was shut down. Facility flushing and waste treatment has continued after shutdown. Waste volume generation and transfers to the tank farms continue, although discharges contain little plutonium. DOE-HQ accountability records report that 67.4 metric tons (MT) of plutonium (Roblyer 1994) were produced in the reactors at the Hanford Site. This includes 12.9 MT of nonweapons-grade plutonium (nominally 9 wt% or higher ^{240}Pu); the rest was weapons grade (nominally 6 wt% ^{240}Pu). This estimate agrees well with independently calculated plutonium production values based on thermal power generation and plutonium conversion factors representing the various reactor fuels. Using this approach, about 62.7 MT of plutonium was processed at the Hanford Site. About 4 MT of plutonium remains in the K Basins and 0.528 MT of plutonium was processed at West Valley, New York. Small quantities of miscellaneous fuels that were processed at the Hanford Site include PRTR (plutonium recycle test reactor), MOX (mixed oxide fuel), thorium fuel, and PWR (Shippingport reactor fuels).

Fuel types produced at the Hanford Site include aluminum-clad base fuel O3N, C5N, K5N, and aluminum-clad driver fuel 03E, C3E, and K5E irradiated in B, C, D, DR, F, H, KE, and KW reactors. Zirconium-clad base fuel, Mark IV, and zirconium-clad driver fuel, Mark IA, were irradiated in N Reactor.

Quantities of plutonium processed (Roetman et al. 1994) through each separations facility and percentage of the total amounts processed are shown in Table A.1.

Table A.1. Plutonium Production by Plant

	Quantity of plutonium processed (MT)	Mass of total plutonium (%)
Bismuth Phosphate	2.70	4.3
T Plant		
B Plant		
REDOX	11.27	18.0
PUREX	48.73	77.7

An estimate of the total plutonium discharged to the Hanford Site waste tanks is about 500 kg. An estimate of about 1,000 kg has been postulated for use in considering criticality issues in waste tanks because of uncertainties about the content of waste discharged to the tanks (Roetman et al. 1994).

The site contains 177 tanks; 149 are SSTs that have no current waste transfer activity and 28 are the newer DSTs. Tank diameters are given in Table A.2. Figure A.1 illustrates a typical waste configuration in the DSTs (unstabilized because waste transfers are fairly recent); Figure A.2 illustrates the waste configuration for the SSTs. Sludge, which consists of solids with interstitial liquid containing water-insoluble chemicals that have precipitated from solution, forms the bottom layer in all the tanks. Salt cake was formed on top of the sludge in some tanks from the crystallization and precipitation of chemicals after the supernatant liquid was evaporated during volume reduction operations.

Table A.2. Tank Diameters

Tank type	No. of tanks	Diameter in m (ft)
SSTs	133 16	6.10 (20) 22.9 (75)
DSTs	28	22.9 (75)

Waste management practices at the Hanford Site required waste be transferred from separations and finishing facilities (or uranium, strontium and cesium recovery operations) to the low-carbon steel tanks only after low concentrations of plutonium were verified and the acid contents were neutralized with sodium hydroxide. The neutralization not only precipitated most of the fissile materials in the waste, but also coprecipitated various metal cations associated with reprocessing or waste management. Such materials were allowed to settle in SSTs, forming sludge layers. Most reprocessing and product purification operations contained sufficient uranium, zirconium, and/or aluminum or used enough iron-containing reagents to neutronically subdue any fissile materials present. The slow settling of alkali-

insoluble materials tended to form pancake-like layers of solids in the 22.9-m (75-ft) diameter waste tanks. As part of subsequent waste management efforts, operations were conducted to recover uranium, cesium, and strontium byproducts of fuel reprocessing from the waste. These operations also lowered heat loads in the tanks. All waste associated with these processes was made alkaline to prevent corrosion of the tanks.

To increase the storage capacity of the tanks, dilute waste supernatant solutions containing water-soluble salts produced by acid neutralization were heated to remove water. Two methods were used: in-tank solidification and successive-pass external evaporation, returning the concentrated waste to the tanks as evaporator bottoms. In both cases, the results were the same. Large quantities of water were removed, the solubility of the salts contained in the wastes was exceeded, and the salts were precipitated and settled out in the tanks, usually resulting in a five- to tenfold reduction in volume. The salts that settled in the tanks became salt cake that formed a layer on top of existing sludge inventories. The evaporation processes also concentrated both the free alkali (sodium hydroxide) and organic complexants in the waste, most of which remained in solution.

As part of an effort to reduce the potential for fluid leakage from SSTs, many of the tanks were salt-well pumped and most of the drainable liquids were transferred to DSTs. This further compacted both the sludge and salt cake layers. The resulting waste contained mainly non-drainable liquids, although some drainable waste remained.

A.2.2 Operational Controls on Waste Transfer

Current criticality controls (CPS-P-465-40000) require that waste transferred from reprocessing facilities to DSTs have a solution concentration limit of less than 0.013 g/L of plutonium (less than 0.05 g/gal). Fissile plutonium is defined as total ^{239}Pu and ^{241}Pu and equivalent ^{235}U and ^{233}U contents. This concentration limit is set to control the cumulative concentration of fissile material in tank solids at or below the operating value of 2.6 g/L as an upper value for settled waste in the tanks.

Plutonium fissile equivalence for ^{233}U is defined as "one gram of ^{233}U shall be assumed equivalent to one gram of ^{239}Pu." Plutonium fissile equivalence of ^{235}U is defined as "when the ^{235}U concentration in uranium exceeds 1 wt%, one gram of ^{235}U in excess of 1 wt% enrichment shall be assumed equivalent to one gram of plutonium." The ^{235}U content of postirradiated Mark IA fuel (preirradiated enrichment of 1.15 wt% ^{235}U average of inner and outer element) is 1.0 wt% when irradiated to 6 percent ^{240}Pu. This is the least irradiated Mark IA fuel processed. All other enriched fuels processed were irradiated to a greater extent and would have less ^{235}U. The 1 wt% ^{235}U value was determined by crediting the ^{238}U associated with ^{235}U as an adequate absorber for ^{235}U above natural concentration of 0.72 wt%. The ^{238}U could not also be credited as an absorber for plutonium calculations in this situation.

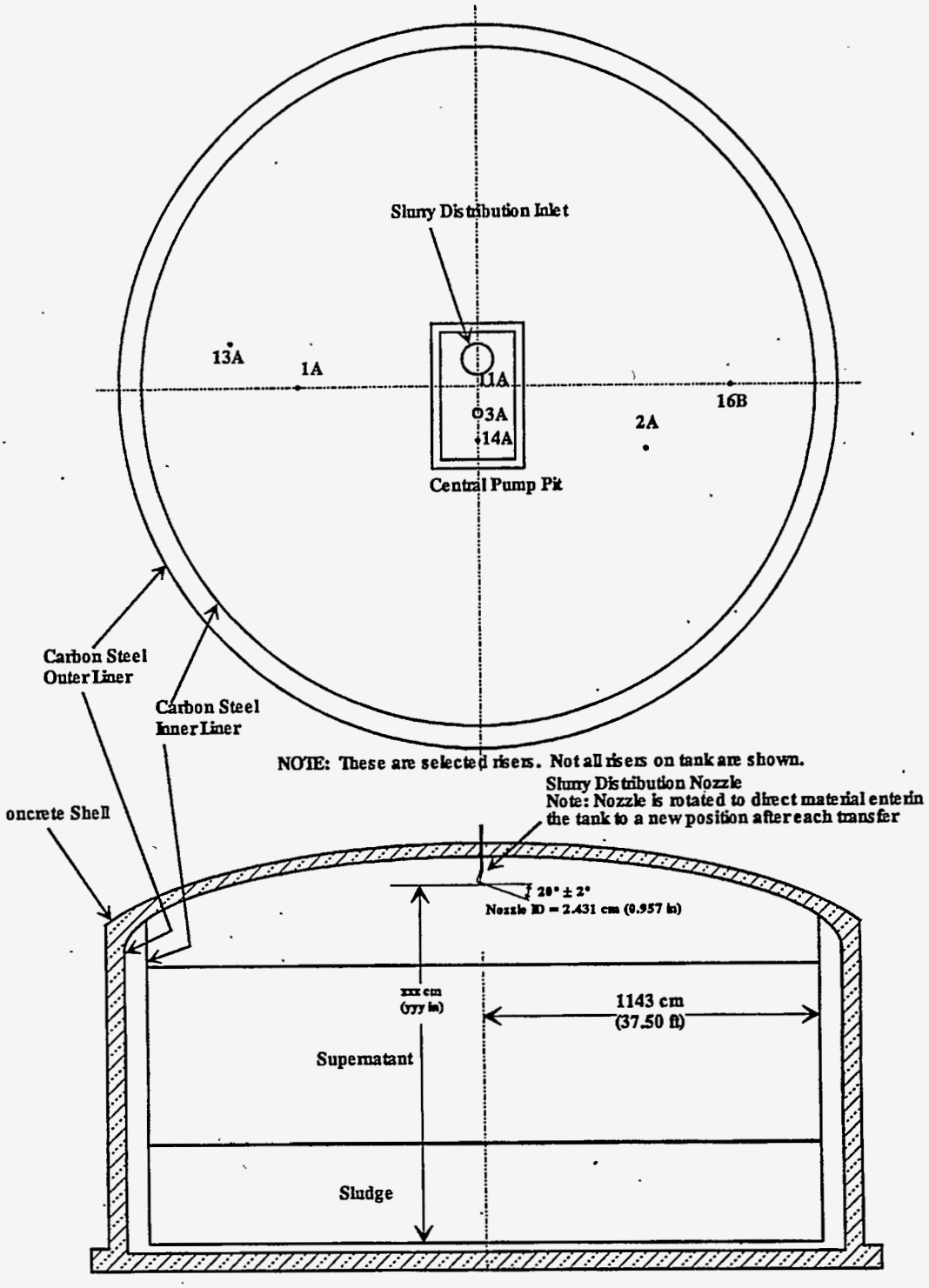

Figure A.1. Schematic for the 28 DSTs at the Hanford Site

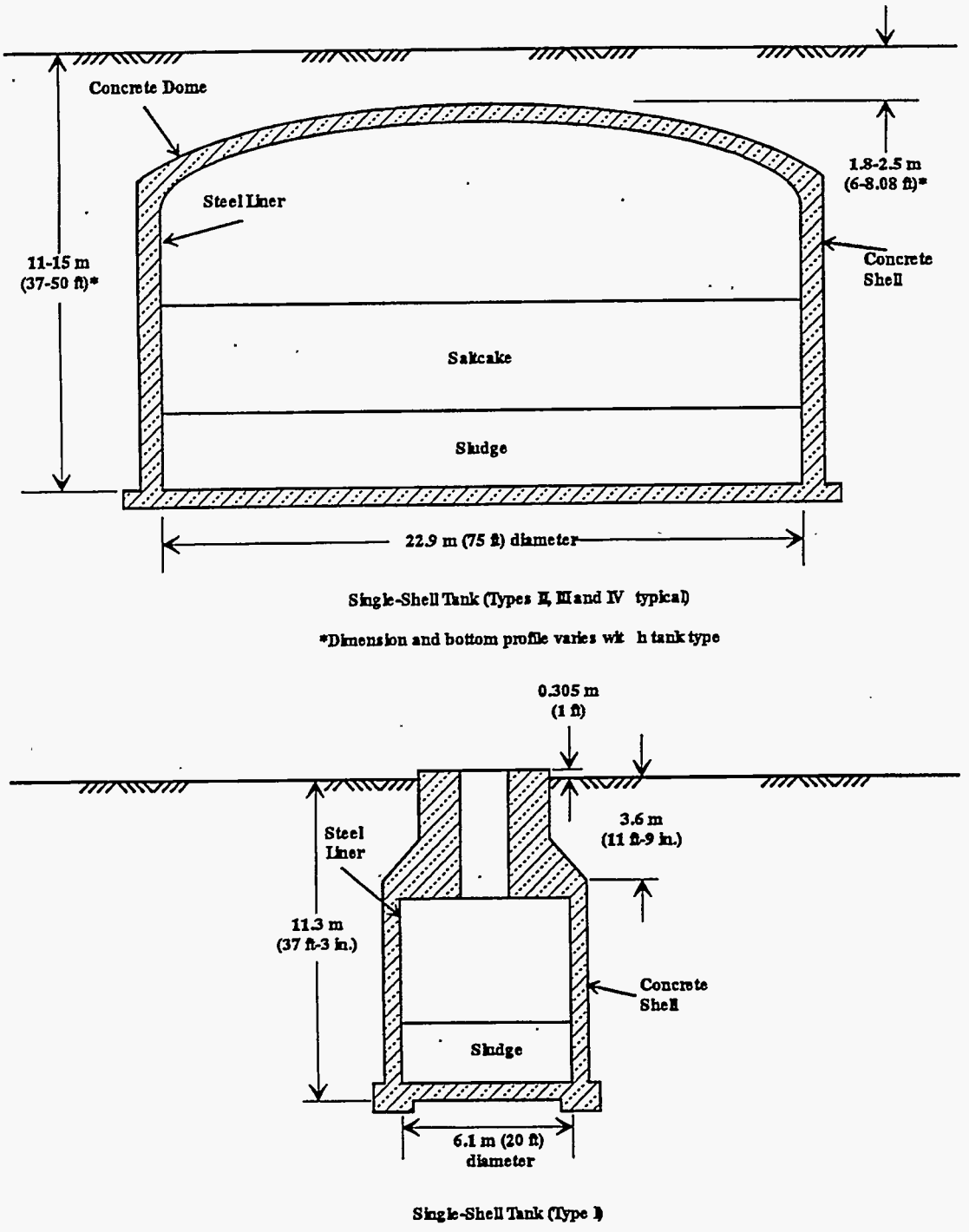

Figure A.2. Schematic for the Two Types of SSTs at the Hanford Site

Neptunium-237 and ^{241}Am are not fissile isotopes but are fissionable in the presence of fast neutrons (Rogers 1996). These isotopes are both present in some waste tanks at low concentrations, but do not contribute to criticality because the tanks contain no fast neutron fields. When the hydrogen-to-actinide (^{237}Np and/or ^{241}Am) atom ratio is ≥5, these actinides are exempt from a need of specification (Tomlinson 1971). All waste has a hydrogen-to-actinide (^{237}Np and/or ^{241}Am) ratio greater than 5 because these actinides are present only at low concentrations and the water content of waste is greater than 5 wt%.

Further, the current controls on Hanford Site tank farms require that an auditable continuous inventory of plutonium and an assessment of the plutonium concentration both in the solids and supernatant shall be maintained for each tank. Waste discharged to the tank farms shall be alkaline (basic) with a pH of at least 8.0, unless a criticality safety evaluation shows that alkalinity is not required. (A low pH by itself can not cause criticality.) Currently, specifications require that waste transferred to tanks have a pH of greater than 10 to control tank corrosion. Verification of compliance shall be documented before each transfer from a generating facility to the tank farms.

These or similar criticality controls were in place when waste was transferred to the SSTs in the past, as documented by (Oberg 1976). Presently waste from generating facilities cannot be transferred to SSTs, nor can transfers be made between SSTs without an approved criticality review and documentation. No fissile material-bearing waste has been transferred to the SSTs since 1980.

A.2.3 Waste Properties Relevant to Criticality Hazard

Waste properties relevant to criticality in Hanford Site waste tanks include fissile material (^{239}Pu, ^{233}U, and ^{235}U) concentrations, neutron absorber concentrations, moderator concentrations, and any chemical or physical fissile material concentrating mechanisms (discussed in the other chapters of this report). Fissile materials are mainly in the sludges that have settled to the bottoms of the tanks. Fissile materials are quite insoluble in the tank waste caustic solutions and are at low concentrations in salt cakes and supernatant. Key parameters affecting criticality include the following:

- Plutonium mass inventory in each tank
- Plutonium concentration in tank waste
- Concentration and identity of neutron absorbers/moderators
- Tank geometry/operations/status.

Fissile materials are found mainly in sludge layers rather than in salt cake or supernatant liquid. Insoluble absorbers are also in the sludge layers. Absorbers of interest and their minimum subcriticality mass ratios (Rogers 1996) are listed in Table A.3.

Table A.3. Minimum Subcriticality Mass Ratio for Selected Absorber Materials

Insoluble absorbers (under tank waste conditions)	Minimum subcriticality mass ratio (absorber/fissile material)
Aluminum (assume 70% insoluble)	910
Bismuth	48,000
Boron	0.09
Cadmium	0.24
Calcium	770
Chromium	135
Copper	130
Iron	160
Lanthanum	121
Manganese	32
Mercury	5
Nickel	105
Silicon	1,400
Thorium	243
Uranium (natural)	770
Zirconium	4,000
Soluble absorbers	
Nitrogen	61
Phosphorus	1,300
Sodium	360

A.2.4 Activity Status of Tanks

SSTs have been inactive since 1981 and no wastes are scheduled to be added to them. The DSTs still receive wastes but, because no fuel separations operations are currently under way, the only waste received is from flushing of PFP and PUREX equipment, tanks, and cells. Any waste added to tank farm tanks is expected to have a very low plutonium concentration. Supernatant transfers from SSTs to DSTs occur infrequently.

A.3 Waste Stream Characterization

This section characterizes the waste streams routed to the tanks. Several aqueous separations, plutonium finishing, and waste treatment processes have been used at the Hanford Site since 1944. Each process generates its own distinctive fissile material-bearing aqueous waste discharged to the underground storage tanks. Both high- and low-level waste containing fissile material was discharged from these processes to the tank farms. The separations processes include the bismuth/phosphate process

conducted at T Plant and B Plant from 1944 to 1956, the uranium recovery process conducted at U Plant from 1952 to 1959, the reduction oxidation (REDOX) process conducted at the REDOX facility from 1952 through 1966, and the plutonium-uranium extraction (PUREX) process conducted at the PUREX facility from 1956 to 1972 and 1983 to 1990. Plutonium finishing processes were conducted at the 234-5 (PFP) facility with wastes discharged to the tank farms from 1973 to the present. Uranium recovery and some cesium and strontium scavenging were conducted at U Plant. Additional cesium and strontium recovery operations were conducted on first cycle waste from the bismuth phosphate process at T Plant and on tank farm supernatant pumped from some tanks to the AR vault for treatment.

A.3.1 Hanford Defined Wastes

Recently, workers at Los Alamos National Laboratory (LANL) compiled available records from the Hanford Site on process flowsheets and waste transfers to tanks. In this appendix we document newly released records and compare our results to LANL's. The flowsheet data and old records on waste stream characterization were used to define a finite set of waste types that represent all the types created and sent to either tanks or cribs. This unique set of waste is called the Hanford Defined Wastes (HDW) and is found in Agnew (1995). Coupled with all the records of transfers to tanks, out of tanks to recovery facilities and evaporators, and treated waste or concentrates back to tanks, the HDW have been used in a computer algorithm to define the contents in tanks, both total and split into sludge (with interstitial liquids) and supernate liquids (includes salt cake). The Agnew estimates of total plutonium inventories in the Hanford Site SSTs is listed in Table A.4 and compared with three other independent estimates. As can be seen, the estimated plutonium content differs significantly between the SSTs. The plutonium inventory estimated for each of the DSTs using two sources is included in Table A.5. Because plutonium concentration and content are the main concern for criticality, resolution of some of the uncertainties shown in the tables may be warranted.

This chapter is keyed toward evaluating the waste in the 29 larger tanks reported to contain more than 10 kg of plutonium or equivalent fissile material and the 4 smaller tanks (with 6.1 m diameter) containing more than 0.75 kg plutonium. The 10-kg and 0.75-kg fissile material screening values are set to allow focusing on the tanks of most interest to addressing the criticality issue. These screening values are a factor of 106 below the minimum critical area density in pure water (240 g/ft^2) reported by Carter et al. (1969) for the tanks. Applying this areal density limit in water is conservative when compared to sludges. If the tanks contain less than 10 kg or 0.75 kg fissile material, respectively, a concentrating mechanism of more than 100 would be required in the horizontal direction to approach a critical limit. This is considered incredible when the processes to add waste to the Hanford tanks are considered. The tanks with less than 10 kg or 0.75 kg of fissile material, as applicable, will be evaluated, but with less intensity unless analysis shows that they may contain higher quantities of plutonium. We have identified 33 tanks that have higher concentrations of plutonium than this screening value as determined by any one of four methods used. The tanks are listed in Table A.6 and are identified in Tables A.4 and A.5 by footnotes.

Table A.4. Single-Shell Tank Plutonium Inventory Comparison

Tank	Waste Status Summary[a] (KL)			ASA source term and sample data[b]				HDW model (Rev. 3)[c] Pu (g)	WESTREN[d]		TRAC-summary TI-057 03/12/85[e]		HDW Model (Rev. 3)[c] ratio sum
	Sludge	Salt	Liquids	Sludge (g Pu/L)	Salt (g Pu/L)	Liquids (g Pu/L)	Total Pu (g)		Total Pu (Bq)	Pu (g)	Pu (Ci)	Pu (g)	
A-101[f]	11.4	3,596	0.0	6.52 E-04	4.40 E-03	4.40 E-03	15,828.70	3,730.00	4.46 E+12	1,943.13	2.00 E+03	32,258.06	234
A-102	56.8	83.27	15.1			1.80 E-03	27.25	792.00	4.57 E+10	19.90	3.00 E+02	4,838.71	20.8
A-103	1,385.3	0	18.9			5.00 E-04	9.46	702.00	7.36 E+12	3,205.16	4.00 E+02	6,451.61	6.19
A-104[f]	106.0	0	0.0	1.09 E-01			11,551.82	16,100.00	2.36 E+13	10,277.42	6.00 E+02	9,677.42	6.45
A-105[f]	71.9	0	0.0	1.40 E-01			10,053.72	1,760.00	1.00 E+13	4,354.84	2.00 E-06	3.23 E-05	59.6
A-106[f]	473.1	0	0.0	7.67 E-02		4.70 E-05	36,265.03	19,900.00	6.74 E+13	29,351.61	1.00 E+03	16,129.03	11.4
AX-101	11.4	2,820	0.0	5.00 E-05	5.00 E-05	5.00 E-05	141.56	4,700.00	1.06 E+11	46.16	3.00 E+02	4,838.71	42.6
AX-102	26.5	109.8	11.4		1.82 E-03	1.82 E-03	219.95	6,940.00	4.08 E+10	17.77	1.00 E+02	1,612.90	3.2
AX-103	7.6	416.4	0.0		4.20 E-05	4.20 E-05	17.49	1,670.00	2.86 E+11	124.55	0.00002	3.23 E-04	59.6
AX-104	26.5	0	0.0	1.49 E-01			3,934.51	647.00	1.42 E+13	6,183.87	3.00 E+02	4,838.71	59.6
B-101[f]	427.7	0	0.0	2.16 E-02			9,238.43	13,100.00	1.67 E+13	7,272.58	5.00 E+02	8,064.52	54.5
B-102	68.1	37.85	15.1		4.00 E-05	4.00 E-05	2.12	142.00	7.13 E+09	3.11	5.00 E+01	806.45	1,130
B-103	223.3	0	0.0			6.80 E-05	0.00	52.30	1.00 E+10	4.35	2.00 E+02	3,225.81	8,830
B-104	1,139.3	261.2	3.8	4.07 E-03	4.07 E-03		5,692.83	393.00		0.00	1.00 E+02	1,612.90	2,690
B-105	151.4	1,007	0.0	2.46 E-04	2.46 E-04		285.38	150.00	8.45 E+09	3.68	1.00 E+01	161.29	6,070
B-106	439.1	0	3.8			1.60 E-05	0.06	107.00	2.05 E+09	0.89	1.00 E+00	16.13	6,690
B-107	620.7	0	3.8	5.14 E-03			3190.60	79.60	7.49 E+12	3,261.77	4.00 E+01	645.16	4,160
B-108	355.8	0	0.0				0.00	71.10		0.00	4.00 E+00	64.52	6,030
B-109	480.7	0	0.0			3.34 E-06	0.00	1,660.00	3.58 E+09	1.56	5.00 E-01	8.06	335
B-110	927.3	0	3.8				0.00	485.00		0.00	2.00 E+02	3,225.81	1,240
B-111	893.3	0	3.8	2.81 E-03			2,510.06	2,560.00		0.00	3.00 E+01	483.87	223
B-112	113.6	0	11.4				0.00	189.00		0.00	4.00 E+00	64.52	949
B-201[g]	106.0	0	3.8	9.19 E-02			9,739.56	24.40	1.71 E+13	7,446.77		0.00	4,520

Table A.4. (cont'd)

Tank	Waste Status Summary[a] (KL)			ASA source term and sample data[b]				HDW model (Rev. 3)[c] Pu (g)	WESTREN[d]		TRAC-summary TI-057 03/12/85[e]		HDW Model (Rev. 3)[c] ratio sum
	Sludge	Salt	Liquids	Sludge (g Pu/L)	Salt (g Pu/L)	Liquids (g Pu/L)	Total Pu (g)		Total Pu (Bq)	Pu (g)	Pu (Ci)	Pu (g)	
B-202[g]	102.2	0	0.0	1.01 E-02		1.15 E-06	1,032.17	23.50	9.47 E+11	412.40	2.00 E+02	3,225.81	4,520
B-203[g]	189.3	0	3.8	1.13 E-02			2,138.53	43.50	7.74 E+11	337.06	7.00 E-01	11.29	4,520
B-204[g]	185.5	0	3.8	1.28 E-02			2,373.95	42.70	4.35 E+12	1,894.35	7.00 E+00	112.90	4,520
BX-101	159.0	0	3.8	1.67 E-03			265.16	4,270.00	5.73 E+11	249.53	5.00 E+02	8,064.52	53.2
BX-102	363.4	0	0.0			1.89 E-06	0.00	591.00		0.00	3.00 E+01	483.87	541
BX-103	234.7	0	22.7			1.49 E-04	3.38	960.00	2.61 E+11	113.66	2.00 E-04	0.00	239
BX-104	363.4	0	11.4	1.23 E-02		3.44 E-04	4,473.23	254.00	7.88 E+12	3,431.61	6.00 E+01	967.74	9,440
BX-105	162.8	11.36	18.9	2.83 E-03	3.04 E-04	3.04 E-04	469.80	37.80	1.04 E+12	452.90	1.00 E-03	0.02	9,440
BX-106	143.8	0	0.0			1.22 E-04	0.00	328.00	2.71 E+08	0.12	1.00 E-03	0.02	879
BX-107	1,302.0	0	3.8	3.22 E-03		8.10 E-05	4,192.88	281.00	5.34 E+09	2.33	5.00 E+01	806.45	2,320
BX-108	98.4	0	0.0				0.00	23.80		0.00	5.00 E+00	80.65	2,000
BX-109	730.5	0	0.0			6.70 E-05	0.00	88.10	2.72 E+08	0.12	6.00 E+01	967.74	10,000
BX-110	772.1	0	11.4	1.06 E-03		2.26 E-06	818.49	619.00	1.12 E+07	0.00	2.00 E+01	322.58	1,070
BX-111	196.8	412.6	3.8			1.86 E-04	0.70	2,000.00	2.28 E+08	0.10	2.00 E+00	32.26	852
BX-112	620.7	0	3.8			2.16 E-04	0.82	209.00	2.09 E+10	9.10	1.00 E+01	161.29	1,940
BY-101	412.6	1,052	0.0				0.00	3,840.00		0.00	4.00 E-02	0.65	878
BY-102	0.0	1,048	0.0				0.00	3,440.00		0.00	4.00 E-03	0.06	849
BY-103[f]	18.9	1,495	0.0				0.00	5,320.00		0.00	9.00 E+02	14,516.13	679
BY-104	151.4	1,385	0.0		1.97 E-03		2,729.06	1,940.00	6.28 E+12	2,734.84	2.00 E+02	3,225.81	1,200
BY-105	166.5	1,737	0.0		2.90 E-05	2.90 E-05	50.38	3,700.00		0.00	9.00 E+01	1,451.61	1,040
BY-106	359.6	2,070	0.0	1.93 E-05	1.93 E-05		46.85	5,950.00		0.00	3.00 E+01	483.87	918
BY-107	227.1	779.7	0.0				0.00	1,670.00		0.00	3.00 E+01	483.87	1,110
BY-108	582.9	280.1	0.0				0.00	710.00		0.00	3.00 E+01	483.87	1,920
BY-109	314.2	1,287	0.0				0.00	4,240.00		0.00	8.00 E-05	0.00	853

Table A.4. (cont'd)

Tank	Waste Status Summary[a] (KL)			ASA source term and sample data[b]				HDW model (Rev. 3)[c] Pu (g)	WESTREN[d]		TRAC-summary TI-057 03/12/85[c]		HDW Model (Rev. 3)[c] ratio sum
	Sludge	Salt	Liquids	Sludge (g Pu/L)	Salt (g Pu/L)	Liquids (g Pu/L)	Total Pu (g)		Total Pu (Bq)	Pu (g)	Pu (Ci)	Pu (g)	
BY-110	389.9	1,117	0.0				0.00	2,340.00		0.00	5.00 E+01	806.45	1,150
BY-111	79.5	1,658	0.0				0.00	4,740.00		0.00	2.00 E-01	3.23	849
BY-112	18.9	1,083	0.0				0.00	3,090.00		0.00	1.00 E-04	0.00	852
C-101	333.1	0	0.0				0.00	4,470.00		0.00	1.00 E+02	1,612.90	63.9
C-102[f]	1,601.1	0	0.0	2.76 E-02		9.40 E-05	44,189.12	40,700.00	2.44 E+09	1.06	2.00 E+03	32,258.06	27.1
C-103[f]	234.7	0	503.4	1.54 E-03		1.54 E-03	1,135.13	17,000.00	4.47 E+11	194.66	3.00 E+02	4,838.71	9.79
C-104[f]	1,116.6	0	0.0	5.40 E-02		1.33 E-03	60,295.05	25,500.00	4.38 E+14	190,741.94	7.00 E+02	11,290.32	38.5
C-105[f]	492.1	0	18.9	7.40 E-02		1.32 E-02	36,662.25	6,990.00	9.50 E+13	41,370.97	2.00 E+03	32,258.06	49
C-106[f]	745.6	0	121.1	1.32 E-01		1.58 E-02	100,333.99	76,100.00	1.08 E+14	47,032.26	3.00 E+02	4,838.71	12.6
C-107[f]	1,040.9	0	0.0	3.44 E-02		7.45 E-03	35,806.10	9,220.00	2.20 E+12	958.06	3.00 E+02	4,838.71	69.1
C-108	249.8	0	0.0				0.00	20.60		0.00	9.00 E+01	1,451.61	11,100
C-109	234.7	0	15.1				0.00	4.80		0.00	1.00 E+00	16.13	47,100
C-110	669.9	0	3.8	3.94 E-03		2.47 E-03	2,648.91	90.30	3.08 E+10	13.41	1.00 E+02	1,612.90	4270
C-111	215.7	0	0.0				0.00	846.00		0.00	7.00 E+01	1,129.03	144
C-112	393.6	0	0.0	5.00 E-03		1.40 E-05	1,968.20	1,030.00	3.48 E+08	0.15	6.00 E+01	967.74	299
C-201	7.6	0	0.0	6.40 E-02			484.48	0.41	1.62 E+12	705.48	2.00 E-02	0.32	30,300
C-202	3.8	0	0.0				0.00	0.00		0.00	6.00 E-02	0.97	NA
C-203	18.9	0	0.0				0.00	1.64		0.00	6.00 E-03	0.10	14,600
C-204	11.4	0	0.0			1.35 E-06	0.00	0.82	4.43 E+08	0.19	2.00 E-05	0.00	19,900
S-101	923.5	647.2	45.4	6.80 E-04			628.01	6,510.00		0.00	2.00 E+02	3,225.81	208
S-102	15.1	2,063	0.0	1.31 E-03	1.01 E-03	1.01 E-03	2,103.29	2,090.00	7.01 E+07	0.03	2.00 E+01	322.58	3,900
S-103	37.9	836.5	64.3		1.70 E-03	1.70 E-03	1,529.61	1,350.00	2.00 E+12	870.97	2.00 E+00	32.26	3,900
S-104	1,109.0	0	3.8	1.08 E-02			11,977.25	5,450.00	2.52 E+13	10,974.19	2.00 E+02	3,225.81	319
S-105	7.6	1,718	0.0		3.42 E-06	3.42 E-06	5.88	1,550.00		0.00	1.00 E+01	161.29	3,900

Table A.4. (cont'd)

Tank	Waste Status Summary[a] (KL)			ASA source term and sample data[b]				HDW model (Rev. 3)[c] Pu (g)	WESTREN[d]		TRAC-summary TI-057 03/12/85[e]		HDW Model (Rev. 3)[c] ratio sum
	Sludge	Salt	Liquids	Sludge (g Pu/L)	Salt (g Pu/L)	Liquids (g Pu/L)	Total Pu (g)		Total Pu (Bq)	Pu (g)	Pu (Ci)	Pu (g)	
S-106	106.0	1,692	15.1	4.96 E-02	5.75 E-06	5.75 E-06	5,266.42	7,080.00	1.89 E+13	8,230.65	1.00 E+00	16.13	26.1
S-107	1,109.0	261.2	53.0	7.10 E-02	2.80 E-05	2.80 E-05	78,748.15	29,200.00	1.81 E+14	78,822.58	1.00 E+03	16,129.03	34.4
S-108	15.1	2,271	0.0	1.76 E-03	8.75 E-07	8.75 E-07	28.63	2,170.00	3.98 E+11	173.32	3.00 E+01	483.87	3,900
S-109	49.2	2,101	0.0	9.54 E-04	1.10 E-05	1.10 E-05	70.05	4,240.00	3.52 E+12	1,532.90	3.00 E+00	48.39	26.1
S-110	495.8	980.3	0.0				0.00	5,220.00	8.26 E+10	35.97	9.00 E+01	1,451.61	114
S-111	526.1	1,692	37.9	2.78 E-04	1.10 E-05	1.10 E-05	165.29	4,400.00	1.50 E+11	65.32	9.00 E+00	145.16	156
S-112	18.9	1,961	0.0		2.83 E-06	2.83 E-06	5.55	2,780.00	7.62 E+10	33.18	1.00 E+00	16.13	50.4
SX-101	423.9	1,298	3.8	1.36 E-04	1.36 E-04	4.63 E-06	234.82	1,910.00	6.09 E+14	265,209.68	2.00 E+02	3,225.81	1,130
SX-102	442.8	1,612	0.0	3.37 E-03	2.64 E-03	2.64 E-03	5,753.99	3,210.00		0.00	2.00 E+01	322.58	3,900
SX-103[f]	435.3	2,029	3.8	1.12 E-02	1.17 E-02	1.17 E-02	28,696.51	4,160.00	2.12 E+12	923.23	2.00 E+00	32.26	855
SX-104	514.8	1,809	0.0		7.80 E-04	7.80 E-04	1,411.20	3,270.00	5.59 E+09	2.43	2.00 E+02	3,225.81	1,240
SX-105	276.3	2,309	0.0	1.26 E-04	5.14 E-06	5.14 E-06	46.68	4,050.00	2.38 E+07	0.01	2.00 E+01	322.58	1,280
SX-106	45.4	1,760	230.9	5.00 E-03	5.66 E-04	5.66 E-04	1,353.96	2,730.00		0.00	3.00 E-04	0.00	822
SX-107	393.6	0	0.0				0.00	2,650.00	3.39 E+08	0.15	3.00 E+02	4,838.71	2,530
SX-108	329.3	0	0.0				0.00	1,040.00		0.00	3.00 E+02	4,838.71	993
SX-109	0.0	946.3	0.0				0.00	1,810.00		0.00	2.00 E+02	3,225.81	4,730
SX-110	234.7	0	0.0				0.00	335.00		0.00	3.00 E+02	4,838.71	1,840
SX-111	473.1	0	0.0	1.51 E-03		1.35 E-06	714.42	505.00	1.41 E+12	614.03	4.00 E+02	6,451.61	1,950
SX-112	348.2	0	0.0				0.00	302.00		0.00	2.00 E+02	3,225.81	2,160
SX-113	98.4	0	0.0				0.00	2.02		0.00	6.00 E+01	967.74	50,200
SX-114	685.1	0	0.0				0.00	1,300.00		0.00	4.00 E+02	6,451.61	1,150
SX-115	45.4	0	0.0	1.94 E-01			8,802.40	60.90	1.68 E+13	7,316.13	1.00 E+02	1,612.90	1,230
T-101[f]	382.3	0	3.8			4.70 E-05	0.18	11,400.00	1.07 E+09	0.47	5.00 E-05	0.00	9.63
T-102	71.9	0	49.2	1.26 E-03		2.90 E-05	92.04	1,980.00		0.00	1.00 E-06	0.00	24.3

Table A.4. (cont'd)

Tank	Waste Status Summary[a] (KL)			ASA source term and sample data[b]				HDW model (Rev. 3)[c] Pu (g)	WESTREN[d]		TRAC-summary TI-057 03/12/85[e]		HDW Model (Rev. 3)[c] ratio sum
	Sludge	Salt	Liquids	Sludge (g Pu/L)	Salt (g Pu/L)	Liquids (g Pu/L)	Total Pu (g)		Total Pu (Bq)	Pu (g)	Pu (Ci)	Pu (g)	
T-103	87.1	0	15.1			1.40 E-05	0.21	1,980.00		0.00	1.00 E-01	1.61	22.3
T-104[f]	1,673.0	0	11.4	7.40 E-03		1.52 E-04	12,381.70	442.00	2.19 E+13	9,537.10	1.00 E+02	1,612.90	1,820
T-105	370.9	0	0.0	4.30 E-03		2.20 E-03	1,595.00	102.00		0.00	2.00 E+02	3,225.81	2,310
T-106	71.9	0	7.6	8.20 E-03		1.79 E-04	591.06	1,780.00	1.58 E+12	688.06	2.00 E+01	322.58	28.7
T-107	647.2	0	34.1	4.20 E-03		5.31 E-03	2,899.37	82.60	1.51 E+10	6.58	5.00 E+01	806.45	4,270
T-108	166.5	0	0.0			1.22 E-04	0.00	35.00		0.00	5.00 E+00	80.65	4,810
T-109	219.5	0	0.0			5.40 E-05	0.00	62.60		0.00	5.00 E-01	8.06	5,030
T-110	1,423.2	0	11.4			3.77 E-06	0.04	324.00		0.00	2.00 E+02	3,225.81	2,870
T-111	1688.1	0	0.0	3.94 E-03		1.35 E-06	6,651.15	370.00		0.00	1.00 E+02	1,612.90	2,920
T-112	227.1	0	26.5			3.00 E-05	0.79	44.60	1.81 E+09	0.79	2.00 E+02	3,225.81	2,710
T-201	106.0	0	3.8				0.00	24.40		0.00		0.00	4,520
T-202	79.5	0	0.0				0.00	18.30		0.00	3.00 E-01	4.84	4,520
T-203	132.5	0	0.0				0.00	30.50		0.00	3.00 E+00	48.39	4,520
T-204	143.8	0	0.0	1.51 E-03		1.52 E-03	217.18	33.10	4.54 E+10	19.77		0.00	4,520
TX-101	317.9	0	11.4			3.22 E-03	36.54	5,010.00		0.00	3.00 E-05	0.00	61.4
TX-102	0.0	821.3	0.0				0.00	879.00		0.00	9.00 E-08	0.00	9,440
TX-103	594.2	0	0.0			2.57 E-04	0.00	371.00	8.08 E+11	351.87	9.00 E-07	0.00	5,030
TX-104	0.0	242.2	3.8		1.39 E-03	1.39 E-03	341.73	199.00	1.94 E+12	844.84	3.00 E-04	0.00	9,440
TX-105	0.0	2,305	0.0		5.66 E-04	5.66 E-04	1,304.67	2,540.00		0.00	4.00 E-04	0.01	9,440
TX-106	0.0	1,715	0.0		2.00 E-05	2.00 E-05	34.29	1,370.00		0.00	3.00 E-08	0.00	4,410
TX-107	0.0	132.5	3.8		3.92 E-03	3.92 E-03	533.46	24.90	1.36 E+13	5,922.58	9.00 E-07	0.00	9,440
TX-108	0.0	507.2	0.0		7.90 E-05	7.90 E-05	40.07	395.00		0.00	6.00 E-01	9.68	15,200
TX-109	0.0	1,453	0.0		1.12 E-03	1.12 E-03	1,633.67	378.00		0.00	2.00 E+02	3225.81	1,820
TX-110	0.0	1,749	0.0		7.80 E-05	7.80 E-05	136.40	1,790.00		0.00	1.00 E+01	161.29	1,500

Table A.4. (cont'd)

Tank	Waste Status Summary[a] (KL)			ASA source term and sample data[b]				HDW model (Rev. 3)[c] Pu (g)	WESTREN[d]		TRAC-summary TI-057 03/12/85[e]		HDW Model (Rev. 3)[c] ratio sum
	Sludge	Salt	Liquids	Sludge (g Pu/L)	Salt (g Pu/L)	Liquids (g Pu/L)	Total Pu (g)		Total Pu (Bq)	Pu (g)	Pu (Ci)	Pu (g)	
TX-111	0.0	1,400	0.0				0.00	1,410.00		0.00	1.00 E+00	16.13	1,180
TX-112	0.0	2,456	0.0				0.00	2,620.00		0.00	6.00 E-02	0.97	5030
TX-113	0.0	2,297	0.0				0.00	1,990.00		0.00	5.00 E+01	806.45	1,180
TX-114	0.0	2,025	0.0				0.00	2,100.00		0.00	5.00 E+00	80.65	4,730
TX-115	0.0	2,422	0.0				0.00	2,410.00		0.00	5.00 E-01	8.06	19,600
TX-116	0.0	2,388	0.0				0.00	958.00		0.00	6.00 E-10	0.00	5,660
TX-117	0.0	2,369	0.0				0.00	1,480.00		0.00	3.00 E-09	0.00	5,470
TX-118[f]	0.0	1,313	0.0	1.60 E-03	3.28 E-03	3.28 E-03	4,306.62	64,300.00	3.22 E+09	1.40	9.00 E+02	14,516.13	4.02
TY-101	446.6	0	0.0	5.05 E-03			2,255.48	163.00	5.15 E+12	2,242.74	2.00 E+02	3,225.81	2,100
TY-102	0.0	242.2	0.0		1.74 E-04		42.06	160.00	2.69 E+16	1.17 E+07	3.00 E+00	48.39	5030
TY-103	613.2	0	0.0	1.54 E-02			9,442.82	253.00	7.10 E+10	30.92	3.00 E+02	4838.71	4190
TY-104	174.1	0	0.0	5.62 E-03		3.60 E-05	978.50	1,140.00	1.80 E+12	783.87	8.00 E+00	129.03	19600
TY-105	874.3	0	0.0	1.78 E-03			1,556.32	66.70	1.20 E+12	522.58	7.00 E+01	1129.03	19600
TY-106	64.3	0	0.0	1.25 E-03			80.11	0.26	7.22 E+10	31.44	8.00 E+00	129.03	237000
U-101	83.3	0	11.4				0.00	9.00		0.00	2.00 E+00	32.26	9440
U-102	162.8	1,185	68.1	7.40 E-03	2.41 E-04	2.41 E-04	1,506.32	1,900.00	2.20 E+12	958.06	1.00 E-05	0.00	9,440
U-103	121.1	1,601	49.2	1.84 E-03	3.10 E-04	3.10 E-04	734.44	2,390.00	2.68 E+10	11.67	4.00 E-09	0.00	9,440
U-104	461.8	0	0.0	2.09 E-04			96.51	408.00	3.41 E+10	14.85	1.00 E-07	0.00	17,100
U-105	121.1	1,321	140.0	2.61 E-03			316.12	2,350.00	6.80 E+12	2,961.29	5.00 E-02	0.81	9,530
U-106	98.4	700.2	56.8		1.00 E-06	1.00 E-06	0.76	1,300.00	2.81 E+09	1.22	2.00 E-07	0.00	9,440
U-107[f]	56.8	1,363	117.3	9.20 E-03	1.00 E-05	1.00 E-05	537.13	14,000.00	1.04 E+12	452.90	7.00 E-05	0.00	26.2
U-108[f]	109.8	1,571	90.8	6.31 E-04	1.19 E-06	1.19 E-06	71.24	11,000.00	9.11 E+11	396.73	1.00 E+01	161.29	10.3
U-109[f]	181.7	1,499	71.9	7.62 E-02	4.25 E-03	4.25 E-03	20,519.81	6,780.00	5.28 E+13	22,993.55	6.00 E-02	0.97	50
U-110	704.0	0	0.0			3.73 E-06	0.00	88.00		0.00	2.00 E+02	3,225.81	4,850

Table A.4. (cont'd)

Tank	Waste Status Summary[a] (KL)			ASA source term and sample data[b]				HDW model (Rev. 3)[c] Pu (g)	WESTREN[d]		TRAC-summary TI-057 03/12/85[e]		HDW Model (Rev. 3)[c] ratio sum
	Sludge	Salt	Liquids	Sludge (g Pu/L)	Salt (g Pu/L)	Liquids (g Pu/L)	Total Pu (g)		Total Pu (Bq)	Pu (g)	Pu (Ci)	Pu (g)	
U-111	98.4	1,147	0.0	2.63 E-04	7.27 E-04	7.27 E-04	859.65	1,120.00	5.94 E+10	25.87	2.00 E+00	32.26	4,020
U-112	170.3	0	15.1				0.00	989.00		0.00	3.00 E-01	4.84	120
U-201	15.1	0	3.8				0.00	644.00		0.00	9.00 E-11	0.00	26.1
U-202	15.1	0	3.8			1.15 E-06	0.00	644.00	4.04 E+08	0.18	1.00 E-10	0.00	26.1
U-203	7.6	0	3.8			1.72 E-06	0.01	325.00		0.00	1.00 E-10	0.00	26.1
U-204	7.6	0	3.8	2.53 E-03			19.15	322.00	2.20 E+10	9.58	3.00 E-11	0.00	26.1
Total inventory in grams							630,181.88	563,041.25		1.25 E+07 w/o TY-102 787791.15		347,629.09	

(a) Waste Tank Summary Report for Month Ending February 29, 1996, WHC-EP-0182-95.
(b) Tank Waste Source Term Inventory Validation, WHC-SD-WM-ER-400.
(c) Hanford Tank Chemical and Radionuclide Inventories: HDW Model Rev. 3, May 1996.
(d) Radionuclide and Chemical Inventories for the Single Shell Tanks, WHC-SD-WM-TI-565, Rev. 1.
(e) Preliminary Estimation of the Waste Inventories in Hanford Tanks Through 1980, SD-WM-TI-057, Rev. O-A.
(f) 22.9 m diameter tanks with greater than 10 kg plutonium.
(g) 6.1 m diameter tanks with greater than 0.754 kg plutonium.

Table A.5. Double-Shell Tank Estimated Plutonium Inventory Comparison

Tank	Waste status volume (KL)[a]			HDW Model (Rev. 3)[b] Pu (g)	Baselined[c] Pu (g)	HDW model (Rev. 3) ratio sum
	Sludge	Salt	Liquid			
AN-101	0	0	4,088	1,310	12.3	NA
AN-102	337	0	3,759	6,810	5,182	NA
AN-103	354[d]	0	68	6720	70	2.71 E+01
AN-104	999	0	3,013	4,700	5,573	NA
AN-105	0	0	4,269	8700	140	NA
AN-106	64	0	1,514	708	344	NA
AN-107	507	0	3,494	4,580	3,077	NA
AP-101	0	0	2,790	463	13.7	NA
AP-102	0	0	4,156	2,620	5.1	NA
AP-103	0	0	95	887	0	NA
AP-104	0	0	3,157	0	8.7	NA
AP-105	0	0	583	4,940	1.6	NA
AP-106	0	0	405	2,280	1.7	NA
AP-107	0	0	95	0	0.3	NA
AP-108	0	0	106	946	0.5	NA
AW-101	318	0	3,948	8,890	3,490	1.09E+04
AW-102	3.8	0	356	3,470	47.7	NA
AW-103[e]	1,374	0	572	18,100	44,791	4.62E+01
AW-104	678	420	3,157	551	5,360	1.22E+03
AW-105[e]	1124	0	288	12,600	22,947	5.44E+01
AW-106[e]	799	322	912	4,310	14,003	2.74E+01
AY-101[e]	314	0	3,229	23,100	24,336	7.40E+00
AY-102	121	0	3,630	9,650	8,702	2.85E+01
AZ-101[e]	132	0	3,365	9,750	19,249	2.30E+01
AZ-102[e]	360	0	3,259	12,500	27,186	1.62E+01
SY-101	2,006[d]	0	71.9	7,470	1,472	NA
SY-102[e]	269	269	1,170	41,200	4,1387	1.35E+01
SY-103	2,169[d]	0	632	3,750	3,670	NA

(a) Waste Tank Summary Report for Month Ending February 29, 1996, WHC-EP-0182-95.
(b) Hanford Tank Chemical and Radionuclide Inventories; HDW Model Rev. 3, May 1996.
(c) Baseline Report WHC-SD-WM-TI-640 as of January 1, 1995, plus updates to April 1996.
(d) Double Shell Slurry.
(e) Tanks with estimated greater then 10 kg plutonium.

The LANL waste model (Agnew 1996) can be used to help identify some criticality-related conditions in the waste tanks. Because, the current model was not designed to address criticality concerns, many neutron absorber concentrations are overestimated and the plutonium content is underestimated in some streams transferred to the tank farms. LANL has agreed to enter appropriate documented feed stream compositions that can be supplied into the existing model in FYs 96 and 97 and issue a revision that would support the needs of criticality evaluations. Finally, not all waste transfer records and all actinide separation processing records have been released from classified storage. Therefore, some of the data cells in the following tables are blank at this time.

Table A.6. Tanks With Enough Fissile Material To Warrant Further Consideration

22.9-m diameter single-shell tanks				
A-101	A-104	A-105	A-106	
B-101				
BY-103				
C-102	C-103, C-104	C-105	C-106	C-107
S-104	S-106	S-107		
SX-103				
T-101	T-104			
TX-118				
U-107	U-108	U-109		
6.1-m diameter single-shell tanks				
B-201	B-202	B-203	B-204	
22.9-m diameter double-shell tanks				
AW-103	AW-105	AW-106		
AY-101				
AZ-101	AZ-102			
SY-102				

A.3.2 PUREX

As discussed earlier, 77.7 percent of the plutonium produced was separated using the PUREX process. The chronology of the separations discussions start with the most recent process, PUREX, and works backwards in time. Three main fuel types and some other miscellaneous fuels were reprocessed at the PUREX facility from 1956 to 1990. These fuel types include aluminum-clad fuel, thorium fuel, and zirconium-clad fuel. The quantities of fuel and aqueous waste streams directed to the tank farms are listed in Table A.7. The following sections present the chemical content of the waste streams for the processing facility. The sections are organized by fuel type.

A.3.2.1 Zirconium-Clad Fuel Reprocessing Wastes

Zirconium-clad fuel was reprocessed at the PUREX facility during a number of campaigns. The dates, quantity of fuel, average exposure of fuel, and plutonium content are listed in the Table A.8. The flowsheet values (Allen 1982), actual waste transfer volumes (from processing records), and sample analyses are given for each stream sent from the PUREX facility to the tank farms, waste fractionation facility, and/or 242 A Evaporator.

Table A.7. Fuel Processed at PUREX and Associated Waste Volumes

Fuel Type	Quantity of Fuel Charged (MT)	Cladding Waste Volume (l)	High Level Waste (CAW) (l)	Canyon Sump Waste (l)	Organic Wash Waste (l)	Acid Cell or Lab Waste (l)
Aluminum Clad	73,701 U	952,539,993				0
Thoria 1966 1970-1971	 188 Th [223 kg ^{233}U] 416 Th [628 kg ^{233}U]	 1,400,000	 859,200	 1,154,000	 3,749,000	 1,060,000
Zirconium Clad 1983-90 1967-72	 3920 U 887 U	 22,298,929	 6,337,605	 10,767,571	 16,675,000	 10,624,840
PRTR, SEFOR, Coproduct, Pu-Al Alloy, & Mixed Oxide						

Table A.8. Zirconium-Clad Fuels Processed at PUREX

Campaigns date	N Reactor fuel reprocessed through dissolvers (MTU)	Fuel exposure (average MWd/MTU)	^{235}U content ave % total uranium	Plutonium content (kg)	Uranium processed through solvent extraction (MTU)
1983-1989 A01 through A06	3920 (30 cold, 3299 enriched to 0.94% and 591 to 1.15%)	1281	0.80 (>0.72% 3130 kg,)	3702	6140
1967-1972	887	1762		1000	
MTU =					

The N Reactor fuel elements consisted of uranium alloy 601 enriched to the appropriate ^{235}U content (natural 0.712 to 1.15 wt%) and clad with zircalloy 2. These fuel elements were irradiated at N Reactor then shipped to PUREX for reprocessing.

The aqueous waste streams from reprocessing this N Reactor fuel through the PUREX and REDOX reprocessing plants were transferred to tank farms, the waste fractionization facility, and the 242 A Evaporator. The nuclear material control records were used to determine quantities of plutonium, uranium, and neptunium discharged from separations facilities to the tank farms, waste fractionization facilities, and evaporators.

3920 MT of zircalloy-clad uranium was reprocessed at PUREX from 1983 to 1989 at near flow-sheet conditions based on processing Mark IV and Mark IA fuel elements at an average preenrichment of 0.988% uranium-235 at N Reactor. Six campaigns were reprocessed at PUREX from 1983 to 1990; 2 fuels grade (greater than 9 wt% ^{240}Pu) and 4 weapons-grade (6 wt% ^{240}Pu) fuel. The fuel elements charged to a dissolver were always blended to maintain a ^{235}U content of less than 1 wt% in any single charge. Cold (unirradiated) uranium and recovered plutonium were recycled within the solvent extraction system as needed to blend for criticality control and to meet product specification requirements during these campaigns. As a result, the quantity of uranium processed through the solvent extraction system was considerably greater than the volume of uranium processed through the head end.

A.3.2.1.1 Zircalloy Decladding Waste

Zircalloy decladding waste quantities and compositions for the 1983-1990 campaigns discharged to AW-103 and AW-105 tanks are listed in Table A.9 per flowsheet, process records, and the HDW model for comparison. Nuclear material control (NMC) process records were used to determine measured quantities of plutonium and uranium transferred to the specific waste tanks. The records are summarized in Appendix E of Serne et al. (1996). The NMC records indicate that 8.64 kg of plutonium and 11,697 kg uranium were transferred to the DSTs in zircalloy decladding waste from PUREX tank TK-E5 from 1983 to 1990. The zircalloy decladding waste consisted of one or two declad batches from each dissolver charge, a batch of spent metathesis solution, and a metathesis rinse batch, along with some tank water flushes and steam jet transfer dilutions. The quantities of plutonium, uranium, the volume of decladding waste transferred, and the associated uranium/plutonium mass ratios are shown by month for campaigns AO1 through AO6 in Appendix E of Serne et al. (1996). Appendix E of Serne et al. (1996) also includes the underground tank receiving the waste and the fuel processed through the PUREX Head End and Solvent Extraction. References for this data are included in Appendix D.

Table A.9. Decladding Waste Sludge Formation in AW-103 and -105 Receiver Tanks

Tank	Time Receiving	Declad Waste Added (L)	Sludge Buildup (L)	Fraction Sludge Formation
AW-103	Oct 1983 - Dec 1988	13,470,000	1,031,400*	0.076
AW-105	June 1984 - Feb 1990	8,590,000	729,550*	0.085
*Difference between starting heel and ending sludge volume for these time periods.				

The PUREX reprocessing plant records were used to determine actual volumes transferred from tank TK-E5 and a jet dilution of 5 vol% was applied to account for the water added to facilitate transfer to the tank farm. The total zirconium processed during the 1980's was calculated to be 284,000 kg based on the processing of 3,299 MTU of Mark IV fuel, 591 MTU Mark IA fuel, and 30 MTU of cold uranium (Mark IV) with cladding. The average amount of zirconium cladding for 0.94 wt% enriched fuel is 70.2 kg/MTU and for spike (enriched to average 1.15 wt%) fuel is 85.4 kg/MTU (PUREX Tech Manual). About 5 wt% (15,240 kg) of the zirconium (Schofield 1991) was processed through the PUREX HA

column with the uranium feed stream and exited the PUREX plant in the NZCAW waste stream from tank TK-F16. The remaining 95 wt% (269,000 kg) exited the PUREX plant from TK-E5 as decladding waste. The total uranium processed through the head end was 3920 MTU including the 30 MTU cold zircalloy 2-jacketed uranium at startup in 1983.

Decladding waste from the PUREX dissolvers was sampled in tanks D2 and E3 before centrifuging or in tank E5 (both 5,000-gal tanks) after centrifuging, nitrite addition, and neutralization. These tanks were agitated and duplicate samples were obtained for plutonium, uranium, and pH analysis. For samples taken from TK-D2 and -E3, solids were allowed to settle and the liquid analyzed for plutonium and uranium. For samples taken from TK-E5 after the waste had been centrifuged and neutralized, only sample solution and acid soluble fines were analyzed with the solution. Some plutonium and/or uranium as fines could have not been accounted for by the sampling procedure of withdrawing the sample or by analyzing potential insoluble fines. On verification that all batches contained less than 500 g plutonium, that the plutonium content was less than 0.013 g/L, and that the pH was greater than 12, the waste was transferred to the tank farm receiver tanks AW-103 or AW-105. Tank transfers were effected by steam jet, which resulted in about a 5 vol% water increase for each transfer. Water flushes were also used after each batch transfer of decladding solution, metathesis rinse of the dissolver, and dissolver rinse.

The total E5 waste volume transferred was 24,516,000 L including the 5 vol% jet dilution or 6254 L/MTU. The total uranium and plutonium determined by NMC sample analysis of each batch transfer were 11,697 kg and 8,638 g, respectively. The average uranium and plutonium concentration in the waste was calculated to be 0.525 g/L of uranium and 0.00039 g/L of plutonium and is listed in the process records column of Table A.10.

Maximum plutonium monthly average concentrations of up to 0.0012 g/L were observed in this decladding waste stream. This is well below the criticality limit concentration of 0.013 g/L plutonium for waste stream transfers to the tank farms.

Zircalloy 2 (Perry 1963) cladding contains O.25 wt% iron, 0.05 wt% nickel, and 1.4 wt% tin. This amounts to an average iron content of 176 g/MTU and nickel content of 35 g/MTU processed through the PUREX dissolvers. Carbon steel shoes on the zircalloy fuel elements (Jacobs 1986) contributed about 130 g/MTU of iron if we assume that half the shoes were charged to the dissolver. Corrosion of the dissolver and dissolver coil during the coating removal process (Jacobs 1986) amounted to about 196 g/MTU of iron, 52 g/MTU of chromium, and 25 g/MTU of nickel.

Table A.10. Plutonium and Associated Insoluble Absorbers in Zirflex Decladding Waste

Waste property	Flowsheet[a]	Hanford- defined waste[b]	Process records[c]	Sludge content projected from process records	Mass ratio per process records (absorber/Pu)
Vol (L/MTU)	4,427	5,376	5,764		
sp gr	1.07	--	1.06		
Settled vol% solids	--	10.5	8.1[d]		
Pu (g/l)	0.0013	0.00176	0.00039	0.0048	
U (g/l)	0.18	0.74	0.525	6.48	1,346
Fe (g/l)	--	2.2	0.087-0.117[e]	1.07-1.44[e]	223-300
La (g/l)	--	--			
Zr (g/l)	16.4	9.1	11.0	136	28,200

(a) G.K. Allen, et al., PFD-P-020-00001, Rev A4, Purex Flowsheet - Processing N Reactor Fuels, September 1985.
(b) S. F. Agnew, LA-UR-94-2657, Hanford Defined Wastes: Chemical and Radionuclide Compositions, September 1995.
(c) Appendix B information, Chemistry Laboratory Reports, Fuel Charging and Characterization Data, and Tank Farm Data.
(d) 103-AW and 105-AW Tank Samples evaluation and Table 5.
(e) Based on iron content of zircalloy cladding and steel clips, and corrosion of the dissolver coils during zircalloy decladding. (Ltr. L.L. Jacobs to K. E. Plummer March 14, 1986 and SAR 003). Iron added as ferric nitrate to AFAN starting in February 1985 (amounted to an additional 174 g/MTU or 0.028 g/l in waste stream).

The quantity and average composition of important criticality-related components of zirconium-clad fuel reprocessing waste streams from 1983 to 1990 are listed in Table A.10. These figures are compared to the flowsheet values, the LANL HDW estimates, and PUREX process records. Based on process records that estimate sludge formation at 8.3 vol% determined by sludge accumulation in tank AW-103, the projected plutonium concentration is two orders of magnitude less than the 2.6-g/L criticality limit. Also, uranium, iron, and zirconium absorbers are projected to be present at much higher concentrations than needed to ensure that the associated plutonium concentrations remain subcritical.

A.3.2.1.2 Neutralized Zirflex Current Acid Waste (NZCAW)

The aqueous NZCAW waste contained more than 99 percent of the nonvolatile fission products, plutonium and uranium losses from the HA column, and associated absorbers. This waste was treated in the PUREX Plant by concentrating in EF-6 and sugar denitrating in tank F15. After sugar denitration, the waste was agitated, sampled, and sent to F-16 for neutralization. Analysis was made for plutonium, uranium, iron, nickel, fluoride, and chromium as well as for pH. Metals were introduced to this stream by several mechanisms. Iron in this stream consists of iron that was added to uranium metal to form a stable fuel alloy in the reactor, ferrous ammonium sulfamate that was added as a reducing agent to the IBX and 2N columns, iron from dissolvers that corroded during the fuel dissolution process, and corrosion of the E-F6, 3WB, and 1UC concentrators, and T-U6 acid vacuum fractionator. Iron impurities in the PUREX uranium product were a negligible <40-ppm iron. Chromium and nickel were introduced by corrosion of the same vessels, as fuel impurities, and as a fission product in the irradiated fuel.

Aluminum was introduced as aluminum nitrate in the dissolution process and as an alloying element in the uranium fuel.

The quantity and average composition of important criticality-related components of neutralized Zirflex current acid waste stream from 1983 to 1990 are listed in Table A.11, which compares the flowsheet values, the LANL HDW estimates, and the process records. The projected plutonium concentration in the sludge formed in the tank farm tanks from this stream is more than two orders of magnitude less than the 2.6-g/L criticality limit and both iron and aluminum are present at much greater concentrations than those needed to ensure subcriticality for the associated plutonium concentrations. This conclusion is supported by process records. The source and quantity of several important absorbers are listed in Table A.12. The majority of this waste stream was received in tanks AZ-101 and -102. The actual volumes of waste transferred to the various receiving tanks are listed in Table A.13.

Table A.11. Neutralized Zirflex Current Acid Waste Transferred from TK-F16 (Based on MTU Irradiated Fuel Plus Cold Uranium Processed Through Solvent Extraction)

Waste property	Flowsheet[a]	Hanford defined waste[b]	Process records[c]	Projected sludge content based on process records	Mass ratio based on process records (insoluble absorber/Pu)
Vol (l/MTU)	885	699	1032		
sp gr	1.25	---	0		
Settled vol% solids	17	3.9	4.4		
Pu (g/L)	0.003	0.0034	0.0028	0.064	
U (g/L)	0.84	9.14	0.67 (1.1)	15.2	239 (289)
Al (g/L)	---	9.18	12.4 (8.3)	23.6	258 (assuming 70% insoluble) (2074)
Cr (g/L)	---	0	0.36	8.2	129
Fe (g/L)	---	6.55	5.57 (3.4)	127	1989 (1214)
Ni (g/L)	---	0	0.17 (0.36)	3.9	61 (95)
Zr (g/L)	---	0	3.8	86.4	1357

(a) (Allen 1995)
(b) (Agnew 1995)
(c) Nuclear Material Control Records, Campaign Reports, Chemistry Laboratory Reports, Fuel Charging and Characterization Data, and Tank Farm Data.

Table A.12. Sources and Quantity of Some Insoluble Absorbers in the NZCAW

Source	Sources and quantity of some insoluble absorbers in NZCAW (g/MTU)			
	Iron	Aluminum	Chromium	Nickel
Uranium alloy (601)[a]	325	750	<65	<100
SX reductant[b]				
IBX	3,535			
2N	493			
Dissolver corrosion[c]	200		53	25
Aluminum addition in dissolver[b]		12,000		
Concentrators corrosion[d]	1,200		318	150
Sodium hydroxide impurity[e]	<1			<1
Total	5,753	12,750	371	175

(a) Standard N Fuels Uranium (Weakly 1979)
(b) G.K. Allen, et al., PFD-P-020-00001, Purex Flowsheet - Processing N Reactor Fuels, 1982.
(c) Letter, L.L.Jacobs to K.E. Plummer N Basin Trip Report, March 1986
(d) Van der Cook, ARH-1649
(e) Kupfer 1996

Table A.13. Sludge Volume Formed in Tanks from NZCAW

Tank	Time period	Zirflex high level waste added (L)	Accumulated solids (L)	Solid volume fraction
AY-101	September 1983	10,688	[a]	----
AY-102	October 1983	252,145	[a]	----
AZ-101	Nov 1983 to April 1986	2,357,827	104,000 (~10" sludge depth 7" to 17")	0.044
AZ-102	May 1984 to Mar 1990	1,971,219	Solids received by this stream are indistinguishable because other waste was received simultaneouly	----
AZ-103	Sept 1985 to Dec 1985	47,384	[a]	----
AW-101	July 1984	47,971	[a]	----
AW-102		32,631	[a]	----
AW-104		182,774	[a]	----

(a) Insufficient solids to allow accurate measurement of solids buildup.

A.3.2.1.3 Canyon Sump and Ammonia Scrubber Bottoms Waste

The canyon sump waste was received in Tank F-18, then sampled, neutralized, and discharged to tank farm tanks. Ammonia scrubber bottoms were transferred through Tank F18 periodically, but the quantity of waste from the scrubber bottoms was a very small fraction of the total waste. This canyon sump and ammonia scrubber waste stream was routed to Tanks AW-101, -102, -104, and -105 during the 1980s. Uranium is the only consistently significant insoluble neutron-absorber present in the canyon sump waste. Flowsheet, HDW model, and process records values for volume, sp. gr., volume percent solids, and plutonium and uranium content are compared in Table A.14 with projected plutonium and uranium sludge content and the uranium-to-plutonium mass ratio of sludge as projected by process records.

Table A.14. PUREX Canyon Sump Waste Plus Ammonia Scrubber Bottoms Accumulated in Tank F-18

Waste property	Flowsheet[a]	Hanford defined waste[b]	Process records[c]	Projected sludge content based upon process records (average)	Mass ratio based on process records (absorber/Pu)
Vol (l/MTU)	545	10,117[d]	1979		
sp gr	1.02	----	0		
Settled vol% solids	--	2	0.07[e]		
Pu (g/l)	0.003	0.000076	0.00081	1.1	
U (g/l)	1.8	0.11	1.59	2318	1963

(a) (Jacobs 1985)
(b) (Agnew 1996)
(c) Appendix D
(d) Includes organic wash and acid fractionator cell waste.
(e) Uranyl trioxide hydrate has a particle density of about 6 (Katz 1986), which gives a bulk density of about 3 and results in a settled sludge volume of about 0.07 vol% of the waste stream assuming uranium is the predominant metal contributor to solids.

A.3.2.1.4 Organic Wash Waste and Acid Fractionator Sump Waste

The organic wash waste and acid fractionator cell sump waste contained very small concentrations of plutonium in large quantities of waste and were not considered a concern. The volumes per MTU average 2716 L/MTU Appendix E of Serne et al (1996) for organic wash waste and 1731 L/MTU Appendix E of Serne et al. (1996) for the acid fractionator cell waste. The amount of plutonium in each stream was very low, averaging 0.000101 g/L and 0.000017 g/L, respectively, and with average uranium-to-plutonium ratios of 4220 and 428. Few solids are associated with organic wash waste or acid fractionator cell sump waste. Some organic wash waste solids may form from the uranium and manganese content, but they would be expected to be only about 0.02 vol%. The chemical composition of the organic wash wastes indicated by the flowsheet and process records are shown in the Table A.15. Only 182 g of plutonium were reported in the acid fractionator waste; 89 g went to AW-101 and 79 g

Table A.15. Organic Wash Waste Transferred from Tanks TK-G8 and TK-R8

Waste property	Flowsheet[a]	Hanford defined waste[b]	Process records average[c]	Mass ratio insoluble absorber/Pu based on process records
Volume (l/MTU)	615	Included with canyon sump and acid fractionator waste	2,716	
sp gr	1.02			
Pu g/L	0.00026		0.000101	
U g/L	0.55		0.426	4220
Na_2CO_3 g/L	12.7			
$NaNO_3$ g/L	2.55			
MnO_2 g/L	0.52			
NaOH g/L	0.40			
$NaNO_2$ g/L	0.76			

(a) (Jacobs 1985)
(b) (Agnew 1996)
(c) (Appendix E of Serne et al. 1996)

went to AW-105. The low uranium-to-plutonium mass ratio (420) for the acid fractionator sump waste is not a criticality concern because of the low quantity of plutonium involved and because the waste stream was distributed to several tanks and mixed with other waste over a number of years.

The uranium content of the organic wash waste (average uranium-to-plutonium mass ratio of 4220) provided sufficient neutron absorption to maintain the waste much below the minimum required subcriticality value of 770. This waste was transferred to Tanks AW-101, AW-102, AW-103, AW-104, and AW-105. Tank AW 104 received 1094 g of plutonium from this stream between July 1986 and March 1990 at an average uranium-to-plutonium mass ratio of 2460. Tank AW-101 received 467 g of plutonium from this stream between July 1984 and March 1986 at a uranium-to-plutonium mass ratio of 3750. Tanks AW-102 received 80 g, AW-105 received 43 g, and AW-103 received 1 g from this stream. This waste transfer data is itemized in Appendix E of Serne et al. 1996..

A.3.2.2 Aluminum Clad Fuel Waste to Tank Farms

Irradiated aluminum clad fuels were processed at PUREX starting in January 1956 after cold runs were completed in the latter part of 1955. These runs continued through 1972 while other fuels were run intermittently. Aluminum cladding was removed from fuel elements in the PUREX dissolver in boiling sodium nitrate solution while adding sodium hydroxide. The resulting solution was removed from the

dissolvers and transferred to the C farm tanks from tank TK-D2. The dissolver was then rinsed with water that was transferred to the same C Farm tank. Typical 03N fuel elements contained about 42 g Al (as cladding and in AlSi bonding layer) per kg of uranium. The iron specification in the aluminum alloy (M-388) used for cladding after 1957 was between 0.45 and 0.77 wt%. An iron content of 0.5 wt% was assumed, which gives 209 g/MTU as a basis for the iron content in Table A.16.

The composition of the aluminum cladding waste as listed in flowsheets, HDW, and process records is compared in Table A.16. The projected plutonium concentration for sludge formed from this waste, assuming 6 vol% solids formation on settling in the tank farm, is 0.03 g/L, which is a factor of about 87 below the criticality limit of 2.6 g/L. Uranium, aluminum, and iron are present as insoluble neutron absorbers in sufficient quantity to ensure that the waste is subcritical. Uranium, by itself, is present at 2.2 times the concentration required to maintain this waste subcritical at the existing fissile content. The tanks receiving the cladding waste, quantities of waste transferred, time period of transfers, and sludge formation volume are listed in Table A.17.

Table A.16. Aluminum Cladding Waste

Component	Flowsheet[a]	Hanford Defined Waste[b]	Process Records[c]	Projected sludge concentration	Projected Ratio Based on Process Records (Insoluble Absorber/ Pu Ratio)	Projected Mass Ratio Sum Based on Process Records (Insoluble Absorber/ Pu Ratio Sum)
Volume (L/MTU)	785	1442	1292			
Sp Gr	1.27	1.15	1.19			
Settled vol% solids		8.1	6			
Pu (g/L)		0.00153	0.0017	0.03		
U (g/L)		2.78	2.9	58	1,706	2.2
Al (g/L)	57.5	23.0	32.4			
Fe (g/L)			0.16[d]	2.7	94.1	0.59
Na (g/L)	138.2		86			
Si (g/L)	0.20		0.56			
NO_3 (g/L)	9.1		37.2			
NO_2 (g/L)	78.7		41.4			
OH (g/L)	21.1		17			
Total						> 2.8

(a) (Matheison 1968)
(b) (Agnew 1996)
(c) (Anderson 1990)
(d) (Kupfer 1996) Aluminum alloy iron content 209 g/MTU

Table A.17. Sludge Formation in Receiving Tanks from Aluminum Cladding Removal Waste

Tank	Time period	Aluminum cladding waste added (liters)	Accumulated solids (liters)	Solid volume fraction
C-104	1956			
C-105	1957			
C-106	1958			
C-101	1960			
C-102	1960 to 1965			
C-111	1957 to 1960			
C-112	1960 to 1961			
C-102	1965 to 1969			
C-107	1961 to 1962			
C-108	1961			
C-104	1970 to 1972	3816	108	2.5

A.3.2.2.1 Neutralized Current Acid Waste (NCAW) for Aluminum Clad Fuel Processing

The aqueous NCAW waste from processing aluminum-clad fuel contained more than 99 percent of the nonvolatile fission products, plutonium and uranium losses from the HA column, and associated absorbers. This waste coming from the concentrator was originally neutralized and transferred to the A Tank Farm. In the early 1960s denitration was conducted with sugar, which reduced the amount of caustic that had to be added and the amount of waste that would have to be transferred. The sugar was destroyed in the process. After sugar denitration, the waste was agitated, sampled, and sent to Tank TK-F16 for neutralization. Analysis was made for plutonium and uranium, as well as for pH. Insoluble neutron absorbers were introduced to this stream by several mechanisms. Iron in this stream results from iron added to uranium metal to form a stable fuel alloy in the reactor, the addition of ferrous ammonium sulfamate as a reducing agent to the IBX, 2D, and 3A columns, and corrosion of the E-F6, 3WB, and 1UC concentrators and T-U6 acid vacuum fractionator. Iron impurities in the PUREX uranium product were negligible (<40 ppm). Chromium and nickel were introduced by corrosion of the same vessels, as fuel impurities, and as a fission products in the irradiated fuel. Aluminum was introduced as an impurity in the uranium fuel. The sources and quantities of some insoluble neutron absorbers in this waste stream are listed in Table A.18.

Table A.18. Sources and Quantity of Some Insoluble Absorbers in the NCAW

Source	Sources and Quantity of Some Insoluble Absorbers in NCAW (g/MTU)			
	Iron	Aluminum	Chromium	Nickel
Uranium Alloy (501)[a]	125	<150	<65	<100
SX Reductant[b]				
IBX	1041			
2DF	868			
3AS	729			
Dissolver Corrosion[c]	-0-		-0-	-0-
Concentrators Corrosion[d]	1200		318	150
Total	3963	<150	318	150

(a) Standard N Fuels Uranium (Weakly 1979)
(b) Matheison, W. E., G. A. Nicholson, Purex Chemical Flowesheet - Processing of Aluminum-Clad Fuels, ARH-214 Del, Feb. 15, 1968.
(c) Letter, L.L.Jacobs to K.E. Plummer N Basin Trip Report, March 1986
(d) Van der Cook, ARH-1649

The quantity and average composition of important criticality-related components of the neutralized current acid waste stream from 1956 to 1967 are listed in Table A.19, which compares the flowsheet values, the LANL HDW estimates, and the process records. The projected plutonium concentration in the sludge formed in the tanks from this stream is more than two orders of magnitude less than the 2.6-g/L criticality limit Both iron and aluminum are present at much higher concentrations than needed to ensure subcriticality for the associated plutonium concentrations. This conclusion is supported by process records. The majority of this waste stream was received in A Farm tanks.

Beginning in 1967, instead of being neutralized and going directly to the tank farm, this stream was sent to B Plant for strontium and cesium removal. Because the process records are being declassified and have not yet been evaluated, the values are not included in Table A.18 at this time. It appears that the plutonium content should be near 0.002 g/L and this stream contains a high concentration of iron from the use of ferrous sulfamate reductant in the PUREX process and from corrosion of concentrators. If the sludge formed from this stream was 4 vol%, a resulting plutonium concentration of about 0.05 g/L would result. This is a factor of about 52 less than the criticality limit. Sufficient iron is present to provide an insoluble absorber-to-plutonium mass ratio of about 12,000, which results in a mass ratio sum of about 75. Sludge formed in the A Farm tanks from this stream is subcritical by a large margin.

Table A.19. Neutralized Current Acid Waste from Aluminum Clad Fuel Processing

Component	Flowsheet[a]	Hanford Defined Waste[b]	Process Records[c] 1956-1967 (Anderson)	Mass Ratio Based on Process Records (Absorber/Pu)
Volume (L/MTU)	156	1573	177	
Sp Gr	1.14	----		
Settled vol% solids		3.9		
Pu g/l	0.0018	0.0014		
U g/l	0.067	2.55		
Al g/l		0	4.1	
Cr g/l		0.42	1.8	
Fe g/l	21.0	6.55	22.3	12,000
Na g/l	37.1	32.0	32.2	
PO_4 g/l	1.43	0	1.9	
SO_4 g	82	15.2	86.4	

(a) (Matheison 1968)
(b) (Agnew 1996)
(c) (Anderson 1990)

A.3.2.2.2 Organic Wash Waste from Processing Aluminum-Clad Fuel

The organic wash waste from the Number 1 organic wash cycle (TK-G8) and Number 2 organic wash cycle (TK-R8) were transferred to the A Farm tanks with the boiling waste until 1969. After 1969 the organic wash waste was transferred to low-level waste in C Farm tanks. The organic wash waste contained very small quantities of plutonium in large quantities of waste. The amount of plutonium expected in this stream is very low, 0.0001 g/L. The process record uranium value given by Anderson (1990) of 0.036 g/L results in a uranium-to-plutonium ratio of about 360. Few solids are associated with organic wash waste. Some organic wash waste solids may form from the uranium and manganese content, but they would be expected to be only about 0.02 vol%. The chemical composition of the organic wash wastes, as indicated by Anderson (1990), is 0.04 M $NaNO_3$, 0.13 M Na_2CO_3, and 0.004M MnO_2. The low uranium-to-plutonium mass ratio (360) for the organic waste is not a criticality concern because of the low quantity of plutonium involved and because the waste stream was transferred intermittently with other waste streams to several tanks and mixed with other waste over a number of years.

A.3.2.2.3 Acid Fractionator Sump Waste

Acid fractionator sump waste was transferred to a crib during processing of aluminum-clad fuels. Therefore, none of this waste should have entered the Hanford Site tanks and it need not be considered further.

A.3.3 Thorium Fuel Waste to Tank Farms

Thorium was processed through the PUREX plant during two time periods. The quantities of thorium and ^{233}U processed during each period are listed in Table A.7. Uranium-233 discharges to the tank farms during thorium fuel processing were from coating waste, high-level waste, canyon sump waste, organic wash waste streams, and plant flush waste. This waste was sent to Tank C-102 as the first tank in a cascading series of tanks during the 1966 campaign and to Tank C-104 as the first tank in a cascading series during the 1970-1971 campaign (Hess 1991).

The thorium fuel, received as powder and wafers, was packaged in aluminum cans. The aluminum cans were dissolved in sodium nitrate and sodium hydroxide solution and slurried from the dissolver carrying some thorium and uranium with them. This stream was centrifuged to remove entrained solids and the recovered solids were dissolved and added to the plant feed. The waste solution and slurry passing through the centrifuge was neutralized and transferred to C Farm (C-102 in 1966 and C-104 in 1970-1971). The composition of this stream is listed in Table A.20 by flowsheet and process records for comparison. If the assumption is made that this stream contains about 5 vol% solids, it would form a sludge that contains 0.052 g/L ^{233}U, which is a factor of about 50 less that the criticality limit. Sufficient aluminum neutron absorber seems to be present to maintain this waste in a subcritical condition for the projected uranium concentration.

The neutralized thorium high-level waste (1WW) was accumulated in tank TK-F18 and transferred to C farm (tanks C-102 in 1966 and C-104 in 1970-1971). This waste came from the HA column, was concentrated in the EF-6 concentrator, sugar denitrated, neutralized in TK-F18, and then transferred to C Farm. The composition of this stream is compared by flowsheet and record values in Table A.21. The projected ^{233}U concentration for sludge formed from this waste, assuming 4 vol% solids formation on settling in the farm tank, is 0.125 g/L, which is a factor of about 21 below the criticality limit of 2.6 g/L. Thorium, aluminum, and iron are present as insoluble neutron absorbers in sufficient quantities to ensure that the waste is subcritical. Thorium by itself is present at 3.5 times the concentration required to maintain this waste subcritical at the existing fissile content of this stream.

Table A.20. Thorium-Aluminum Coating Waste from TK-E5

Waste property	Flowsheet[a]	Hanford defined waste[b]	Process records[c]	Sludge content based upon process records (average)	Insoluble absorber to plutonium mass ratio based on process records (absorber/Pu)
vol (L/MTTh)	2760	Not Specified	3703		
sp gr	1.14				
settled vol% solids			(5)		
^{233}U (g/L) [total mass]	---		0.0026 [3.7kg]	0.052	
Th (g/L) [total mass]	0.32		0.26 [363 kg]	5.2	100
Al (g/L)	21.1		17.7		

(a) Smith 1970
(b) Agnew 1996
(c) ARH-2127 PD PUREX Process Operation and Performance 1970 Thoria Campaign

Table A.21. Thorium - Neutralized 1WW Waste from TK-F18

Waste property	Flowsheet[a]	Hanford defined waste[b]	Process records[c]	Sludge content based upon process records (average)	Mass ratio based on process records (absorber/Pu)
vol (L/MTTh)	2027	Not Specified	2273		
sp gr	1.13				
settled vol% solids			4[d] 90.9 L		
^{233}U (g/L) [total mass]	0.0021		0.005 [4.3kg]	0.125	
Th (g/L) [total mass]	1.93		4.23 [3632 kg]	106	845
Al (g/L)	9.18				
Fe (g/L)	1.4				

(a) Smith 1970
(b) Agnew 1996
(c) ARH-2127 PD PUREX Process Operation and Performance 1970 Thoria Campaign
(d) Assumed value, not supported by tank farm sludge formation measurements related to waste volume transfers.

The thorium organic wash waste was accumulated in Tanks TK-G8 and TK-R8, neutralized, and transferred to the C Farm receiver tanks. The composition of this stream as listed in flowsheets and process records is compared in Table A.22. The projected ^{233}U concentration for sludge formed from this waste, assuming 0.5 vol% solids formation on settling in the farm tank, is 0.3 g/L. This is a factor of about 9 below the criticality limit of 2.6 g/L. Thorium and manganese are present as insoluble neutron absorbers in sufficient quantity to ensure that the waste is subcritical.

Table A.22. Thorium - Organic Wash Waste from TK-G8 and TK-R8

Waste property	Flowsheet[a]	Hanford defined waste[b]	Process records[c]	Sludge content based upon process records (average)	Mass ratio based on process records (absorber/Pu)
vol (L/MTTh)	4250	Not Specified	9813		
sp gr	1.01				
settled vol% solids			(0.5)		
^{233}U (g/L) [total mass]			0.0015 [5.4 kg]	0.30	
Th (g/L) [total mass]			0.34 [1271 kg]	68	228
$NaNO_3$ (g/L)	13.1				
Mn (g/L)	0.65				

(a) Smith 1970
(b) Agnew 1996
(c) ARH-2127 PD PUREX Process Operation and Performance 1970 Thoria Campaign

Canyon sump waste was collected in Tank TK-F18, neutralized, and transferred to C farm tanks during the thorium campaigns. The waste uranium and thorium compositions of this stream are listed in Table A.23. The projected ^{233}U concentration for sludge formed from this waste, assuming 0.2 vol% solids formation on settling in the farm tank, is about 3.1 g/L. This is just above the criticality limit of 2.6 g/L. Thorium is present on the average of 1.3 times the amount required to maintain the sludge formed from this stream in a subcritical condition. The quantity of sludge formed from this stream is small and, if distributed evenly over the tank sludge in a C farm tank, would amount to a sludge thickness of less than 1 cm. This waste was transferred between other waste transfers to the same C farm tank and would result in a mixed sludge with the cladding, 1WW, and organic wash waste. This stream does not present a criticality safety issue.

Table A.23. Thorium - Canyon Sump Waste from Tank TK-F18

Waste property	Flowsheet[a]	Hanford defined waste[b]	Process records[c]	Projected sludge content based upon process records (average)	Mass ratio based on insoluble absorber per process records (absorber/Pu)
vol (L/MTTh)	-----	Not Specified	3054		
sp gr					
settled vol% solids			(0.2)		
^{233}U (g/L) [total mass]			0.0062 [7.2 kg]	3.1	
Th (g/L) [total mass]			1.97 [2270 kg]	986	318

(a) Smith 1970
(b) Agnew 1996
(c) ARH-2127 PD PUREX Process Operation and Performance 1970 Thoria Campaign

Plant flushes were made before starting the thorium runs and after completing them. These flushes were collected in Tanks TK-F18, TK-E5, TK-G8 and TK-R8, neutralized, and transferred to C Farm tanks. The waste uranium and thorium compositions of these flushes are listed in Table A.24. The projected ^{233}U concentration for sludge formed from this waste, assuming 0.1 vol% solids formation on settling in the farm tank, is about 3.6 g/L. This is above the criticality limit of 2.6 g/L. Thorium is present on the average of 0.96 times the amount required to maintain the sludge formed from this stream in a subcritical condition. The quantity of sludge formed from this stream is small and, if distributed evenly over the tank sludge in a C farm tank, would amount to a sludge thickness of less than 1 cm. This waste does not present a criticality safety issue in the tank farm.

Table A.24. Thorium - Flush and Lab Waste from PUREX

Waste property	Flowsheet[a]	Hanford defined waste[b]	Process records[c]	Projected sludge content based upon process records (average)	Mass ratio based on process records (absorber/Pu)
vol (L/MTTh)	7610	Not Specified	9142		
sp gr					
vol% solids			(0.1)		
^{233}U (g/L) [total mass]			0.0036 [12.4 kg]	3.6	
Th (g/L) [total mass]			0.84 [2906 kg]	233	234

(a) Smith 1970
(b) Agnew 1996
(c) ARH-2127 PD PUREX Process Operation and Performance 1970 Thoria Campaign

A.3.4 REDOX

The REDOX process was the first continuous solvent extraction process used at the Hanford Site. It was developed at the Argonne National Laboratory. The REDOX process operated between 1952 and 1966 in the 202-S Building. Waste from the REDOX process was added to tank farm tanks as coating waste, high-level waste, and sump waste.

The REDOX process was a continuous counter-current column extraction process. The uranium and plutonium were separated from fission products and held in aqueous solution by manipulating the plutonium valence so that the two actinides could be preferentially extracted with hexone (methyl isobutyl ketone) and then separated from one another.

The design production or feed rate of the REDOX Plant was 3.1 tons of irradiated uranium reactor fuel per day. The product of the REDOX Plant was a liquid plutonium nitrate solution. The process was designed so that the high-level waste stream from REDOX would contain at least 10,000 ppm iron, with reference to plutonium.

Two types of waste were sent to underground tank storage: coating waste and REDOX high-level waste. The major components of the waste exiting the REDOX process were chromium, zirconium, iron, silicon, aluminum, sodium, and nitrate compounds.

Aqueous waste streams were directly transferred to underground tanks if analytical results were within the established limits for discharge. Initially, all of the liquid waste from the REDOX Plant was transferred to the S Tank Farm.

Based on two uranium and two plutonium purification cycles, detailed flowsheet data and process data, REDOX wastes transferred to tank farms are given in Table A.25.

The REDOX aluminum-cladding waste is low in plutonium to give a projected sludge concentration of 0.04 g/L, assuming 6 vol% sludge formation on settling. It also has a uranium-to-plutonium mass ratio of 1284 and an aluminum mass ratio many times above the minimum required for neutron absorption to ensure subcriticality. The REDOX high-level waste is low in plutonium to give a projected sludge concentration of 0.005 g/L, assuming 4 vol% sludge formation on settling. It has a uranium-to-plutonium mass ratio of 1900, an iron-to-plutonium mass ratio of 893 and a chromium-to-plutonium mass ratio of 57,700. These add up to many times the minimum mass ratio sum required to ensure subcriticality in this waste stream.

A.3.5 Bismuth Phosphate Process Wastes

The bismuth/phosphate process was the first chemical process used at the Hanford Site to separate plutonium from irradiated reactor fuel elements. The bismuth/phosphate process operated between 1944 and 1956 in the 221-T Building and between 1945 and 1952 in the 221-B Building.

Table A.25. Typical REDOX Waste Compositions

Component	Al cladding		High level	
	Flowsheet[a]	Process records[b]	Flowsheet[a]	Process records[b]
Volume (L/MTU)	750	1,196	3425	2655
Sp Gr	1.21	1.19	1.39	1.29
Pu, g/L	0.001	0.0026	0.0004	0.0001
U, g/L	1.33	3.34	0.15	0.19
$NaAlO_2$, M	1.91	1.2	0.93	1.2
NaOH, M	0.61	1.0	1.44	0.69
$NaNO_3$, M	0.80	0.6	4.37	4.83
$NaNO_2$, M	1.44	0.9	--	--
Na_2SiO_3, M	0.027	0.02	--	--
$Na_2Cr_2O_7$, M	--	--	0.10	0.066
Na_2SO_4, M	--	--	0.020	0.031
$Cr(OH)_3$, M	--	--	0.003	0.045
$Fe(OH)_3$, M	--	--	0.006	0.016

(a) Crawley, 1960
(b) Anderson, 1990

In this batchwise process, the plutonium valence was manipulated so the plutonium could be coprecipitated with bismuth phosphate, separated from uranium and the bulk of the fission products, and redissolved and reprecipitated several times for purification. Four major waste streams were sent to underground tanks from the bismuth phosphate process.

- Coating waste containing <0.1% of the plutonium
- Metal waste (MW) from extraction containing the greatest majority of the uranium, about 90 percent of the original fission product activity and 0.5 to 1.0 percent of the plutonium
- First decontamination cycle waste containing about 10 percent of the original fission product activity and 2 percent of the plutonium
- Second decontamination cycle waste containing less than 0.1 percent of the original fission product activity and about 1 percent of the plutonium.

The coating waste and the first decontamination cycle waste were combined initially but later kept separate for disposal.

The major cation components of the waste from the bismuth/phosphate process were uranium, silicon, chromium, iron, zirconium, bismuth, cerium, sodium, and aluminum. The major anion in most cases was nitrate, with lower concentrations of phosphate compounds. Typical compositions of the waste, as calculated from process flowsheets, are given in Table A.26.

Table A.26. Typical Bismuth Phosphate Waste Composition

Component	Coating waste	Metal waste	First cycle waste	Second cycle waste
Gallons/MTU	377[a,b]	3,800	2,756[b]	2,400
Specific Gravity	1.18			
Pu, g/l	1.7 E-04	1.7 E-04	4.8 E-04	2.8 E-04
U, g/l	0.70	69.4	~0	~0
NaOH, M	0.39	--	--	--
$NaNO_3$, M	0.83	0.58	0.80	0.67
$NaAlO_2$, M	0.82	--	--	--
Na_2SiO_3,M	0.005	--	--	--
$NaNO_2$, M	0.62	--	--	--
Na_2CO_3, M	--	0.88	--	--
Na_2SO_4, M	--	0.25	--	--
Na_3PO_4, M	--	0.39	0.47	0.45
$Fe_2(SO_4)_3$, M	--	--	0.014	0.013
$(NH_4)_2SiF_6$, M	--	--	0.036	0.030
$(NH_4)_2SO_4$, M	--	--	0.014	0.013
$Cr(NO_3)_3$, M	--	--	0.002	0.002
NH_4NO_3, M	--	--	--	0.027

(a) Includes water and dilute nitric acid rinses.
(b) Coating waste and first cycle wastes mixed for disposal.

A.3.6 Uranium Recovery Waste Stream

Metal waste (waste containing the bulk of the uranium and fission products) from the bismuth phosphate plants were collected in underground storage tanks beginning in 1944. This waste was later removed from the underground tanks and processed through the Uranium Recovery Plant to recover uranium. The Uranium Recovery Plant began operation in 1952.

Uranium recovery waste consisted of combined, neutralized, and concentrated RAW and ROW streams. The composition and volume per metric ton of this waste stream transferred to the tank farms is listed in the Table A.27. In November 1954, scavenging of the uranium recovery waste with ferrocyanide began. It resulted in the disposition of supernatant to the B-C Crib from the Uranium Recovery Plant and transfer of more concentrated waste to the tank farms. The projected plutonium concentration of sludge formed from this waste, based on a 4 vol% sludge formation volume, is less than 0.004 g/L. This is more than two orders of magnitude less than the criticality limit of 2.6 g/L. The uranium and iron content of this waste provide an insoluble neutron absorber mass ratio sum of greater than 60, which results in waste conditions far below subcriticality.

Table A.27. Volume and Composition of Uranium Recovery Waste

Waste property	Uranium recovery waste[a]	Hanford defined waste[b]	Process records
volume (l/MTU)	14,400	27,570	
% solids		2.8	
pH	>9.5	--	
sp gr	1.398	1.148	
Pu (g/L)	0.00014	0.000066	
U (g/L)	0.62	0.95	
Na (g/L)	174	89.9	
Fe (g/L)	1.34	0.11	
Cl (g/L)	0.98	3.64	
NO_3 (g/L)	383	160	
SO_4 (g/L)	33.0	13.6	
PO_4 (g/L)	23.8	12.4	
CO_3 (g/L)	--	11.5	

(a) HW-19140, Uranium Recovery Technical Manual, Chemical Development, November 10, 1951.
(b) S. F. Agnew, LA-UR-94-2657, Hanford Defined Wastes: Chemical and Radionuclide Compositions, September 1995.

A.3.7 Plutonium Finishing Plant Waste

PFP waste was transferred to the 242-T Evaporator Facility receiving tank (TK-R1) beginning in May 1973 because of a criticality concern in the cribs. Until then, PFP waste had been transferred to the cribs. PFP waste transferred to the 242-T Evaporator Facility consisted of high- and low-level salt waste and was transferred from the Z Plant D5 tank. This waste was neutralized in the 242-T Evaporator Facility and then concentrated in the 242-T Evaporator. The evaporator was shut down in 1976. PFP resumed operations in 1978 and its waste was routed to Tank TX-118 until 1981, when the PFP waste was diverted to the DST SY-102.

A.4 Plutonium and Absorber Concentrations in Waste

Fissile and absorber material concentrations in the underground storage tanks have been calculated from actual analysis of only a few samples of tank waste. In general, the fissile materials are in the sludges formed in the underground tanks. These sludges were formed by settling/precipitation in the tanks from the introduced slurries. The fissile content of supernatant is less than 0.0005 g/L for most tanks. Salt cakes formed from evaporation of water from the supernatants also contain very low concentrations of fissile material and do not approach criticality.

The ratios of selected neutron absorbers to plutonium for the sludge fraction of tank contents were calculated for each tank using either predicted contents or actual measurements. The calculations were based on the following two sets of tank concentration and inventory information:

- Historical Tank Content Estimate (HTCE) Model Revision 3 estimates (Agnew et al. 1996)
- Estimates of average tank plutonium and absorber concentrations from sample data for a selected number of tanks based on Tank Characterization Reports (TCR) (Hartley et al. 1996).

The elements analyzed as neutron absorbers were shown in Table A.3 and are listed here again for convenience: Sodium (Na), Aluminum (Al), Iron (Fe), Chromium (Cr), Bismuth(Bi), Lanthanum (La), Zirconium (Zr) as $ZrO(OH)_2$, Nickel (Ni), Manganese (Mn), Calcium (Ca), Nitrate (NO_3), Silicon (Si), and Uranium (U).

The plutonium concentrations, which were given in activity units (pCi/g), had to be converted to mass units (ug/g) to calculate the mass ratios of the individual neutron absorbers to plutonium. The individual element-to-plutonium mass ratios were then divided by the element-specific minimum absorber-to-plutonium ratio needed to ensure subcriticality (Rogers 1996). The minimum subcritical ratios determine the minimum relative concentrations for the absorber materials that, if present individually with the plutonium, would provide subcriticality for any degree of moderation. Therefore, a ratio greater than 1.0 should indicate subcritical conditions. The individual absorber-to-plutonium ratios may be summed to give an overall assessment of the subcriticality conditions of the tank contents.

The subcriticality conditions in the tank can be further refined by summing the criticality ratios of the soluble and insoluble neutron absorbers separately. The sum of the criticality ratios for the insoluble neutron-absorbing elements demonstrates an added measure of subcriticality because there is added assurance that the insoluble elements will remain in close proximity with the plutonium in the tank sludge under the caustic tank conditions. The insoluble absorbers were: iron, chromium, bismuth, lanthanum, zirconium, nickel, manganese, and uranium.

Aluminum can become soluble under conditions associated with a pH of 14 or higher, so for this analysis, only 70 percent of the aluminum was assumed to be insoluble. Tables A.28 and A.29 give the total ratio sum and the ratio sum for the insoluble absorbers-to-plutonium for the sludge for the single- and double-shell tanks, respectively.

Table A.28. Plutonium Criticality Ratios - Single-Shell Tanks

Tank name	High Pu tanks	Agnew Pu conc (ug/g)	Agnew ratio sum	Agnew insolubles ratio sum	TCR mean Pu conc (ug/g)	TCR ratio sum	TCR insolubles ratio sum
A101	*	4.48	234.00	173.00	NA	NA	NA
A102		35.50	20.80	13.40	NA	NA	NA
A103		118.00	6.19	3.53	NA	NA	NA
A104	*	115.00	6.45	3.76	NA	NA	NA
A105	*	16.90	59.60	47.00	NA	NA	NA
A106	*	64.60	11.40	7.07	NA	NA	NA
AX101		21.90	42.60	32.30	NA	NA	NA
AX102		207.00	3.20	2.15	NA	NA	NA
AX103		16.90	59.60	47.00	NA	NA	NA
AX104		16.90	59.60	47.00	NA	NA	NA
B101	*	18.50	54.50	13.90	NA	NA	NA
B102		0.83	1,130.00	750.00	NA	NA	NA
B103		0.15	8,830.00	2,700.00	NA	NA	NA
B104		0.21	2,690.00	525.00	NA	NA	NA
B105		0.17	6,070.00	394.00	NA	NA	NA
B106		0.15	6,690.00	362.00	NA	NA	NA
B107		0.10	4,160.00	1,010.00	NA	NA	NA
B108		0.14	6,030.00	511.00	NA	NA	NA
B109		2.77	335.00	28.40	NA	NA	NA
B110		0.42	1,240.00	474.00	0.54	2,052.69	235.13
B111		2.42	223.00	135.00	1.58	453.02	80.13
B112		1.15	949.00	112.00	NA	NA	NA
B201		0.16	4,520.00	1,820.00	18.40	64.85	46.25
B202		0.16	4,520.00	1,820.00	NA	NA	NA
B203		0.16	4,520.00	1,820.00	NA	NA	NA
B204		0.16	4,520.00	1,820.00	NA	NA	NA
BX101		14.4	53.2	37.9	NA	NA	NA
BX102		2.05	541.00	125.00	NA	NA	NA
BX103		2.31	239.00	155.00	NA	NA	NA
BX104		0.06	9,440.00	6220.00	NA	NA	NA
BX105		0.06	9,440.00	6220.00	NA	NA	NA
BX106		1.57	879.00	56.90	NA	NA	NA
BX107		0.17	2,320.00	522.00	0.93	960.18	101.70
BX108		0.19	2,000.00	442.00	NA	NA	NA
BX109		0.09	10,000.00	4,280.00	NA	NA	NA
BX110		0.61	1,070.00	121.00	NA	NA	NA
BX111		1.57	852.00	36.70	NA	NA	NA

Table A.28. (cont'd)

Tank name	High Pu tanks	Agnew Pu conc (ug/g)	Agnew ratio sum	Agnew insolubles ratio sum	TCR mean Pu conc (ug/g)	TCR ratio sum	TCR insolubles ratio sum
BX112		0.25	1,940.00	266.00	NA	NA	NA
BY101		1.57	878.00	56.60	NA	NA	NA
BY102		1.64	849.00	31.30	NA	NA	NA
BY103	*	2.12	679.00	25.60	NA	NA	NA
BY104		1.02	1,200.00	152.00	NA	NA	NA
BY105		1.22	1,040.00	93.70	NA	NA	NA
BY106		1.51	918.00	55.10	NA	NA	NA
BY107		1.09	1,110.00	127.00	NA	NA	NA
BY108		0.56	1,920.00	386.00	0.75	2,009.56	397.83
BY109		1.59	853.00	32.30	NA	NA	NA
BY110		1.02	1,150.00	135.00	0.06	381.56	381.56
BY111		1.64	849.00	31.30	NA	NA	NA
BY112		1.70	852.00	32.90	NA	NA	NA
C101		9.22	63.90	29.80	NA	NA	NA
C102	*	16.70	27.10	13.80	NA	NA	NA
C103	*	51.30	9.79	4.80	NA	NA	NA
C104	*	15.60	38.50	24.50	NA	NA	NA
C105	*	8.59	49.00	19.60	NA	NA	NA
C106	*	66.40	12.60	8.07	NA	NA	NA
C107	*	6.38	69.10	23.90	NA	NA	NA
C108		0.06	11,100.00	4,770.00	NA	NA	NA
C109		0.01	47,100.00	33,600.00	5.55	161.41	83.51
C110		0.10	4,270.00	1,010.00	1.31	590.80	91.40
C111		2.86	144.00	48.30	NA	NA	NA
C112		1.78	299.00	185.00	0.98	2,514.46	1,955.79
C201		0.03	30,300.00	25,900.00	NA	NA	NA
C202		0.00	NA	NA	NA	NA	NA
C203		0.05	14,600.00	11,100.00	NA	NA	NA
C204		0.04	19,900.00	16,100.00	NA	NA	NA
S101		4.48	208.00	102.00	NA	NA	NA
S102		0.18	3,900.00	3,110.00	NA	NA	NA
S103		0.18	3,900.00	3,110.00	NA	NA	NA
S104	*	3.17	319.00	84.40	4.59	256.85	72.76
S105		0.18	3,900.00	3,110.00	NA	NA	NA
S106	*	23.50	26.10	8.38	NA	NA	NA
S107	*	18.30	34.40	17.10	0.00	NA	NA
S108		0.18	3,900.00	3,110.00	NA	NA	NA
S109		23.50	26.10	8.38	NA	NA	NA

Table A.28. (cont'd)

Tank name	High Pu tanks	Agnew Pu conc (ug/g)	Agnew ratio sum	Agnew insolubles ratio sum	TCR mean Pu conc (ug/g)	TCR ratio sum	TCR insolubles ratio sum
S110		5.85	114.00	78.90	NA	NA	NA
S111		4.33	156.00	112.00	NA	NA	NA
S112		12.80	50.40	27.70	NA	NA	NA
SX101		0.89	1,130.00	360.00	NA	NA	NA
SX102		0.18	3,900.00	3,110.00	NA	NA	NA
SX103	*	1.46	855.00	92.40	NA	NA	NA
SX104		0.76	1,240.00	472.00	NA	NA	NA
SX105		0.92	1,280.00	521.00	NA	NA	NA
SX106		1.58	822.00	59.70	NA	NA	NA
SX107		0.40	2,530.00	1,790.00	NA	NA	NA
SX108		1.22	993.00	232.00	NA	NA	NA
SX109		0.19	4,730.00	4,010.00	NA	NA	NA
SX110		0.75	1,840.00	1,110.00	NA	NA	NA
SX111		0.60	1,950.00	1,210.00	NA	NA	NA
SX112		0.50	2,160.00	1,420.00	NA	NA	NA
SX113		0.04	50,200.00	4,950.00	NA	NA	NA
SX114		1.13	1,150.00	401.00	NA	NA	NA
SX115		0.88	1,230.00	463.00	NA	NA	NA
T101	*	47.30	9.63	35.60	NA	NA	NA
T102		17.30	24.30	64.50	NA	NA	NA
T103		18.40	22.30	54.30	NA	NA	NA
T104	*	0.20	1,820.00	243.00	2.28	220.18	43.89
T105		0.22	2,310.00	404.00	2.26	471.10	367.83
T106		16.50	28.70	31.30	NA	NA	NA
T107		0.10	4,270.00	1,020.00	NA	NA	NA
T108		0.14	4,810.00	869.00	NA	NA	NA
T109		0.18	5,030.00	786.00	NA	NA	NA
T110		0.18	2,870.00	870.00	NA	NA	NA
T111		0.18	2,920.00	1,260.00	2.26	275.55	157.90
T112		0.17	2,710.00	1,450.00	NA	NA	NA
T201		0.16	4,520.00	1,,820.00	NA	NA	NA
T202		0.16	4,520.00	1,820.00	NA	NA	NA
T203		0.16	4,520.00	1,820.00	NA	NA	NA
T204		0.16	4,520.00	1,820.00	NA	NA	NA
TX101		11.20	61.40	47.80	NA	NA	NA
TX102		0.06	9,440.00	6,220.00	NA	NA	NA
TX103		0.18	5,030.00	330.00	NA	NA	NA
TX104		0.06	9,440.00	6,220.00	NA	NA	NA

Table A.28. (cont'd)

Tank name	High Pu tanks	Agnew Pu conc (ug/g)	Agnew ratio sum	Agnew insolubles ratio sum	TCR mean Pu conc (ug/g)	TCR ratio sum	TCR insolubles ratio sum
TX105		0.06	9,440.00	6,220.00	NA	NA	NA
TX106		0.15	4,410.00	3,390.00	NA	NA	NA
TX107		0.06	9,440.00	6,220.00	NA	NA	NA
TX108		0.06	15,200.00	7,630.00	NA	NA	NA
TX109		0.20	1,820.00	397.00	NA	NA	NA
TX110		0.24	1,500.00	319.00	NA	NA	NA
TX111		0.29	1,180.00	239.00	NA	NA	NA
TX112		0.18	5,030.00	330.00	NA	NA	NA
TX113		0.29	1,180.00	239.00	NA	NA	NA
TX114		0.19	4,730.00	323.00	NA	NA	NA
TX115		0.05	19,600.00	8,660.00	NA	NA	NA
TX116		0.17	5,660.00	355.00	NA	NA	NA
TX117		0.17	5,470.00	348.00	NA	NA	NA
TX118	*	214.00	4.02	2.10	NA	NA	NA
TY101		0.26	2,100.00	366.00	NA	NA	NA
TY102		0.18	5,030.00	330.00	NA	NA	NA
TY103		0.17	4,190.00	1,870.00	NA	NA	NA
TY104		0.05	19,600.00	8,660.00	NA	NA	NA
TY105		0.05	19,600.00	8,660.00	NA	NA	NA
TY106		0.01	237,000.00	18,400.00	NA	NA	NA
U101		0.06	9,440.00	6,220.00	NA	NA	NA
U102		0.06	9,440.00	6,220.00	NA	NA	NA
U103		0.06	9,440.00	6,220.00	NA	NA	NA
U104		0.05	17,100.00	6,520.00	NA	NA	NA
U105		0.06	9,530.00	6,220.00	NA	NA	NA
U106		0.06	9,440.00	6,220.00	NA	NA	NA
U107	*	23.50	26.20	8.38	NA	NA	NA
U108	*	44.70	10.30	6.13	NA	NA	NA
U109	*	11.80	50.00	24.10	NA	NA	NA
U110		0.09	4,850.00	1,590.00	4.07	272.69	117.74
U111		0.14	4,020.00	2,430.00	NA	NA	NA
U112		4.10	120.00	46.20	NA	NA	NA
U201		23.50	26.10	8.38	NA	NA	NA
U202		23.50	26.10	8.38	NA	NA	NA
U203		23.50	26.10	8.38	NA	NA	NA
U204		23.50	26.10	8.38	NA	NA	NA

NA = not applicable.

Table A.29. Neutron Absorber-to-Plutonium Mass Ratios for Solids in Double-Shell Tanks

Tank Name	High Pu Tanks (>10 kg)	Agnew Pu Conc (ug/g)	Agnew Ratio Sum	Agnew Insolubles Ratio Sum	TCR Mean Pu Conc (ug/g)	TCR Ratio Sum	TCR Insolubles Ratio Sum
AN101		0.00	NA	NA	NA	NA	NA
AN102		0.00	NA	NA	NA	NA	NA
AN103		42.50	27.10	20.60	NA	NA	NA
AN104		0.00	NA	NA	NA	NA	NA
AN105		0.00	NA	NA	NA	NA	NA
AN106		0.00	NA	NA	NA	NA	NA
AN107		0.00	NA	NA	NA	NA	NA
AP101		0.00	NA	NA	NA	NA	NA
AP102		0.00	NA	NA	NA	NA	NA
AP103		0.00	NA	NA	NA	NA	NA
AP104		0.00	NA	NA	NA	NA	NA
AP105		0.00	NA	NA	NA	NA	NA
AP106		0.00	NA	NA	NA	NA	NA
AP107		0.00	NA	NA	NA	NA	NA
AP108		0.00	NA	NA	NA	NA	NA
AW101		0.07	10900.00	9500.00	NA	NA	NA
AW102		0.00	NA	NA	NA	NA	NA
AW103	*	9.87	46.20	11.80	NA	NA	NA
AW104		0.58	1220.00	1040.00	NA	NA	NA
AW105	*	8.92	54.40	18.60	NA	NA	NA
AW106	*	42.50	27.40	20.60	NA	NA	NA
AY101	*	103.00	7.40	4.55	NA	NA	NA
AY102		39.20	28.50	21.90	NA	NA	NA
AZ101	*	41.90	23.00	17.80	NA	NA	NA
AZ102	*	41.00	16.20	10.30	NA	NA	NA
SY101		0.00	NA	NA	NA	NA	NA
SY102	*	85.10	13.50	3.28	NA	NA	NA
SY103		0.00	NA	NA	NA	NA	NA

NA = not available

HTCE (Agnew) plutonium and absorber concentrations were estimated for 12 of the 28 DSTs and for all 149 SSTs. One of the SSTs, C-202, did not have criticality ratio estimates calculated because the HTCE analysis reported a 0.0 concentration for plutonium. The 14 tanks for which TCR sample tank average concentration contents were measured [see Hartley et al. (1996)] were all SSTs.

The tables contain 8 columns with the following information:

- Tank name
- Designation of tanks with high Pu (using as *) [see Section A.3.1 for discussion/rationale]
- The estimated total Pu concentration in the tank solids (from Agnew et al. 1996)
- The sum of the ratio of all neutron absorbers-to-Pu ratio using Agnew et al. (1996)
- The sum of the ratio of the insoluble neutron absorbers-to-Pu ratio using Agnew et al. (1996)
- The average concentration of Pu measured in tank solids from actual measurement (TCR)
- The sum of the ratio of all neutron absorbers-to-Pu ratio using measured data (TCR)
- The sum of the ratio of insoluble neutron absorbers-to-Pu ratio using measured data (TCR).

These evaluations show Tanks TX-118 and AW-103 as the only tanks with more than 10 kg of plutonium to have a minimum total absorber-to-plutonium mass ratio sum of less than 10. These results support the conclusion that Hanford Site tank waste is subcritical, but additional evaluations are warranted.

In a separate analysis, we used Appendix C (Waste Sample Data and Analysis) of Braun et. al. (1994), which describes analyses of tank sample concentrations for plutonium and absorber materials. The samples were taken from Hanford Site tank waste from 1974 to 1994, with the majority of the samples taken before 1989. Figure C-14 in Braun et. al. (1994) is a histogram of the plutonium concentration in 221 solid samples; the maximum plutonium concentration was reported as 0.547 g/L. Figure C-24 in Braun et. al. (1994) shows a histogram of the ratio sum for insoluble neutron absorbers for 236 solid samples. The insoluble absorbers used in the analysis were uranium, iron, manganese, chromium, and nickel. Eighteen of the 236 samples had ratio sums of less than 1, with about 55 samples having ratio sums of less than 10.

Each tank was evaluated for its potential for criticality based on the following eight criteria.

- Plutonium concentration <1 g/L
- Individual insoluble mass ratio for any absorber >1.0
- Sum of insoluble mass ratios >1.0
- Individual soluble mass ratio >10.0

- Sum of soluble mass ratios >10.0
- Thickness of sludge layer <20 in.
- For tanks with no sample information - similarity between tanks in a waste-type tank grouping that has at least one tank sampled and meet three of the first five criteria
- For tank groups or miscellaneous tanks that have no sample information - similar to tank groups with sample information or based on waste type.

Based on combinations of these criteria, all of the tanks were judged to be subcritical.

A.5 Discussion of Active Tanks (Double-Shell Tanks)

As shown in Table A.5 or A.29 seven DSTs were estimated to have more than 10 kg plutonium. Because theses tanks are considered still active, they were evaluated in groups based on the types of waste received. The bulk of each tank's plutonium content is actually verified by analysis or is assumed to be in the waste sludge. The supernatant in these tanks contain almost negligible concentrations of plutonium. Salt cake inventory is not reported in these tanks except for AW-106, which is reported to contain 322,000 L of salt cake. Typical measured supernatant concentrations of plutonium are listed in Table A.30.

Table A.30. Supernatant Plutonium Concentration for Double Shell Tanks with more than 10 kg of plutonium

Tank	Date of Sample	Recent Supernatant Plutonium Concentration[a] (μg/l)
AW-103	September 1994	0.35
AW-105	August 1994	3.7
AW-106	November 1994	7.0
AY-101	October 1994	321
AZ-101	May 1989	11.4
AZ-102	August 1989	473
SY-102	March 1990	3.6
(a) (Tusler 1995)		

PUREX zirconium decladding waste was received in Tanks AW-103 and AW-105 during the 1980's to form sludge layers on existing solids in the tanks. Neutralized current acid waste was received in Tanks AZ-101 and AZ-102. AW-106 received waste from several unrelated sources.

A.5.1 Waste in Tanks AW-103 and AW-105

A schematic of the waste in Tank AW-103 is shown in Figure A.3, along with the waste introduction and core sample locations for the core sample obtained January 23, 1989. Core samples were obtained at about an 8.2-m radius in tanks AW-103 and AW-105. Results of the AW-103 core sample analysis listed in Table A.31 for the composite of segments 4 and 5R indicate that the decladding waste, settled as sludge in the tank, has a plutonium concentration of 0.0327 g/L. Results of comparing the segment 4 and 5R composite analysis with the segment 6-10 (material from lower level in the sludge) segment composite analysis imply that a sludge heel existed in the tank before PUREX zirconium decladding waste was introduced in November 1983. The segment 6 through 10 composite analysis suggests that a heel of other waste with little plutonium and zirconium and more aluminum was present in Tank 103-AW before decladding waste was added in 1983. The decladding waste had substantial zirconium, while the initial heel had no significant zirconium and the heel contained significantly more aluminum than the zirconium cladding waste.

The Waste Tank Summary Report (Hanlon 1996) indicates a sludge content for AW-103 of 1,374,000 L and a supernatant content of 572,000 L. The same report indicates a sludge content of 1,124,000 L and a supernatant content of 288,000 L for AW-105. These sludge volumes are thought to have been representative of the sludge volume in 1989 and 1990 when sampling occurred. The quantity of sludge represented by core height for each tank is AW-103, 7 full segments or 1,380,000 L and for AW-105, 4 full and one partial segment for 853,000 L.

Table A.32 also shows the results of the tank AW-105 sludge core sample analysis along with comparisons of projected sludge compositions based on process records for both tanks. Similar comparisons of the measured neutron absorber-to-plutonium mass ratios with process record estimated ratios are shown in Table A.33.

Comparing process record sludge concentration projections with actual tank sample analysis for representative layers of waste, some significant differences are apparent. As determined by AW-103 and AW-105 sludge analysis, the plutonium content of the accumulated sludge is significantly higher than shown by NMC records of zirconium decladding waste batches transferred to these tanks during the 1980s. The zirconium content, as determined by sludge analysis and volume, is about a factor of two higher than was expected based on the total zirconium determined to be added to the two tanks from fuel elements processed in PUREX. The actual masses of fuel processed through the PUREX Plant are known, so actual quantities are known for the zirconium in decladding waste. This makes zirconium the most accurately known constituent in the waste stream.

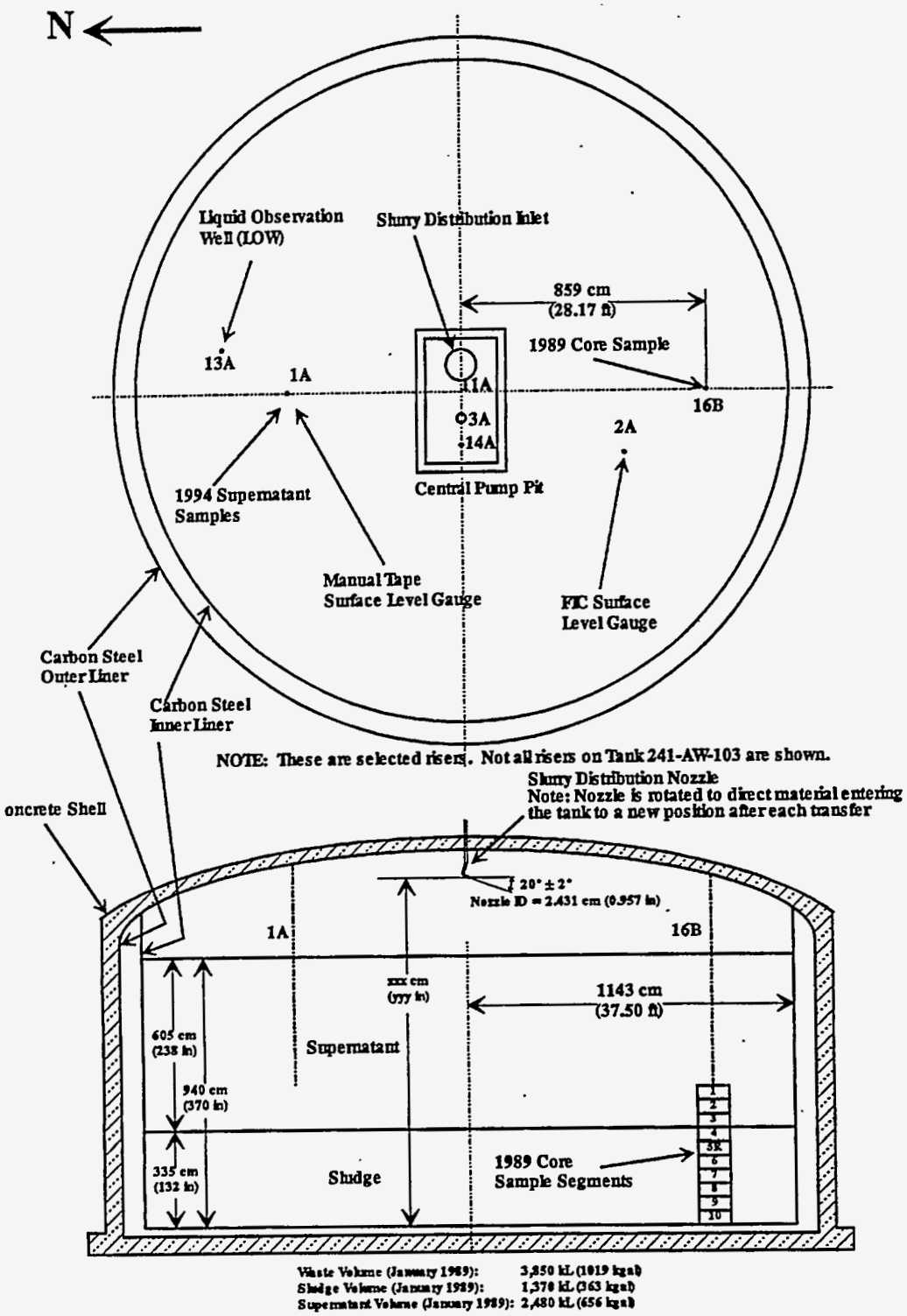

Figure A.3. Schematic of Tank AW-103 Showing Waste Introduction Location

Table A.31. AW-103 and AW-105 Tank Waste Analysis

Sludge analyte	Sludge analysis (g/l)				
	AW-103 segments[a] based on 1.43 Sp Gr		AW-105 segments[b] based on 1.39 Sp Gr for 3-6 and 1.50 Sp Gr for 7		Cladding waste projected concentrations based on process records[c]
	4-5R	6-10	3-6	7	
Pu	0.0327	0.0094	0.063	0.0058	0.0048
U	17.9	11.6	26.4	18.8	6.48
Al	3.46	11.0	4.89	54.9	
Cr	0.38	2.95	1.21	26.3	
Fe	1.13	1.16	7.90	29.1	1.07-1.44
La	3.62	0.23	3.54	0.25	
Zr	251.7	102.7	322	35.4	136

(a) (Hodgson, 1995)
(b) (Tingey, 1994)
(c) Calculated from Table A.10

Table A.32. AW-103 and AW-105 Sludge Insoluble Neutron Absorber-to-Plutonium Ratios

Insoluble absorber	Tank AW-103 segments 4 and 5R absorber/Pu mass ratios and ratio sums		Tank AW-105 segments 3-6 absorber/Pu mass ratios and ratio sums		Process records projected for declad waste, absorber/ Pu mass ratios and ratio sums	
U	547	----	419	-----	1346	----
Al	105	0.08	54.3	0.06		
Cr	12	0.09	19.2	0.14		
Fe	35	0.22	125	0.78	223	1.4
La	111	0.92	56.2	0.46		
Zr	7697	1.92	5111	1.28	28,200	7.1
Total		3.23		2.72		8.5

Differences in plutonium content between the plant sending and the tank farm receiving the waste may be explained by sampling uncertainties in the plant batch-sampling procedures. The fines might not always have been representatively collected and analyzed. When NMC decladding waste samples were obtained from Tanks TK-D2 and TK-E3, collected solids were not analyzed. The plant centrifuge was assumed to have removed the solids before the waste was transferred to the TK-E5 neutralization tank. Starting in March 1994, when NMC samples were obtained from TK-E5, any undissolved fines from the samples were not analyzed. Some difficulties were observed in plutonium sampling by operating personnel (Harlow 1986) and the procedures were changed in 1987 to include analysis of fines.

Because fines were observed to be a concern in this stream, it could also be implied that fines may settle out of the supernatant unevenly in the tank farm receiving tank. The observation that the zirconium content of the sludge is greater than expected by a factor of about two could support a concern that uneven settling may have occurred. The waste was introduced into the tanks from near the top center of the tank through a pipe with an internal diameter of 0.957 cm angled about 20° from the horizontal and extending out less than 0.1 m. This angled pipe was rotated after each batch transfer to distribute the waste in different directions. The discharge rate of about 2.8 L/s would put the slurry at about an 8-m radius for a 7-m drop in elevation from the nozzle discharge point.

Obtaining core samples of the sludge as a function of radius in at least one of these receiving tanks and conducting a comparative analysis on the analytical results would be valuable. This would show whether the plutonium or zirconium is distributed unevenly.

Analysis of the 1990 AW-105 sludge sample showed a plutonium concentration of 0.063 g/L, which is about a factor of 50 less than the criticality concentration limit. Analysis of the 1989 AW-103 sample showed a concentration of 0.033 g/L, which is a factor of about 80 below the limit. The zirconium-to-plutonium mass ratio was 5111 in this AW-105 sample and 7697 in the AW-103 sample. These ratios are more than sufficient to ensure subcriticality. The insoluble absorber-to-plutonium mass ratios for AW-103 and AW-105 are listed in Table A-32, along with the insoluble absorber-to-plutonium mass ratio sums. The insoluble neutron absorber-to-plutonium mass ratio sums for the upper sludge in these tanks are 3.2 for AW-103 and 2.7 for AW-105 and 8.5, as indicated by the process records. These results indicate that the decladding waste is far below criticality.

A.5.2 Waste in Tank AW-106

The current Waste Tank Summary report (Hanlon 1996) indicates that tank AW-106 contains 799,000 L of sludge, 322,000 L of salt cake, and 912,000 L of supernatant. No sludge or salt cake samples were analyzed for this tank. Tusler suggests that the AW-106 sludge should be the same as for AW-105 sludge, even though the sludge inventories are not related. Tusler concludes with a baseline recommended plutonium inventory of 13,988 g in AW-106. AW-105 received mainly PUREX zirconium-cladding waste starting in June 1984. Tank AW-106 received miscellaneous waste from A-106 in 1980, from B Plant in 1982, from AW-103 early in 1983. It also received miscellaneous waste from AW-102 from 1985 to 1989, from AP-105 in 1988, from AY-102 in 1989, and from an evaporator mini run in 1993 (Tusler 1995, Brevick 1995).

The tank HDW Model Rev 3 report (Agnew et al. 1996) indicates a much lower plutonium inventory in Tank AW-106 at 4310 g. It is recommended that the waste in this tank be core sampled and analyzed to provide supportive technical data for a more thorough evaluation of the criticality safety issue in this tank. In either case (baseline or HDW Rev 3), the plutonium concentration is more than one order of magnitude less than the criticality limit of 2.6 g/L and the waste is expected to be in a subcritical condition.

A.5.3 Waste in Tank AY-101

Tank AY-101 is reported (Hanlon 1996) to contain 314,000 L of sludge (76 cm deep) and 3,229,000 L of supernatant with no salt cake. Waste transfers into tank AY-101 include dilute noncomplexed waste from B Plant in 1981, dilute complexed waste from B Plant in 1983, waste from Tank AZ-102 in 1984, and miscellaneous smaller waste transfers from B Plant, PUREX [a very small amount of plutonium was added from NZCAW (22 g) and canyon sump waste (9 g)], saltwell pumping, and the 300 Area.

A sample containing supernatant and sludge (labeled 101-AY-1) was obtained from AY-101 December 29, 1994. This sample consisted of approximately 60 vol% settled solids and 40 vol% clear supernatant liquid. The liquid and settled solids were separated and analyzed and the results reported in an internal memo (Herting to Jones February 27, 1996). The settled solids were considered sludge. The sample represents a grab sample of the supernatant and sludge thought to be obtained near the top of the sludge in the tank.

The sludge (settled solids) analysis for plutonium and insoluble absorbers is listed in Table A.33. The results listed are an average of a sample and a duplicate sample (very close agreement between sample and duplicate analysis) taken from the grab sample settled solids (Herting 1996a). Insoluble neutron absorber-to-plutonium ratios and ratio sums are also included in Table A.34. The results show that the sludge plutonium concentration is two orders of magnitude less than the criticality limit of 2.6 g/L. The top portion of sludge in this tank contains sufficient insoluble absorbers (mass ratio sum of 19.8) present to preclude a criticality concern. Consideration should be given to obtaining and analyzing a full core sample of the sludge in this tank because the projected plutonium inventory (3.9 kg) implied by this grab sample evaluation is considerably less than the baselined (24 kg) and HDW Model Rev 3 (23 kg) values (see Table A.5). Based on the sources of waste added to this tank, the grab sample evaluation appears more reasonable than the baselined or HDW Rev 3 values, but a good core sample evaluation of the sludge in this tank appears to be warranted. In either case, the plutonium concentration is more than one order of magnitude below the 2.6-g/L criticality limit. The insoluble neutron absorber-to-plutonium mass ratio is greater than 2 and the waste would be subcritical.

Table A.33. AY-101 Sludge Analysis and Insoluble Absorber to Plutonium Mass Ratios

Analysis	Settled sludge (average of sample and duplicate)	AY-101 insoluble absorber/Pu mass ratio	AY-101 insoluble absorber/Pu mass ratio sum
Sp Gr	1.38		
Pu (g/l)	0.0124		
U (g/l)	Not Analyzed		
Al (g/l)	48.5 (70% of total)	3912	4.3
Fe (g/l)	16.6	1341	8.4
Mn (g/l)	2.8	226	7.1
Total			19.8

A.5.4 Waste in Tanks AZ-101 and AZ-102

Tank AZ-101 is reported (Hanlon 1996) to contain 132,000 L of sludge and 3,365,000 L of supernatant with no salt cake. Waste transfers to this tank included waste from Tank SY-102 in 1982, Tank AY-102 in 1983, and PUREX NZCAW in 1983 through 1986. According to NMC transfer records, 9,700 g of plutonium were added with this stream. Additional small volumes of noncomplexed waste were transferred to this tank.

Two core samples of AZ-101 waste were obtained by the push mode sampling method in April and May 1989 and analyzed for chemical and radionuclide content. Before the tank was sampled, six sludge-level measurements were made and an average sludge level determination of 43 cm (17 in. or 177,000 L) was calculated. Two segments were obtained for each core. The first sample core obtained from riser #15F consisted of one segment with 280 g of supernatant and one segment obtained by suction consisting of 200 g of dark brown solids and 118 g of drainable liquid. The solids were soft, creamy, and sticky and did not maintain the cylindrical shape of the sampler after extrusion. Also, the solids obtained did not necessarily represent sludge strata in the tank because the second segment was obtained by suction from the bottom of the tank. Suction was used because the sampler was started at the bottom of the tank and could not be pushed or rotated. Analysis of the sample solids is listed in Table A.34.

Table A.34. AZ-101 Tank Sludge Analysis Compared to Projections from Process Records

Sludge analyte	Sludge analysis of Cores 1 and 2 (g/l)		
	AZ-101 Core 1 solids[a] based on 1.7 Sp Gr	AZ-101 Core 2 solids[b] based on 1.67 Sp Gr	Projected NZCAW waste sludge concentrations based on process records[c]
	Segment 2 obtained by suction	Segments 1 and 2 composite	
Pu	0.095	0.16	0.064
U	----	16.4	15.2
Al	52.5	26.6	23.6
Cr	4.36	1.26	0.6
Fe	111	182	157
Ni	4.69	8.6	3.9
Zr	24.2	79.7	86.4

(a) (Letter from M. E. Peterson to A. J. Diliberto September 29, 1989)
(b) (Gray W. J., September 1993)
(c) Taken from Table A.11

The second core sample was obtained from riser # 24D and consisted of two segments. The upper segment (#89-013) was 39.4 cm long, dark brown in color, retained its cylindrical shape after extrusion, and consisted of 305 g of solids with no drainable liquid. The lower segment (#89-014) was 48 cm long and consisted of 109 g drainable liquid and 208 g solids. Some concern about the strata representativeness of the lower segment is noted because about 17.9 cm of drainable liquid was present between

the layers of solids. The total height of solids obtained in the samplers (39.4 cm in upper segment and 25.7 cm in lower segment) is in excess of the expected average solids height (43 cm) in the tank by about 22 cm. A composite sample was made from these two segments and analyzed. Results of the composite sample are listed in Table A.35, along with the results from the first core and projected concentrations based on process records. Insoluble neutron absorber-to-plutonium mass ratios and ratio sums were calculated from these analyses. They are listed in Table A.35, along with the projected mass ratios based on process records.

Table A.35. AZ-101 Sludge Insoluble Neutron Absorber-to-Plutonium Ratios

Insoluble absorber	Tank AZ-101 Core 1 segment 2 absorber/Pu mass ratios and ratio sums		Tank AZ-101 Core 2 segments 1 & 2 absorber/Pu mass ratios and ratio sums		Process records projected NZCAW insoluble absorber/Pu mass ratios and ratio sums	
U	----	----	124	-----	-----	----
Fe	1168	7.30	1413	8.83	1946	12.2
Cr	46	0.34	8.6	0.14	----	----
Al (70%)	387	0.43	140	0.15	----	----
Ni	49.4	0.47	66.9	0.64	59	0.56
Zr	225	0.06	617	0.15	1331	0.33
Total		8.60		9.91		13.09

Four 1-cm-thick layer sections (subsamples L1, L2, L3, and L4) of these two segments were analyzed and reported in Hodgson 1995b. The results of these layer samples indicate that the solids at the bottom of the tank (about 6 cm from the bottom-sample L3) consist of waste with considerably greater aluminum, chromium, silver, manganese, sodium, chloride, nitrite, and sulfate than the three higher layers. The lower layer also had considerably lower concentrations of barium, calcium, cadmium, cerium, iron, nickel, and zirconium. The next layer sample (L4 obtained 44 cm up from the bottom of segment 2, not necessarily from the bottom of the tank, because liquid layers existed in the sample between these two locations) indicated that the layer consisted principally of the NZCAW waste with a minor mix of tank heel waste of L3 composition. These observations imply that AZ-101 had a heel of about 18 cm, then about 25 cm of NZCAW waste was added above it.

Results show that the bulk sludge plutonium concentration is about 0.16 g/L or less by sample analysis of the sludge in Tank AZ-101 and by projections from process record data, which is considerably less than the 2.6 g/L criticality limit. Sufficient insoluble absorber content (by factors of 8.6 to 13, mainly iron) is associated with the NZCAW sludge plutonium to ensure subcriticality by both sample analysis of the sludge in Tank AZ-101 and by projections from process record data.

A.5.5 Waste in Tank SY-102

Tank SY-102 is reported (Hanlon 1996) to contain 269,000 L of sludge and 1,169,000 L of supernatant with no salt cake. Tank SY-102 began receiving waste in 1977. Waste transferred to this

tank from 1977 to 1981 was supernatant from the 241-S, -SX, -T, and -U tank farms (Jungfleish 1984) as feed to the 242-S and 242-A Evaporators. In 1981 SY-102 began receiving sludge and dilute non-complexed waste from T Plant decontamination processes and dilute noncomplexed waste from 222-S Laboratory. In 1982 waste from PFP consisting of slurry and transuranic solids began being added to this tank. Salt well liquids from 200 West Area tanks were received in SY-102 until 1983 and after 1993.

The sludge accumulated in the tank is expected to have come from three sources. The first is precipitate of manganese dioxide and hydrous manganese hydroxide from wastes added in 1977. Some may have accumulated from transferring REDOX waste from S and SX tank farms before 1981. This waste contained high concentrations of aluminum, chromium, and iron. The third source was PFP slurry wastes added after 1981. The sludge from PFP wastes is expected to contain plutonium and ^{241}Am in it.

Three sampling and analysis events have occurred for Tank SY-102. The first core sample was obtained from riser 1B in October 1988. Push mode core samples were obtained in 1990 and a supernatant grab sample was obtained in 1994.

The 1988 core sample consisted of four segments. The top two (segments 1 and 2) consisted of supernatant and the bottom two (segments 3 and 4) consisted of sludge. The bottom sludge segment (4) contained 38.1 cm of recovered sludge. The top portion of this segment was analyzed and the results are listed in Table A.36. Insoluble neutron absorber-to-plutonium mass ratios are given in Table A.37.

Table A.36. Tank SY-102 Sludge Insoluble Neutron Absorber Analysis and Comparison to Projections from Process Records

Sludge analyte	SY-102 Sludge insoluble absorber composition (g/L)	
	SY-102 cores 16 and 17 composite solids[a] based on 1.8 sp gr	Projected PFP waste sludge concentrations based on process records[b]
Pu	0.018	
U	3.5	
Al	82.1	
Ca	20.7	
Cr	34.0	
Fe	73.6	
Ni	1.85	
Mg	3.56	
Mn	19.6	

(a) (Winters 1995)
(b) Records have not been declassified at this date.

Table A.37. SY-102 Sludge Insoluble Neutron Absorber to Plutonium Ratios

Insoluble absorber	Tank SY-102 core 16 and 17 sludges composite absorber/Pu mass ratios and ratio sums		Process records projected PFP insoluble absorber/Pu mass ratios and ratio sums	
Al (70%)	3193	3.51		
Ca	1150	1.49		
Cr	1889	14.0		
Fe	4089	25.6		
Ni	103	0.98		
Mg	198	----		
Mn	1089	34.0		
U	194	0.25		
Total		79.8		

Sludge sample analysis evaluations show low plutonium concentrations (0.018 g/L) and high concentrations of insoluble neutron absorbers. This ensures that this waste is in a highly subcritical condition. As the process records for the PFP wastes are obtained and evaluated, we expect them to support this conclusion.

As mentioned earlier in the report, Tank SY-102 is of special importance because a mixer pump will be installed in the tank. The mixer pump could rearrange the sludge particles. Analyses presented in Chapter 4 suggest that discrete particle separation is not very likely and that the potential for this tank to go critical is extremely low, if not nonexistent.

A.6 Summary and Conclusions

The relevant criticality safety properties of Hanford Site underground stored waste was characterized in this appendix using currently available information. This chapter identified relevant fissile materials, neutron absorbers, and moderators related to criticality in waste streams sent to the tank farms and in the waste currently in the tanks. It also considered waste treatment processes that have been conducted on the waste over time. Additional information needed to provide more conclusive estimates of the contents of some of the tanks with the highest plutonium inventories is identified.

The approach to identifying properties relating to criticality in existing waste storage tanks was to determine the batchwise composition of discharges from the processing facilities to the tank farm storage tanks. NMC records were used for plutonium, uranium, and neptunium transfers because they have been well documented and reviewed for accuracy and because they identified the Hanford Site tanks that received each batch of waste. The NMC records included an accountability volume that was compared, where possible, to plant waste discharge volumes as supportive information. Where possible, the settled sludge concentration of fissile material and insoluble neutron absorbers in tanks that may contain fissile

material in concentrations higher than 10 kg was determined based on the historical accumulation of process waste streams and by core sample analysis results. These two approaches to estimating inventories were compared and discrepancies discussed.

The results show that the fissile material concentrations in all of the Hanford Site tank waste is likely at subcritical values and that sufficient insoluble neutron absorbers are present to maintain subcritical conditions under safe storage and retrieval operations. Additional sampling of tank waste is recommended for some selected tanks to verify tank fissile material and insoluble absorber content.

We made the following final conclusions in the development of this appendix.

- The plutonium or equivalent plutonium concentration in most of the waste tank sludge is at least one to two orders of magnitude less than the 2.6-g/L criticality limit as determined by both process records and tank sample analysis results.

- The plutonium or equivalent plutonium concentration in the supernatant and salt cake in most tanks (those for which defensible data are available) is at least three orders of magnitude less than the 2.6-g/L criticality limit as determined by tank sample analysis.

- Process records and tank sample analysis indicate that the waste contains sufficient insoluble neutron absorbers to render the fissile material subcritical.

- Additional sampling and analysis of some tanks (tanks with high plutonium inventories) should be conducted to verify that the fissile and insoluble neutron absorber materials are at concentrations similar to the predictions, which clearly would maintain subcritical conditions as long as waste remains homogeneous.

- Any effort to remove the sludge waste (i.e. tank contents retrieval) or change its configuration (mixer pump operation, continued waste disposal, etc.) that may result in an increase in plutonium concentration and/or removal of insoluble neutron absorbers from the waste must be evaluated for effect on the criticality state of the waste before beginning the operation.

A.7 References

References for this appendix are contained in the Chapter 7 reference list.

This page intentionally left blank.

Appendix B

Physical Processes Related to Solid Segregation

Appendix B
Physical Processes Related to Solid Segregation

Solid particle movement affects the transport of tank wastes both directly and indirectly. Indirectly, sediment transport changes the properties and rheology (density, viscosity, shear stress, bottom roughness, and heat transfer coefficient) of the waste mixture in Hanford tanks. These changes, in turn, affect the flow velocities of particles and solution and temperature distributions within tanks. Changes in temperature distributions may also affect the solubility of some chemicals causing precipitation or dissolution of specific chemical compounds, thus affecting particle size, solid and fluid densities, and waste rheology.

Natural processes in tanks can directly suspend and transport solids by creating flow (for example, induced by buoyancy due to heat and presence of gases). In addition, human activities related to waste tank maintenance (such as mixer jet-pumps and injection of new wastes into tanks) can cause particle transport. Suspended solids will settle in the tank at different locations, depending on the capacity of flow to transport specific solids. Both suspended and bottom solids can adsorb dissolved wastes and then migrate and settle in a different location in the tank. The potentially nonuniform deposition of contaminated suspended solids and the direct adsorption of soluble contaminants by the bottom sediment may build up the specific solids in the tank bottom, that can be subject to subsequent resuspension or desorption. However, contaminant adsorption by solids can also reduce concentrations in supernate solution and bring neutron absorbers present in the waste sludge/salt cake into close contact with insoluble fissile materials. Thus the impacts of mass transfer from solution to solid, and vice versa, can have either favorable or deleterious effects on the potential for criticality, dependent upon the reactions that dominate.

In this section, the potential physical processes that could promote segregation of solids in the Hanford waste tanks are evaluated.

B.1 Solid Transport Mechanisms

Transport, deposition, and resuspension processes can rearrange particle distributions through their complex interdependency with flow, rheology, and bottom roughness/resistance to flow. Hydraulic and environmental engineers have investigated sediment transport in natural environments most extensively, and this knowledge is very useful to assessing particle movement in Hanford tanks. Solid/sediment transport is generally controlled by geometric/channel characteristics, fluid properties, flow characteristics, and solid properties (Raudkivi 1967, Graf 1971, Vanoni 1975, Simons and Senturk 1977, Onishi, 1994a).

In this section, the mechanisms of particle transport, deposition and resuspension are described in general terms. Important properties of solids and fluids that affect particle transport are also discussed.

This section describes particle settling velocity and initiation of motion with their functionalities, mostly derived from studies of alluvial streams. The transport, deposition, and resuspension of sediments is also covered here to identify which variables control the mechanisms and relationships that are also acting on solids in the Hanford tanks.

B.1.1 Solid Properties

The various properties of solid particulate relevant to solid segregation are discussed in this section.

B.1.1.1 Solid Types

Solids/sediments are composed of a variety of minerals. In the natural environment (such as rivers) the most common mineral is usually quartz, because of its great resistance to weathering and abrasion (Leliavsky 1966, Richards 1982). However, solids in Hanford tanks are formed through various chemical reactions and consist of a wide variety of chemical compounds, e.g., $NaNO_3(s)$, $NaNO_2(s)$, $Al(OH)_3$ (s), and other Al, Pb, Fe, Mn oxyhydroxides (Reynolds and Herting 1984, Tank Waste Science Panel 1991, Castaing 1994, DiCenso et al. 1995, Onishi and Hudson 1996).

Solid particles can be divided into two types; cohesive and non-cohesive solids. Non-cohesive solids are those consisting of discrete particles whose movement depends only on particle properties (size, shape, and density) for given transport and erosion forces (Vanoni 1975, Jansen et al. 1979). The main properties of non-cohesive solids that relate to solid/sediment transport are particle size, shape, density, and fall velocity. Sand and gravel are examples of non-cohesive sediments. Cohesive solids, on the other hand, are those whose movement depends also on the strength of cohesive bonds between particles. They flocculate (or aggregate) and the aggregate properties depend on sediment type, type and concentration of ions in the water, and flow conditions (Krone 1962; Mehta et al. 1989). Fine silt and clay are often cohesive sediments. The fine-grained sludges in Hanford tanks are also thought to be cohesive particles.

B.1.1.2 Solid Sizes

The most important property of the solid particle is its size (Vanoni 1975; Simons and Senturk 1977). Particle sizes may be defined by volume, weight, fall velocity, and sieve size, and various size parameters such as Feret's diameter, Martin's diameter, and projected area diameter. Because the size and shape of grains in sediments vary over wide ranges, descriptions are based on groupings into different size classes. Table B.1 shows a commonly used grade scale with associated sieve sizes (Lane 1947, Vanoni 1975). Note that particle behavior on a sieve and probability of falling through the sieve depends on many factors, such as particle size and shape, mesh size and shape, duration of sieving, and sieve loading. Some recommendations for the sieve loading were reported in Shergold (1946) and Jansen et al. (1979). For fine particles, the pipet method is commonly used to obtain particle sizes. The pipet method relies upon the falling velocity attribute to describe particle size. Usually size distributions are plotted as normal or log-normal distributions, and geometric means and standard deviation of the particle distribution are determined.

Table B.1. Solid Size Classification (adapted from Vanoni 1975)

Class Name	Sizes (mm)	Sieve Mesh Opening per inch	
		Tyler	U.S. Standard
BOULDERS			
very large	4,096 - 2,048		
large	2,048 - 1,024		
medium	1,024 - 512		
small	512 - 256		
COBBLES			
large	256 - 128		
small	128 - 64		
GRAVEL			
very coarse	64 - 32		
coarse	32 - 16		
medium	16 - 8	2.5	
fine	8 - 4	5	5
very fine	4 - 2	9	10
SAND			
very coarse	2.000 - 1.000	16	18
coarse	1.000 - 0.500	32	35
medium	0.500 - 0.250	60	60
fine	0.250 - 0.125	115	120
very fine	0.125 - 0.062	250	230
SILT			
coarse	0.062 - 0.031		
medium	0.031 - 0.016		
fine	0.016 - 0.008		
very fine	0.008 - 0.004		
CLAY			
coarse	0.004 - 0.002		
medium	0.002 - 0.001		
fine	0.001 - 0.0005		
very fine	0.0005 - 0.00024		

B.1.1.3 Shape of the Solid Particles

The most pertinent shape parameters are sphericity and roundness. Sphericity is defined as the ratio of surface area of a sphere of the same volume as the particle to the actual surface area of the particle to describe relative motion between the falling particle and the fluid (Wadell 1932, Simons and Senturk 1977). Roundness is the ratio of the average of the corners and edges of a particle to the radius of a circle inscribed in the maximum projected area of the particle (Vanoni 1975). Roundness is important for abrasion, but has a negligible impact on the hydrodynamic behavior of the particles.

Both of these parameters tend to decrease with decreasing size of the particles (Simons and Senturk 1977). Because of practical difficulties in obtaining sphericity and roundness, a more common parameter is a shape factor, SF defined as

$$SF = \frac{c}{\sqrt{ab}} \qquad \text{(B.1)}$$

where a, b, and c are the length of the longest, intermediate and shortest mutually perpendicular axes of the particle. The fall velocity can be expressed as a function of SF and a particle Reynolds number (Vanoni 1975), as discussed in Section B.1.1.5.

B.1.1.4 Specific Weight of the Solid Particles

The specific weight of quartz is 2.65. Other minerals include feldspar, chert, and carbonates, whose specific weights are 2.55-2.76, 2.65, and 2.85, respectively (Vanoni 1975). However, many solids in the waste tanks have different specific weights from these values, for instance $NaNO_3$(s), and $NaNO_2$(s) have specific weights of 2.26 and 2.17, while aluminum and iron oxides that are present in the Hanford sludge in the form of boehmite, gibbsite, ferrihydrite, goethite, hematite, and magnetite have specific weights of 3.44, 2.4, 3.96, 4.77, 5.26 and 5.18, respectively (Lide 1995). Crystalline plutonium oxide is much heavier (specific weight of 11.46), but no value is available for amorphous Pu hydrous oxide. Further, many solids, including Pu may be co-precipitated or adsorbed on other solids, and thus may have specific weights significantly lower than that of the pure PuO_2 crystal solids.

B.1.1.5 Fall Velocity of Spheres

The fall velocity of a sphere is given by (Raudkivi 1967; Vanoni 1975)

$$w^2 = \frac{4}{3}\frac{g d_s}{C_D}\left(\frac{\rho_s - \rho}{\rho}\right) \qquad \text{(B.2)}$$

where C_D = drag coefficient,
d_s = sediment diameter,
g = gravitational acceleration,
w = fall velocity, and
ρ and ρ_s = density of fluid and solid particle respectively.

Rouse (1937a,b) presented the drag coefficient as a function of a particle's Reynolds number or the auxiliary scale of the non-dimensionalized submerged weight of the particle, as shown in Figure B.1. A particle Reynolds number (R) and submerged weight (F) in Figure B.1 are calculated by using equations B.3 and B.4

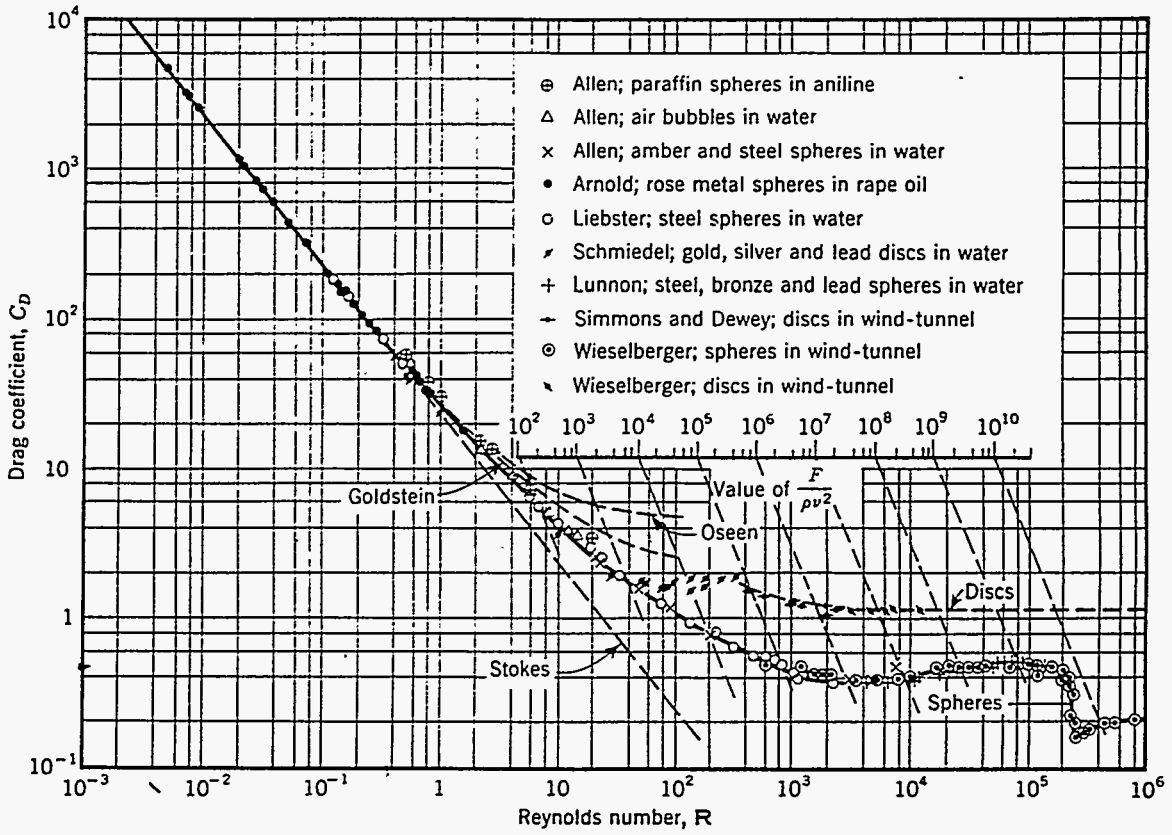

Figure B.1. Drag Coefficient of Spheres as a Function of Reynolds Number (Rouse 1937b)

$$R = \frac{w d_s}{\nu} \tag{B.3}$$

$$F = \frac{\pi d_s^3}{6}(\gamma_s - \gamma) \tag{B.4}$$

Where ν = kinematic viscosity
γ_s = specific weight of the solid
γ = specific weight of the liquid
d_s = sediment diameter.

Rouse (1937b) also presented the fall velocity of a quartz sphere as a function of particle size and water temperature or particle Reynolds number, as reported by Leliavsky (1966), Raudikivi (1967), Vanoni (1975), and Graf (1971). For a Reynolds number of less than 0.1, the fall velocity (w) is given by the Stokes law

$$w = \frac{g d_s^2}{18\nu}\left(\frac{\gamma_s - \gamma}{\gamma}\right) \tag{B.5}$$

An effect of particle shape on the fall velocity was reported by McNown et al. (1951). They relate the fall velocity as a function of a particle Reynolds number (R), a shape factor (SF), and resistance factor (K), defined as: $F/(3\pi\mu w d_s)$, where μ is the dynamic viscosity of the fluid.

B.1.1.6 Effects of Solid Concentrations on Fall Velocity

The fall velocities determined by Eqs. B.2 and B.5 are valid for a single spherical particle in a quiescent infinite fluid. If only a few closely spaced particles are in a fluid, they will fall in a group with a velocity that is higher than that of a single particle falling alone. On the other hand, if particles are dispersed throughout the fluid, the interference between neighboring particles will reduce (or hinder) their fall velocity (Raudkivi 1967). Thus the effective size of individual particles decreases with increasing fine sediment concentrations. Simons and Senturk (1977) reported that the main changes in fluid properties caused by increasing the fine sediment concentration are increases in viscosity and specific weight of the sediment-fluid mixture. The hindered settling velocity may be expressed using (Richardson and Zaki 1954, , Jansen et al. 1979) as

$$\frac{w}{w_0} = (1-c)^{\alpha} \tag{B.6}$$

where c = sediment concentration
w_0 = fall velocity without sediment concentration effects
α = constant, a function of the particle Reynolds number, R.

The values of α reported by Richardson and Zaki (1954) are shown in Table B.2.

Table B.2. Values of the Exponent Constant α in Hindering Fall Velocity

Particle Reynolds Number $R = w_0 d_s/\nu$	Exponent Constant α
<0.2	4.65
0.2 - 1.0	$4.35R^{-0.03}$
1.0 - 200	$4.45R^{-0.1}$
>200	2.39

For cohesive sediment, at higher concentrations (c) (above 300 milligrams per liter), continuing aggregation or break-up of cohesive sediment affect the sediment fall velocity. Another way to express the fall velocity in this case is,

$$w = A\ c^{\frac{4}{3}} \tag{B.7}$$

where A is constant. At sediment concentrations above approximately 10 grams per liter, sediment settling is hindered by the close spacing of settling aggregates. In this case, the resulting fall velocity is commonly expressed by,

$$w_h = w\ (1 - k_1 c)^5 \tag{B.8}$$

where k_1 = constant,
w_h = hindered fall velocity.
c = sediment concentration.

For laminar flow conditions, there are some simpler expressions available (Govier and Aziz 1972), including the following Famulado and Happel formula:

$$\frac{w}{w_0} = \frac{1}{1 + k_2 c^{\frac{1}{3}}} \tag{B.9}$$

where k_2 = a constant in the range of 1.30±0.24.

B.1.2 Fluid Properties and Flow Characteristics

The fluid properties that affect particle segregation are described in this section.

B.1.2.1 Fluid Properties

The main fluid properties to affect sediment transport (or particle settling velocity) are fluid viscosity and density (and lesser extent heat capacity). Relevant to the Hanford tank wastes, Mahoney and Trent (1995) obtained the following equation for the liquid viscosities, based on the viscosity data obtained from the literature for $NaNO_3$ solutions:

$$\mu_L = a_4\ \exp([a_0 + a_1 C + a_2 C^2]/T) \tag{B.10}$$

where, a_k = coefficients fit from experimental data as shown in Table B.3
T = solution temperature, (°K)
C = weight percentage (concentration) of the solute.

Table B.3. Coefficients for Equation B.10 Based on Experimental Measurements of $NaNO_3$ Solutions (Mahoney and Trent [1995])

Coeff.	Value
a_4	5.8044 x 10-6 Pa-s
a_0	1489.9 K
a_1	-0.97874 K
a_2	0.19490 K

The correlation is thought to give estimates that are within 10 % of the actual value for solutions with 0 to 90 wt. % $NaNO_3$ in the temperature range from 273 to 433 °K. Mixtures of fluids and sediment with high sediment concentrations likely exhibit non-Newtonian flow characteristics (Govier and Aziz 1972, Trent and Eyler 1993). There are many models for the rheological behavior of non-Newtonian fliuds (Mahoney and Trent 1995). These include power law or Ostwald-DeWaele (Bird et al. 1960), Cross (1965), Carreau, (Ellwood et al. 1990), biviscous, (Kalyon et al. 1993), Bingham (Bird et al. 1960), Casson (Bird et al. 1960), Herschel-Bulkey (Bird et al. 1960), and Gay (Dabak and Yucel 1987) models. A Bingham model for shear stress, for example, is expressed as

$$\tau = -\left\{\mu_\infty + \frac{\tau_0}{\sqrt{\frac{1}{2}\Pi_D}}\right\} D \qquad for\ \frac{1}{2}\Pi_D > \tau_0^2 \qquad \text{(B.11)}$$

and

$$D = 0, \quad for\ \frac{1}{2}\Pi_D < \tau_0^2$$

where
- D = shear rate tensor
- $\prod_D$ = second invariant of the shear rate tensor
- τ_0 = yield strength
- μ_∞ = Newtonian viscosity at high shear rate.

The preceding Bingham model has been fit to Hanford tank wastes for use in other tank waste modeling (Trent and Eyler 1993; Onishi 1995). A different approach was used in the TEMPEST modeling performed in for this report. This modeling effort is described in Section 3.0.

No viscosity correlation for multi-component, solid-liquid waste mixtures is available due to the complexity of the solid-liquid mixtures and their interactions. The development of such a relationship

for uniform spherical particles has been the subject of numerous theoretical and experimental efforts (Mahoney and Trent 1995). One common approach is to extend Einstein's viscosity relationship to apply at finite particle volume concentrations (Onishi and Hudson 1996). The type of relationship which results is typically of the form

$$\mu_M = \mu_L(1 + 2.5C_V + 14.4C_V^2 + \ldots) \quad \text{(B.12)}$$

where C_V = the particle volume fraction
μ_M = viscosity of a mixed electrolyte solution
μ_L = viscosity of a pure electrolyte solution (one salt component only).

Similar expressions have been provided by a number of authors including Frankel and Acrivos 1967. Relationships of this form apply for uniform spherical particles with low to moderate particle volume loadings. As the particulate volume loading approaches maximum packing, the predicted viscosities will deviate significantly from those observed. A model of this form does not include any colloidal or large aspect ratio effects, which make the mixture viscosity much more non-linear than that predicted by Equation B.12.

Some empirical formulas estimate the fluid density for a multi-component solution (Mahoney and Trent 1995, Onishi and Hudson 1996). For the Hanford tank wastes, the following formulas for the liquid density, ρ_L (kilograms per cubic meter) are suggested by Mahoney and Trent (1995):

$$\rho_L = 1171.8 - 9.140C - 0.7758T + 0.4866T^2 + 4.318m_{OH} \quad \text{(B.13)}$$

or its simplified form,

$$\rho_L = 1245.8 - 9.824C - 1.0606T + 0.6812T^2 \quad \text{(B.14)}$$

where, C = the weight percent of the all aqueous species to the total solution weight,
m_{OH} = the molality of hydroxide in the solution
T = solution temperature, °K.

The slurry mixture density (ρ_M) is a function of the solid and the liquid density, as well as the solids fraction, and can be expressed as Onishi and Hudson (1996) state:

$$\rho_M = \frac{\rho_L}{\left(1-\chi_S\left(1-\frac{\rho_L}{\rho_S}\right)\right)} \tag{B.15}$$

where, ρ_s = solid particle density, (or volume weighted average density for mixtures)
χ_s = solid mass fraction (wt. of solids/wt of total slurry).

Important flow characteristics, that are required with the above equations to predict particle settling velocities in a mechanically disturbed regime, are flow discharge/velocity, depth of fluid, and width of flow, energy slope, and shear/yield stresses, as follows.

Similar to the density formula (Eq. B.15), single-phase liquid heat capacity (c_{pL}) may be expressed by (Mahoney and Trent 1995)

$$c_{pL} = a_0 + a_1 C + a_2 T + a_3 C^2 T \tag{B.16}$$

where, a_0, a_1, a_2, and a_4 = empirically determined coefficients
T = temperature in °K.

Currently, no data are available to develop an empirical formula for heat capacity of the multicomponent fluid in Hanford tanks. Heat capacities for a liquid-solid (gasless) mixture (C_{PM}) and a bubbly mixture (liquid-solid-gas) (C_{PB}) for potential application to the Hanford wastes are estimated in (Mahoney and Trent 1995) as follows:

$$c_{pm} = \frac{n_L \rho_L c_{pL} + (1-n_L)\rho_s c_{ps}}{n_L \rho_L + (1-n_L)\rho_s} \tag{B.17}$$

and,

$$c_{pb} = (1-n_G) c_{pm} \tag{B.18}$$

where, ρ_L = density of the liquid phase in the mixture
ρ_s = particle density of the representative solid
c_{pL} = heat capacity of the representative liquid
c_{ps} = heat capacity of the representative solid
n_L = porosity that is filled with liquid (volume fraction in the mixture filled with liquid)
n_G = porosity that is filled with gases (volume fraction in mixture filled with gas

B.1.2.2 Flow Characteristics

Important flow characteristics must be known in order to predict whether particles will be suspended and potentially separated from other particles during deposition: these characteristics are flow discharge/ velocity, depth, width, energy slope, and shear/yield stresses. One of the main characteristics of the sediment-laden flow is the interaction between flow and sediment transport. For example, in a waste tank, a sufficiently fast flow transports solids. The transport of solids changes properties and rheology (density, viscosity, shear stress, bottom roughness, and heat transfer coefficient) of the waste mixture in the tanks (Onishi et al. 1995). These changes, in turn, affect the flow velocity and temperature distributions. Changes in temperature and chemical species distributions may also affect the solubilities of some chemicals, causing either precipitation or dissolution of specific chemical compounds, thus affecting particle size, solid and fluid densities and rheology, which affect the flow velocities in the tanks (Onishi and Hudson 1996). Continual feedback or interrelationship between the variables controlling particle transport changes these patterns; so these complications must be considered when performing either simple or complex calculations.

Interactions between flow and sediment have been investigated most intensively in alluvial streams (Leliavsky 1966, Raudkivi 1967, Richards 1982). It is well known that flow affects sediment transport, which controls the hydraulic roughness and channel geometry through bed formation and sediment deposition and erosion (Vanoni 1975, Onishi 1994a). The hydraulic roughness and channel geometry, in turn, affect the flow (Simons and Senturk 1977).

For example, it is common to find multiple flow velocities and sediment transport rates for the same rate of discharge from, or depth of flow within a given channel, depending on the bed form (Nordin 1989). Thus to predict the flow within a channel requires knowledge of the relationships among flow parameters, fluid and sediment properties, and the hydraulic roughness and resulting friction factors affected by sediment transport.

Numerous methods and formulas are available to predict the interdependencies between flow, sediment transport and hydraulic roughness and to calculate sediment transport rates in rivers (Onishi 1994a). These relationships and empirical equations are an integral part of numerical sediment transport models/codes (Vanoni 1975; National Research Council 1983; Fan 1988; Onishi 1994a). These relationships and empirical equations include:

Einstein-Barbarossa (Einstein and Barbarossa 1952)
Garde-Raju (Garde and Raju 1966)
Simons-Richardson-Haynie (Simons and Richardson 1966; Haynie and Simons 1968)
Engelund (1966)
Znamenskaya (1967)
Raudkivi (1967)
Kennedy-Alam-Lovera (Alam and Kennedy 1969; Lovera and Kennedy 1969)

Maddock (1969)
Mostafa-McDermid (Mostafa and McDermid 1971)
Brownlie (1983).

As summarized by Raudkivi (1967),Vanoni (1975), and Onishi (1994a), most of these predictors are based on the concept that a specific variable (e.g., friction factor, hydraulic radius, or cross-sectional area) can be divided into two components, one corresponding the skin friction (grain roughness), and the other accounting for the form drag (bed forms).

Many of these methods were compared against measured data obtained from the Colorado River in Colorado (Vanoni 1975), the Niobrara River in Nebraska (Vanoni 1975), and the Sacramento River in California (Nakato 1990). These comparisons show wide variations among predictions, resulting from incomplete understanding of the relationship between bed forms and hydraulic roughness. Among these predictors, Brownlie reveals the best match to the measured data (Onishi 1994a).

B.1.3 Controlling Parameters for Solid Transport

Flow, solid/sediment transport, and bottom roughness/flow-field geometry are interdependent. In general, the following parameters are relevant for the solid/sediment transport (Vanoni 1975, Simons and Senturk 1977): water discharge, Q; solid/sediment discharge, Q_s; flow channel bottom width, b; mean fluid flow depth, d; friction factor, f; channel plan geometry, m; depth/hydraulic radius, r; energy gradient, S; mean velocity, V; fluid kinematic viscosity, ν; fluid density, ρ; solid particle density, ρ_s; mean falling velocity, w; geometric mean size of bottom solid material, d_s; geometric standard deviation of bottom solid material, σ_s; and gravitational acceleration constant, g.

It is important to select appropriate independent variables as input data to obtain unique solutions for unknowns (the dependent variables) for a specific problem. Table B.4 provides guidelines for selection of independent variables (Vanoni 1975).

B.1.4 Initiation of Solid Motion

As the flow over a sediment (or in this case sludge and/or salt cake) surface increases from zero, flow-induced forces (lift and drag) acting on the solid particle increase. When these forces exceed the submerged weight of the particle, the solid particles start to move. This critical condition for initiation of motion has been correlated to the velocity using the following relationship (Leliakovsky 1966),

$$V_{critical} = kW^{1/6} \qquad \text{(B.19)}$$

where, $V_{critical}$ = critical velocity to initiate solid particle movement
k = constant
W = dry particle weight in air.

Table B.4. Guidelines for Selection of Independent and Dependent Variables in Alluvial Streams (adopted from Vanoni 1975)

Time Frames	Independent Variables		Dependent Variables	Functional Relationships	
	Properties of Fluid Sediment, and Others	Flow Characteristics		Single Values	Multiple Values for Some Ranges
Short-Term	ν ρ, ρ_s, d_s,σ_s, w, g	Q, d, m	Q_s, b, r, V, s, f	X	
		d, S, m	Q, Q_s, b, r, V, f		X
		r, S, m	Q, Q_s, b, d, V, f		X
		Q, S, m	Q_s, b, d, r, V, f		X
Long-Term	ν, ρ, ρ_s, g	Q, Q_s	m, b, d, r, V, S, f, d_s, σ_s, w,	X	

Subsequently, many researchers, including Shields (1936) and White (1940), correlated the flow intensity controlling initial particle movement and subsequent sediment transport rate to velocity, shear stress, or stream power (product of shear stress and velocity), as summarized by Leliavsky (1966), Henderson (1966), Raudkivi (1967), Vanoni (1975), Graf (1971), Simons and Senturk (1977), Jansen et al. (1979), and Richards (1982). Assuming the initiation of motion is determined by bed shear stress (τ_o), specific weight difference ($\gamma_s - \gamma$) between sediment and water, d_s, ρ, and ν, the following dimensional analysis yields the well known Shields diagram for the initiation of motion (Shields 1936).

$$\frac{\tau_o}{(\gamma_s - \gamma) d_s} = F\left(\frac{U_* d_s}{\nu}\right) \qquad \text{(B.20)}$$

where F = functional relationship
U_* = the velocity shear (τ_0/ρ).

Figure B.2 clearly indicates a significant difference among different particle sizes for the critical shear stresses needed to erode bottom sediments. The most easily erodible sediment is a particle having the particle Reynolds number (R) of around 10, while very small particles (having smaller particle Reynolds number) exhibit greater resistance to being entrained by a given flow. This resistance is mainly due to the cohesiveness of most small particles. Thus, a given flow can clearly segregate specific sized particles by selectively eroding some solid particles. Further, it is not the smallest particles that are eroded first as the flow rate increases from zero.

When flow conditions reach the critical stage of the initiation of motion, some bottom solid particles start to move. Initially, they will roll and slide along the bed with increasing velocity; some will make jumps and hops. With a further increase in velocity, some particles will be suspended by turbulence and

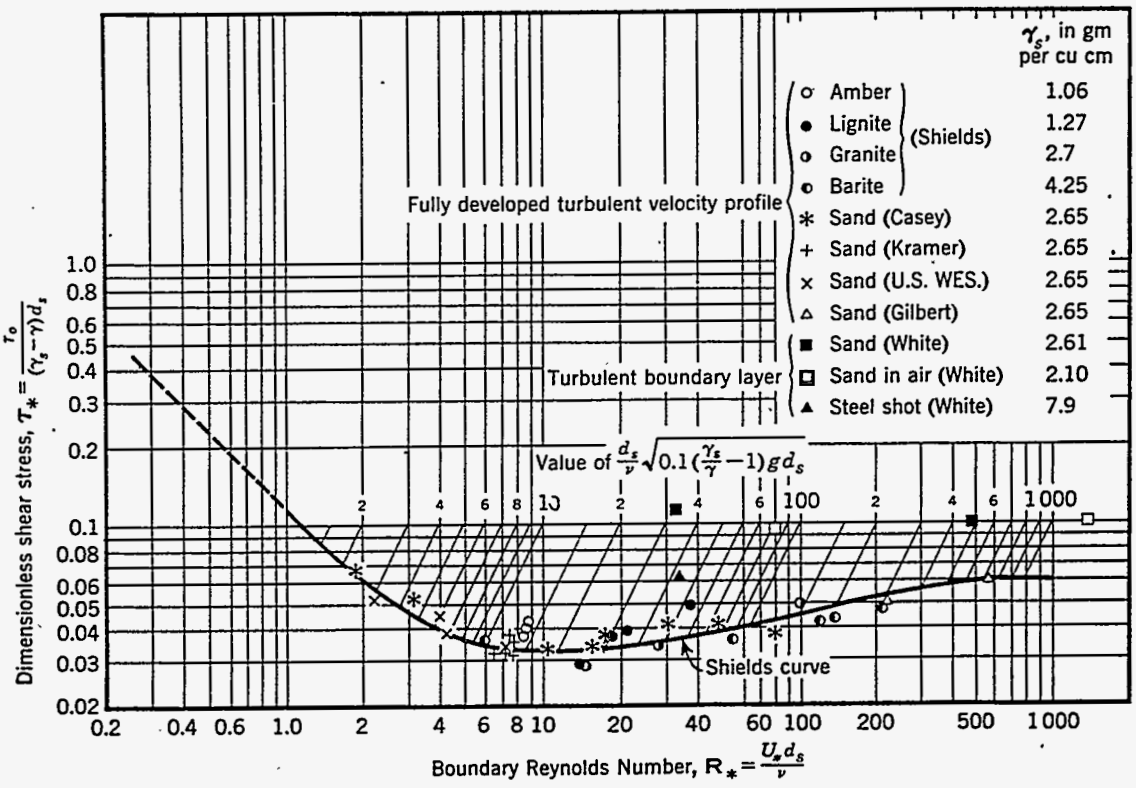

Figure B.2. Shields Diagram (Shields 1936, Vanoni 1975)

move away. The rolling, sliding, hopping, and jumping portion is called bed load, while the remainder that is predominately suspended above the bed and seldom falls back into the interface is called suspended load. Thus, sediment transport is the sum of the bed and suspended loads.

B.1.5. Critical Condition for Cohesive Solids

Unlike non-cohesive solids, the fall velocity of cohesive solids and the critical shear stress for erosion and deposition depend not only on the solid properties (density and diameter), but also on the electrochemical environment of the solid, flow characteristics and solid past history of transport, deposition, and resuspension, (phenomena such as flocculation and consolidation) as described in Vanoni (1975). Few studies have been made that address the initiation of movement of cohesive particles and knowledge of these phenomena are very limited (Krone 1962, Partheniades 1962, Onishi et al. 1993, Onishi 1994b).

Since Sundborg (1956) derived the critical shear stress for cohesive solids, some studies have correlated the stress to shear strength (S_v) and plasticity index (Ip). For example, Dunn (1959) conducted

measurements with sediments ranging from sand to silty clay, and obtained the following relationship for critical shear stress for cohesive sediments with a plasticity index between 5 and 16:

$$\tau_{CR} = 0.001\ (S_v + 180) \cdot \tan\ (30 + 1.73 I_p) \qquad \text{(B.21)}$$

where S_v = Shear Strength
I_p = plasticity index.

The critical shear stress increases with plasticity index, I_p. Some of these studies provide a wide range of critical shear stress for erosion, as shown in Table B.5.

Another important consideration is the formation of aggregates on the critical shear stress. The larger the aggregation, the smaller the critical shear stress for erosion (Krone 1962). The shear strength of various aggregates, based on a San Francisco Bay sediment are shown in Table B.6.

Table B.5. Critical Shear Stresses for Cohesive Sediments

Authors	Critical Shear Stresses N/m^2
Dunn (1959)	0.058 - 0.24
Smerdon and Bearsley (1961)	0.0038 - 0.024
Flaxman (1962)	0.11 - 0.72
Abdel-Rahmann (Vanoni 1975)	0.0072 - 0.043

Note that zero order aggregates are made up of the sediment particle themselves. The first order aggregate is made up with zero aggregates, second order aggregate is made up with first order aggregates, and so on. These values clearly indicate the more the cohesive sediment aggregates, the less able the aggregates become to remaining stuck in the bed sediment, and the lower the critical shear stress for erosion. The transport, deposition and erosion of cohesive sediment will be further discussed in Section B.1.8.

Table B.6. Shear Strength of Aggregates

Orders of Aggregates	Shear strength N/m_2
0	2.2
1	0.39
2	0.14
3	0.14
4	0.082
5	0.036
6	0.020

B.1.6 Bed Forms

The common bed forms are ripples, bars, dunes, transition, flat bed, and antidunes, listed in the general order of their occurrence with increasing velocity, Froude number, and sediment transport rates (Raudkivi 1967; Vanoni 1975; Jansen et al. 1979). Among the bed forms,, ripples are the smallest, with wave lengths and heights up to approximately 30 cm and 3 cm, respectively. Bars have wave lengths and heights comparable to the stream channel width and flow depth. Dunes are larger than ripples, but smaller than bars. With increasing velocity, dunes will disappear from the bed to form a flat bed, thus significantly reducing the friction factor/hydraulic roughness. In the transition from dune to flat bed, the bed is mainly covered by low-amplitude ripples and dunes, interspersed with flat bed. Antidunes have a nearly sinusoidal form with a wave length of $2\pi V^2/g$ and variable height, depending on flow depth and velocity. Antidunes are always accompanied by in-phase waves of the water surface.

Predictions of the bed forms have been studied theoretically, experimentally, or by field observations (Kennedy 1963; Simons and Richardson 1966). Simons and Richardson (1966) provides the bed form prediction as a function of mean particle diameter and stream power (defined as the product of bottom shear stress and velocity).

B.1.7. Solid/Sediment Discharge Rate Formulas

There have been many formulas for calculating solid/sediment discharges of bed materials (mostly non-cohesive sediment), since DuBoys (1879) in the last century presented a relationship between sediment discharge, particle mean diameter, and the shear stress acting on the bed. Many of these formulas correlate the sediment discharge to shear stress, velocity, or stream power as well as fluid and solid properties. For example, DuBoys' formula relates the bed loads to shear stress by (Vanoni 1975)

$$q_s = \chi_o \tau_o (\tau_o - \tau_c) \tag{B.22}$$

where q_s = sediment discharge per unit width (= Q_s/b),
χ_o = coefficient.
τ_o = bed shear stress, and
τ_c = critical bed shear stress for initiation of motion.

The values of τ_c and τ_o are solely functions of a median bed sediment size. Many other formulas, e.g., Meyer-Peter (Meyer-Peter and Muller 1948) and Shields (1936), use a similar concept of correlating the sediment discharge to shear stress. Some relate the sediment discharge directly or indirectly to velocity, including the Einstein bed load function (Einstein 1950) and Colby (1964a,b). Einstein postulated that a sediment particle moves if the instantaneous hydrodynamic lift force exceeds the particle weight, and that the motions should be expressed statistically. A third group of formulas relating to stream power are represented by those of Engelund and Hansen (1967), Ackers and White (1973), and Yang (1973, 1979). Yang hypothesized that the sediment transport rate is related to the rate of energy dissipation, which in turn can be expressed by the stream power (product of velocity and shear stress),

which he called the unit stream power. These formulas have been summarized in many publications (Rouse 1950; Leliavsky 1966; Raudikivi 1967; Graf 1971; Vanoni 1975; Simons and Senturk 1977; Jansen et al. 1979; Richards 1982). Required input data and their output for some formulas are summarized by Nakato (1990), as shown in Table B.7.

Table B.7. Input Data Requirements and Output for Some Sediment Discharge Formulas (Adapted from Nakato 1990)

Sediment Discharge Formula	Independent Variables		Dependent Variables (Output)
	Properties of Fluid Sediment	Flow Characteristics	
Ackers-White	$\nu, \gamma, \gamma_s, D_{35}$	d, d, U_* (or S)	Q_T
Einstein-Brown	$\nu, \gamma, \gamma_s, D_{50}$	U_{*b} (or r_b and S)	Q_B
Engelund-Fredsoe	$\nu, \gamma, \gamma_s, D_{50}$	V, d, S	Q_B and Q_S
Engelund-Hansen	γ, γ_s, D_{50}	V, U_* (or r_b and S)	Q_T
Inglis-Lacey	$\nu, \gamma, \gamma_s, D_{50}$	V, d	Q_T
Karim	$\nu, \gamma, \gamma_s, D_{50}$	q, d, S	Q_T
Meyer-Peter-Muller	$\nu, \gamma, \gamma_s, D_{90}, D_{si}, P_i$	V, U_{*b} (or r_b and S)	Q_B
Rijn	$\nu, \gamma, \gamma_s, D_{16}, D_{50}, D_{84}, D_{90}$	V, d, S	Q_B and Q_S
Schoklitsch	D_{si}, P_i	q, S	Q_B
Toffaleti	ν, T, $\gamma, \gamma_s, D_{65}, D_{si}, P_i$	V, d, S	Q_B and Q_S
Yang	$\nu, \gamma, \gamma_s, D_{50}$	V, d, S	Q_T

A major problem the engineer faces is not how to calculate the sediment discharge for given hydraulic and sediment parameters, but which sediment discharge formula to use. The following 23 methods are representative sediment discharge formulas applicable to non-cohesive bed sediment under uniform steady conditions and are reviewed by Onishi (1994a):

DuBoys (DuBoys 1879; Vanoni 1975)
Schoklitsch (Shulits 1935; Vanoni 1975)
Shields (Shields 1936; Vanoni 1975)
Meyer-Peter (Meyer-Peter and Muller 1948; Vanoni 1975)
Meyer-Peter-Muller (Meyer-Peter and Muller 1948)
Einstein-Brown (Brown 1950)

Einstein Bed Load Function (Einstein 1950)
Laursen (1958)
Colby (1964a,b)
Bagnold (1966)
Blench Regime Formula (Blench 1966)
Engelund-Hansen (Engelund and Hansen 1967)
Inglis-Lacey (Inglis 1968)
Toffaleti (1969)
Graf (1971)
Shen-Hung (Shen and Hung 1972)
Ackers-White (Ackers and White 1973)
Yang (1973, 1979)
Maddock (1976)
Engelund-Fredsoe (Engelund and Fredsoe 1976)
Karim (Karim and Kennedy 1981)
Brownlie (1981a, b)
Rijn (1984a, b)

Vanoni (1975) compared the following 13 sediment discharge formulas against observed data for the Colorado River at Taylor's Ferry, Colorado, and Niobrara River near Colby, Nebraska: DuBoys, Schoklitsch, Shields, Meyer-Peter, Meyer-Peter-Muller, Einstein-Brown, Einstein Bed Load Function, Laursen, Colby, Blench Regime Formula, Engelund-Hansen, Inglis-Lacey and Toffaleti formulas. These comparisons show large variation (several orders of magnitude) in predictions among these formulas and from field data (see Figure B.3 for the Colorado River). The Toffaleti, Colby, Inglis-Lacey, and Engelund-Hansen formulas predicted values closer to the measured data for these river conditions than other sediment discharge formulas.

D_{16}, D_{35}, D_{84}, D_{90}, and D_{si} = bed sediment diameter such that 16, 35, 84, 90, and Si percent are finer, respectively
Q_T, Q_B, and Q_S = total, bed, and suspended sediment load, respectively
P_i = ith fraction of bed material group
q = water discharge per unit channel width
γ_b = hydraulic radius of bed only (cross sectional area of flow divided by wetted perimeter)
T = water temperature, °K,
U_* = shear velocity
U_{*b} = shear velocity evaluated at bed surface

Other parameters are as previously defined.

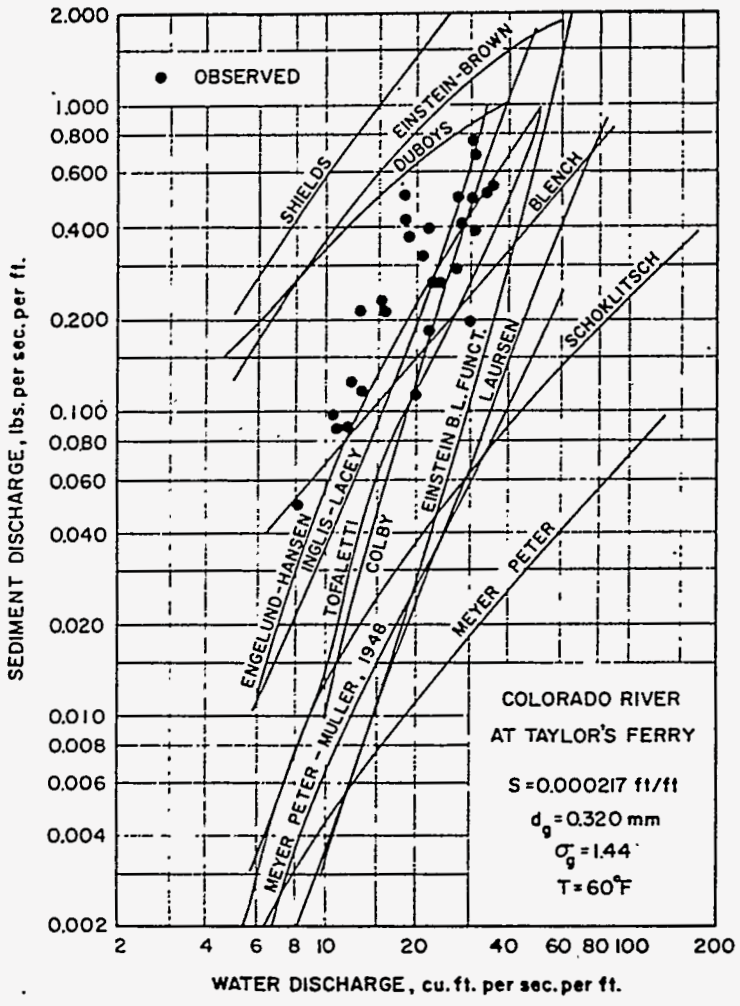

Figure B.3. Comparison of Predicted and Observed Total Sediment Discharges for the Colorado River at Taylor's Ferry, Colorado (Vanoni, 1975)

Yang and Molinas (1982) compared the following six formulas with 1259 data sets from laboratory flumes and five rivers: Colby, Engelund-Hansen, Shen-Hung, Ackers-White, Maddock, and Yang. The five rivers were the Niobrara River in Nebraska, the Middle Loup River in Nebraska, Mountain Creek in South Carolina, the Rio Grande in New Mexico, and the Mississippi River in Missouri. All six formulas predicted the total sediment load in the rivers within approximately 200% error, as shown in Table B.8, showing both mean values and the distributions of the ratio of the computed to the measured total sediment load. Among them, the Yang and Shen-Hung formulas show better results, followed by Ackers-White, and Engelund-Hansen. However, the Shen-Hung formula is limited to small rivers because it uses a dimensionally nonhomogeneous parameter in the formula (Yang and Molinas 1982).

Table B.8. Evaluation of Six Sediment Discharge Formulas for Five Rivers (Yang and Molinas 1982)

Sediment Discharge Formulas	Ratio of Computed Values to the Measured Total Sediment Load					
	Mean	Frequency of Occurrence (%)				Standard Deviation
		In ratio of 0.75-1.25 (%)	in 0.5-1.5 (%)	0.25-1.75 (%)	0.5-2.0 (%)	
Ackers-White	1.50	31	61	75	80	0.80
Corby	0.61	13	29	71	33	0.66
Engelund-Hansen	1.51	34	58	72	79	0.75
Maddock	0.49	24	43	56	45	0.48
Shen-Hung	1.18	43	71	80	81	0.61
Yang	1.12	50	76	95	88	0.44

A series of performance tests of sediment discharge formulas by many researchers clearly demonstrates a wide range of variations and limitations for these formulas. Among the 23 formulas discussed, the Engelund-Hansen, Inglis-Lacey, Toffaleti, Ackers-White, and Yang formulas show the most acceptable results over a wide range of flow and sediment conditions (Onishi 1994a). However, users must be very careful to select several formulas and test them for a specific application.

B.1.8 Solid transport, Deposition and Resuspension

B.1.8.1 Solid Transport

Solid/sediment transport is commonly expressed by the following advection-diffusion equation (National Research Council 1993; Onishi 1994a, 1994b):

$$\frac{\partial c}{\partial t}+\nabla\cdot(uc) = \nabla\cdot(\epsilon\nabla c)+G_s \qquad \text{(B.23)}$$

where c = solid concentration
ϵ = dispersion coefficient
G_s = solid erosion and deposition rates.

The erosion and deposition rates are usually formulated separately for cohesive and non-cohesive sediments (Onishi et al. 1993). The most commonly used methods to determine the sediment erosion and deposition rates are discussed as follows (National Research Council 1993; Onishi 1994a).

B.1.8.2 Solid Deposition and Erosion

Particle erosion and deposition depends not only on fluid flow and solid characteristics, but also on actual concentration of solids in the fluid.

For non-cohesive solids:

$$G_s = \frac{Q_s - Q_{sa}}{\Delta A} \quad \text{for erosion} \tag{B.24}$$

$$G_s = \frac{Q_{sa} - Q_s}{\Delta A} \quad \text{for deposition} \tag{B.25}$$

where ΔA = unit bottom surface area to and from which solid will be deposited or eroded
Q_s = sediment transport capacity for the given flow per unit surface area
Q_{sa} = actual sediment transport rate per unit surface area.

A_s can be evaluated by various sediment transport discharge formulas [Einstein (1950), Toffaleti (1969), Ackers and White (1973), Yang (1979) formulas], discussed in Section B.1.7 above.

For cohesive solids (Partheniades 1962; Krone 1962):

$$G_s = M \left(\frac{\tau_o}{\tau_{CR}} - 1\right) \quad \text{for erosion} \tag{B.26}$$

$$G_s = w\ c \left(1 - \frac{\tau_o}{\tau_{CD}}\right) \quad \text{for deposition} \tag{B.27}$$

where, M = erodibility coefficient
w = particle(or agglomerate) fall velocity
τ = bed shear stress
τ_{CD} = critical shear stress for deposition
τ_{CR} = critical shear stress for erosion.

The fall velocity, w in Equation B.27 may be determined by Equation B.2 or B.5, if the solids concentration is relatively low and cohesive solids do not form many aggregates. However, as discussed

in Section B.1.1.5, at higher concentrations (above 300 milligrams per liter), continuing aggregation or break-up of cohesive solids affects the sediment fall velocity. Thus, the fall velocity becomes a function of solids concentration under this condition (See Equations B.6 through B.9).

Teeter (1988) and Krone (1962) conducted experiments specifically to obtain parameters in Equations B.7, B.26 and B.27 with Buzzards Bay sand, and Clinch River (Tennessee) sediments. The erosion and deposition parameters values shown in Tables B.9 and B.10 are obtained by Teeter's experiments.

Table B.9. Cohesive Sediment Erosion Parameters

Erosion Variables	Sediment Sizes mm $0.002<d_s<0.014$	Sediment Sizes mm $0.014<d_s<0.030$	Sediment Sizes mm $0.030<d_s<0.072$
τ_{CR} (N/m^2)	0.0060	0.6 - 0.16	> 0.6
M (g/m^2-s)	4.2×10^{-3}	--	--

Table B.10. Cohesive Sediment Deposition Parameters

Deposition Variables	Sediment Sizes mm $0.002<d_s<0.014$	Sediment Sizes mm $0.014<d_s<0.030$	Sediment Sizes mm $0.030<d_s<0.072$
τ_{CD} , N/m^2	0.043	0.33	0.42
w, cm/s	6.0×10^{-4}	0.104	0.202
A	1.8×10^{-5}	3.2×10^{-3}	6.4×10^{-3}

Many sediment transport and contaminant transport codes available have incorporated these sediment transport, deposition, and erosion formulas to evaluate behavior of sediment and sediment sorbed contaminant, as evaluated and summarized in National Research Council (1993) and Onishi (1994a,b).

B.2 References

References for this appendix are contained in the Chapter 7 reference list.

Appendix C

Analysis to Determine the Volume of Liquid Entrained by a Single Air-Lift Circulator

Appendix C
Analysis to Determine the Volume of Liquid Entrained by a Single Air-Lift Circulator

This analysis was performed to determined whether an air-lift circulator is capable of entraining 2100 gpm of liquid. Analysis requires understanding the geometric features of an air-lift circulator and applying correlations to predict the flow in the appropriate geometry. This discussion is organized as follows. The geometry of the air-lift circulator is provided first. Correlations to predict the flow in that geometry follow. The predicted pressure drops, as a function of target gas and liquid flow rates, are provided at the end of the discussion.

C.1 Abstract Representation of the Air-Lift Circulator

Air is supplied at the bottom of an open-ended pipe that is enclosed in a larger diameter shroud, Figure C.1. The larger diameter shroud extends somewhat below the air supply pipe. The buoyant air released from the air supply pipe rises inside the shroud, and in the process entrains some liquid into the bottom of the shroud. The total flow rate of entrained liquid depends on air supply rate, the geometry of the air-lift circulator, and the physical properties of the liquid.

In the Hanford tanks, the system is complicated by the suspended solids contained in the slurry that constitutes the liquid. No specific correlations in the literature predict the pressure drop in suspension of solid-liquid mixtures using gas bubbles. It is assumed the slurry is a liquid with a density and viscosity equal to the slurry density.

This assumption is justified when the suspended particles are relatively small, which is the case of Hanford slurries and sludges. In any case, the assumption is consistent with the goal of the analysis, which is to determine whether the entrained liquid flow rate used in a TEMPEST prediction documented by Eyler (1984) is reasonable. The TEMPEST analysis made similar assumptions regarding flow of the mixture. So, any uncertainty resulting from treating the slurry mixture as a liquid is also embedded in the result of the TEMPEST simulation.

C.2 Method of Analysis

The flow rate inside the shroud may be predicted by recognizing the pressure drop calculated for flow outside the shroud must be equal to the calculated flow inside the shroud. That is, pressures at points 3 and 1 in Figure C.1 can be determined without knowledge of the gas flow rate through an understanding, of single phase flow relations that apply outside the shroud. In addition, the pressure

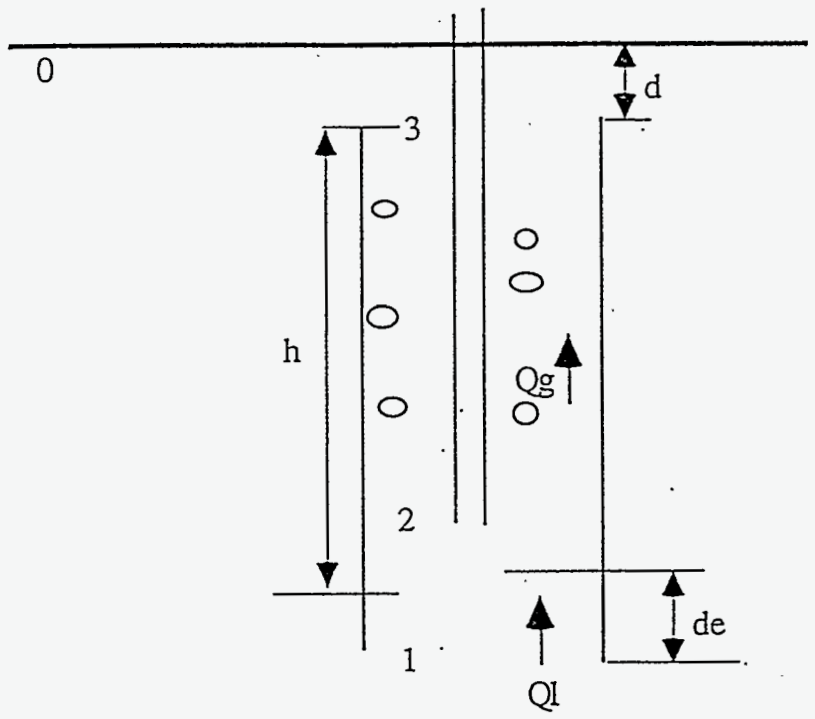

Figure C.1. Schematic Representation of the Air-Lift Circulator

difference between points 3 and 1 depends on the gas and liquid flow rates inside the shroud. If the gas flow rate is known, entrained liquid flow rate will assume the value that ensures pressure differences between points 3 and 1 must be the same when calculated using relations that apply outside the shroud and inside the shroud.

Because no flow losses occur outside the shroud, the pressure drop everywhere outside the air-lift circulator can be predicted using Bernoulli's equation along a stream line connecting the free surface of the liquid and the entrance of the shroud. This equation gives a second relation for the pressure difference between points 1 and 3, $P_1 - P_3$, which depends on the entrained liquid flow rate entering the air-lift circulator.

The pressure drop inside the air-lift circulator can be analyzed by dividing the air-lift circulator into two regions. This first is the region from points 1 to 9 which describes developing single phase flow. The second region is the loss from points 2 to 3, which we will predict using a correlation for gas-liquid flow in a vertical pipe. The sum of the pressure drop in the two regions is the pressure difference between points 1 and 3, $P_1 - P_3$. This pressure difference will depend on the unknown entrained liquid flow rate Q_l, the known gas flow rate Q_g, and the air-lift circulator geometry.

The two methods of relating the pressure drop $P_1 - P_3$ to the entrained liquid flow rate, Q_1 result in two equations and two unknowns. Thus, the system can be manipulated to obtain the solution for the entrained liquid flow rate.

The pressure difference between the free surface and the shroud entrance, point 0 and point 1 respectively, is described by Bernoulli's equation for single phase flow:

$$P_1 - P_0 = \rho_L g(h+d) - \tfrac{1}{2}\rho_L V_{L1}^2 = \rho_L g(h+d) - \rho_L Q_{L1}^2 \Big/ 2A^2 \qquad \text{(C.1)}$$

where P_1 = the static pressure at point 1
P_0 = the static pressure at point 0
ρ_L = the density of the slurry between the surface and point 1
h = the height of the external tube or shroud
d = the immersion depth of the top of the tube
g = the acceleration due to gravity
A = the cross-sectional area of the shroud
Q_{L1} = the entrained liquid, or slurry, flow rate
V_L = the velocity of the liquid at point 1.

The static pressure at the exit of a pipe with subsonic flow is equal to the local ambient pressure. So, the pressure difference between the surface and point three varies hydrostatically. This statement can be quantified by:

$$P_3 - P_0 = \rho_L g(d) \qquad \text{(C.2)}$$

where P3 = the static pressure at point 3.

Taking the sum of (C.1) and (C.2) results in

$$P_1 - P_3 = \rho_L gh - \tfrac{1}{2}\rho_L V_{L1}^2 = \rho_L gh - \rho_L Q_{L1}^2 \Big/ 2A^2 \qquad \text{(C.3)}$$

Equation (C.3) may be used to determine the pressure drop based on flow that occurs outside the air-lift circulator.

The pressure drop between points 1 and 2 cannot be determined exactly, but may be bounded. The upper bound is estimated from loss coefficients for flow at a pipe entry and the frictional loss for fully developed flow in the short entry region.

$$P_1 - P_2 = \rho_1 g(d_e) + \left(K_{loss} + f d_e / D\right) \rho_1 V_1^2 / 2 \qquad \text{(C.4)}$$

where K_{loss} = the loss coefficient associated with developing flow
d_e = the distance between the air-lift circulator entrance and the exit of the gas supply tube (see Figure C.1)
D = the diameter of the shroud
f = the friction factor in single phase flow.

The lower bound is $P_1 - P_2 = 0$. The upper bound estimate will under predict the entrained flow rate, and is used in this appendix.

More refined estimates are not possible because published values of K_{loss} account for the entire loss that accrues during flow development. In the case of an air-lift circulator, the liquid flow is not fully developed at the air injection point, so the pressure loss is smaller.

The pressure drop between points 2 and 3 must be predicted based on correlations for the pressure drop in a gas-liquid flow. Several correlations to predict the pressure drop in the gas-liquid flow in vertical circular pipes are published in Govier and Aziz (1987). However, Govier and Aziz recommend the correlations for gas-liquid mixtures may be applied to predict flow of crude oil, which often contains some entrained particulate.

Because of the existence of the air-lift supply tube inside the shroud, the air-lift circulator is not a circular pipe. Instead, it is an annulus with a very small internal pipe. Govier and Aziz provide no recommendations to account for the difference between annular flow and pipe flow. To estimate the flow in the annulus, the correlations for pipe flow were adapted by substituting the hydraulic diameter of the annulus for the diameter of the pipe. This method is commonly recommended in flow of single phase fluids.

The hydraulic diameter D_h is defined as $D_h = 4A/P$ where A is the cross-sectional area of the flow region and P is the perimeter of the flow region. For a circular pipe, the hydraulic diameter and the diameter are equal.

Only one of the correlations recommended in Govier and Aziz (1987) applies to large diameter pipes. This correlation was the one recommended by Ros (1961) and extended by Duns and Ros (1963). This correlation was selected to predict the entrained liquid flow rate in the air-lift circulator.

The Ros correlation involves numerous intermediate steps to calculate the pressure drop. The procedure is described in an order that facilitates calculation, rather than one that describes the phenomenology of 2-phase flow.

The Ros correlation states that the pressure drop ΔP in the 2-phase region can be decomposed into three parts. These parts are the hydrostatic pressure head ΔP_{HH}, the change in kinetic energy with height ΔP_{KE}, and the frictional pressure loss, Δpf. The sum of the three contributions equals the total pressure drop. So,

$$\Delta P = \Delta P_{HH} + \Delta P_{KE} + \Delta P_f \tag{C.5}$$

The hydrostatic head can be calculated using

$$\Delta P_{HH} = \left[E_g \rho_g + (1 - E_g)\rho_1\right] gz \tag{C.6}$$

where E_g = the average volume fraction of the gas in the 2-phase region
ρ_g = the density of the gas in the 2-phase region
ρ_l = the density of the liquid in the 2-phase region
z = the length of the region containing both liquid and gas phases.

For most gas-liquid pipe flows, including the one under consideration, Ros recommends neglecting the kinetic energy change. So, $\Delta P_{KE} = 0$.

The frictional pressure drop is estimated using

$$\Delta P_f = \frac{2 f_r V_{SL}^2 \rho_L}{D_h}\left(1 + \frac{V_{SG}}{V_{SL}}\right) z \tag{C.7}$$

where f_r = the friction factor in gas-liquid flow
V_{SL} = the superficial liquid velocity
V_{SG} = the superficial gas velocity.

The superficial liquid and gas velocities may be determined using $V_{SG} = \frac{Q_g}{A}$ and $V_{SL} = \frac{Q_L}{A}$, respectively, where Q_{LS} the volumetric flow rate of liquid and Q_g, is the volumetric flow rate of gas.

To evaluate (C.6), and (C.7), a model is required to predict the gas volume fraction E_g and the friction factor f_r in a vertical gas-liquid flow. The procedure to predict them follows.

The first step of the procedure requires specifying the flow rates of the liquid and gas phase and determining the physical properties of both phases. The second step involves computing the magnitude of four dimensionless parameters:

The liquid velocity number

$$N_{VL} = V_{SL}\sqrt[4]{\rho_L / g\sigma}, \tag{C.8}$$

The gas velocity number

$$N_{VG} = V_{SG}\sqrt[4]{\rho_L / g\sigma}, \tag{C.9}$$

The pipe diameter number

$$N_D = D_H\sqrt[4]{\rho_L / g\sigma}, \tag{C.10}$$

and the liquid viscosity number

$$N_L = \mu_L\sqrt[4]{g / \rho_L\sigma^3} \tag{C.11}$$

where σ = the surface tension of the slurry in air
μ_L = the viscosity of the slurry.

The next step is to identify the flow regime. For brevity, this discussion will focus on the region referred to as Region I by Ros. This region is also referred to as the bubble and slug or froth flow regime. In this regime, the liquid phase is continuous; the gas phase is discontinuous and forms bubbles. The focus will be on this region because it is based on data for a range of pipe diameters that includes those of the air-lift circulators.

Region I occurs when $N_{vg} < L_1 + L_2 N_{VL}$, where L_1 and L_2 are functions of N_D. The functional relation is illustrated in Govier and Aziz (1987). The flow in the air-lift circulator is predicted to fall in this region. The friction factor is calculated as follows. First, the slip number, N_s, is calculated using:

$$N_S = F_1 + F_2 N_{VL} + F_3' \left(\frac{N_{VG}}{1 + N_{VL}} \right) \quad \text{(C.12)}$$

with

$$F_3' = F_3 - \frac{F_4}{N_D} \quad \text{(C.13)}$$

where F_1 = is an empirical constant
F_2 = is an empirical constant
F_3 = is an empirical constant
F_4 = is an empirical constant.

The values of F_1, F_2, F_3, and F_4 are provided as a function of N_L in a figure in Govier and Aziz (1987). The slip velocity, S, is then calculated using

$$S = N_S \Big/ \sqrt[4]{\rho_L \Big/ g\sigma} \quad \text{(C.14)}$$

The gas void fraction E_G may be calculated using

$$S = \frac{V_{SG}}{E_G} - \frac{V_{SL}}{(1 - E_G)} \quad \text{(C.15)}$$

The hydrostatic pressure head may be determined using (C.6).

The remaining steps determine the frictional pressure drop, ΔPf [see Equation (C.7)]. The friction factor is determined using

$$f_r = f_1 \left(\frac{f_2}{f_3} \right) \quad \text{(C.16)}$$

where f_r = is an empirical constant
f_1 = is an empirical constant
f_2 = is an empirical constant
f_3 = is an empirical constant.

The magnitude of f_1, is determined from a figure in Govier and Aziz (1987), which is a modified Moody diagram. The magnitudes of f_2 and f_3 account for hold up effects. The constant f_2 is obtained as a function of $:_1 V_{SG} / V_{SL} N_D^{2/}$ and is shown in a figure in Govier and Aziz (1987). The constant f_3 is determined algebraically using

$$f_3 = 1 + f_1 \sqrt{V_{SG} / 50\ V_{SL}} \tag{C.17}$$

After f_r is determined, it may be used to evaluate the frictional pressure drop using (C.7).

Finally, the pressure drop between points 1 and 3 can be determined using

$$P_1 - P_3 = \rho_1 g(d_e) + \left(K_{loss} + f^{d_e} / D \right) \rho_1 V_1^2 / 2 + \Delta P \tag{C.18}$$

where ΔP is calculated using Equation (C.5).

C.3 Results of Analysis

The procedure described in Section C.2 was applied to verify the entrained flow rate in the air-lift circulator could meet or exceed 2100 gpm used by Eyler (1984). The entrained rate is possible, if the pressure drop inside the air-lift circulator caused by a specific air and liquid flow rate is less than that outside the circulator.

Values of the pressure drop were predicted using the following parameters:

Air flow rate: 50 scfm minimum (George et al. 1996). The lower bound on the entrained liquid flow rate was obtained by applying the ideal gas law to obtain the volumetric flow rate at the hydrostatic pressure at the entrance of the shroud. It was assumed the shroud entrance was submerged 30 ft below the free surface of the liquid. This assumption provided a very conservative value for the air-flow rate because the correlations predict lower liquid entertainment rates for lower air flow rates. The value used was 26.5 cfm.

Temperature: >200°F (George et al. 1996).

Height-of air-lift circulator: 22 ft long and 17 ft long.

Diameter of air-lift circulator shroud: 30 in. (George et al. 1996).

Diameter of air supply line 1 in.

Distance between bottom of air supply line and bottom of air-lift circulator 6 in.

Entrained liquid flow rate used by Eyler (1984): 2100 gpm.

The physical properties used for the entrained fluid were estimated to be equal to those of water at standard conditions. The density of the slurry is expected to exceed this value.

The pressure drop between points 1 and 3 determined using C.3 and the one determined using C.18 are provided in Table C.1; these values correspond to the physical properties just described. In both cases, the pressure drop that would occur when 2100 gpm was entrained in the shroud was less than the pressure drop outside the shroud; that is, the value based on C.18 was less than that calculated using C.3. These calculations imply that 2100 gpm can be entrained for the physical properties evaluated.

The same procedure was used to predict the pressure drop, using all properties described previously, with one modification. The specific gravity of the slurry was assumed to be s.g. = 2, an upper bound estimate for the specific gravity. The flow rate of at least 2100 gpm was also found to be achieved for this specific gravity.

The pressure drops are provided in Table C.2. Higher pressure drops were achieved both inside and outside the shroud; this is a hydrostatic effect. However, the pressure drop inside the shroud was smaller than the drop outside, indicating that more than 2100 gpm of fluid would be entrained.

The pressure drop inside and outside the shroud were then predicted using all properties applied to the predictions in Table C.1, except the viscosity of the liquid was assumed to be 2 centipoise. The pressure drop predictions are provided in Table C.3. The entrained flow rate of 2100 gpm was achieved. In fact, the numerical predictions were entirely insensitive to the viscosity of the fluid in the range applied. This situation is typical of turbulent pipe flows.

This analysis concluded the air-lift circulators will entrain at least 2100 gpm for the range of physical properties anticipated in Hanford tanks. The conclusion suggests that the parameters selected by Eyler (1984) are applicable to predict the suspension of solids in DSTs.

Table C.1. Pressure Drop Predicted Assuming the Slurry has Physical Properties Equal to Water at Standard Conditions

Height of Air-Lift Circulator (ft)	Pressure Drop $P_3 - P_1$ (Pa)	
	Based on C.3	Based on C.18
22	6.57×10^4	6.23×10^4
17	5.04×10^4	4.81×10^4

Table C.2. Pressure Drop Predicted Assuming the Slurry has a Specific Gravity of 2 and Other Properties Same as Table C.1

Height of Air-Lift Circulator (ft)	Pressure Drop $P_3 - P_1$ (Pa)	
	Based on C.3	Based on C.18
22	1.31×10^5	1.26×10^5

Table C.3. Pressure Drop Predicted Assuming the Slurry has a Viscosity of 2 cP and Other Physical Properties Same as Table C.1

Height of Air-Lift Circulator (ft)	Pressure Drop $P_3 - P_1$ (Pa)	
	Based on C.3	Based on C.18
22	6.57×10^4	6.23×10^4

C.4 References

References for this appendix are contained in the Chapter 7 reference list.

Appendix D

Concentration Ratio of Plutonium (IV) Hydroxycarbonate and Plutonium (IV) HydroxyEDTA Complexes

Appendix D
Concentration Ratio of Plutonium (IV) Hydroxycarbonate and Plutonium (IV) HydroxyEDTA Complexes

Concentrations of $Pu(OH)_4(CO_3)_2^{4-}$, and $Pu(OH)EDTA^-$ in a typical waste tank supernatant can be compared to evaluate the significance of organic complexes of Pu(IV). For this purpose, Tank B-109 where the estimated concentration of (EDTA) is about an order of magnitude higher than carbonate concentration was chosen.

The formation of $Pu(OH)_4(CO_3)_2^{4-}$ complex is represented by the reaction:

$$Pu^{4+} + 4OH^- + 2CO_3^{2-} = Pu(OH)_4(CO_3)_2^{4-} \qquad (D.1)$$

According to the mass action law, the concentration of the complex is related to the concentrations of the unbound species by the relationship:

$$[Pu(OH)_4(CO_3)_2^{4-}] = K_1^c[Pu^{4+}][OH^-]^4[CO_3^{2-}]^2 \qquad (D.2)$$

where [ ] represents concentrations, and K_1^c is the conditional equilibrium constant for reaction (D.1).

Experimental data listed in Weigel et al. (1986) indicates that Pu(IV) forms a hydroxy complex with EDTA ligand. The stoichimetry of this complex has been indicated to be $Pu(OH)EDTA^-$. This complex is the only known Pu-EDTA complex and at present, no evidence of other Pu-EDTA complexes exists. The formation of $Pu(OH)EDTA^-$ complex from unbound component reactant species can be represented by the reaction:

$$Pu^{4+} + OH^- + EDTA^{4-} = Pu(OH)EDTA^- \qquad (D.3)$$

The concentration of $Pu(OH)EDTA^-$ is related to the unbound reactant species by the relationship:

$$[Pu(OH)EDTA^-] = K_3^c[Pu^{4+}][OH^-][EDTA^{4-}] \qquad (D.4)$$

where [ ] represents concentrations, and K_3^c is the conditional equilibrium constant for reaction (3). The concentration ratio of complexes $[Pu(OH)_4(CO_3)_2^{4-}]$ and $Pu(OH)EDTA^-]$ can be computed using the Equations (D.2) and (D.4):

$$[Pu(OH)_4(CO_3)_2^{4-}]/[Pu(OH)EDTA^-] = K_1^c[Pu^{4+}][OH^-]^4[CO_3^{2-}]^2/K_3^c[Pu^{4+}][OH^-][EDTA^{4-}] \qquad (D.5)$$

This relationship can be furthur simplified to:

$$[Pu(OH)_4(CO_3)_2^{4-}]/[Pu(OH)EDTA^-] = K_1^c[OH^-]^3[CO_3^{2-}]^2/K_3^c[EDTA^{4-}] \quad (D.6)$$

The conditional constants, K_1^c and K_3^c (for ionic strength of 0.2) were calculated from data listed by Yamaguchi et al. (1994) and Katz et al. (1986). Assuming the free (unbound) concentrations of the ligands are equivalent to the total concentrations found in Tank B-109 [OH^-=1.29M, CO_3^{2-} =3.17×10^{-4}M, and EDTA =8.13×10^{-3}], the concentration ratio is computed as:

$$[Pu(OH)_4(CO_3)_2^{4-}]/[Pu(OH)EDTA^-] = 3.02 \times 10^{49}[1.29]^3[3.17 \times 10^{-4}]^2/7.24 \times 10^{16}[8.13 \times 10^{-3}] \quad (D.7)$$

From Equation (D.7) the concentration ratio $[Pu(OH)_4(CO_3)_2^{4-}]/[Pu(OH)EDTA^-]$ is calculated to be 1.1×10^{28}. The magnitude of this ratio indicates that in tank supernatants (in which carbonate concentrations are typically higher than concentrations of organics, such as EDTA), the dominant Pu(IV) species would be Pu-hydroxycarbonate complexes and the concentrations of Pu-organic complexes such as $Pu(OH)EDTA^-$ would be insignificant.

A tank with high EDTA and low CO_3^{2-} concentrations was purposely selected. As shown in Equation (D.6), the ratio of $Pu(OH)_4(CO_3)_2^{4-}$ to $Pu(OH)EDTA^-$ complexes varies as the cube of the free hydroxide, square of the free carbonate, and inversely with the free EDTA concentrations. Tanks with low hydroxide and carbonate, but high EDTA supernatant concentrations, would lower the ratio, but it would take an unrealistic combination of these three variables (a condition not encountered so far in Hanford tank supernatants) to lower the ratio to a point where $Pu(OH)EDTA^-$ complex becomes significant.

D.1 References

References for this appendix are contained in the Chapter 7 reference list.

Appendix E

Laboratory Experiments to Support Criticality Issues

Appendix E
Laboratory Experiments to Support Criticality Issues

A detailed review of Pu chemistry, as it relates to criticality issues, was presented in Section 2.0. All the available data reviewed indicated that Pu in Hanford Site fuel reprocessing waste streams can potentially undergo three different types of reactions. These were, precipitation as a distinct solid phase, precipitation as a solid solution with other components that are present in certain specific process-dependent waste streams (La, Bi, and Zr), and adsorption onto major hydroxide or oxyhydroxide components such as Al, Fe, Cr, and Mn. The available tank characterization data does not contain details on the speciation of plutonium in the waste phases (supernate, salt cake, and sludge). Therefore, the waste stream analyses were even less detailed, subsequent changes during aging in the tanks are largely uncharacterized, and no definite conclusion could be reached about the dominant chemical reactions and phase partitioning of plutonium in current waste tank environments. The review of plutonium chemistry relevant to waste tank environment raised the following questions:

1. During neutralization of the wastes (for typical compositions of Hanford Site waste, see Agnew 1995), does plutonium form chemical bonds with the neutron absorbers (mostly iron and aluminum hydroxides) through mainly adsorption reactions?

2. To what extent does Pu form solid solutions with compatible components, such as La, Bi, and Zr, upon neutralization of waste streams?

3. Because Hanford Site waste streams were apparently oversaturated with respect to $PuO_2 \cdot xH_2O$, did Pu precipitate as a distinct solid phase (coagulated by the large masses of iron and aluminum hydroxides)?

4. Does aging of the sludge solids release plutonium from neutron absorbers into separate solid phases that could settle out during retrieval?

5. What is the nature of aged solid phases, that is, the extent to which Fe and Al hydroxides have converted to oxyhydroxides or oxides during decades of higher temperature aging in waste tanks?

6. What are the likely particle size distributions of neutron absorbing Al and Fe solid phases, and, if present, the distinct particles of $PuO_2 \cdot xH_2O$?

A set of experiments is being proposed to answer these important questions.

E.1 Adsorption Experiments

To answer the first question and to reduce the differences that are likely to occur in interpreting the results of the experiments, the test plan should eliminate the possibility of forming separate plutonium phases that do not contain neutron absorbers. Thus the concentration of plutonium in the test solutions should be far below the expected solubility limit for hydrated plutonium oxide under the conditions to be studied. Also, no metal ions other than neutron absorbers (Fe or Al) should be present. The solutions should simulate the $NaNO_3$, $NaNO_2$, Na_2CO_3, and NaOH concentrations present in the neutralized waste stream solutions. Two sets of experiments need to be conducted, with and without the presence of Na_2CO_3, to determine whether in a typical Hanford waste stream environment, adsorption is likely to be a dominant mechanism. A measured lowering of the plutonium concentration in a solution that is known to be undersaturated with respect to $PuO_2 \cdot xH_2O$ during contact with iron or aluminum precipitate (formed before the plutonium is added) would prove that chemical bonding occurred between plutonium and the neutron absorbers. If adsorption does occur, aging the mixtures over a period of months, and then performing desorption measurements on the solids, would indicate the strength of the plutonium bonding to the neutron absorbers (mainly Al and Fe hydroxides).

A second test would start with the Pu, Al and Fe in acid solution. The next step would be to perform the neutralization reaction using NaOH. The resultant Pu solution, as well as the solids, would be analyzed for Pu concentration and solid morphology, mineralogy, and particle size, respectively. The slurry would be aged at a higher temperature in the presence of air. After set times, the Pu in solution and within solid particles would be measured again to identify changes. Specific changes of interest include amorphous solids turning into crystalline material, particle sizes increasing with time, and an increase or decrease in concentration of plutonium in the solution. Care would be needed to keep the slurry pH constant; or at least the effects of pH (and other variables) would have to be considered when interpreting the change in plutonium concentration in the solution.

E.2 Solid-Solution Formation Experiments

Experiments would be set up to test the potential solid solution formation of Pu with waste stream components, such as $ZrO(NO_3)_2$, $La(NO_3)_3$, and $Bi(NO_3)_3$. Neutralization experiments would be conducted with NaOH and Na_2CO_3 solutions with $NaNO_2$ as the holding reductant. These tests would not include all the other tank components, such as Al, Fe, Cr, Mn, and PO_4.

At least one additional experiment would use a Hanford Site tank waste composite that includes ligands, such as OH^-, NO_3^-, NO_2^-, CO_3^{2-}, F^-, Cl^-, PO_4^{3-}, SO_4^{2-} and acetate, and metal ion components, such as Na, Al, Si, Fe, Bi, K, Zr, Mg, Ca, Sr, Cr, Mn, Ni, B, Ce, Pb, and U in proportions matching overall Hanford Site tank waste from a given process such as bismuth phosphate or zirconium decladding processes. If warranted, several specific waste streams could be simulated using stable components traced with Pu.

Following precipitation, aliquots of the precipitate would be aged at room temperature and at 90°C. Ultra-filtered sample solutions would be analyzed periodically for up to one year for Pu concentration. After six months and again after one year, solid samples would be separated by a float/sink technique and analyzed using TEM/SEM/EDAX to determine whether the Pu is hetero- or homogeneous; the bulk and surface morphology, primary particle size, and mineralogy of the major constituents; and the association of plutonium with the various particles within the precipitate matrix. This process assumes that not enough plutonium will be present to observe discrete plutonium-rich particles. (TEM and SEM require about 0.1% by weight of an element to "see" identify) Settling studies would be performed to determine if plutonium preferentially reports to more- or less-buoyant phases. These characterization tests would be used to determine the extent to which plutonium is likely to partition into solid solution phases (especially in the first experiments with a simple set of components). These tests would also be used to determine the extent to which plutonium would associate with particular types and sizes of solid phases in the waste tank environment after acid metal-rich waste streams are neutralized and aged.

E.3 Plutonium Solid Phase Formation Experiments

Hanford waste streams apparently were oversaturated with respect to $PuO_2 \cdot xH_2O$. Therefore, Pu could have precipitated as a distinct solid phase and been coagulated by the large masses of Fe and Al hydroxides. A set of experiments may be conducted with solutions oversaturated with respect to $PuO_2 \cdot xH_2O$ and containing $Fe(NO_3)_3$, and $Al(NO_3)_3$ and $NaNO_2$. These solutions would be neutralized with NaOH and Na_2CO_3. Aliquots of the resulting precipitates would be examined before and after aging at room temperature and at 90°C using the TEM/SEM/EDAX techniques.

Because reverse strike (acidic stream added to basic solution) was also used to neutralize some of the Hanford Site waste streams, a reverse strike experiment may be conducted. In the reverse strike experiment, pH would be adjusted by adding a simulated acid waste stream to concentrated NaOH in the presence of $NaNO_2$ as a holding reductant. The precipitate would then be examined using the same methods used for the precipitate produced by adding caustic to the simulated acid waste to determine the nature of resulting Pu solid phase.

Following precipitation, the precipitate would be aged at room temperature and 90°C. Ultra- filtered sample solutions would be analyzed periodically for up to one year for Pu concentration. After six months and again after one year, solid samples would be separated by float/sink technique and analyzed using TEM/SEM/EDAX to determine Pu hetero/homogeneity within the precipitate matrix. Settling studies would be performed to determine the particle size distribution and whether plutonium preferentially reports to more- or less-buoyant phases or separates out into a distinct solid phase.

E.4 Tests on Actual Hanford Waste Tank Sludges

To more fully answer questions 4 through 6, it would be ideal to conduct tests on actual Hanford Site waste tank sludges. The results would then be compared to the results obtained using the simulated waste stream. Using physical separation methods, such as sink/float, any plutonium solid phases that

are present would be expected to separate into the heavy (sink) fraction. Measuring plutonium in the fractions would determine where the plutonium would likely end up in settling solids. The measurements also would be used to characterize the plutonium-rich fractions. The plutonium concentration would be expected to increase enough in the plutonium-rich fractions following separation from the dominant, but less dense, sludge matrix that the plutonium itself might be seen by TEM/SEM/EDAX. This result would allow acquisition of much information specific to plutonium. Such characterization would also potentially resolve the question about whether aging of sludge solids causes a concomitant release of plutonium from neutron absorbers into separate solid phases that could preferentially settle out during retrieval.

Characterization of the major sludge components using analytical techniques, such as selective extraction, x-ray diffraction, and particle size distribution, also would help answer the following questions related to the nature of aged solid phases.

- To what extent have Fe and Al hydroxides converted to more crystalline oxyhydroxides or oxides during decades of high-temperature aging in waste tanks?

- What are the likely particle size distributions of neutron-absorbing aluminum and iron solid phases and, if present $PuO_2 \cdot xH_2O$?

Data obtained by these characterizations would be used to validate the data obtained through bench-scale tests described in Sections E.1 through E.3.

E.5 References

References for this appendix are contained in the Chapter 7 reference list.

Appendix F

Limited Solubility Solid Phases in Hanford Waste Tank Sludges

Appendix F
Limited Solubility Solid Phases in Hanford Waste Tank Sludges

F.1 Hanford Sludge Characterization Studies

The high level waste (HLW) generated during the Pu separation process was rapidly neutralized (caustic strike—direct or reverse) before storage in waste tanks. Direct caustic strike involved adding caustic (sodium hydroxide containing unknown concentrations of sodium carbonate) to the waste; reverse caustic strike involved titrating the acidic waste into a caustic solution. Experimental data from literature indicate that such rapid neutralization of Fe and Al containing acidic solutions results in the formation of microcrystalline/X-ray amorphous compounds of limited solubilities. These compounds may consist of hydroxides, silicates, phosphates, and carbonates, depending on the types and concentrations of various ligands present in the waste streams. In addition to Fe and Al, other dissolved metals such as Bi, Ce, Cr, La, Mn, Pb, Ni, U, and Zr that were present in the acid waste streams upon neutralization may have precipitated as compounds of limited solubilities (hydroxides, oxyhydroxides, silicates, and phosphates).

Recently, sludge samples from a number of Hanford waste tanks have been collected and characterized according to their physical and chemical properties (Colton et al. 1994, Liu et al. 1995, Lumetta et al. 1996, Temer and Villareal 1995, 1996). These tanks have been categorized based on the major type of wastes being stored (Hill et al. 1995). The waste types and the grouping of these sludge-characterized tanks (19 SST, and 4 DST) are tabulated (Tables F.1 and F.2). According to Hill et al. (1995), group I (consisting of 22 SST) is the most significant category of tanks because it contains (by volume) 37% of salt cake, 12% of sludge, 21% of supernatant, 42% of interstitial liquid, and 28% of the total waste volume of all the 149 single-shell tanks.

The characterization of sludges from 21 SST and 4 DST, conducted by Colton (1994), Liu et al. (1995), Lumetta et al. (1996), Temer and Villareal (1995, 1996), consisted of measuring physical properties such as the settling properties and size distribution of particles. Also, the chemical characterization of sludges included total chemical and radiological analyses, solubilities in water and in an alkaline solution, compound identification using x-ray and electron diffraction, and chemical analyses using electron beam techniques (scanning and transmission electron microscopy with x-ray analysis). Both water soluble and insoluble solid phases were identified in these characterization studies. However, only data collected about water-insoluble solid compounds (from sludges) are listed in Table F.3.

The data show that Al in Hanford waste tank sludges may exist in a number of compounds of limited solubilities, such as aluminum hydroxide, boehmite [α-AlOOH], amorphous and crystalline alumino-silicates of variable composition, sodium aluminate [$NaAl(OH)_4$], variscite [$AlPO_4 \cdot 2H_2O$], Cr-substituted gibbsite[$Al_{(1-x)}Cr_x(OH)_3$], and cancrinite [$Na_4Al_3(SiO_4)_3CO_3$].

Table F.1. Types of Wastes Stored in Selected Single- and Double-Shell Hanford Tanks

SORWT Group[a]	Tank #	Waste types[b]				Watch List Status[c]
		Primary	Secondary	Tertiary	Other	
I	S-107	R	EB	CW	IX-MIX	N
III	BY-104	TBP-F	EB-ITS	CW	IX	F
III	BY-110	TBP-F	EB-ITS	1C	CW	F
IV	S-104	R	-	-	-	N
IV	SX-108	R	-	-	-	H
V	BX-105	TBP	CW	IX	EB	N
V	BX-109	TBP	CW	1C	IX	N
VII	B-202	224	-	-	-	N
X	C-107	1C	CW	SRS	-	N
X	T-107	1C	CW	R	LW	F
X	U-110	1C	CW	R	LW	N
XII	BX-107	1C	TBP	CW	IX	N
XIII	C-108	TBP-F	1C	CW	OWW	F
XIII	C-109	TBP-F	1C	CW	IX	F
XIII	C-112	TBP-F	1C	CW	IX	F
XV	T-111	2C	224	DW	-	O
XVI	B-110	2C	5-6	FP	IX	N
XVI	B-111	2C	5-6	FP	IX	N
XXII	TY-104	TBP	1C-F	DW	MIX-R	F
Ungrouped	B-104	2C	EB	TBP	1C	N
Ungrouped	T-104	1C	-	-	-	N
DS tank	AW-105	PL	CWR	EB	DW	N
DS tank	SY-101	R	EB	DW	CW	G
DS tank	SY-102	DW	Z	-	-	N
DS tank	SY-103	R	EB	DW	CW	G

(a) Groupings based on Hill et al. (1995)
(b) See Table F.2 for waste definitions. Tanks may contain wastes from several processes. Primary: Waste contributing to the highest sludge volume, Secondary: Waste to the second highest sludge volume, Tertiary: Waste to the third highest sludge volume, Other: Mixture of wastes contributing lesser sludge volumes.
(c) F: ferrocyanide, G: Gas generation, H: High- heat, N: Non-watch status, O: Organics

Many of these compounds may have formed initially upon caustic additions to the acidic wastes. Some of these compounds may also have formed from alteration of precipitated compounds during decades of aging within the tank environment.

Table F.2. Description of Selected Waste Types Stored in Hanford Waste Tanks

Waste	Description
1C	First decontamination cycle waste from $BiPO_4$ process (~24% is cladding waste)
1C-F	1C waste scavenged with ferrocyanide additions
2C	Second decontamination cycle waste from $BiPO_4$ process
224	Final decontamination waste from $BiPO_4$ process
5-6	Waste from Tank 5-6 at B- plant resulting boil-over from $BiPO_4$ process
CW	Aluminum Cladding waste (after 1964 Zircalloy cladding) from PUREX process
CWR	Cladding (Aluminum and Zircalloy) waste from REDOX process
DW	Decontamination waste from T-plant containing mainly 0.24M $NaNO_2$ solution
EB	Slurry product from the evaporators
EB-ITS	In-tank solidifed EB waste
FP	Fission products waste produced in B Plant and Hot Semiworks
IX	Ion exchange waste from the cesium recovery process at the B Plant
IX-MIX	IX and miscellaneous wastes
LW	Waste from 222-S laboratory
MIX-R	Miscellaneous wastes with R waste (high-level waste from the REDOX process)
OWW	Organic solvent wash waste from the PUREX Plant
PL	Low-level waste from PUREX plant
R	High-level waste from the REDOX process
SRS	Sludge feed from strontium extraction process at the B Plant
TBP	Uranium extraction process waste from U Plant
TBP-F	Uranium extraction process waste from U Plant - scavenged with ferrocyanide additions
Z	Plutonium Finishing Plant waste

F.2 Aluminum-Containing Solid Phases

Precipitation experiments conducted by Barnhisel and Rich (1965) and Hsu (1966) indicated that rapid caustic addition (resulting in neutral or alkaline conditions) to Al-bearing solutions results in precipitation of bayerite [β-$Al(OH)_3$] or nordstrandite [γ-$Al(OH)_3$] or both; whereas, slow caustic titration (with pH conditions below neutral) precipitates gibbsite [α-$Al(OH)_3$]. Hsu (1977) also indicated that if anions, such as phosphate and silicate, are present during neutralization, phases, such as phosphates and silicates, may form instead of hydroxide phases. Other experimental data obtained by Hsu (1966) and Chesworth (1972) showed that neutralization of Al-containing high ionic strength solutions result in the formation of boehmite-like (pseudoboehmite) precipitates. Presence of carboxylic acids also promotes the formation of pseudoboehmite (Kodama and Schnitzer 1980; Violante and Violante 1980; Kwong and Huang 1981; Violante and Huang 1985). Data obtained by Violante and Violante (1980) showed the type of carboxylic acid, the molar ratio of Al to carboxylic acid, and the pH influence the type of aluminum hydroxide precipitates.

This page intentionally left blank.

Compounds		Hanford Wa									
Name	Composition	I	III		IV		V		VII	X	
		S-107	BY-104	BY-110	S-104	SX-108	BX-105	BX-109	B-202	C-107	T-107
Aluminum hydroxide	$Al(OH)_3$			●			●	⊖			
Boehmite	AlOOH	●	●		●	●			⊖	●[b]	●
Aluminosilicate (amor)	variable	⊖	⊕			⊕				⊕	
Aluminosilicate (cryst)	variable				⊖[c]		●				●
Sodium Aluminate	$NaAl(OH)_4$										
Variscite	$AlPO_4 \cdot 2H_2O$										⊖
Cr- gibbsite	$Al_{(1-x)}Cr_x(OH)_3$										
Cancrinite	$Na_4Al_3(SiO_4)_3CO_3$										
Ferrihydrite	$Fe(OH)_3$										
Goethite	α-FeOOH	⊕	⊕	●[f]	⊖	⊕	●	●		●	
Ferric bismuth silicate	$Fe_2Bi(SiO_4)_2OH$			⊕[h]					●[i]		●
Fe- bismuth phosphate	?										⊖
Cr- ferrihydrite	$Fe_{(1-x)}Cr_x(OH)_3$		⊖								
Jacobsite	Fe_2MnO_4					⊕					
Theophrastite	$Ni(OH)_2$		⊖	⊖							
Bismuth Oxide	Bi_2O_3										
Uranyl hydroxide	$UO_2(OH)_2$	●	⊖[n]	●[n]	⊖	●	●	●			●
Calcite/aragonite	$CaCO_3$						⊕				
Hydroxyapatite	$Ca_5(PO_4)_3OH$		●	●				⊕	⊖		
La- Pyrophosphate	$La_4(P_2O_7)_3$										
Zirconium Oxidehydrate	$ZrO_2 \cdot xH_2O$	⊕								⊕	
Pb-hydroxyphosphate	$Pb_5(PO_4)_3OH$									⊕	
Grimaldite	CrOOH			⊕							
Quartz	SiO_2										

●: >10 wt %, ⊕: 2 - 9 wt%, ⊖: <2 wt%. [a] Sort on Radioactive Waste Type (SORWT) Model -applicable to only single shell tanks (Hill et
[f]maghemite (γ-Fe_2O_3), [g]akagenite (β-FeOOH), Fe-silicate (amorphous), [i]Mn-La-Fe-Bi silicate (Temer and Villareal, 1995), [j]$BiPO_4$, [k] $Fe_{(1-x)}M$
Data Sources: AW-105, B-111, BX-107, C-112, S-104, SY-101, SY-102, SY-103, T-104, and T-111 (Liu et al. 1995). B-110, C-109, C-11
B-104, B-202, BX-105, BX-109, C-108, S-104, T-107, and TY-104 Temer and Villarreal, 1995, 1996)

tified in Selected Hanford Waste Tank Sludges

ste Tanks (Characteristic Groups based on SORWT Model[a])														
	XII	XIII			XV	XVI		XXII	Ungrouped		Double Shell Tanks			
U-110	BX-107	C-108	C-109	C-112	T-111	B-110	B-111	TY-104	B-104	T-104	AW-105	SY-101	SY-102	SY-103
●	⊕	●	●	●			⊕			⊕	⊖		⊕	⊕
●			●	⊖							●		●[b]	
	●									●				●
	●	⊖	⊖	⊖[d]			⊖	⊕	⊕	●[e]	⊖		⊖	
⊖												●		
	●									●				
												●	●	⊖
⊕			⊕	⊖			⊖							
	●			●	●	●	●	●		●	⊖		⊖	
⊕		⊕	⊕		●						⊕		⊕[g]	
	●				●		●		●	●				
	⊕					●[j]								
	⊖				⊖					⊖	⊖			
⊕[k]					⊖									
		●	⊕	⊖			⊖	⊖						
⊕[l]	⊕		⊕		⊕		⊖[m]	●						
		⊕		●[n]				●	⊕				⊖	
			⊕[o]	●							⊖			
		●	⊕	●[p]	●			⊖					⊖[q]	
					⊕									
											●			
			⊕											
⊖						⊕								
			⊕	⊖									⊖[r]	

al. 1995). [b]$(Al_2O_3)_x$• y H_2O, [c]K-Al silicate (Temer and Villarreal, 1995), [d]$NaAlSi_3O_8$ and $Al_2Si_2O_5(OH)_4$, [e]Na-Al silicate, n_xOOH, [i]$Bi_{(1-x)}Mn_xO_3$, [m]$Bi_{(1-x)}Cr_x(OH)_3$, [n]β-U_3O_8, [o]$CaSO_4$, [p]hydroxyapatite and $Mg_3(PO_4)_2$, [q]$CaFPO_3 \cdot 2H_2O$, [r]SiO_2• x H_2O (amorphous), 2, and U-110 (Colton et al., 1994). BY-104, BY-110, C-107, S-107, and SX-108 (Lumetta et al. 1996).

Data from the Hanford waste tanks (Table F.3) indicate that boehmite (α-AlOOH) is the dominant Al-bearing solid phase in many of the tanks that have high ionic strength conditions, thus conforming with experimental observations of Hsu (1977) and Chesworth (1972). In waste tanks (U-110, C-109, C-112, AW-105, and SY-102) in which aluminum hydroxide or aluminum silicate phases coexist with boehmite, it likely that all these phases are at equilibrium, or phase conversion may be occuring indicating disequilibrium conditions. In some of the tanks, aluminosilicate phases seem to predominate, indicating the influence of silicate in controlling the nature of precipitating Al-solid phases. It is interesting to note that in tanks BX-107 and T-104, the dominant Al-solid phases are the silicates and phosphate, suggesting the presence of other ligands during the rapid neutralization of waste streams results in solid phases other than hydroxides or oxyhydroxides. Phase stability relationships (Lindsay 1979) suggest that varicite [$AlPO_4 \cdot 2H_2O$] may have existed in certain Hanford waste streams even before the caustic strike. One of the waste tanks (SY-101) contains a sodium aluminate phase. Occurrence of this phase has been attributed to very high hydroxyl concentrations (Liu et al. 1995). Minor to trace amounts of cancrinite has been found in some of the tanks (U-110, C-109, C-112, and B-111). Because of a lack of experimental data, it is difficult to assess whether cancrinite was one of the initial Al-bearing solid phases that precipitated during the neutralization process or formed during the decades-long aging of sludges.

F.3 Iron-Containing Solid Phases

The literature review indicated that a significant amount of data exists about the formation and transformation of iron hydroxides, oxyhydroxides, and oxides. The data has been summarized by Schwertmann and Taylor (1989) and Schwertmann and Cornell (1991). The formation and transformation pathways for various hydrolytic iron compounds are schematically shown in Figure F.1. Available data (Schwertmann and Cornell 1991) indicate the formation of iron hydroxide, oxyhydroxide, and oxide phases depend mainly on Eh-pH conditions, presence of ligands, rate of oxidation, and time and temperature during the aging of precipitates. The data indicate that rapid neutralization of acidic Fe(III) solutions results in the formation of ferrihydrite. Depending on pH and temperature conditions, ferrihydrite is known to transform into either goethite or hematite. This transformation is the most probable pathway for the formation of iron hydroxide and oxyhydroxide compounds in Hanford HLW. When subjected to caustic strikes and concomitant high pH conditions, Fe(III) containing HLW may have initially precipitated ferrihydrite-like compounds. During aging, this precipitate subsequently may have altered to goethite or hematite. Sludge characterization data (Table F.3) show that in a number of waste tanks, goethite is the principal Fe-oxyhydroxide phase. Presence of goethite indicates almost a complete transformation of ferrihydrite in these tank sludges. Other tanks (BX-107, C-112, T-111, B-110, B-111, T-104, and AW-105) contain mainly ferrihydrite or a mixture of ferrihydrite and goethite, suggesting that no or a partial transformation of initially precipitated Fe-hydroxide material. Maghemite (γ-Fe_2O_3) has been identified in Tank BY-110 sludge indicating a transformation pathway either through the initial formation of green rust or magnetite. Also, akaganeite (β-FeOOH) has been found as the principal Fe-bearing phase in sludge from Tank SY-102 indicating partial neutralization and aging in the presence of chloride. Iron also occurs as a ferric bismuth silicate solid phase in a number of tanks (T-107, BX-107, T-111, B-111,B-104, and T-104) that contain

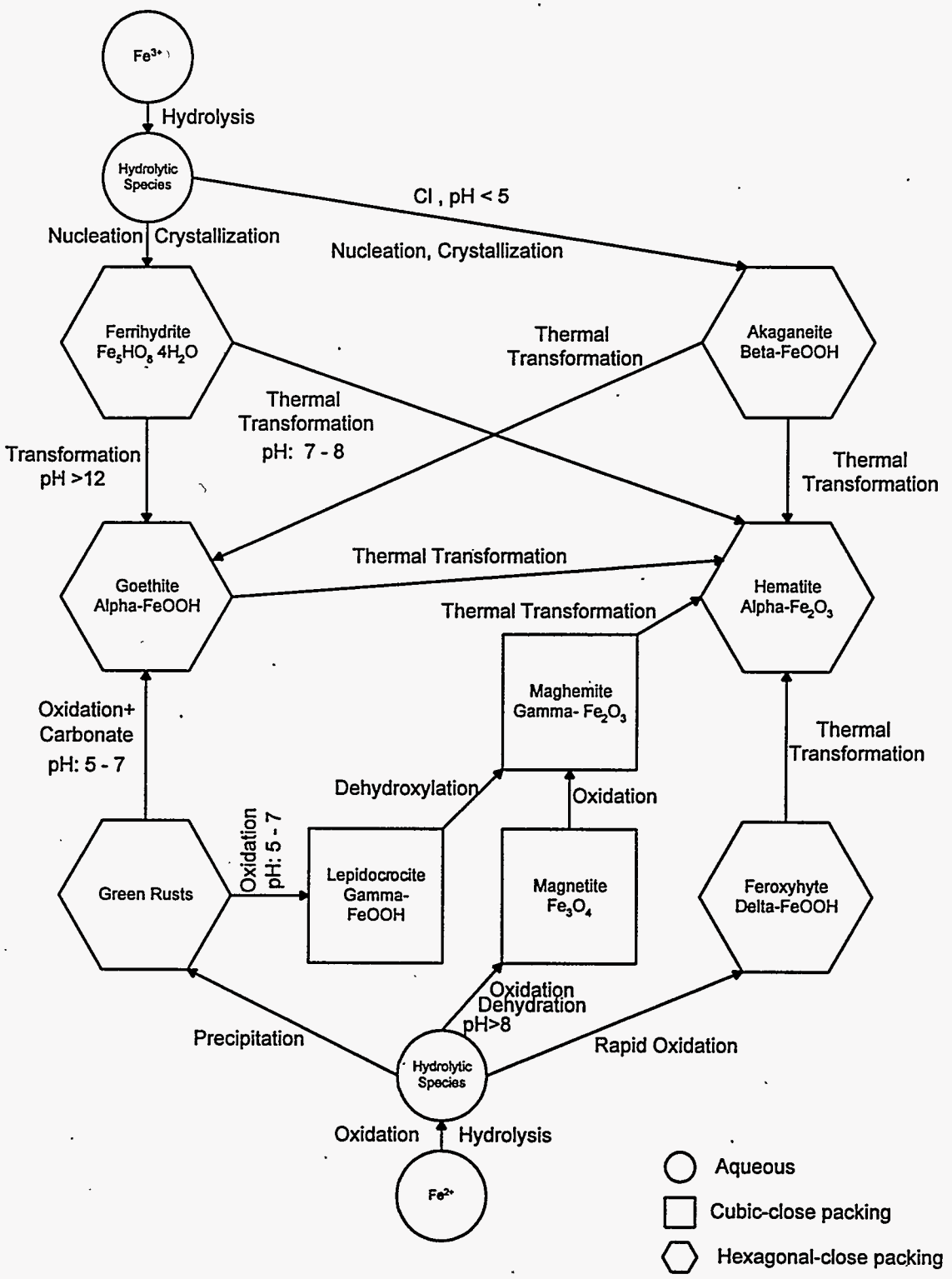

Figure F.1. Formation and Tranformation Pathways of Iron Hydroxides, Oxyhydroxides, and Oxides

neutralized waste streams from the bismuth phosphate process. A few tanks contain minor or trace amounts of Fe-bismuth phosphate. In some cases, ferric bismuth silicate and ferric bismuth phosphate phases coexist with ferric-hydroxide and oxyhydroxide phases. Such coexistence of Fe-bearing solid phases in tank sludges suggests the presence of other cationic and anionic constituents, such as Bi, Si, and PO_4, in waste streams also control the type of Fe solid phases that precipitate.

F.4 Other Solid Phases

Data in Table F.3 show that U in HLW waste streams has precipitated mainly as a hydroxide, except in two cases (BY-110 and C-112) where U is found as an oxidic phase (β-U_3O_8). Bismuth in wastes originating from bismuth phosphate processes is found in the form of bismuth oxide, ferric bismuth silicate, bismuth phosphate, and ferric bismuth phosphate. Lanthanum in sludges has been detected in the form of pyrophosphates (AW-105, T-111). Zirconium in neutralized cladding removal wastes apparently precipitates as a hydrated oxide (S-107, C-107, AW-105). Other waste stream constituents, such as Ca and Pb, have been found mainly in the form of hydroxyphosphate.

Minor constituents in the waste streams, such as Cr and Mn, have been found either as a pure phase or as solid solutions with major components. For instance, Cr occurs as grimaldite (CrOOH) in sludges of waste tanks BY-110, U-110, and B-110; whereas it is found in solid solution forms with Al (SY-101, SY-102, and SY-103), Fe (BY-104, BX-107, T-111, T-104, and AW-105), and Bi (B-111). Manganese is found in solid solution phases with Fe (SX-108, U-110, T-111), and Bi (U-110).

Solid phases of Pu and other radionuclides present in trace concentrations in sludges were not detected because of limitations of the analytical techniques used in the characterization studies. Depending on the solid matrix, compound identification using XRD requires each phase be present at least 1 wt %. Electron beam techniques (SEM and TEM) can detect compounds if they are present in minimum concentrations of 0.1% by weight. Because total concentrations of Pu in Hanford sludges are well below these detection limits, it is not feasible to detect Pu solid phases, unless these solids are separated and concentrated using appropriate processes. However, Pu solid phase forms in the sludges are expected to be analogous to the solid phases of minor elements (Pu can exist either as a pure phase or as solid solution phases) depending on the electrolyte chemistry of the waste stream, rate and degree of neutralization, and time and temperature of aging of resulting sludges.

In summary, the compound identification data collected from the sludge characterization studies indicates that

- Upon rapid neutralization, Al and Fe (major components of acidic waste streams) precipitate as hydroxides, silicates, and phosphates. These compounds occur as pure and solid solution phases depending on the waste chemistry (type and concentrations of other constituents such as, Bi, Cr, and Mn).

- Microcrystalline aluminum and iron hydroxide phases upon aging transform into crystalline phases such as boehmite and goethite.

- Uranium in sludges occurs mainly as a hydroxide phase and in three cases as an oxide phase.

- Minor constituents in waste streams (Cr and Mn) occur as pure phases and also as solid solutions with major constituents (Al, Fe, and Bi) as a function of waste chemistry.

- Although solid phases of Pu and other trace constituents were not identified sludges (because of limitations in analytical techniques), by analogy, Pu in sludges is expected to occur as a pure phase or as solid solutions.

F.6 References

References for this appendix are contained in the Chapter 7 reference list.

Distribution

No. of Copies

OFFSITE

2 DOE/Office of Scientific and Technical Information

ONSITE

13 **Westinghouse Hanford Company**

D. G. Baide (3)	S2-48
G. S. Barney	T5-12
D. R. Bratzel	S7-14
R. J. Cash	S7-14
G. N. Hanson	S5-05
J. P. Harris III	S2-48
D. W. Jepsen	G2-04
R. P. Marshall, Jr.	H5-61
T. S. Vail	R2-54
J. E. Van Beek	S2-48
J. A. Voogd	H5-03

No. of Copies

16 **Pacific Northwest National Laboratory**

N. D. Foote	K7-10
G. R. Golcar	P7-20
L. M. Liljegren	K7-15
S. V. Mattigod	K6-81
Y. Onishi	K9-33
M. R. Powell	P7-19
K. R. Savard	K9-04
R. J. Serne	K6-81
G. A. Whyatt (3)	P7-19
Information Release (5)	K1-06